Investigating Cardiac Metabolism and the Effect of Novel Metabolic Modulation Therapy on Cardiac Physiology and Exercise Capacity in Aortic Stenosis: A Multi-Parametric Cardiac Magnetic Resonance Study

Dr Shveta Monga MBBS MRCP

St Cross College
University of Oxford



A thesis submitted for the degree of
Doctor of Philosophy in Medical Sciences
Trinity Term 2023

I dedicate this work to my son, *Kiansh*

Declaration

This thesis is entirely my own work unless otherwise indicated. It has not been submitted, either wholly or substantially, for another degree at this University, or for a degree at any other institution. I have acknowledged assistance from colleagues and collaborators where relevant.

The total word count, excluding abstract, front matter and bibliography is 44,065 words

Abstract

Aortic stenosis is a major cause of morbidity and mortality in the western world. Whilst symptomatic patients with severe AS are treated with valve replacement surgery, there remains uncertainty about the best treatment for asymptomatic severe AS. Current guidelines recommend wait and watch strategy and offer surgery on occurrence of symptoms or evidence of systolic dysfunction. The annual rate of sudden cardiac death in asymptomatic severe AS remains close to 1%.

Aortic disease is both a disease of the valve and myocardium. The valve mechanisms and structural LV changes secondary to pressure overload have been extensively studied before, but no medical therapy directed at the valve processes has so far shown beneficial effect on cardiac physiology or disease progression. Changes in cardiac metabolism in pressure overload hypertrophy seem to play an important role in pathophysiology of AS and transition to decompensation. The healthy human heart uses fatty acids as the main energy source ~70% of adenosine triphosphate (ATP) requirements. In AS, there is substrate shift with downregulation of fatty acid oxidation (FAO) and increased reliance on glycolysis, with evidence of myocardial lipid accumulation and impairment of myocardial energetics. Peroxisome proliferator activated receptor-alpha (PPAR-α) plays a central role in FAO signalling and controlling lipid homeostasis in the heart. Downregulation of this transcriptional factor is associated with the metabolic alterations and subsequent lipotoxicity in AS, which ultimately causes reduced ATP production and heart failure. However, it is unclear whether these metabolic changes have a cause or effect relationship with the two main pathological features of AS, left ventricular (LV) pressure loading and LV hypertrophy, and their relationship with myocardial fibrosis (which is commonly seen in AS), is unclear.

Furthermore, it is yet unknown whether modulating cardiac metabolism would have any beneficial effect on disease progression or outcomes in AS.

This thesis set out to establish the relationship between metabolic remodelling and cardiac structure and physiology in AS. It then evaluates the role of novel metabolic modulator therapy in asymptomatic moderate-severe AS.

In Chapter 3 and 4, patients across the spectrum of AS were studied with advanced CMR imaging and phosphorus-31 magnetic resonance spectroscopy (^{31}P-MRS) and cardiopulmonary exercise testing (CPET) respectively. It is demonstrated that metabolic changes, specifically myocardial lipid accumulation (steatosis) and impaired cardiac energetics appear to occur early in the disease process. In addition, whilst impairment in cardiac energetics is related to degree of LV hypertrophy, steatosis appears to be more related to the degree of LV pressure loading from valve obstruction. Furthermore, these patients despite being asymptomatic with normal LVEF have evidence of subclinical LV dysfunction which occurs early in the disease process. Moreover, these patients though able to exercise to volitional exhaustion without developing symptoms have reduced average peak VO_2 and VE/VCO_2, both of which are predictors of outcome in cardiac disease.

In Chapter 4 and 5, the effect of the PPARα agonist Fenofibrate was evaluated on cardiac metabolism and physiology in a randomised double-blind placebo-controlled study. Fenofibrate reduced myocardial triglyceride content significantly after 6 months' treatment with evidence of in vivo fatty acid oxidation upregulation. It also caused a modest improvement in cardiac energetics. However, this modulation did not show any measurable improvement in cardiac physiology or exercise capacity.

Together, these data show that myocardial metabolic remodelling plays an important role in pathophysiology and progression of AS. The novel finding from this research is that metabolic changes occur early in the AS disease process and are associated with early

subclinical systolic and diastolic dysfunction. This highlights that metabolic remodelling may play a causal role in disease progression. This research has also shown, for the first time, that metabolic alterations in AS are amenable to modulation with a PPARα agonist, with some improvement in cardiac physiology but the benefit of such modulation in advanced disease remains questionable. Whether targeting earlier disease would yield different results remains unanswered.

Publications during this DPhil

1. **Monga S**, Valkovič L, Tyler D, et al. Insights Into the Metabolic Aspects of Aortic Stenosis With the Use of Magnetic Resonance Imaging. *J Am Coll Cardiol Img.* null2022, 0 (0).**https://doi.org/10.1016/j.jcmg.2022.04.025**

2. Moritz J. Hundertmark,A Adler, C Antoniades, **Shveta Monga**, et al.Assessment of Cardiac Energy Metabolism, Function, and Physiology in Patients With Heart Failure Taking Empagliflozin: The Randomized, Controlled EMPA-VISION Trial. **https://doi.org/10.1161/CIRCULATIONAHA.122.062021**

Other manuscripts in draft and under peer review

1. **Monga S,** Valkovič L, Mahmod M, Myerson SG, Neubauer S, Rider O. Metabolic phenotyping in Aortic stenosis: Results from a multi-parametric CMR study - in revision with Circulation imaging.

2. **Monga S**, Valkovič L, Myerson SG, Neubauer S, Mahmod M, Rider O. A prospective double-blind placebo-controlled study of novel metabolic therapy in Aortic stenosis – in draft

Presented abstracts

1. Metabolic Phenotyping In Aortic Stenosis: Insights From A Multi-Parametric Cardiac Magnetic Resonance Study
   Monga S, Valkovič L, Mahmod M, Myerson SG, Neubauer S, Rider O.
   Presented as moderated poster at ESC Congress 2022, Barcelona.

2. Metabolic Phenotyping In Aortic Stenosis: Insights From A Multi-Parametric Cardiac Magnetic Resonance Study
   Monga S, Valkovič L, Mahmod M, Myerson SG, Neubauer S, Rider O.
   Young Investigator award finalist at BSCI/ BSCCT annual conference September 2022, Bath.

3. A randomised controlled trial of Fenofibrate in moderate – severe AS: A Multi-Parametric Cardiac Magnetic Resonance Study
   Monga S, Valkovič L, Mahmod M, Myerson SG, Neubauer S, Rider O.

Young Investigator runner-up award at BSCMR annual conference October 2022, Liverpool.

4. Characterisation of metabolic phenotype in AS: Insights from a Multi-Parametric Cardiac Magnetic Resonance Study
   Monga S, Valkovič L, Mahmod M, Myerson SG, Neubauer S, Rider
   Awarded CVRI Early career travel grant for presentation, AHA, November 2022, Chicago
   Moderated poster presentation at AHA scientific sessions, November 2022, Chicago.

5. A randomised controlled trial of Fenofibrate in moderate – severe AS: A Multi-Parametric Cardiac Magnetic Resonance Study
   Monga S, Valkovič L, Mahmod M, Myerson SG, Neubauer S, Rider O.
   Moderated poster at AHA scientific sessions, November 2022, Chicago.

Acknowledgements

The work presented in this thesis would not have been possible without the expertise and support of my supervisors, to whom I am forever indebted. Prof Oliver Rider, my primary supervisor, who has been a tremendous source of encouragement, insight, and direction through the many learning stages of this thesis. Prof Stefan Neubauer for giving me this life-changing opportunity and supporting me throughout this DPhil. Prof Saul Myerson for his time and expertise and always encouraging my endeavours. I am grateful for the rigorous academic, scientific, and clinical training that I received from my supervisors throughout the course of this DPhil.

I feel privileged to have been able to work with an outstanding group of colleagues, collaborators, and mentors whose scientific enthusiasm and diligence is remarkable.

I am extremely grateful to my close friends and colleagues within OCMR who made this journey an enjoyable and memorable one. My immediate neighbours in the fellow's office William Watson, Peregrine Green, Matthew Burrage for their constant advice, support, and friendship. I am also thankful to Moritz Hundertmark, Mayooran Shanmuganathan, Jenny Rayner, Rina Ariga, Betty Raman, Ladislav Valkovič, Ferenc Mózes, Andrew Lewis, Andrew Apps, Valantou Nikolaidou and Rebecca Chamley as well as the excellent team of nurses and radiographers for their support. It has been an honour to know such talented and inspiring group of people. I am also thankful to the Clinical Cardiovascular Research Facility team for their support in running the study visits as well as the clinical research team for their help during this research.

My sincere and heartfelt thanks go to all the patients and volunteers who gave up their time to participate in my research. I acknowledge and thank the British Heart Foundation for granting me the Clinical Research Training Fellowship and supporting this research. I

acknowledge the funding support from Radcliffe Department of Medicine, Biomedical Research centre and John Fell fund for this project.

Finally, I would like to thank my parents, Surinder and Sandhya Monga, for their lifelong love and unwavering support and encouragement. My sister, Surbhi, who enthuses me with her own achievements and has provided limitless support over the years. My nephew, Armaan, for his light banter that cheered me up from time-to-time and kept me entertained through these years.

Above all, my deepest thanks to my husband, Kushal, whose commitment and work ethics are beyond remarkable and a constant source of inspiration. I feel blessed to have his endless love and encouragement, which has allowed me the opportunity to follow my dreams. My son, Kiansh, for those lovely cuddles that gave me strength beyond belief and to whom this thesis is dedicated.

Table of Contents

Contents

Abstract i

Publications during this DPhil iv

Acknowledgements vi

List of Figures xiii

List of Tables xvi

List of Abbreviations xviii

1 Chapter One 1

Introduction 1

1.1 Aortic Stenosis 1

1.2 Progression of disease 2

1.3 Pathophysiology of Aortic Stenosis 7

1.3.1 Valvular mechanisms 7

1.3.2 Myocardial mechanisms 11

1.4 Normal cardiac metabolism 17

1.4.1 Normal substrate selection 18

1.4.2 Normal mitochondrial oxidative phosphorylation and ATP homeostasis 24

1.4.3 Normal Creatine Kinase Shuttle 26

Role of PPARα signalling pathways in the normal heart 27

1.4.4 27

1.5 Cardiac metabolism in hypertrophied heart 31

1.5.1 Substrate shift with FAO downregulation in pressure-overload 31

1.5.2 Glucose metabolism in pressure overload hypertrophy 33

1.5.3 Anaplerosis (upregulation of pathways that replenish the pools of metabolic intermediates) and cardiac lipotoxicity 33

1.5.4 Impaired myocardial energetics (PCr/ATP and CK flux) 36

1.5.5 PPARα downregulation and consequent abnormal lipid homeostasis in pressure overload hypertrophy 36

1.5.6 Oxidative stress and mitochondrial dysfunction in hypertrophy 39

1.5.7 Myocardial steatosis and LV dysfunction in hypertrophy 39

1.6 Role of Magnetic resonance spectroscopy (MRS) in AS 41

1.6.1 ^{1}H-MRS for assessing lipid metabolism 43

1.6.2 ^{31}P-MRS for assessing high-energy phosphate metabolism 43

1.6.3 Other MRS techniques 44
1.7 Exercise capacity assessments 47
1.7.1 Cardiopulmonary Exercise Test (CPET) 47
1.7.2 Six-minute walk test (6MWT) 48
1.8 Summary of Research rationale 49
1.9 Aims of this Research 50
1.9.1 Correlational study (detailed in chapter 3 and 4) 51
1.9.2 Randomised double-blind placebo-controlled study/Ox-FAST – Oxford: Fibrates in Aortic Stenosis (detailed in chapter 5 and 6) 51
2 Chapter Two 52
Methods 52
2.1 General methods 52
2.2 Eligibility Criteria 52
2.2.1 Inclusion criteria 52
2.2.2 Exclusion criteria 53
2.3 Study assessments 54
2.3.1 Visit 1 - Screening and Baseline assessments 54
2.3.2 Visit 2 - Safety and compliance assessment (3 months ± 7 days) 56
2.3.3 Visit 3 – End of treatment assessments (6 months ± 7 days) 56
2.3.4 Visit 4 – Study completion (1 month after end of treatment) 57
2.3.5 COVID-19 modification to the study schedule 59
2.4 Clinical assessment 59
2.4.1 Anthropometry 59
2.4.2 Blood Pressure 59
2.4.3 ECG 59
2.4.4 Bloods 59
2.5 Six-minute walk test 60
2.6 Cardiopulmonary exercise testing (CPET) 60
2.6.1 CPET protocol 61
2.6.2 CPET results 62
2.7 Imaging assessment 64
2.7.1 Echocardiography 64
2.7.2 CMR scan protocol 64
2.8 Summary 83
3 Chapter Three 84
Role of metabolic phenotyping in Aortic stenosis 84

3.1 Abstract 84
3.1.1 Background 84
3.1.2 Purpose 84
3.1.3 Methods 84
3.1.4 Results 85
3.1.5 Conclusions 85
3.2 Introduction 86
3.3 Methods 87
3.4 Study Design 88
3.5 Statistical Analysis 91
3.6 Results 91
3.6.1 Study population 91
3.6.2 The Relationship between hypertrophy and metabolism 93
3.6.3 AS related pressure overload quartiles 103
3.6.4 LV pressure gradient quartiles 110
3.7 Discussion 119
3.7.1 Effect of LV hypertrophy 119
3.7.2 Effect of pressure overload (both AVG and LVG) 121
3.8 Blood parameters and cardiac metabolism 122
3.9 Conclusions 123
3.10 Rationale for metabolic therapy in AS 123
4 Chapter Four 125
Effect of cardiac metabolism on exercise capacity in AS 125
4.1 Abstract 125
4.1.1 Introduction 125
4.1.2 Methods 125
4.1.3 Conclusion 126
4.2 Introduction 127
***4.3* Methods** 130
4.3.1 Study population 130
4.3.2 Study assessments 131
4.3.3 Statistical analysis 131
4.4 Results 132
4.4.1 Characteristics of the population 132
4.4.2 Functional capacity in AS 135
4.5 Discussion 137

4.5.1 LV structure and exercise capacity in AS 138
4.5.2 LV function and exercise capacity in AS 138
4.5.3 Cardiac metabolism and exercise capacity 140
4.6 Conclusions 142
4.7 Limitations 142
5 Chapter Five 144
A prospective double blinded randomised controlled trial of metabolic modulation therapy in Aortic stenosis 144
5.1 Abstract 144
5.1.1 Background 144
5.1.2 Methods 144
5.1.3 Results 145
5.1.4 Discussion 145
Introduction 146
5.2 Methods 148
5.2.1 Study drug dose, duration and randomisation 148
5.2.2 Study visit schedule 150
5.2.3 Study population 150
5.2.4 Study end points 151
5.2.5 Data acquisition and analysis 152
5.3 Results 156
5.3.1 Study population 156
5.3.2 Primary Outcome 161
5.3.3 Secondary outcomes 162
***5.4* Discussion** 179
5.5 Limitations and future directions 185
5.6 Conclusions 187
6 Chapter Six 188
The effect of metabolic modulation on cardio-respiratory fitness and exercise capacity in AS 188
6.1 Abstract 188
6.1.1 Background 188
6.1.2 Methods 188
6.1.3 Results 188
6.1.4 Conclusions 189
6.2 Introduction 189
6.3 Methods 190

6.3.1 Data acquisition 191
6.3.2 Data analysis 191
6.4 Results 192
6.4.1 Study population 192
6.4.2 Cardiopulmonary exercise testing parameters 195
6.4.3 Spirometry results 197
6.4.4 Six-minute walk test 200
6.4.5 Exercise parameters and CMR measures of LV structure and function 201
6.4.6 Exercise parameters and CMR parameters of cardiac metabolism 210
6.4.7 Main predictors of peak VO_2 210
6.5 Discussion 210
6.5.1 Effect of LV peak systolic strain parameters and stroke volume on peak VO_2 211
6.5.2 LV diastolic function and Peak VO_2 212
6.5.3 Main predictors of Peak VO_2 213
6.6 Limitations 213
6.7 Conclusions 213
7 Chapter Seven 215
General conclusions and Future directions 215
7.1 General Conclusions 215
7.2 Future directions 221
8. **References** 223

List of Figures

Chapter 1 Figures

Figure 1.1: Prevalence of Aortic Stenosis as a function of age (Page 1)

Figure 1.2: Illustration of structural and metabolic changes that occur in aortic stenosis as the disease progresses. (Page 6)

Figure 1.3: Established mechanisms of valve injury and previously targeted interventions (Page 11)

Figure 1.4: Structural remodelling in Aortic stenosis (Page 14).

Figure 1.5: Three main steps of cardiac metabolism, cardiac glucose and long chain fatty acid metabolic pathways (Page 20)

Figure 1.6: Metabolic flexibility of the heart (Page 23)

Figure 1.7 (A) and (B): Role of peroxisome proliferator-activated receptor (PPAR) α in normal cardiac fatty acid metabolism (Page 29)

Figure 1.8: Anaplerosis depicting pyruvate entry into competing reactions. Oxidation via pyruvate dehydrogenase vs anaplerotic carboxylation to malate via malic enzyme. (Page 35)

Figure 1.9: Potential role of genomic alterations as causative factors in the chain of events leading from compensated hypertrophy to cardiac failure. (Page 38).

Chapter 2 Figures

Figure 2.1: Flowchart of study visits (Page 58).

Figure 2.2: Upright bicycle ergometer used for CPET testing (Page 62).

Figure 2.3: 9-panel plot result from a patient with AS. (Page 63)

Figure 2.4: CMR scan protocol (Page 65).

Figure 2.5: Timeline for CMR protocol (Page 66).

Figure 2.6: Comparison of ^{31}P-MRS Spectroscopy techniques (Page 68)

Figure 2.7: Cardiac energetics data from a patient with aortic stenosis (Page 70)

Figure 2.8: Left ventricular contours for volume and function (Page 72)

Figure 2.9: CMR tagging images of a long (left) and short axis (right) view in early diastole (Page 74).

Figure 2.10: **A**) ^{1}H-MRS voxel position and graphic representation **B**) Results from a patient with AS. (Page 77)

Figure 2.11: CMR acquisition of aortic valve images. (Page 78)

Figure 2.12: Late gadolinium acquisition images showing myocardial fibrosis in an AS patient (Page 80).

Figure 2.13: T1-map analysis from a mid-ventricular slice. **A.** ShMOLLI T1 maps (acquired and contoured image). **B**. MOLLI long T1 maps (acquired and contoured image), Page 81.
Figure 2.14: **A.** ShMOLLI T1 maps (acquired and contoured image). **B.** MOLLI long T1 maps (acquired and contoured image), Page 82.

Chapter 3 Figures

Figure 3.1: Pictorial representation of the participant groups and CMR protocol for the study (Page 90).
Figure 3.2: Graphic representation of LV structure and function characteristics in relation to LV wall thickness quartiles (Page 98).
Figure 3.3: Graphic representation of cardiac metabolism characteristics in relation to LV wall thickness quartiles (Page 100)
Figure 3.4: Relationship between myocardial fibrosis and cardiac energetics (Page 102)
Figure 3.5: Graphic representation of LV structure and function in relation to AV pressure gradient quartiles (Page 107).
Figure 3.6: Graphic representation of cardiac metabolism characteristics in relation to AV pressure gradient (Page 108).
Figure 3.7: Graphic representation of main LV structure and function findings in relation to total LV gradient quartiles (Page 114).
Figure 3.8: Graphic representation of cardiac metabolism characteristics in relation to LV pressure gradient (Page 116).
Figure 3.9: Correlation matrix of main blood parameters and cardiac metabolism (Page 122)

Chapter 4 Figures

None

Chapter 5 Figures

Figure 5.1: Visit Timeline Ox-FAST (Page 150).
Figure 5.2: Detailed inclusion and exclusion criteria for Ox-FAST (Page 151).
Figure 5.3 Pictorial representation of the study endpoints (Page 152).
Figure 5.4: Overview of CMR Sequences Ox-FAST (Page 154).
Figure 5.5: CONSORT flowchart of randomised controlled trial (Page 157)
Figure 5.6: Changes in MTG levels from baseline to 6 months treatment with Fenofibrate and Placebo (Page 162).
Figure 5.7: Change in PCr/ATP Ox-FAST: Change in Phosphocreatine/ATP ratio from baseline to 6 months treatment with Fenofibrate and Placebo (Page 163).

Figure 5.8: Delta PCr/ATP OxFAST: Scatter plot with bars with mean and 95% confidence intervals of delta PCr/ATP ratio for individual patients in respective cohorts (Page 163).
Figure 5.9 (A) and (B) Change in LV strain parameters as measured by MR tagging from baseline to 6 months in Fenofibrate and Placebo groups (Page 164-165).
Figure 5.10: Bar graph of paired t-test for LVEF in each group showing mean values with 95% confidence intervals (Page 168).
Figure 5.11: Bar graph of paired t-test for LV stroke volume (ml) in each group showing mean values with 95% confidence intervals (Page 169).
Figure 5.12: Bar graph of paired t-test for (A) LV mass index (Kg/m^2) and (B) LV wall thickness (mm) in each group showing mean values with 95% confidence intervals (Page 170).
Figure 5.13: Bar graph of paired t-test for (A) peak diastolic longitudinal strain rate (%/s) and (B) LA volume (ml) in each group showing mean values with 95% confidence intervals (Page 171-172).
Figure 5.14: Counts of patients with late gadolinium enhancement (LGE) in both the groups' pre and post 6 months' treatment (Page 173).
Figure 5.15: Summary of the main changes in free fatty acids and lipid profile in the (A) Fenofibrate and (B) Placebo group (Page 176),
Figure 5.16: Change in free fatty acids and beta-hydroxybutyrate levels in (A) Fibrate group and (B) Placebo group assessed by paired t-test from baseline to 6 months (Page 181).
Figure 5.17: A brief schematic of the ketone body production and oxidation in the liver and heart (Page 182).
Figure 5.18: Summary of the changes in left ventricular (A) circumferential strain, (B) longitudinal strain, (C) ejection fraction and (D) Diastolic longitudinal strain in both the groups (Page 184-185).

Chapter 6 Figures

Figure 6.1 Mean values for the main CPET parameters in the two groups both pre and post treatment and paired t-test results for these parameters i.e. (A) peak VO_2, (B) VE/VCO_2 and (C) VT (Page 196).
Figure 6.2: Graphic representation of pre and post treatment values of 6MWT distance in both the Fenofibrate and Placebo groups (Page 200).
Figure 6.3: Correlation results for comparison between delta change in main LV parameters and peak VO_2 in both the Fibrate and Placebo groups (Page 205).

List of Tables

Chapter 1 Tables

Table 1.1: Disease progression stages in calcific aortic stenosis and current recommended management for each stage (Page 4).

Table 1.2: Overview of available MRS techniques and their potential application (Page 46).

Chapter 2 Tables

None

Chapter 3 Tables

Table 3.0 : Baseline characteristics of study groups (Page 92-93)

Table 3.1: Demographics, clinical and biochemical characteristics in group based on LVH (Page 95).

Table 3.2: Cardiac structure and function in groups based on LVH (Page 97).

Table 3.3: Correlation between LV wall thickness and LV specific functional and metabolic parameters when controlled for both AV and LV gradient (Page 103).

Table 3.4: Demographics, clinical and biochemical characteristics in group based on peak AV gradient (Page 104).

Table 3.5: Cardiac structure and function in groups based on peak AV gradient (Page 106).

Table 3.6: Partial correlation between AV gradient and main LV function and metabolism parameters when controlled for LVWT (Page 109)

Table 3.7: Demographics, clinical and biochemical characteristics in group based on total LV gradient (Page 111).

Table 3.8: Cardiac structure and function in groups based on total LV gradient (Page 113).

Table 3.9: Partial correlation between LV gradient and main LV function and metabolism parameters when controlled for LVWT (Page 118).

Chapter 4 tables

Table 4.1: Demographic, clinical and cardiopulmonary exercise test (CPET) data (Page 133).

Table 4.2: CMR parameters in relation to maximal exercise capacity (MEC), Page 134).

Table 4.3: Relationship between peak VO_2, Age, BMI and CMR parameters (Page 136).

Chapter 5 tables

Table 5.1: Safety and efficacy bloods and laboratory tests Ox-FAST (Page 153).

Table 5.2: Baseline characteristics Ox-FAST: Characteristics at baseline for all patients randomised to treatment (Page 159).

Table 5.3: Baseline CMR characteristics Ox-FAST. All values expressed as mean ± SD (Page 160).
Table 5.4: Change in CMR parameters of LV structure and function from baseline to 6 months in both groups (Page 166-167).
Table 5.5: Paired t-test results for the change in native T1 values, extra- cellular volume fraction, myocardial matrix and cellular volume concentrations pre and post treatment in both fibrate and Placebo groups (Page 174).
Table 5.6: Paired t-test results for blood markers post 6 months treatment with Fenofibrate and Placebo (Page 177-178).

Chapter 6 tables

Table 6.1: Paired t-test results for spirometry, CPET and 6MWT parameters in both the fibrate and placebo groups (Page 198-199).
Table 6.2: Relationship between peak VO_2, maximal oxygen capacity and left ventricular strain parameter results post 6 months treatment for both Fenofibrate and Placebo groups (Page 202).
Table 6.3: Pearson correlation results between delta change in main LV parameters and peak VO_2 in the Fibrate group (Page 204).
Table 6.4: Correlation analysis between post treatment values of peak VO_2 and chosen LV parameters in the Fibrate group (Page 207).
Table 6.5: Correlation between delta change in main CPET parameters and markers of myocardial fibrosis, specifically Native T1 values (ms) and Extracellular volume fraction (%) in (A) Fenofibrate, and (B) Placebo group (page 209).
Table 6.6: Main predictors of peak VO_2 in the study (Page 210)

List of Abbreviations

AAT	Aspartate aminotransferase
AS	Aortic Stenosis
ACC	Acetyl Co-A Carboxylase
ADP	Adenosine Diphosphate
ANT	Adenosine Nucleotide Translocase
ATGL	Adipocyte triglyceride lipase
ATP	Adenosine Triphosphate
AVA	Aortic valve area
AVR	Aortic valve replacement
BMI	Body mass index
BNP	Brain natriuretic peptide
^{13}C-MRS	13-Carbon Magnetic resonance spectroscopy
CPT	Carnitine Palmitoyl Transferase
CK	Creatine Kinase
Cr	Creatine
CMR	Cardiac Magnetic Resonance
CPET	Cardiopulmonary Exercise Test
DAG	Diacylglycerol
DGAT	Diglyceride acyl transferase
ECV	Extracellular volume
EDV	End diastolic volume
EF	Ejection fraction
ESV	End systolic volume
ETC	Electron transport chain
FAT	Fatty acid translocase
FABPc	Fatty acid binding protein C
FEV	Forced Expiratory volume
FFA	Free fatty acids
FVC	Forced vital capacity
GLUT	Glucose transporters

^{1}H-MRS	Proton magnetic resonance spectroscopy
^{2}H-MRS	Deuterium magnetic resonance spectroscopy
HBP	Hexosamine biosynthetic pathway
HCM	Hypertrophic cardiomyopathy
HDL	High Density Lipoprotein
HF	Heart failure
LA	Left atrium
LCAD	Long chain acyl co-A dehydrogenase
LDL	Low Density Lipoprotein
LGE	Late gadolinium enhancement
L(p)a	Lipoprotein-a
LV	Left ventricle
LVH	Left ventricular hypertrophy
MCAD	Medium chain acyl co-A dehydrogenase
ME	Malic enzyme
MRI	Magnetic resonance imaging
MRS	Magnetic resonance spectroscopy
MTG	Myocardial triglyceride content
^{23}Na -MRS	23-Sodium magnetic resonance Spectroscopy
^{31}P-MRS	31-Phosphorus magnetic resonance Spectroscopy
PCr	Phosphocreatine
PDH	Pyruvate Dehydrogenase
PPAR	Peroxisome proliferator-activated receptor
PGC-1α	PPAR gamma coactivator 1α
Pi	Inorganic phosphate
RER	Respiratory Exchange Ratio
TCA	Tricarboxylic Acid
VO_2	Volume of oxygen
VE	Minute ventilation
VCO_2	Volume of carbon dioxide
VT	Ventilatory Threshold
WT	Wall thickness

1 Chapter One

Introduction

1.1 Aortic Stenosis

Aortic Stenosis (AS) is a major cause of cardiac morbidity and mortality. There is an exponential increase in prevalence of AS with age, with 0.2% in the 50–59-year group, 1.3% in the 60–69-year group, 3.9% in of the 70–79-year group, and 9.8% in those aged 80–89 years. The incidence of new AS is 5 per 1,000 per year, with the initial mean age of patients being 60 years,[1] due to the predominance of degenerative aetiologies (**Figure 1.1**). This makes it a currently a major societal and economic burden, which given the ageing population is likely to be increased in the future.[2]

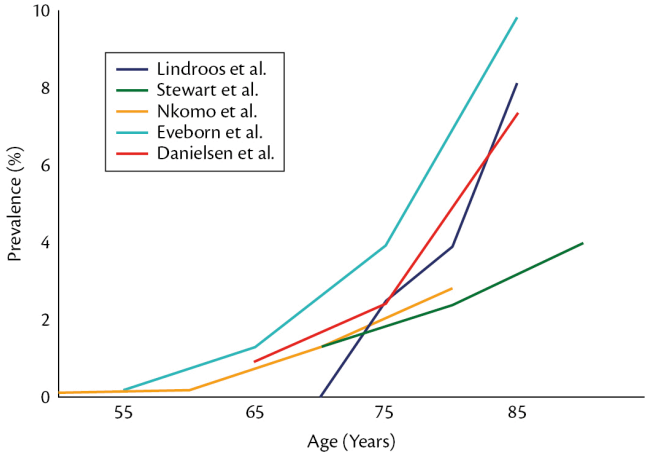


Figure 1.1: The prevalence of aortic stenosis as a function of age.[2, 3] *The prevalence of aortic stenosis (AS) according to age in the following population-based series from the USA or Europe: Lindroos et al. (Finland), in which AS was defined as an aortic valve area of < 1.2 cm^2; Stewart et al. (Cardiovascular Health Study, USA), in which AS was defined as a peak aortic jet velocity of > 2.5 m per sec; Nkomo et al. (USA), in which AS was defined as an aortic valve area of < 1.5 cm^2; Eveborn et al. (Tromsø Study, Norway), in which AS defined was as a mean gradient of ≥ 15 mmHg; Danielsen et al. (AGES-Reykjavik Study, Iceland), in which AS was defined as an indexed aortic valve area of ≤ 0.6 cm^2 per m^2*

Degenerative AS develops over many years and slowly progresses at the molecular, cellular and tissue levels. Current guidelines recommend aortic valve replacement (AVR) as the definitive treatment for severe AS, but only after the onset of clinical symptoms such as chest pain, breathlessness, and syncope, or when there is impaired left ventricular (LV) systolic function.[4] However, there is uncertainty about the best treatment for asymptomatic severe AS patients with preserved LV systolic function. Previous trials of medical therapy include trials of 3-hydroxy-3-methyl-glutaryl-coenzyme A (HMG Co-A) reductase inhibitors (statins), angiotensin converting enzymes inhibitors and bisphosphonates [5,6,7],but all have failed to show any significant therapeutic effects that could translate clinically and the pathophysiological mechanisms that underlie the transition from compensated pressure overload state to heart failure are poorly understood.

Therapeutic options beyond AVR are currently limited but hold great promise not only in the elderly patients at high or prohibitive risk for surgery due to multiple comorbidities, but also to delay timing of AVR in young patients who may require more than one surgery in their lifetime. Alternative therapeutic options may also help improve myocardial response and recovery in severe AS undergoing AVR and potentially improve outcomes after surgery. There is thus an urgent need to understand the pathophysiological processes leading to decompensation in AS at the most fundamental level to improve preventive and therapeutic strategies**.**

1.2 Progression of disease

Progression of AS is not entirely predictable. A preclinical phase of aortic sclerosis, where the aortic valve cusps are thickened without significant blood flow limitation, occurs prior to the development of calcific AS (**Table 1.1**), but the rate of progression may differ from individual to individual. Indeed, population studies have suggested that by the age of 85 years

old, only half of the population would have developed aortic sclerosis. The conversion from sclerosis to stenosis affects approximately 2% of patients per year, but there are no clear methods for identifying who will progress, nor for predicting the rate of disease advancement in an individual.[8,9] However, observational data has suggested that individuals with the greatest valve calcification are at higher risk of early progression of AS.[10]

Table 1.1: Disease progression stages in calcific aortic stenosis and current recommended management for each stage (AS, Aortic Stenosis; AVR, Aortic valve replacement; LV, left ventricular; LVEF, LV ejection fraction

Disease stage	Sub-stage	Description	Management
At risk of AS	N/A	• Bicuspid aortic valve (or other congenital valve anomaly), aortic valve sclerosis • No obstruction to blood flow • No symptoms	• Clinical and echocardiographic follow-up every 3–5 years • No indication of AVR
Mild or moderate AS	N/A	• Mild-to-moderate leaflet calcification of a bicuspid valve or tricuspid valve with some reduction in systolic motion • Mild or moderate AS • Early LV diastolic dysfunction might be present, normal LVEF • No symptoms	• Clinical and echocardiographic follow-up every 3–5 years for mild AS and every 1–2 years for moderate AS • No indication of AVR
Severe AS	Asymptomatic severe AS with normal LV systolic function	• Severe leaflet calcification or congenital stenosis with a severely reduced leaflet opening • Severe AS • LV diastolic dysfunction, normal LVEF • No symptoms	• Clinical and echocardiographic follow-up every 6–12 months • Indication of AVR (Class IIa) if stenosis is very severe and low surgical risk
	Asymptomatic severe AS with LV systolic dysfunction	• Severe leaflet calcification or congenital stenosis with a severely reduced leaflet opening • Severe AS • LVEF of <50% • No symptoms	• Indication of AVR (Class I)
	Symptomatic severe AS	• Severe leaflet calcification or congenital stenosis with a severely reduced leaflet opening • Severe AS • LV diastolic dysfunction, impaired LV longitudinal systolic function and pulmonary hypertension may be present • Symptoms: exertional dyspnoea, angina, syncope or pre-syncope and decreased exercise tolerance	• Indication of AVR (Class I)

AS is both the disease of valve and myocardium, and response of the myocardium is equally important in determining progression and development of symptomatic disease. LV hypertrophy develops as a result of increased afterload, which is believed to normalise LV wall stress and preserve systolic function.[11,12] However, there is wide individual heterogeneity when it comes to degree of hypertrophy and progression to heart failure.[13,14]. I sought to understand in this research whether metabolic changes underlie this variability.

Figure 1.2 gives a brief overview of the structural and metabolic changes in AS.

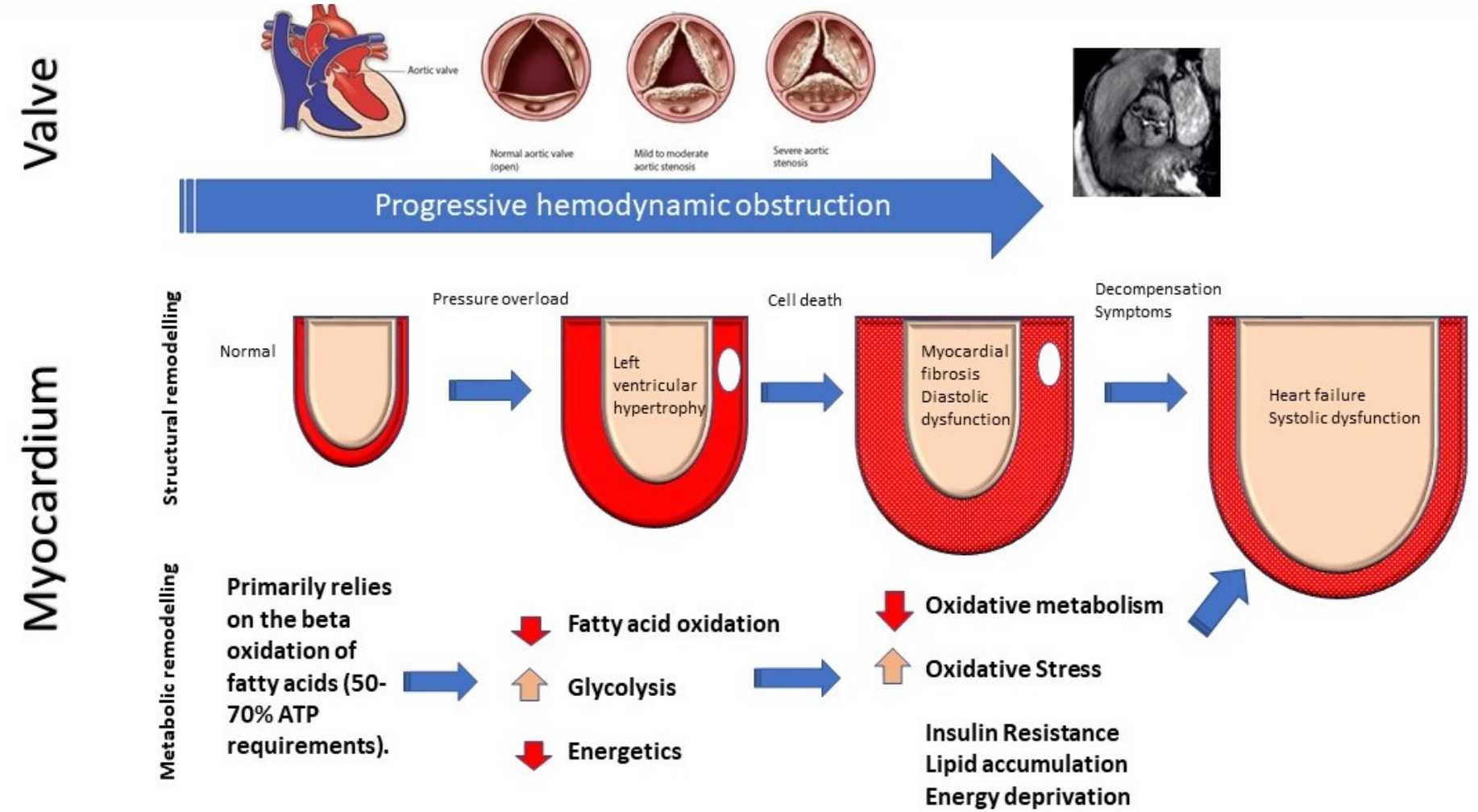


Figure 1.2: Illustration of structural and metabolic changes that occur in aortic stenosis as the disease progresses.

1.3 Pathophysiology of Aortic Stenosis

It is clear that AS is not a passive degenerative disorder of aging related to mechanical stress but incorporates active cellular processes that affect both the valve leaflets and the myocardium, which I have expanded on further below.

1.3.1 Valvular mechanisms

AS progresses over several decades during which the valve leaflets undergo extensive fibro-calcific tissue remodelling.[15] Biomechanical stress is recognised to play a significant role in the initiation and progression of the disease. The most widely accepted hypothesis is that hemodynamic stress leads to lipid infiltration that in turn allows for inflammation and calcification.[16] Like atherosclerotic lesions, the lipoproteins [including LDL-cholesterol and lipoprotein Lp(a)] infiltrate and undergo oxidative modifications. These oxidized lipoproteins are cytotoxic and can stimulate both the inflammatory response and the mineralisation. Once inflammatory cells, like macrophages and T lymphocytes, are recruited in the sub-endothelium, they release enzymes, such as matrix metalloproteinase, which degrade collagen, elastin and proteoglycans of the aortic cusps. Inflammation promotes the mineralisation of valve interstitial cells, the main cellular components of the aortic valve. The transformation of valve interstitial cells into myofibroblasts and osteoblast-like cells is determined by several signalling pathways having reciprocal crosstalk.[17] These different valvular mechanisms that have been implicated in the pathophysiology of AS have been the target of previous clinical trials and are briefly discussed below.

1.3.1.1 Atherosclerosis like process

The extensive scientific evidence that degenerative AS likely represents an active process similar to that of atherosclerotic disease has led to the suggestion that the risk factors for atherosclerosis are also common to AS and include older age, male gender, smoking, arterial

hypertension, high levels of Lp(a) and LDL cholesterol.[15] This recognized association between atherosclerosis, cholesterol, and calcific aortic valve disease has been the basis for major larger studies evaluating the efficacy of LDL-lowering therapy in retarding AS progression. Three large randomized clinical trials (SALTIRE, SEAS and ASTRONOMER) reported between 2005 and 2010 assessing the impact of statins on either AS progression by echocardiographic parameters or outcome using a composite of cardiovascular events. These studies randomised patients with mild to moderate AS to treatment with several different statins. No statistically significant difference was found for any of the measured parameters of disease progression or other cardiovascular outcomes.[18,19,20]

Sub analysis of the ASTRONOMER trial (Aortic Stenosis Progression Observation: Measuring Effects of Rosuvastatin) showed that in patients with mild to moderate AS, elevated levels of Lp(a) were associated not only with faster progression of AS but also with significantly worse clinical outcomes after multi-variable adjustment. In addition, single-nucleotide polymorphisms in the Apo-B and IL10 genes have been suggested to play a role in the risk of developing AS. Given the potential role of Lp(a) in AS progression, drugs that reduce Lp(a) levels like Niacin, antisense-specific Lp(a) inhibitors, and PCSK9 inhibitors[21] are seen to be promising future alternatives. Further basic research is ongoing before such a treatment can be evaluated in a clinical setting.

Whether lipid-lowering therapy could slow or halt progression of valvular mechanisms that underpin AS is still unknown. Although the initial evidence in the literature seems to be unfavourable, currently there is a growing idea that these therapies may have a benefit only if given early in the disease process, when inflammation (and not calcification) is the predominant process, in contrast to severe or advanced AS, where calcification (and not inflammation) predominates.

1.3.1.2 Osteoporosis like process (Imbalance of calcium homeostasis*)*

Another school of thought is that the calcium deposition and bone mineralization, which when established in late-stage calcific aortic valve disease, severely impedes normal mechanical operation of the aortic valve. Valve calcification assessed with computed tomography (CT) is one of the stronger independent predictors of adverse clinical outcomes in AS.[22,23] Dysregulation of serum calcium and phosphate is hypothesized to promote development of calcific aortic valve disease, the cellular basis of which remains an active topic of research in AS.[24]

The calcification hypothesis implies that treatments for bone diseases (bisphosphonates or denosumab) might have a beneficial effect on vascular and valvular calcification while maintaining bone health. The recently published SALTIRE 2 trial, however, showed that neither denosumab (which inhibits osteoblast activity) nor alendronic acid (which reduces bone absorption and release of calcium in the circulation) affect progression of aortic valve calcification in patients with calcific aortic AS.[25] Vitamin K supplementation is another attractive option to replenish vascular vitamin K stores and ensure full activation of Matrix Gla protein (MGP) for optimal calcification inhibition. Vitamin K supplementation in rats showed regression of warfarin-induced vascular calcification.[26] In line with this, a first in-man RCT has demonstrated that vitamin K supplementation decelerated valvular calcification on CT in a small group of patients with calcific aortic valve disease.[27]The effectiveness of vitamin K supplementation to reduce or hold calcification progression is currently subject of investigation in clinical trials.[28]

1.3.1.3 *Renin-Angiotensin Aldosterone system (RAS)*

The RAAS cascade is another important player in cardiovascular disease, also being involved

in pathological processes involving both the valve and myocardium in calcific aortic valve disease.[29,30] However, observational retrospective studies investigating the Angiotensin converting enzyme (ACE) inhibitor effects on aortic valve disease progression has provided conflicting results. Treatment with ACE inhibitors has been shown to be associated with less aortic valve calcification[31] but did not appear to slow haemodynamic progression.[32] In relation to the LV hypertrophic response, the Ramipril in Aortic Stenosis (RIAS) RCT performed in OCMR, showed a modest but significant reduction of myocardial hypertrophy in patients with calcific aortic valve disease treated with Ramipril.[6] Finally, clinical observational studies have suggested that ACE inhibitors and Angiotensin receptor blockers (ARB) are associated with favourable effects on symptoms and improved survival in patients with calcific aortic valve disease.[33] Again RCT data are required to validate this observation. Overall, valve mechanisms have been the target of multiple interventional trials as described above but none so far has shown the ability to halt the progression of calcific AS or induce its regression. **Figure 1.3** below summarises the valve processes and targeted interventions.

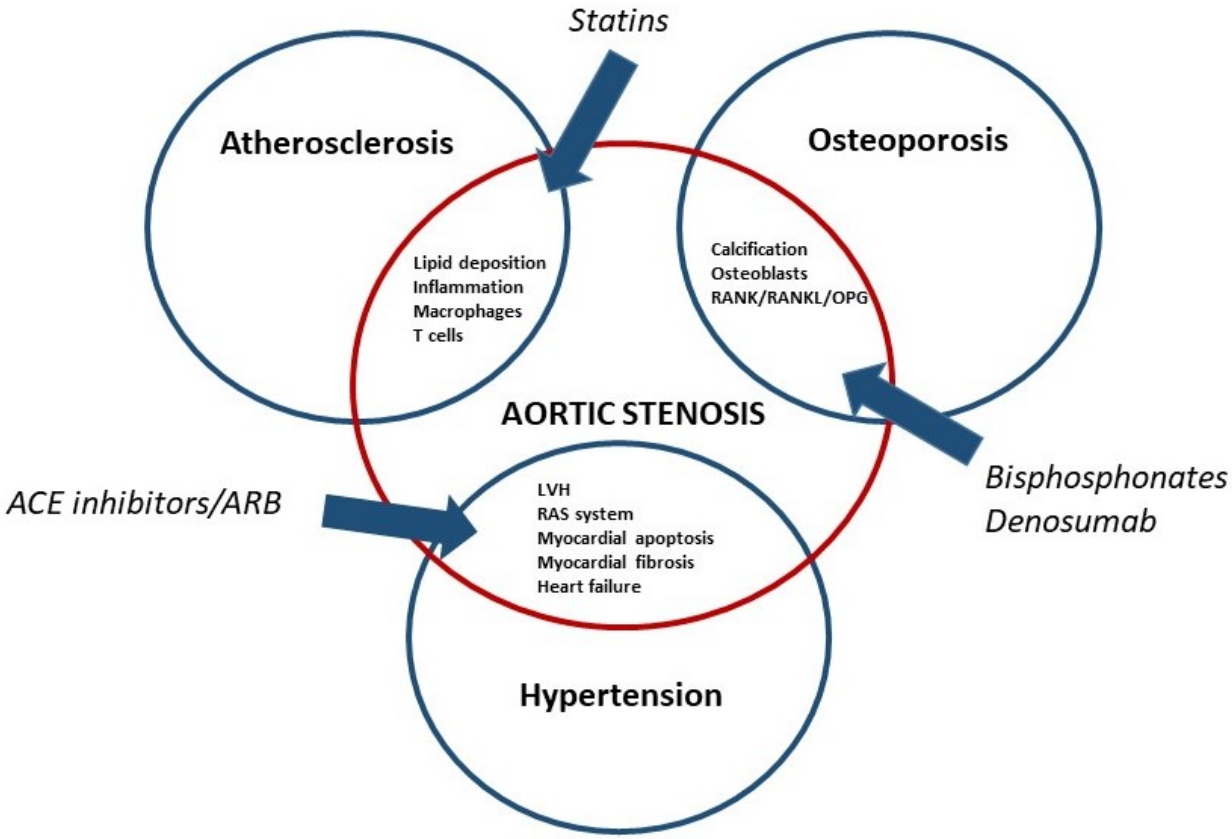


***Figure 1.3**: **Established mechanisms of valve injury and previously targeted interventions.** ACE indicates angiotensin-converting enzyme; ARB, Angiotensin Receptor Blockers; RANKL, receptor activator of nuclear factor-κB ligand; LVH, left ventricular hypertrophy: RAS, Renin Angiotensin system*

1.3.2 Myocardial mechanisms

Although the primary insult in AS is valve stenosis, the myocardial response to this is highly relevant to the clinical course. The myocardial response depends not only on the severity of AS itself, but also on a multitude of additional factors like age, sex, coexistent coronary artery disease, hypertension, and genetic influences, as these contribute significantly to myocardial remodelling. LV pressure overload in AS is a pathological process that elicits myocyte hypertrophy and alterations in extracellular matrix composition, both of which contribute to increases in LV stiffness and failure. There is significant clinical and experimental evidence to suggest that when AVR is performed after the development of significant LV diastolic dysfunction and heart failure symptoms, the LV structural

remodelling process including LVH and myocardial fibrosis that ensued from long-standing AS may not be readily reversible.[34,35] Thus, elucidation of cellular and metabolic pathways that contributes to myocardial structural and functional remodelling in AS will not only provide clinically relevant prognostic information but translation of these metabolic pathways into diagnostic and prognostic applications could be utilised to direct appropriate timing for AVR or explore new therapeutic options.

Below, I first expand on the myocardial structural changes in AS dividing them into myocardial hypertrophy, myocardial fibrosis and LV contractile dysfunction before dwelling into the intricacies of metabolic cascade in AS. I, further, explore avenues for better risk stratification and potential therapeutic options targeting metabolic phenomenon.

1.3.2.1 Pressure overload hypertrophy

Pressure overload, which is defined here as total LV pressure sufficient to cause LVH, in AS manifests as two distinct but overlapping structural changes (**Figure 1.4**). The first one is characterised by LV hypertrophy where the increase in wall thickness and mass act to limit the increase in wall stress created by AS-induced pressure overload state [36] in line with the law of Laplace (i.e. wall stress is related directly to intra-cavity pressure and cavity radius, but inversely to wall thickness). However, these compensatory mechanisms i.e., myocyte hypertrophy and stretching, occur at the expense of increased myocardial oxygen consumption, altered LV function and increase filling pressures.[37] Once the adaptive mechanisms to pressure overload are exhausted, either because of extreme sarcomere extension or marked LVH with increased diastolic stiffness preventing adequate LV filling, the LV becomes unable to maintain a normal stroke volume in the setting of limited preload reserve causing afterload mismatch. Consequently, systolic wall stress becomes markedly elevated, and LVEF decreases.[38] LV dilation might be present in this late phase, with eccentric LV remodelling or hypertrophy.

This above concept, however, is operative, and perfect hypertrophic compensation often does not occur. In some cases, the amount of hypertrophy that develops seems excessive, afterload is reduced to subnormal levels, and ejection performance is normal or supernormal.[39] In some cases, hypertrophy is inadequate to normalize wall stress and ejection fraction is decreased.[40] In other cases, there is concentric remodelling with little hypertrophy, a pattern in which LV wall thickness is increased but chamber size is decreased.[41] What causes this variable response is not fully known. Metabolic interactions in AS may explain this variability, and I explore this possible hypothesis in detail in Chapter 3.

1.3.2.2 Myocardial fibrosis

The second process occurs within the hypertrophied myocardial extra-cellular matrix (ECM) and causes progressive myocardial fibrosis which in turn results in reduced ventricular compliance and diastolic dysfunction. Interstitial myocardial fibrosis, myocyte degeneration, and apoptosis are early structural changes in patients with severe AS. In the hypertrophied myocardium, areas of fibrosis coalesce with areas of myocyte apoptosis, and a pathological sequence of myocyte hypertrophy followed by apoptosis and replacement fibrosis has been described.[42,43,44] These changes occur predominantly in the sub-endocardial layers, leading first to interstitial and later to replacement fibrosis during disease progression. The extent being related to increasing LV filling pressures and decreased LVEF. Cardiac Magnetic Resonance (CMR) imaging detected mid wall fibrosis has been shown in various prospective clinical studies to be an independent predictor of mortality in patients with moderate and severe AS and of incremental value in the prognostic model to ejection fraction.[45]

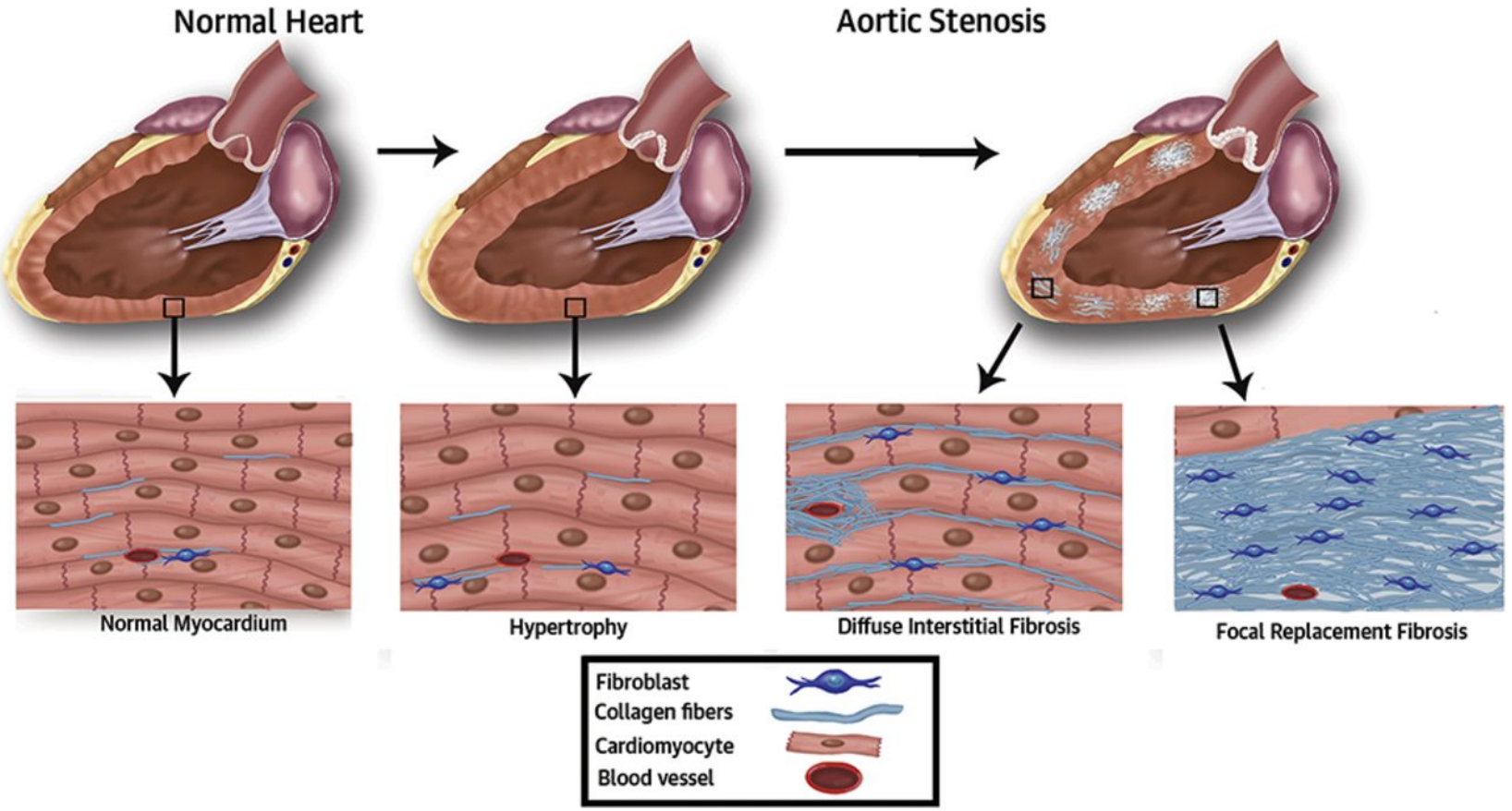


Figure 1.4: Structural remodelling in Aortic stenosis*: Progressive myocardial hypertrophy associated with myocyte apoptosis and replacement fibrosis Modified from source* [45]

1.3.2.3 Myocardial perfusion and contractile dysfunction

1.3.2.3.1 *Longitudinal function*

In pressure overload state, the increase in wall stress and intra myocardial pressure as well as the reduction in myocardial blood flow occurs mainly in the sub-endocardium where the myocardial fibres are oriented longitudinally.[46] Increase in sub-endocardial wall stress and associated ischemia are found in patients with AS even in the absence of significant coronary artery disease.[47] These are related to the severity of AS, haemodynamic load on the LV, and reduced diastolic perfusion time and may represent the substrate for LV longitudinal dysfunction, which is an early finding in patients with significant AS even in the presence of a normal LVEF. Compensatory changes in LV geometry with increased relative wall thickness and preserved radial and circumferential function, mainly determined by mid-wall myocardial fibres, may explain the preservation of LVEF in these patients.[36] A reduction in peak systolic longitudinal strain and circumferential strain has been shown to predict adverse outcomes in asymptomatic AS patients.[48]

1.3.2.3.2 *Diastolic function*

This also has an important role in the pathogenesis of symptoms and the progression to HF in patients with AS. It appears early in the disease process as a result of LVH and interstitial fibrosis with subsequent impaired relaxation and increased LV chamber stiffness.[49] Recent studies have shown that increasing baseline grades of diastolic dysfunction are associated with adverse clinical outcomes.[50]

1.3.2.3.3 *Right Ventricle (RV) in AS*

The right and left ventricle are closely attached through the interventricular septum sharing common fibres that encircle both ventricles, and are constraint into the pericardial space,

which justifies the functional interdependence between the two chambers.[51, 52] The alteration in LV afterload and function in AS might therefore be transmitted to the RV through the interventricular septum, as already observed in some experimental models of AS.[53]

Traditionally, RV dysfunction in AS was thought to be a direct consequence of increased systemic pulmonary artery pressure (PAP) due to advanced LV dysfunction and increased LV end-diastolic pressure. However, PAP is not always the true indicator of RV function. In AS with normal LVEF, increased RV afterload may be present before detectable pulmonary hypertension.[54] RV adaptation to chronic afterload is by increased contractility thus a high normal RV ejection fraction (RVEF) and increased RV strain in these patients may indicate early decompensation. Hypertrophied, stiff LV might be aided by increased RV contractility in asymptomatic severe AS to maintain the normal stroke volume across the stenosed valve. There are studies suggestive that a hyperdynamic RV may be considered a novel early objective marker of decompensated AS.[55] Larger studies establishing the role of RV functional assessment in asymptomatic severe AS remain pending.

Overall, AS is not a disease entity limited to the aortic valve, but rather could be compared to a cardiomyopathy like process that is characterized by a concomitant deep alteration in the whole heart structure and function.[56] It yet remains to be explored how the above structural changes tie in with the metabolic alterations that accompany AS. Whether there exists a cause or effect relationship between the two that might explain variability in outcomes amongst individuals with the same amount of pressure overload and hypertrophy. This research aims to understand the underlying reciprocity between the structural and metabolic myocardial response to chronic pressure overload in AS well as explore avenues for metabolic modulation in AS.

1.4 Normal cardiac metabolism

As a continually working aerobic biological pump, the adult human heart has the highest energy demand for adenosine triphosphate (ATP) per gram of tissue of any organ ~ 6 kg daily.[57] The heart conducts its pumping function by converting the chemical energy stored in fatty acids, glucose and other substrates into the mechanical energy of actin-myosin interaction of myofibrils.

Normal cardiac metabolism comprises of three key stages (as illustrated in **Figure 1.5**).
The first stage is substrate utilization i.e., cellular uptake of different carbon substrates (glucose, fatty-acids, lactate, ketones, branch chain amino acids) followed by their utilisation via substrate specific metabolic pathways, (β-oxidation for fatty acids, and glycolysis for glucose), to generate acetyl coenzyme-A (acetyl CoA) which then enters the tricarboxylic acid (TCA) or Krebs cycle. In the adult heart, fatty acids are the main source of ATP production, accounting for 60%–90% and the remaining 10%–40% comes from glucose, amino acids, pyruvate, lactic acid, ketone bodies, and other sources.[58]
The second stage - Oxidative phosphorylation (Oxphos) involves electron shuttling from cytosolic to mitochondrial reducing equivalents (via the glycerol phosphate and malate-aspartate shuttle), then transfer of energy by electrons from reducing equivalents to O_2 via the electron transport chain (ETC) complexes and generation of an electrochemical proton gradient within the mitochondrial intermembrane space. The free energy of this gradient is coupled to the synthesis of ATP from ADP + Pi by the F0, F1-ATPase contributing >95% of ATP synthesis under aerobic conditions.[59] The heart has no excess capacity for energy production over energy utilization and during maximal exercise cardiac muscle uses 90% of its oxidative capacity.[60]

The third stage, Phosphotransfer, refers to delivery of ATP from mitochondria to sites of use, i.e., facilitated diffusion. This involves ADP-ATP exchange across the inner mitochondrial membrane by adenine nucleoside translocase (ANT) and propagation of local ATP/ADP disequilibria by the CK system. The CK system plays an important role in myocardial ATP metabolism by maintaining ADP and Pi levels high in the mitochondria (CK mitochondrial isoform), where ATP is generated, and low at sites of ATP utilization (CK muscle isoform), thereby enhancing the efficiency of the ATP utilization processes. Besides CK, there are minor contributions from adenylate kinase, other phosphotransfer systems and direct adenine nucleotide channelling.[61, 62]

1.4.1 Normal substrate selection

1.4.1.1 Fatty acid metabolism

Fatty acid (FA) metabolism is a multi-step process including uptake into the cytosol, transport across the mitochondrial membrane and oxidation within the mitochondria finally resulting in the breakdown of FA for energy production (highlighted in **Figure 1.5** in yellow). Although short chain FAs can traverse the plasma membrane passively, the transport of long chain fatty acids is facilitated by transport proteins including fatty acid translocase (FAT/CD36) [63] and the plasma membrane fatty acid binding protein (FABPc). In the cytosol, free fatty acids are esterified to fatty acyl CoA, which is either esterified to triglycerides (TG) and stored as lipid droplets in the myocardium available for oxidation or converted to long-chain acylcarnitine by carnitine palmitoyl transferase I (CPT I) located in the outer mitochondrial membrane prior to entering the mitochondria, a critical regulatory step that determines FA oxidation rates. The turnover of myocardial TG is high, and FA derived from myocardial TG stores provides a significant proportion of substrates for mitochondrial FAO and has also been shown to be involved in the regulation of FAO through the activation of

peroxisome proliferator-activated receptor-α (PPARα) and PPARγ coactivator-1α (PGC1α).[64,65,66]

Long-chain acylcarnitine is then transported into the mitochondrial matrix and converted back to long-chain acyl-CoA by carnitine palmitoyl transferase II (CPT II). Acyl-CoA then enters β-oxidation, generating acetyl-CoA and the reducing equivalents NADH and $FADH_2$, which are not only used for ATP production via the electron transport system but also regulate glucose oxidation.[67] Adenine nucleotide translocase (ANT) transfers ATP and ADP into and out of the mitochondria. The transfer of ATP to the utilization site (e.g., myofibril) involves the creatine kinase (CK) shuttle, which catalyses the conversion between ATP and phosphocreatine (PCr).[62] (shown in **Figure 1.5**).

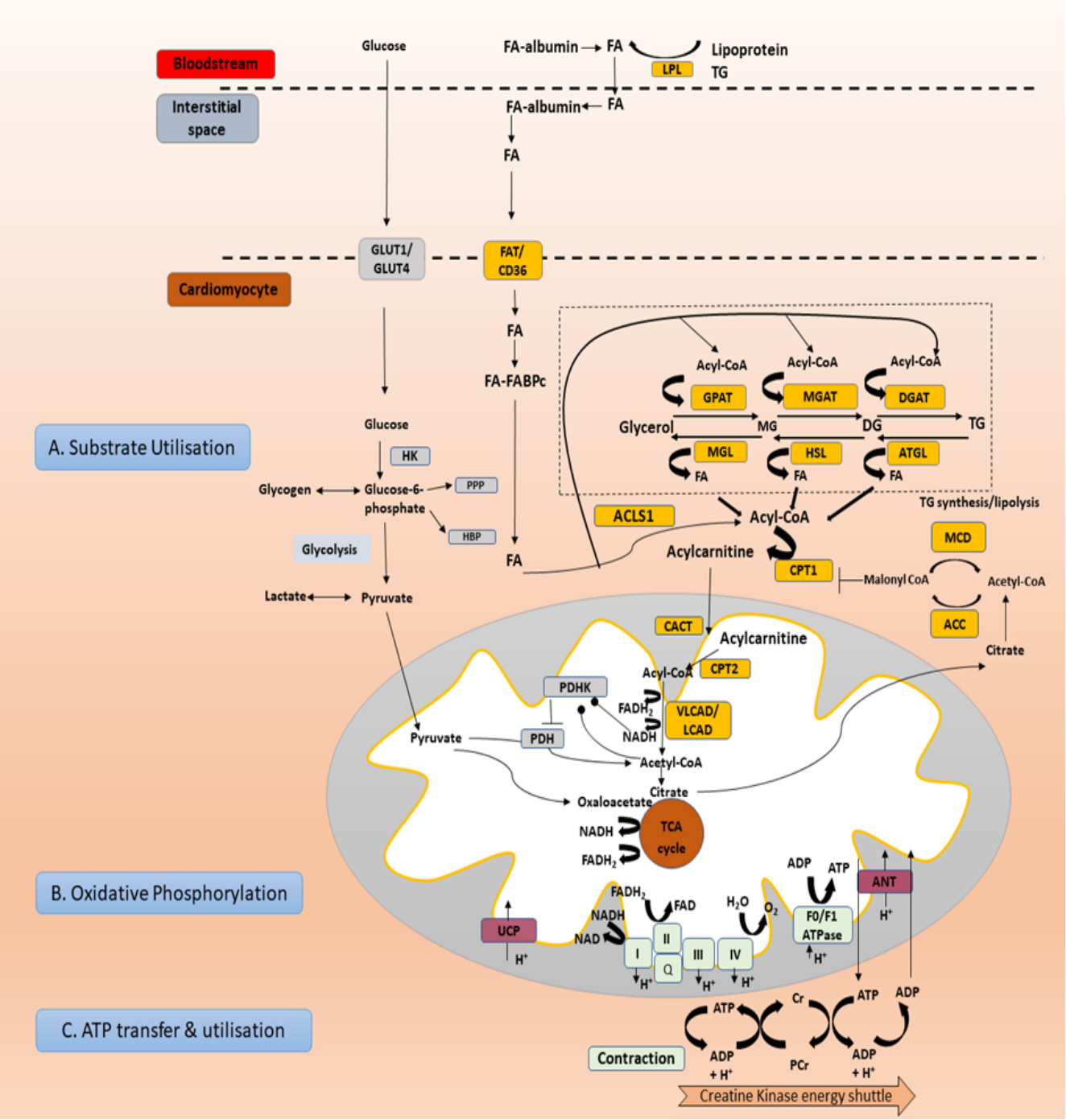


***Figure 1.5**: **Three main steps of cardiac metabolism (highlighted in blue), cardiac glucose (grey) and long chain FA (yellow) metabolic pathways.** FA, besides glucose, are the main substrates for cardiac energy metabolism. [FA, fatty acid; TG, triglycerides; FAT/CD36;fatty acid translocase; FABPc, fatty acid binding protein; GPAT, glycerol phosphate acyltransferase; MGAT, monoglyceride acyltransferase; DGAT, diglyceride acyltransferase; DG, diglycerides; ATGL, adipose triglyceride lipase; MG, monoglycerides; HSL, hormone sensitive lipase; ACLS-1, long chain fatty acyl-coA synthestase-1; MCD, malonyl Co-A decarboxylase; ACC, acetyl co-A carboxylase; CPT, carnitine palmitoyl transferase; CACT, carnitine-acylcarnitine transporter; VLCAD, very long chain acyl co-A dehydrogenase; LCAD, long chain acyl co-A dehydrogenase; PPP, pentose phosphate pathway; HBP, hexokinase biosynthetic pathway; HK, hexokinase; PDHK, pyruvate dehydrogenase kinase; PDH, pyruvate dehydrogenase; TCA, tricarboxylic acid; UCP, uncoupling proteins; ANT, adenine nucleotide translocase].*

1.4.1.2 Normal glucose metabolism

Under normal conditions, cardiac ATP is mainly derived from FAO, with glucose metabolism contributing less. However, under stress conditions, FAO may be reduced, which is concomitant with increased glucose utilization. Glucose uptake in cardiomyocytes is mediated by glucose transporters (GLUTs), with GLUT1 and GLUT4 as the most abundant isoforms. GLUT4 is predominant in the adult heart.[68, 69, 70] Inside cardiac myocytes, glucose is first phosphorylated to glucose 6-phosphate by hexokinase. Glucose 6-phosphate subsequently goes through multiple metabolic pathways, including glycolysis, pentose phosphate pathway (PPP), and the hexosamine biosynthetic pathway (HBP).

Glycolysis is the most important route for glucose metabolism in a cell, which produces pyruvate, NADH, and ATP.[71] ATP yield from glycolysis, however, contributes only a small portion of the overall ATP pool in the normal heart.[72] In cytosol, pyruvate can be further utilized to form alanine by alanine transaminase or reduced to lactate by lactate dehydrogenase. On the other hand, pyruvate is oxidized (known as pyruvate oxidation) to generate acetyl-CoA by pyruvate dehydrogenase that fuels the TCA cycle in mitochondria.[73] (refer to **Figure 1.5**).

1.4.1.3 Accessory pathways of glucose metabolism

Beside glycolysis, G6P may also be channelled into glycogen synthesis or the pentose phosphate pathway (PPP, see **Figure 1.5**).[74] The PPP is an important source of reduced nicotinamide adenine dinucleotide phosphate (NADPH), which plays a critical role in regulating cellular oxidative stress and is required for lipid synthesis and anaplerosis[75] (discussed in next section 1.4.1.4). The key oxidative enzyme of the PPP is G6P dehydrogenase, which catalyses the first reaction of the pathway to generate NADPH. In

addition to the PPP, a small amount of G6P can enter the hexosamine biosynthetic pathway (HBP, **Figure 1.5**).[76] Because the HBP requires not only glucose but also acetyl-CoA and glutamine, it may serve as a metabolic sensor linking metabolic status to several cellular processes. In the normal heart flux through the PPP and HBP is relatively small.

1.4.1.4 TCA cycle and anaplerosis in the normal heart

Acetyl-CoA, the common end product of glucose and FA oxidation, enters the tricarboxylic acid (TCA) or Krebs cycle to generate guanosine triphosphate, GTP (or ATP), CO_2, and reducing equivalents $NADH_2$.[75] Because Krebs cycle intermediates can be used for many biosynthetic pathways (e.g., amino and nucleic acids), they are constantly removed from the cycle and therefore need to be replaced. The replenishment of the Krebs cycle intermediate pool through pathways independent of acetyl-CoA is called anaplerosis.[77] The carboxylation of pyruvate to malate is an important anaplerotic reaction. This requires NADPH and therefore links anaplerosis to processes that generate (PPP) or consume (lipogenesis, antioxidative defence) NADPH.[78] Anaplerosis is a crucial process in the heart, where impairment rapidly causes contractile dysfunction.[79]

1.4.1.5 Metabolic flexibility in the normal heart

The heart is an omnivore, consuming fuel constantly and using any substrate available. Heart's substrate preference can rapidly change based on the availability of energy substrates supplied to the heart, hormonal status and the changing workload of the heart (**Figure 1.6**). The high rates of ATP production and turnover are critical in maintaining cardiac contractility to deliver blood and oxygen to the other organs. To adapt to substrate availability and energy demand, the heart is 'metabolically flexible' to switch between FA and glucose,[79] an important feature that is usually lost in the diseased heart, for example in the diabetic heart and in the failing

heart. Compared with glucose oxidation, FAO is more carbon-efficient; one mole of palmitate produces about 3-4 times more ATP than one mole of glucose does. On the other hand, glucose oxidation is more oxygen efficient compared with FAO, producing 10-12% more ATP per carbon used for the same amount of oxygen consumed. The balance between cellular energy metabolism and contractile performance is disrupted in cardiac disease.[74, 79]

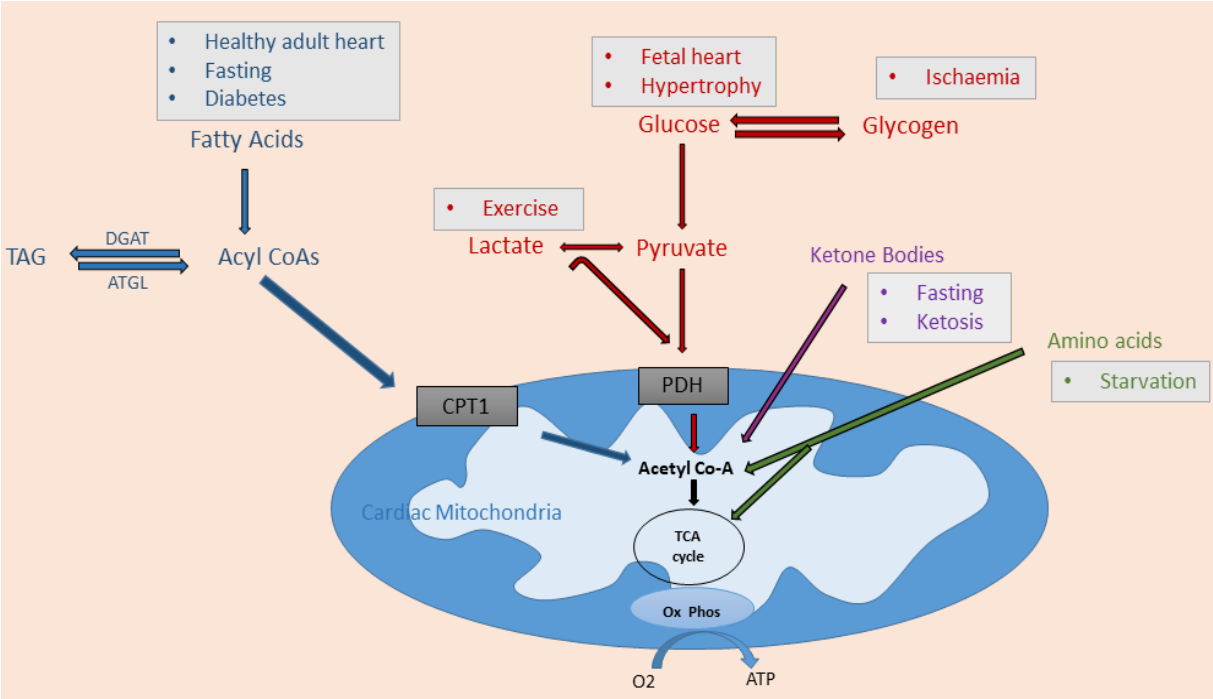


Figure 1.6: **Metabolic flexibility in the normal heart.** The energy-yielding substrates (fatty acids, glucose, ketones, and amino acids, lactate), via specific catabolic pathways, converge on acetyl-CoA production with subsequent entry into the tricarboxylic acid (TCA) cycle. The final step of energy transfer is accomplished through oxidative phosphorylation (OxPhos), supplying >95% of ATP consumed by the heart. The boxes above each metabolic pathway indicate the pathological and physiological condition in which the specific substrate becomes a predominant contributor to metabolism. {ATGL indicates adipose triglyceride lipase; DGAT, diacylglycerol acyltransferase; mCPT1, muscle form of carnitine-palmitoyl transferase-1; PDH, pyruvate dehydrogenase; TAG, triacylglycerol; and TCA, tricarboxylic acid}

1.4.2 Normal mitochondrial oxidative phosphorylation and ATP homeostasis

Mitochondrial oxidative phosphorylation normally contributes ≈95% of myocardial ATP requirements, with glycolysis providing the remaining 5%.[80, 81] The majority of the oxygen consumed by the heart is used for mitochondrial oxidative phosphorylation by the electron transport chain, while the synthesis of ATP derived from glycolysis does not require oxygen. Oxphos involves electron shuttling from cytosolic to mitochondrial reducing equivalents i.e. NADH and $FADH_2$ (primarily via the malate-aspartate shuttle), transfer of energy by electrons from reducing equivalents to O_2 [via electron transport chain (ETC) complexes], and generation of an electrochemical proton gradient within the mitochondrial intermembrane space (by complexes I, III, and IV), as illustrated in **Figure 1.5**. The release of this gradient is coupled to the synthesis of ATP from ADP + inorganic phosphate (Pi) by F0, F1-ATPase (complex V), contributing >95% of ATP synthesis under aerobic conditions. Because of this dependence on oxphos, rates of TCA cycle flux, cardiac work, and O_2 consumption are linearly correlated [82] and at high workloads approach 90% of mitochondrial oxidative capacity.[80] Besides a non-limiting O2 supply, Oxphos capacity in situ requires normal mitochondrial number (mass and biogenesis), dynamics, and unit activity (integrity).

ATP is required for cell viability and myocardial pump function. Cleavage of the terminal phosphate (a phosphoryl bond) by ATPases [ATP → ADP + (Pi)] releases chemical energy that is converted into the work of contraction, ion pumping, synthesis and degradation of large and small molecules, molecular trafficking, and indeed all functions of the cell. Because the amount of ATP in the heart is small (~10 mM, enough for only a few beats) compared with demand (as much as 10, 000 times greater), the myocardial cell must continually re-synthesize ATP to maintain normal cardiac pump function and cellular viability.

Consequently, the rates of ATP utilization and re-synthesis are very large. The concentration of ATP is maintained constant, despite large and variable changes in ATP demand.[83]

The efficiency of ATP production expressed as the ratio of ATP synthesis rate to O_2 consumed (P/O) differs slightly depending on the mix of substrates oxidized: the P/O is ~15% higher for oxidation of glucose only (a condition that occurs only in severe ischaemia) vs. fatty acids only. On a molar basis, however, much more ATP is produced from fatty acid oxidation than from glucose utilization.[81]

ATP re-synthesis by fatty acid oxidation in mitochondria is normally sufficient to meet the dynamic demands for chemical energy and is the primary pathway for ATP synthesis. Under conditions of high ATP demand relative to ATP availability, the myocyte recruits additional pathways for ATP synthesis, namely glycolysis and the phosphotransferase reactions catalysed by creatine kinase (CK) and adenylate kinase (AK). The different pathways for ATP supply have different rates of ATP synthesis: phosphoryl transfer via CK is ~10 times faster than ATP synthesis in mitochondria which is ~20 times faster than glycolysis.[81, 84] The relative contributions of these pathways to overall ATP synthesis changes rapidly in response to changes in fuel supply, hormonal and neural signals, availability of substrates and inhibitors of specific enzyme reactions, and by chemical modification of proteins. During acute increases in work in the normal myocardium, glycogen is used,[83] more glucose is influxed,[85] and phosphocreatine (PCr), the primary energy reserve compound in the heart) is used to support the demand for more ATP.[86] To maintain constant [ATP], the sum of the rates of ATP synthesis by the mitochondria, glycolysis and glycogenolysis, and the phosphotransferase reactions matches the sum of rates of ATP utilization by the sarcomere, ion pumps, etc. This flexible dynamic metabolic network is the normal state of the myocyte.

1.4.3 Normal Creatine Kinase Shuttle

Creatine plays a key role in cellular energy metabolism. The creatine kinase (CK) enzyme reversibly phosphorylates it to phosphocreatine (PCr), shown in **Figure 1.5.** Then, when phosphocreatine is reverted to creatine (Cr), its phosphate bond breaks, and such a break provides enough energy to allow phosphorylating a molecule of adenosine diphosphate (ADP) to adenosine triphosphate (ATP). Thus, PCr acts as an energy reserve to synthesize ATP rapidly, with no need for oxygen. The reaction is the following one:

$Cr + ATP \leftrightarrows PCr + ADP + H^+$

This reaction plays a crucial role in heart contraction.[87] Its roles have been extensively reviewed elsewhere [62] and summarised below:

Transfer of ATP from its production site (mitochondria) to its place of exploitation (neuronal membrane or cytoplasm) is often referred to "the ATP shuttle." To carry out this transport ("shuttle") of ATP energy, Cr first receives the phosphate from ATP near the mitochondria, becoming PCr. It then diffuses through its concentration gradient to the periphery of the cell. Near cytoplasmic ATPase, it donates its phosphate to ADP, effectively forming ATP far away from the mitochondria and delivering it precisely where and when it is required. In doing so, it reverts to Cr and diffuses back, again along its concentration gradient, to the mitochondrion to start the cycle again. The reason why the cell needs this complex mechanism to transport energy between mitochondria and cytoplasmic ATPase is that ATP is a very large molecule, therefore its diffusion through the organelle-filled cytoplasm is slow and cumbersome. By contrast, PCr is a much smaller molecule, thus it diffuses more quickly through the cytoplasm.

Restoration by PCr of ATP concentration in conditions of increased energy demand and in diseases involving a reduced supply of blood or oxygen.[88] In the first scenario, the

consumption of ATP is excessive compared to the ability of the cell to synthesize it. For instance, a muscle exposed to a particularly intense effort/exercise quickly uses more ATP than it can produce, thus exhausting its reserve. In the second scenario, an organ cannot produce enough ATP because of a blood deficiency (ischemia) or an oxygen deficiency (anoxia). For example, in case of a myocardial infarction, phosphocreatine intervenes by transferring its phosphoric group to ADP, to provide ATP at a time when the heart cannot synthesize it due to ischemia. Among all the biochemical reactions that our cells use to synthesize ATP, the one that starts from the Cr/PCr system is the quickest in buffering ATP levels at times of increased energy expenditure.[89]

There is extensive scientific evidence to suggest that failing pressure overloaded heart undergoes substantial metabolic reconfiguration including: substrate switch from FFA to glucose, FAO downregulation, increased reliance on glucose with reduced oxidative metabolism and enhanced glycolysis, impaired mitochondrial respiration[90] and decreased mitochondrial creatine kinase (CK) flux,[88] together with loss of metabolic flexibility to stress. These are partly driven by nuclear receptor and transcriptional co-regulator signalling circuits coordinating substrate selection, mitochondrial oxidative capacity, and energy homeostasis. These include peroxisome proliferator-activated receptor α (PPARα)[91] along with interacting regulators of oxidative metabolism retinoid X receptor α (RXRα), oestrogen-related receptor α (ERRα) and PPARγ coactivator-1α (PGC-1α).[92]

1.4.4 Role of PPARα signalling pathways in the normal heart

PPARs are nuclear hormone receptors and major executors of modulating glucose and lipid homeostasis. PPARα is abundant in tissues with high fatty acid oxidative capacity like heart and liver and participates in the regulation of fatty acid uptake and oxidation thereby maintaining energy homeostasis. In the liver, activation of PPARα induces the expression of

fatty acid transport (FAT) proteins and long-chain acyl-CoA synthetase, which is a prerequisite for FA metabolism.[93] Several key enzymes involved in peroxisomal β-oxidation such as acyl-CoA oxidase (ACO) are also direct targets of PPAR-α.[94] Peroxisomal β-oxidation does not directly provide energy but shortens very long-chain fatty acids, thus allowing their subsequent mitochondrial β-oxidation.[95]

In the heart, activation of PPARα increases the expression of genes involved in three major steps in the cellular fatty acid utilization pathway (**Figure 1.7**):

- Fatty acid transport and esterification (FATP, FAT/CD36, FABP, and ACS),[64,96]
- Fatty acid mitochondrial import (M-CPT I),[97] and
- Mitochondrial (MCAD, LCAD, VLCAD)[98, 99] and peroxisomal β-oxidation (ACO).[95,100]

The developmental expression pattern of the PPARα gene parallels that of FAO enzyme genes in heart.[101] Studies utilizing mice transgenic for human MCAD gene promoter fragments confirmed the importance of PPARα in the transcriptional control of cardiac MCAD expression in vivo. The PPARα response element, Direct repeat 1 (DR1), has been shown to be necessary for appropriate developmental and tissue-limited expression in the MCAD promoter transgenic mice, directing high-level expression in heart and brown adipose, tissues with high capacity FAO systems.[99] These results implicate PPARα as a key component of the gene regulatory program for FAO enzymes in heart.[64, 102]PPARα controls the expression of malonyl Co-A decarboxylase (MCD), which regulates the transport of long-chain fatty acid into mitochondria by governing the level of malonyl Co-A (inhibitor of CPT-1), and pyruvate dehydrogenase kinase (PDK), that phosphorylates and inactivates pyruvate dehydrogenase, thus, limiting the entry of pyruvate into mitochondria and its subsequent oxidation (**Figure 1.7 A and B and Figure 1.5**).[103, 104] PPARα activation also stimulates the expression of the mitochondrial form of HMG-CoA synthase, involved in ketone body synthesis.[105]

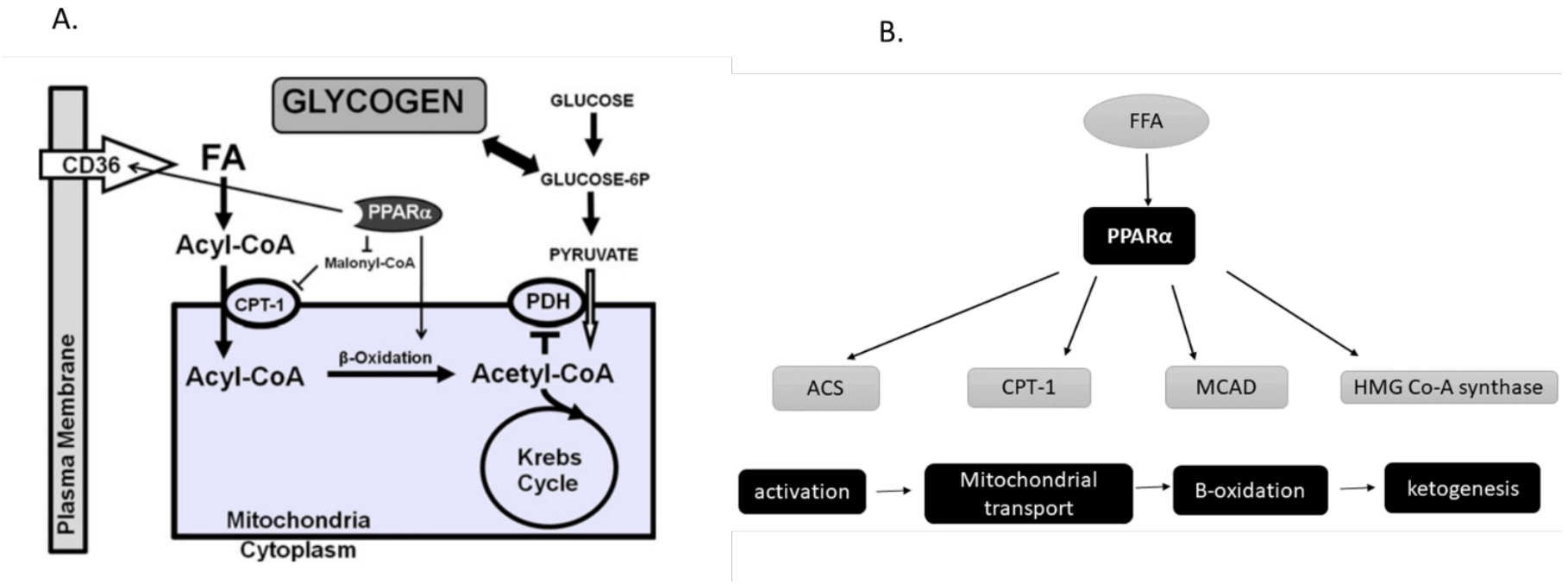


Figure 1.7 (A) and (B): Role of peroxisome proliferator-activated receptor (PPAR) α in normal cardiac fatty acid metabolism*. PPARα induces the expression of fatty acid transport proteins such as FAT/CD36 and acyl co-A synthetase (ACS)**, regulates basal and fatty acid–induced transcription of FAO enzyme gene including medium-chain acyl-CoA dehydrogenase (MCAD) and muscle carnitine palmitoyl transferase (CPT-1). Controls the expression of malonyl Co-A decarboxylase (MCD), and pyruvate dehydrogenase (PDH), which regulates the transport of long-chain fatty acid into mitochondria by governing the level of malonyl Co-A (inhibitor of CPT-1), PPARα activation favours fatty acid oxidation directly by inducing the expression of PDK that phosphorylates and inactivates pyruvate dehydrogenase, thus, limiting the entry of pyruvate into mitochondria and its subsequent oxidation and indirectly through the synthesis of ketone bodies by stimulating the expression of the mitochondrial form of hydroxymethylglutaryl (HMG)-CoA synthase and increased fatty acid oxidation capacity. [FA, fatty acid; CPT, carnitine palmitoyl transferase; PDH, pyruvate dehydrogenase.*

PPARα activation, thus, favours fatty acid oxidation either directly by inducing the expression of pyruvate dehydrogenase kinase or indirectly through the synthesis of ketone bodies and the increased fatty acid oxidation capacity, thus decreasing tissue content of lipids and minimizing lipotoxicity. PPARα also binds to target DNA elements as a heterodimeric partner with the RXR receptor and promotes transcription of genes involved in FA metabolism. PPARα target genes encode enzymes involved in cellular fatty acid oxidation including the peroxisomal, mitochondrial[100] and cytochrome P450 (CYP) pathways.[106] Therefore, transcriptional regulation by PPARα favours fatty acid over carbohydrate utilisation by establishing metabolic pathways for FAO in the heart as well as maintaining high fluxes of the FAO pathway while limiting fluxes through carbohydrate utilisation pathways.

PPARα primarily not only acts as a modulator of energy metabolism but also acts as anti-inflammatory agent.[107] There is growing evidence from animal studies that PPARα activators are involved in integrating inflammatory and hypertrophic pathways thereby governing the pathological outcome of hypertrophy associated fibrosis.[108, 109] Moreover, PPARα double knockout mice subjected to TAC showed much heightened fibrotic and inflammatory gene expressions along with severely aggravated hemodynamic function compared to wild type mice that has undergone TAC.[110] The development and characterization of mice with targeted disruption of the PPARα gene provided definitive evidence for the role of PPARα in the control of the entire cardiac lipid utilization pathway.[104] Although the PPARα −/− mice appear normal under basal conditions, the constitutive expression of proteins and enzymes involved in fatty acid transport (FATP, FAT/CD36, long-chain ACS, M-CPT I, CPT II) and oxidation (SCAD, MCAD, LCAD, VLCAD, short-chain 3-hydroxyacyl-CoA dehydrogenase, ACO) are all significantly lower in heart and liver compared to age-matched controls.[99] In

addition, the increased expression of LCAD, VLCAD, FATP, CD36/FAT, and heart-type FABP which normally occurs in heart or cultured cardiac myocytes upon exposure to PPARα ligands is absent in PPARα −/− mice. Coincident with the decreased expression of these lipid transporters and enzymes of β-oxidation, the myocardial uptake as well as subsequent oxidation of LCFA is markedly reduced in the PPARα −/− mice.[104]Thus, PPARα serves as a key transcriptional integrator for the basal and regulated expression of cardiac fatty acid utilization enzymes. Moreover, *PPARα*$^{-/-}$ mice accumulate myocardial lipid in the context of conditions known to increase FAO rates, such as fasting, indicating that PPARα plays a critical role in the maintenance of cardiac energy and lipid homeostasis by its regulatory influence on cellular fatty acid utilization pathways.[111]

In conclusion, PPARα plays a central role in FAO signalling system and maintaining lipid homeostasis. PPARα can recognize a broad array of ligands, sense wide changes in FA status and dietary inputs. PPARα not only plays a key role in the transcriptional control of substrate switching [112] but artificial ligands for PPARα, such as Fenofibrate, also protect against endothelin-induced cardiac hypertrophy and failure,[113, 114] and cardiac function is seen to be severely damaged in PPARα null mice during pressure overload.[115] In particular, as metabolism may vary from cell-to-cell and tissue-to-tissue, PPARα may act locally to integrate a variety of cell-specific metabolic parameters. The ability of these receptors to respond to distinct metabolic cues provides a potential mechanism to maintain a balance between FA breakdown and storage.[116]

1.5 Cardiac metabolism in hypertrophied heart

1.5.1 Substrate shift with FAO downregulation in pressure-overload

Hypertrophied hearts, such as in AS undergo a shift in substrate metabolism with a preference towards glucose utilisation, as glucose is a more efficient fuel compared to FAs.[117, 118] Long-chain fatty acid oxidation rates are lower in pathologically hypertrophied

hearts than in non-hypertrophied hearts.[117] FA utilisation requires greater oxygen per mole ATP production compared to carbohydrate. Accordingly, a shift in substrate utilisation in LVH to greater dependence upon glucose is anticipated to enhance myocardial efficiency through increasing energy production at lower oxygen cost. There have been multiple attempts to provide insight regarding the impact that substrate shifts have on pressure overload-induced remodelling, however, mixed results have been reported. More recently, it has been suggested that this substrate shift in pressure overload hypertrophy associated with reactivation of other foetal-like hallmarks (e.g., myosin heavy chain isoform switching) contributes towards the progression to overt contractile failure.[119] Studies in mice with either deficient muscle CPT1 to limit fatty acid oxidation[120] or ACC2[121] knockout to promote fatty acid oxidation, suggest that decrease in fatty acid oxidation in the hypertrophic heart is a maladaptive response.[122] Pal et al[123] in their study of patients with symptomatic severe AS discerned no significant impact of CPT-1 inhibitor, perhexiline on the primary symptomatic endpoint, LV systolic function or plasma BNP, whose levels predict outcome in AS. These findings contrast the salutary effect of perhexiline in symptomatic primary LVH caused by HCM,[124] suggesting that strategy to further enhance myocardial substrate switching in favour of carbohydrate utilisation may not be clinically beneficial in LVH associated with pressure overload. More recently, Ritterhoff et al have shown that metabolic switch from FAs to glucose is associated with an increase in anabolic metabolism, which provides glucose-derived aspartate for cellular hypertrophy. Although the hypertrophic growth provides short-term benefits, including reducing wall stress and sustaining cardiac function, it becomes maladaptive and predisposes ton heart failure long-term. Furthermore, preservation of FAO reduces anabolic substrate availability and prevents cardiomyocyte hypertrophy. It remains unclear, however, whether FAO directly regulates hypertrophic growth or whether

attenuation of hypertrophy is a consequence of improved myocardial energetics and function when FAO is preserved.[125]

1.5.2 Glucose metabolism in pressure overload hypertrophy

The pattern of energy substrate utilization that develops in pathological cardiac hypertrophy resembles that in foetal hearts with increased glucose consumption. However, this increase in glucose uptake and glycolysis can occur in the absence of any increase in glucose oxidation, resulting in an uncoupling of glycolysis from glucose oxidation.[122] Indeed, recent studies of failing animal hearts have shown that glucose oxidation rates can be significantly depressed in pathologically hypertrophied hearts than in non-hypertrophied hearts as there is increased reliance on glycolysis and a decrease in overall mitochondrial oxidative metabolism.[126, 127]

1.5.3 Anaplerosis (upregulation of pathways that replenish the pools of metabolic intermediates) and cardiac lipotoxicity

In hypertrophied rat hearts, an 80–90% increase in anaplerotic flux has been observed and is further supported with increased tissue content of malate.[78, 127] A significant increase in the gene expression of malic enzyme without a change in pyruvate carboxylase[78] supported the idea of increased anaplerosis through the pyruvate–malate pathway. Although the increased anaplerotic flux in hypertrophied myocardium is sufficient to maintain overall TCA cycle flux, it reduces the efficiency of ATP production from pyruvate. The hypertrophic heart works to maintain TCA flux by upregulating anaplerosis (**Figure 1.8**). In the hypertrophied heart, the elevated anaplerotic flux occurs via carboxylation of pyruvate through increased expression of the NADPH-dependent, cytosolic malic enzyme. The consequences of shifting single pyruvate molecule from oxidation to anaplerosis reduces ATP generation from 14 to 3 ATP. Anaplerotic entry into the second span of the TCA bypasses several of the NADH-

generating reactions.[128] In addition, the carboxylation of pyruvate to form malate via malic enzyme consumes and depletes NADPH. The reduction in NADPH may represent one of the mechanisms responsible for the reduced triacyl glyceride (TAG) content within the hypertrophic myocardium and hence, TAG oxidation to facilitate energy transduction is not operational.[129, 130] Diacylglycerol (DAG) as well as ceramide species are increased in the hypertrophied heart and have been associated with lipotoxicity, while redirecting these toxic lipid intermediates into the TAG pool prevents lipotoxicity.[131, 132]

Pound et al[78] in their study added further insight into the consequences of enhanced intermediary metabolism in the hypertrophied heart by confirming in isolated perfused rat hearts that pressure overload–induced cardiac hypertrophy results in diminished contractile function in association with a significant increase in malic enzyme linked anaplerosis compared to non-hypertrophied control hearts.

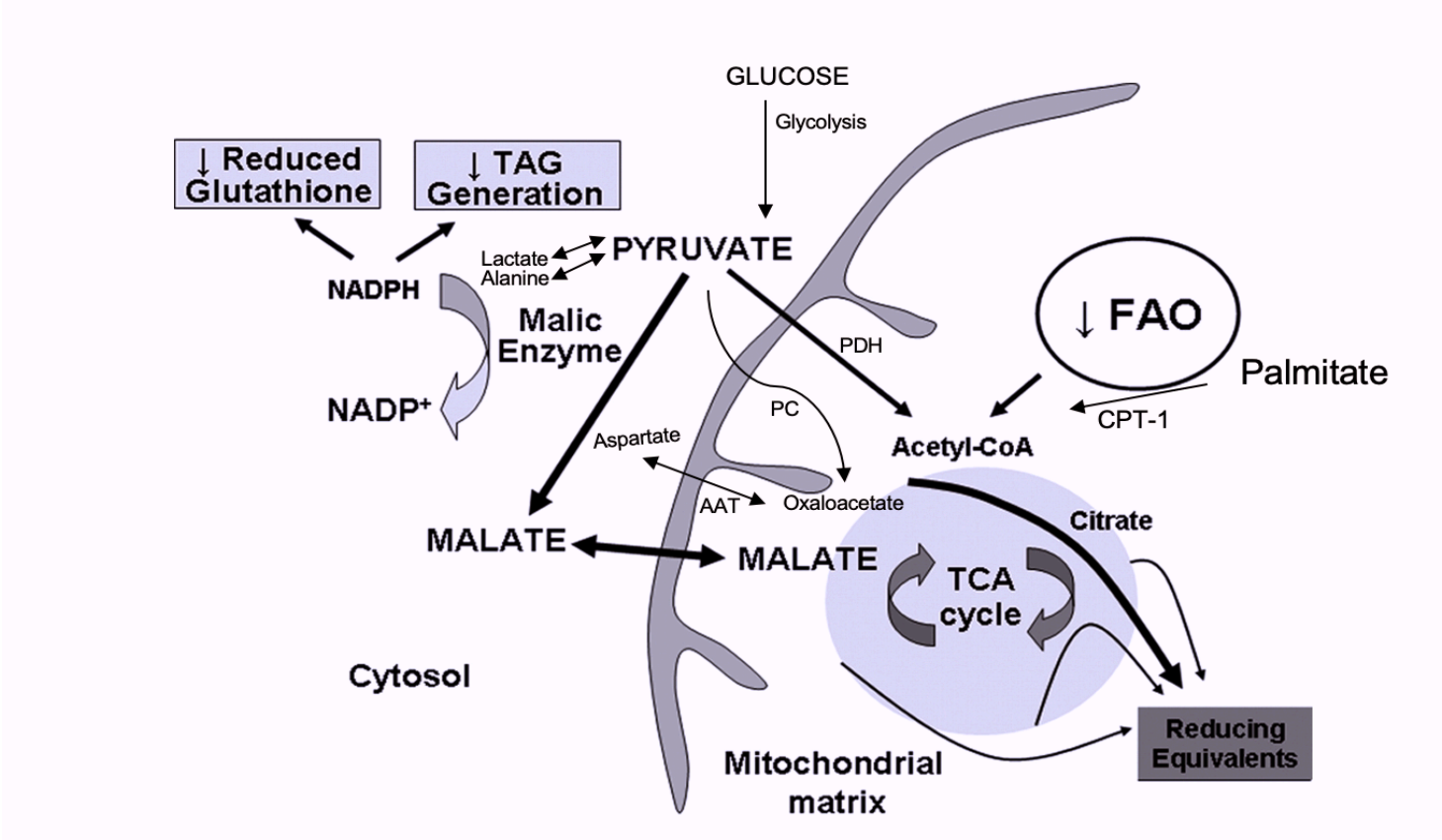


Figure 1.8: Anaplerosis depicting pyruvate entry into competing reactions. Oxidation via pyruvate dehydrogenase (PDH) vs anaplerotic carboxylation to malate via malic enzyme*. Bold arrows indicate the increased action of Malic enzyme in the hypertrophied heart. Acetyl-CoA is produced from long chain fatty acids via β-oxidation and from glycolytic pyruvate via PDH. Anaplerosis contributes malate and oxaloacetate in the second (5 carbon) span of the citric acid cycle and is fuelled by both the amino acids (aspartate) and pyruvate. Enzymes catalysing pyruvate entry into anaplerosis are pyruvate carboxylase (PC) and malic enzyme. Carboxylation of pyruvate, via malic enzyme, consumes NADPH necessary for TAG synthesis and glutathione reduction. Aspartate fuels anaplerosis through aspartate aminotransferase (AAT), producing oxaloacetate.*

1.5.4 Impaired myocardial energetics (PCr/ATP and CK flux)

Cardiac hypertrophy impairs the relationship between ATP demand and production. Myocardial energetic state that is reflected by the ratio of PCr/ATP is significantly decreased in hearts with LVH. The severity of this abnormality is linearly related to the severity of cardiac hypertrophy as well as LV dysfunction.[133] The PCr/ATP ratio, however, is only one indicator of the energetic state of the myocardium and is shown to be reduced in hypertrophied hearts [130]and in HF[134] but PCr/ATP ratio does not directly reflect the rate of ATP production through the CK reaction. ATP levels fall only when PCr levels are substantially depleted, because the CK system strongly favours ATP synthesis above PCr synthesis, this may be more important in the progression to HF in patients with LVH.[135] In the hypertrophied heart, there is initially a decline in PCr pool before any changes in ATP.[136] The decline in PCr is the result of a decrease in total creatine,[137]with the decline in total creatine directly related to the severity of hypertrophy.[138]As the heart moves closer to decompensation, both the PCr and ATP pools begin to decline.[139] LV hypertrophy alone is associated with a reduction in the PCr/ATP; however, there is not a further decline in the PCr/ATP in patients that have transitioned to chronic heart failure.[140] There is, however, a significant decline in CK flux between LV hypertrophy and chronic heart failure.[139] Therefore, at a similar PCr/ATP, the delivery of energy via CK can be dramatically different in pressure overload state.[141]

1.5.5 PPARα downregulation and consequent abnormal lipid homeostasis in pressure overload hypertrophy

Pressure overload-induced hypertrophy results in downregulation of PPARα and subsequent dysregulation of FAO enzyme gene expression, which sets the stage for abnormalities in cardiac lipid homeostasis and energy production.[64, 142](**Figure 1.9**).

Pre-clinical studies using isolated rat hearts subjected to pressure overload[143] showed that myocardial FA oxidation was depressed, whilst glucose uptake was increased. Previous MRS studies[144] of cardiac metabolism in rats after aortic constriction showed that in compensated hypertrophy FA oxidation was suppressed, there was increased reliance on glucose primarily via glycolysis whereas lactate and glucose oxidation were unaffected**.** There was increased pyruvate oxidation suggesting that mitochondrial function was not impaired, This increased flux of pyruvate is mainly through anaplerotic pathways which reduces its availability for oxidation by the PDH complex. As a result, pyruvate oxidation might not sufficiently compensate for the impaired FA oxidation, leading to energetic inefficiency of the Krebs cycle. Furthermore, increased flux through malic enzyme may also affect cardiac function by consuming NADPH which is required for triglyceride synthesis and for defending against oxidative stress.

Thus, reduction in FA oxidation is at the level of β-oxidation or more upstream (cellular uptake or activation of FA). The deficiency of carnitine palmitoyltransferase-1b (CPT1b), a mitochondrial β-oxidation rate-limiting enzyme that controls the uptake of long-chain acyl-CoA in the mitochondria, has shown to result in myocardial lipid accumulation, increased ceramide levels, and worsened pathological myocardial hypertrophy in the cardiac pressure overload model.[120] An alternative concept is that the decline in FA oxidation in the hypertrophic and failing myocardium is the direct consequence of a reduction in the expression of the FA-handling genes concerned, as depicted in **Figure 1.9**.[145]

However, a generalized description of the shift in energy providing metabolism as a simple reduction in fatty acid oxidation with increased carbohydrate use, neglects the balance of carbon flux in and out of the citric acid cycle, and neglects changes in the overall dynamics of lipid utilization/storage that produce physiological effects.[146, 147]

Eventually it appears to be a combination of reduced FAO, upregulation of anaplerosis and glycolysis, reduction in overall TAG volume and turnover rate that gives rise to myocardial lipid accumulation/steatosis.[148]This accumulation provides a source for non-oxidative metabolism of excess FAs to diacylglycerol and ceramide, potentially resulting in lipotoxicity, apoptosis and cardiac dysfunction.[149, 150]

Cardiac lipotoxicity and resulting increased oxidative stress can cause mitochondrial dysfunction and potentially decrease rates of ATP synthesis and may play an important role in the progression from compensated hypertrophy to overt heart failure.[151, 152]

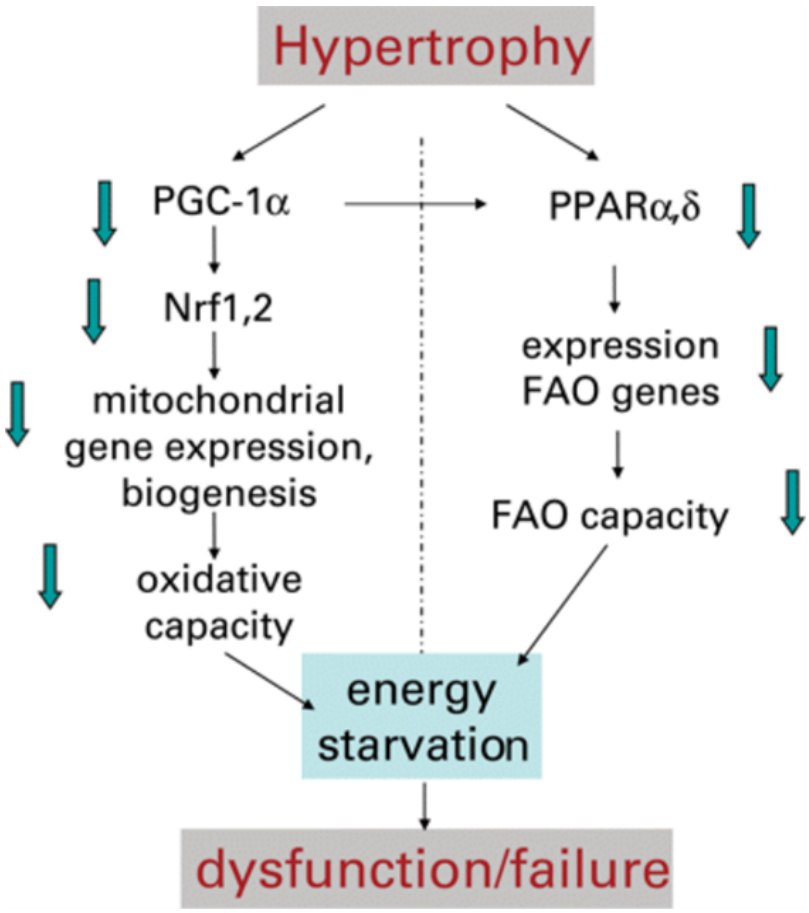


Figure 1.9: Potential role of genomic alterations as causative factors in the chain of events leading from compensated hypertrophy to cardiac failure*. Reductions in PPARϒ-coactivator-1α (PGC1α) and nuclear receptor factor [(Nrf1/2), left side] impair mitochondrial replication and the expression of genes constituting respiratory chain complexes. Concurrently, the expression/activity of PPARs (right side) is reduced leading to diminished expression of FA oxidation (FAO) genes.*

1.5.6 Oxidative stress and mitochondrial dysfunction in hypertrophy

The development and progression of cardiac hypertrophy is associated with changes in the expression of multiple structural, signalling, and metabolic genes.[153, 154] Metabolic changes upon cardiac hypertrophy include substrate oxidative preference and subsequent mitochondrial dysfunction.[155] There is no consistent pattern for how ETC capacity changes in non-failing pressure overload hypertrophy. For example, increased complex I & III activity has been reported in humans with AS and peak gradients of > 80 mmHg compared with control subjects. Conversely, several animal studies have reported unaltered or reduced state 3 rates or complex I/II activities in pressure overload. Uncoupling proteins (UCPs) in the inner mitochondrial membrane allow protons to flow across mitochondrial membrane, and by doing so, generate heat instead of producing ATP.[141] UCPs have been implicated in the pathogenesis of a variety of diseases with energy metabolism dysfunction.[156]

Elevated myocardial triglyceride levels have potential to stimulate apoptotic signal transduction pathways as well as increase mitochondrial uncoupling cardiac proteins (UCPs),[157] which, in turn, are associated with decreased mitochondrial respiratory coupling and low cardiac efficiency.[158] Mitochondrial UCP3 levels were increased in the hypertrophied failing hearts and correlated positively with plasma FFA concentrations.[159,160] Studies of mitochondrial UCP2 mRNA expression in the development of cardiac hypertrophy has yielded contradicting results.[159, 161] The discrepancies could apparently be attributed to differences in subject species and the causes of cardiac hypertrophy.

1.5.7 Myocardial steatosis and LV dysfunction in hypertrophy

Although in humans there is no direct evidence yet whether this is cause or effect, preclinical studies have demonstrated a causal link between steatosis and LV dysfunction. Chiu et al

generated transgenic mice that overexpressed long-chain acyl-CoA synthetase in the heart and showed that mismatch between myocardial FA uptake and utilisation leads to cardiac lipotoxicity. Haematoxylin & Eosin staining revealed vacuolated myocytes, consistent with intracellular accumulation of lipid. There was evidence of DNA fragmentation and increased cardiac ceramide content consistent with stimulation of apoptotic pathways. These were observed after lipid accumulation and before development of significant LV dysfunction, suggesting that lipid-induced programmed cell death contributes to the development of cardiomyopathy.[148] Similarly, Zhou et al showed a causal relationship between abnormal FA metabolism and reduced myocardial contractility in obese Zucker Diabetic Fatty (ZDF) rats. Myocardial TAG was higher in ZDF rats due to under expression of FA oxidative enzymes and PPARα. Ceramide levels were increased compared to controls causing cell apoptosis and lipotoxic cardiomyopathy. A causal relationship was further supported by the fact that antisteatotic agent, Troglitazone, which reduced cardiac triacylglycerol, prevented both cardiac apoptosis and loss of myocardial function.[162]

There is now ever increasing evidence implicating altered myocardial substrate utilisation and consequent steatosis in hypertrophy and heart failure in humans.[110, 131, 151] Mahmod et al have shown that steatosis is present in both symptomatic and asymptomatic severe AS and that it independently correlates with impaired myocardial deformation (strain), a measure of early LV contractile dysfunction.[163] Furthermore, in symptomatic severe AS, positive oil red O staining of lipid deposition (a marker of steatosis) in myocardial biopsies was associated with systolic strain abnormalities. This is supported by a previous study by Marfella et al demonstrating a significant association between myocardial lipid staining and LV dysfunction in AS patients with the metabolic syndrome.[152]

In summary, decreased FAO clearly contributes to the reappearance of the foetal metabolic pattern in hypertrophied and failing hearts that leads to increased reliance on glycolysis

combined with upregulation of anaplerosis to maintain TCA flux and slightly improves myocardial oxygen efficiency, but this metabolic profile is inefficient in utilizing carbon substrates for ATP production during increased energy demand, leading to impaired myocardial energetics and depletion of contractile reserve.[164] With advancing cardiac hypertrophy, perturbations in substrate partitioning and selection become associated with cardiac lipotoxicity and reduced contractile reserve. Despite the recruitment of alternative intermediary pathways to enhance flux through the TCA cycle, cardiac efficiency is incompletely restored with a persistent deficit in the PCr/ATP ratio. PPARα not only serves a critical role in normal cardiac metabolic homeostasis, but also alterations in PPARα signalling likely contribute to the pathogenesis of pressure-overload hypertrophy in AS.[64, 110] Fibrate drugs such as fenofibrate, PPARα activator, have been shown in various animal and clinical studies to inhibit LVH [165]and phenotypic changes in cardiac gene expressions[166] well as to reduce excessive myocardial lipid accumulation.[167] Myocardial lipid accumulation (steatosis) can be directly cardiotoxic and cause unfavourable LV remodelling.[131]

In the studies to date, these metabolic changes have only been studied in mainly animal models and not in real world insulin resistant chronic moderate-severe AS population. However, it is yet unclear how early these metabolic changes occur in the disease process and what role, if any, do they play in decompensation and progression to heart failure. I set to study this precisely in my research and findings are detailed in Chapter 3. Furthermore, considering the critical role of PPARα in lipid homeostasis as detailed above, I sought to determine in this research if PPARα agonists are able to modify cardiac metabolism favourably in AS, detailed later in Chapter 5.

1.6 Role of Magnetic resonance spectroscopy (MRS) in AS

Magnetic resonance spectroscopy (MRS) is the only non-invasive, non-radiation exposure technique for the investigation of cardiac metabolism in vivo.[168] The basic principle enabling

MRS is that the distribution of electrons within an atom cause nucleus in different chemical environments, to experience slightly different magnetic fields. This results in different resonant frequencies, which in turn cause signals from these nuclei to appear as separate peaks in the MR spectrum.[169] MRS uses magnetic resonance signals from nuclei, such as ^{31}phosphorus, ^{1}hydrogen, ^{13}carbon and ^{23}sodium to provide comprehensive metabolic and biochemical information about cardiac muscle. This method is highly versatile and can provide metabolic insights into the role of cardiac metabolism in a wide number of conditions, including hypertensive, valvular, and ischemic heart disease, heart failure, as well as cardiomyopathies. This method can also be used to monitor patient responses to therapeutic interventions: pharmacologic,[170] surgical, or interventional.[171] When combined with cardiovascular magnetic resonance imaging, MRS enables detailed pathophysiologic insights into the inter-relations among cardiac structure, function, and metabolism. However, MRS is currently used primarily as a research tool because of low spatial resolution and reproducibility.

Cardiac MRS uses mostly the same hardware as conventional CMR for patients, typically a 1.5- or 3.0-T magnet (ultra-field [7- to 18-T] for experimental studies), with additional hardware including nucleus-specific coils (e.g., ^{31}P-coil) and a broadband radiofrequency transmitter to excite non-proton nuclei. Specific MRS acquisition sequences, MRS post-processing, and data analysis packages are also required.

In this research, I used advanced MRS techniques, particularly proton (^{1}H-) and phosphorus (^{31}P-) MRS to understand the metabolic intricacies in AS. Below, I introduce the available MRS techniques and their role in cardiac disease.

1.6.1 ^{1}H-MRS for assessing lipid metabolism

^{1}H-MRS is a method capable of detecting and quantifying specific cardiac biomolecules, such as lipids and creatine in normal and diseased hearts in both animal models and humans.[172, 173] In vivo, ^{1}H-MRS is mainly used to provide a window into cardiac metabolism at two different levels. Firstly, lipid (triglyceride) content of the heart is highly dynamic and myocardial lipid overload has been implicated in the pathophysiology of cardiac disease. Thus, measuring lipids will help to better understand their role in the healthy and diseased heart. Secondly, the measurement of total creatine, a crucial actor in the CK system, gives an insight into high-energy phosphate transport and storage but still requires more sophisticated techniques to allow accurate measurement.[174]

Two single-voxel single-shot localization techniques commonly used for ^{1}H-MRS are PRESS (Point Resolved Spectroscopy) and STEAM (Stimulated Echo Acquisition Mode).[175] As the concentration of cardiac proton metabolites is less than 2% of the water concentration, it is necessary to apply water suppression prior to the PRESS or STEAM acquisition using the CHESS (chemical shift selective) sequence. For the purpose of metabolite quantification, the maintenance of steady-state magnetization is important. More details of the method are explained in Chapter 2.

1.6.2 ^{31}P-MRS for assessing high-energy phosphate metabolism

^{31}P-MRS allows the *in vivo* quantification of phosphorus (^{31}P)-containing metabolites involved in energy metabolism, such as phosphocreatine (PCr) and adenosine triphosphate (ATP). Using ^{31}P MRS, various indices of the CK system have been measured to assess mitochondrial energetics, including the PCr/ATP ratio and forward creatine kinase (CK) flux.[176] Cardiac ^{31}P-MRS in humans is typically performed at higher magnetic field strengths of 1.5–3 T and takes 10-30 minutes to acquire. Studies have shown that PCr/ATP is a better

predictor of long-term survival than NYHA functional class or LV EF in several cardiac conditions: dilated cardiomyopathy,[177] hypertrophic cardiomyopathy,[178] HF with preserved ejection fraction,[179] and ischemic heart disease.[180] CK reaction rate and flux can also be probed by ^{31}P-MRS, which provides a more accurate assessment of cardiac energetic state than PCr/ATP alone. Multiple studies have previously demonstrated that both PCr/ATP ratio and CK flux are reduced in symptomatic AS patients,[139, 181] being lowest in those with associated systolic failure,[164] and correlates with LV end-diastolic pressures and end-diastolic wall stress in line with previous histological animal and human studies.[182,183] Some have also shown that impaired energetics in AS are reversible following relief of pressure overload and hypertrophy regression.[184, 185] Further details on ^{31}P-MRS method used in this research are discussed in Chapter 2.

1.6.3 Other MRS techniques

1.6.3.1 *Hyperpolarised ^{13}C MRS*

Hyperpolarized ^{13}C spectroscopy has enabled the assessment of pyruvate metabolism in vivo in humans.[186] The technique potentially provides a window on several important metabolic processes that are essential to cardiac function and vary during differing disease processes, including diabetes,[187] dilated cardiomyopathy,[127] ischemic heart disease,[186] cardiac hypertrophy, and HF.[188]

The metabolism of the injected [1-^{13}C] pyruvate provides information on key metabolic reactions (i.e., lactate dehydrogenase, PDH, and alanine transaminase).[189] Other molecules have also been successfully studied, including [2-^{13}C] pyruvate[190] for investigation of metabolism through the TCA cycle, [1,4-$^{13}C_2$] fumarate[191] or assessment of cellular necrosis, and ^{13}C-bicarbonate,[192] for in vivo assessment of extracellular pH.

In the pressure-overloaded myocardium, there is proposed to be an increase in glycolysis despite a normal level of flux through PDH, leading to increased incorporation of glycolytically derived pyruvate into lactate.[193] Histologic studies in hypertrophied rat hearts have demonstrated that this mismatch between glycolysis and glucose oxidation is the consequence of increased pyruvate carboxylation and lower flux through PDH, resulting in the increased lactate production.[194] Use of hyperpolarized ^{13}C imaging in the pressure-overloaded state in vivo could remarkably improve our understanding of the metabolic alterations and their effect on cardiac function.

The clinical use of hyperpolarized ^{13}C imaging is in its infancy, with only selected centres having the capability to run cardiac scans in humans.

1.6.3.2 Deuterium (^{2}H-) MRS

An alternative metabolic imaging technique to study TCA cycle metabolites is deuterium MRS (DMRS). This has recently been used in combination with an infusion of deuterium-labelled glucose or acetate by Wang et al [195] in rat hearts to determine the rates in vivo of glucose metabolism and the TCA cycle, which dominates mitochondrial ATP production in supporting cardiac function. Though not yet tested in humans, DMRS could be valuable for investigating the metabolic shift from preferred FAO to glucose oxidation under stress and diseased conditions.[196] To develop the DMRS technique for clinical translation, further research is needed to understand the relationship between imaging measures and cardiac pathophysiology in human patients.

Table 1.2 gives an overview of available MRS techniques and their potential application.

Table 1.2: Overview of available MRS techniques and their potential application.

MRS nuclei/technique	Main use	Strengths and limitations	Potential solution	Clinical translation
^{1}H-MRS	• Can detect and quantify cardiac lipids, creatine and choline	• High sensitivity and abundance • Low spatial resolution	• Use of advanced surface coils and higher field strengths.	• Already used in clinical brain and cancer imaging. • Could be adopted for use in clinical cardiac imaging in specialised centres
^{31}P-MRS	• Can detect metabolites involved in high-energy phosphate metabolism in the heart. • Indirectly deduce intracellular pH	• High sensitivity and 100% natural abundance • High quality spectra obtainable even at low field strengths	• Use of advanced surface coils and higher field strengths.	• Could be adopted for use in clinical cardiac imaging in specialised centres
^{13}C-MRS	• Can detect and quantify pyruvate metabolism metabolites	• Low sensitivity and abundance (1%)	• Use of hyperpolarized MRS technique increases signal • Higher field strengths	• Already used in prostate cancer imaging
^{2}H-MRS	• Can detect Tricarboxylic acid (TCA) cycle metabolites	• Low sensitivity and abundance (1%) • Currently only performed at ultra high field strength and in experimental animal models	• Still in developmental stage, not yet used in humans	• Not ready for clinical use
^{23}Na-MRS	• Can detect tissue viability	• Very low sensitivity and concentration • Long acquisition times	• Advanced sequences and coils to improve detection • Higher field strengths	• Not ready for clinical use

1.7 Exercise capacity assessments

1.7.1 Cardiopulmonary Exercise Test (CPET)

Cardiopulmonary exercise testing (CPET) provides assessment of the integrative exercise responses involving the pulmonary, cardiovascular and skeletal muscle systems, which are not adequately reflected through the measurement of individual organ system function. CPET is being used increasingly in a wide spectrum of clinical applications for evaluation of undiagnosed exercise intolerance and for objective determination of functional capacity and impairment. It delivers breath-by-breath gas exchange measures of 3 variables: O2 uptake (VO_2), carbon dioxide output (VCO2), and minute ventilation (VE). These 3 measures are used to derive various other gas exchange patterns that reflect organ-specific maladaptive responses to exercise, particularly when CPET is coupled with standard exercise variables (HR, blood pressure, electrocardiogram), and other hemodynamic measurements during exercise.

CPET evaluation involves an assessment of whether there was maximum volitional effort, as indicated by RER >1.0 to 1.1. Heart rate >85% of predicted also signals maximum effort but is often not achieved in patients with beta blockers/or with chronotropic incompetence. Peak VO_2 remains the gold standard metric of fitness and is the focal point of CPET interpretation if maximum effort was achieved. Peak VO_2 is known to be an important predictor of prognosis in HF patients with a peak VO_2 ≤14 ml/kg/min associated with poor prognosis.[197] For patients who do not achieve maximum effort, O2 uptake variables that are independent of volitional effort are useful i.e., oxygen uptake efficiency (OUES) <1.4 and VO_2 at ventilatory threshold (VT) <9 ml/kg/min indicating a poor prognosis in HF cohort. There are no studies yet assessing the prognostic cut-off of CPET parameters in AS and hence data from HF studies is generally used as a reference guide on overall performance.

A significant proportion of patients with apparently asymptomatic moderate-severe AS exhibit exercise limitation as measured by peak VO_2. CPET therefore has potential as a useful tool for serial monitoring. It can provide valuable information on haemodynamic and physiological components that determine decreased peak VO_2. It is useful to identify 1) patients with a low risk of cardiac death and low risk of progression to symptoms from the AS, and 2) patients with hemodynamic compromise who may improve in functional capacity after therapeutic intervention.

1.7.2 Six-minute walk test (6MWT)

The 6MWT is a physical performance test that evaluates the global and integrated responses of systems involved during physical activity, including cardiopulmonary function, systemic circulation, neuromuscular units, and metabolism.[198] The 6MWT is widely used to stratify risk and guide treatment in patients with congestive heart failure.[199] In asymptomatic patients with aortic valve stenosis, the 6MWT has been shown to be an independent predictor of all-cause and cardiovascular mortality.[200] It is an excellent tool for the measurement of functional status of a patient and is of incremental value to clinical and imaging evaluation. 6MWT can be a useful guide for monitoring disease progression and clinical follow-up intervals in patients with AS.

Participants performed the 6MWT by walking at their own pace back and forth along a 30-metre length corridor around a set of cones spaced 10 metres apart for 6 minutes. The standard validated protocol was followed which is established for use in clinical and research practice. Total distance covered was recorded along with Borg scores for dyspnoea and fatigue.

The findings from the exercise assessment of the study patients and the effect of PPARα agonist on exercise capacity in AS is discussed in detail in Chapter 4 and 6.

1.8 Summary of Research rationale

Lipid metabolism seems to underpin both the metabolic and the hypertrophic mechanisms seen in the pressure-overload state, this may be a common pathway to target as a therapy. MRS, with its recent improvements in technique and advanced processing systems, will prove to be of clinical value in establishing the link between abnormal metabolism and progression from compensated hypertrophy to HF. It could potentially identify metabolic biomarkers to monitor progression of the disease and help in risk stratification in AS. In this way, it not only will be helpful in guiding decision making for valve replacement in addition to currently available imaging tools, but also could help in exploring avenues for precision metabolic therapy.

Thus, a therapeutic approach that alters myocardial substrate selection may target both the cardiac metabolic and the structural effects of pressure overload and is likely to be effective in treating cardiac dysfunction in AS and other pressure-overload disorders. PPAR agonists are one such group of drugs, especially PPAR-α, which play a central role in the FAO signalling system as well as control lipid homeostasis.[64] The ability of PPARα receptors to respond to distinct metabolic cues provides a potential mechanism to maintain a balance between FA breakdown and storage, and their down-regulation in the pressure-overload

hypertrophy state has been shown to have deleterious effects.[116] Fibrates (PPAR-α agonists) are one such group of drugs that hold promise with their ability to up-regulate FAO in cardiac myocytes and reduce lipotoxicity in pressure-overload hypertrophy. Another group that may hold potential are PPAR-γ agonists, Thiazolidinediones, help in adipogenesis and redirect excess free FAs to adipose cells preventing lipotoxicity. In the heart, they also oppose inflammatory pathways and function as a growth suppressor.

The successful translation of therapies targeting cardiac substrate alterations in AS will require a deeper understanding of the interplay between cardiac substrate metabolism, lipid deposition, energy generation, and cardiac function, especially in those with asymptomatic moderate to severe AS and preserved ejection fraction.

1.9 Aims of this Research

- To study the timing of the metabolic changes in AS, mainly myocardial steatosis and energetic deficit and their relationship with structural changes and subclinical LV dysfunction.
- To assess whether upregulating fatty acid metabolism in AS using PPARα agonist, Fenofibrate would alter myocardial lipid accumulation and have any effect on cardiac physiology and exercise capacity.

To achieve this, the research was divided into two sub-studies and involved multi-parametric cardiac magnetic resonance imaging (explained in detail in Chapter 2)

1.9.1 Correlational study (detailed in chapter 3 and 4)

The aim of this study is to study the timing and severity of structural and metabolic changes across the spectrum of AS using advanced cardiac magnetic resonance imaging techniques and biochemical analysis.

I further evaluated if cardiac metabolism in AS could be modulated using a PPAR α agonist, Fenofibrate. The second part of the research sought to determine this.

1.9.2 Randomised double-blind placebo-controlled study/Ox-FAST – Oxford: Fibrates in Aortic Stenosis (detailed in chapter 5 and 6)

The main objective of this study is to assess the effects of a fibrate drug, fenofibrate (a PPARα agonist, a key regulator of lipid metabolism) on myocardial triglyceride content (MTG) and cardiac physiology and exercise capacity in patients with asymptomatic moderate-severe AS.

2 Chapter Two

Methods

2.1 General methods

The study received approval from a Research Ethics Committee (South London, 18/LO/1981). Research was conducted in accordance with institutional procedures and Declaration of Helsinki. Participants were prospectively recruited from clinical activity across three sites: Oxford University hospital NHS trust, Oxford, Great Western hospital NHS trust, Swindon, and Royal Berkshire hospital, Reading. Each participant gave written informed consent to be involved.

Healthy volunteers were recruited from another study with similar protocol and ethics approved by research ethics committee (South Central Oxford C, 15/SC/0004).

The project was funded through British Heart Foundation Clinical Research Training Fellowship (FS/18/17/33514).

2.2 Eligibility Criteria

2.2.1 Inclusion criteria

- Willing and able to give informed consent for participation in the study.
- Male or Female, aged 18 years or above
- Not planned for aortic valve intervention (AVR or TAVI)
- No other significant valvular condition including AR.
- No contraindication to magnetic resonance imaging
- Able (in the investigator's opinion) and willing to comply with all study requirements

2.2.1.1 Correlational study group

- Asymptomatic with diagnosed mild, moderate or severe AS per their clinical echocardiogram findings, but no other valvular condition.

2.2.1.2 Ox-FAST group

- Asymptomatic with diagnosed moderate to severe AS (at least two of the following: aortic valve area <1.5 cm2, peak pressure gradient >36 mmHg or mean pressure gradient >25 mmHg)
- Participant on stable doses of current regular medications for at least 6 weeks prior to entry to the study
- Female participants of childbearing potential ensure effective use of contraception by themselves or their partner during the study and six months thereafter.

2.2.1.3 Healthy volunteers' group : same as section 2.2.1

2.2.2 Exclusion criteria

- Known coronary artery disease, history of angina, myocardial infarction or presence of regional wall motion abnormalities
- Presence of other underlying cardiomyopathy
- LVEF<50%
- Presence of uncontrolled hypertension (BP >160/100 despite medical therapy)
- Presence of type 1 or type 2 diabetes mellitus (known diagnosis of diabetes or fasting blood glucose >7mmol/L)
- Presence of liver impairment (known diagnosis of liver disease or abnormal liver function tests)
- Female participant who is pregnant, lactating or planning pregnancy during the study

- BMI >40 kg/m^2
- Significantly impaired renal function (eGFR<30ml/min)
- Intolerance to or concurrent use of fibrates or PPARα agonists.
- Contraindications to MRI (implantable devices or other metal implants, internal cardioverter-defibrillator, cranial aneurysm clips, metallic ocular foreign bodies, hypersensitivity to gadolinium)
- Inability to tolerate MRI scanning (claustrophobia, inability to lie flat)
- Any other significant disease or disorder which, in the opinion of the investigator, may either put the participant at risk because of participation in the study, or may influence the result of the study, or the participant's ability to participate.

2.3 Study assessments

Both correlational and Ox-FAST study participants underwent screening and baseline assessment as detailed below.

2.3.1 Visit 1 - Screening and Baseline assessments

This included the following:

1. *Eligibility check and informed consent*
2. *History*
3. *Physical Examination (5 mins)*

Anthropometric measurements including height, weight, BMI and waist to hip ratio will be established. Blood pressure and heart rate were recorded. Blood Pressure was recorded as average of 3 supine measures taken over 10 minutes (DINAMAP-1846-SX, Critikon Corp).

4. *Resting 12 lead ECG*
5. *Venous Cannulation and blood collection (15-20 minutes)*

Prior to undergoing CMR scanning, each participant was cannulated to prepare the participant for the administration of contrast agent gadolinium, and at the same time baseline blood samples (25mls) including full blood count, renal function profile (Sodium, potassium, urea, creatinine), liver function tests (Albumin, ALP, ALT, bilirubin), Total cholesterol, HDL cholesterol, calculated LDL cholesterol, Triglycerides, Free fatty acids, NT-pro BNP were taken. istat creatinine was checked to ensure eGFR> 30ml/min prior to administration of the contrast agent.
Patients were instructed to fast at least six hours before the scheduled visit as fasting blood samples will be required.

6. *Cardiac Magnetic Resonance (60-75 mins) including Magnetic Resonance Spectroscopy (MRS) at* 3Tesla MR scanner.

All participants underwent CMR scan and participants were asked for their consent to have their de-identified images stored at the time of initial consent. Participants lay in a supine position and a dedicated CE marked cardiac coil was placed around their chest. Images were obtained using breath hold and ECG gating.

7. *6 minute walk test*

Participants were asked to perform a 6 minute walk test (6MWT) by walking at their own pace back and forth along a 30 metre length for 6 minutes. The standard validated protocol was followed which is established for use in clinical and research practice. Total distance covered was recorded along with Borg scores for dyspnoea and fatigue.

8. Cardiopulmonary Exercise Testing

Cardiopulmonary exercise testing (CPET) was undertaken using an upright bicycle ergometer protocol with simultaneous respiratory gas analysis as previously described.[203] An incremental ramp protocol was utilised whereby workload will be

gradually increased with continual heart rate, blood pressure and ECG recording. Subjects were exercised to volitional fatigue with a corresponding adequate respiratory exchange ratio (RER) achieved as a requirement for satisfactory effort defined as RER of >1.1. Peak oxygen consumption (peak VO_2) was determined by averaging VO_2 measures over 30 seconds of peak exercise. The exercise protocol is a validated incremental protocol with established use in clinical and research practice.

Participants who were eligible were then enrolled into the Ox-FAST sub-study and randomised to either receive fenofibrate or placebo for 6 months after the baseline assessments.

Ox-FAST participants further underwent follow-up assessments at 3- and 6-months intervals as detailed in visit 2 and 3 below.

2.3.2 Visit 2 - Safety and compliance assessment (3 months ± 7 days)

This included the following:

1. *Evaluate the participant's safety by history taking*
2. *Check medication packaging and compliance*
3. *Dispense study medication for the remaining three-month study period*

2.3.3 Visit 3 – End of treatment assessments (6 months ± 7 days)

Same assessments as baseline visit 1 will be undertaken:

1. *History and physical examination*
2. *Resting ECG*
3. *Venous cannulation and blood collection*
4. *CMR and MRS at 3.0T*
5. *6 minute walk test*
6. *Cardiopulmonary exercise testing (CPET)*

2.3.4 Visit 4 – Study completion (1 month after end of treatment)

Visit 4 marked the completion of the study for the individual participant. This follow up was executed via telephone call/email.

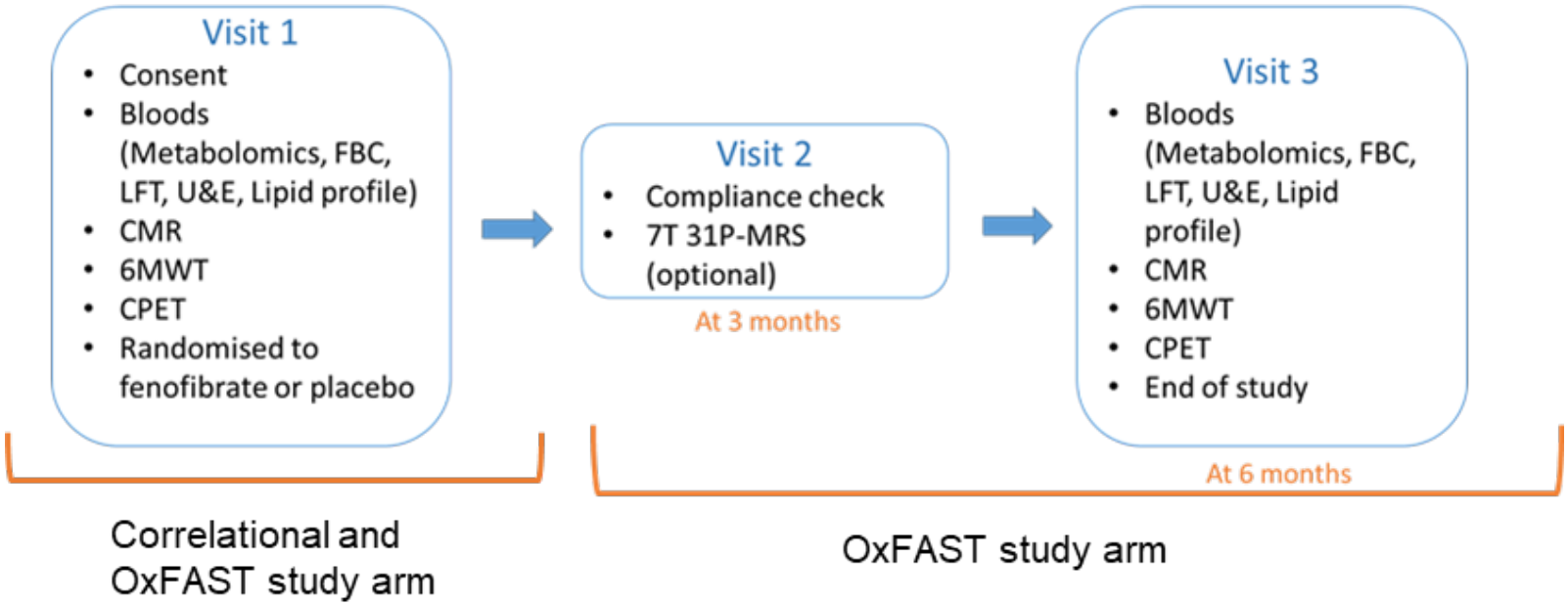


Figure 2.1: Flowchart of study visits

Healthy volunteers only underwent CMR imaging without gadolinium contrast agent administration.

2.3.5 COVID-19 modification to the study schedule

In light of the COVID-19 pandemic and subsequent lockdowns from March 2020, visit schedule was changed to keep face to face patient contact to minimum. A decision was made to conduct visit 2 (3-month follow-up) via telephone/email and only arrange face to face follow-up where needed. Amendment to the protocol was submitted and approved by the REC committee in November 2020.

2.4 Clinical assessment

History included assessment of inclusion and exclusion criteria as explained above in section 2.2 and drug history including allergies.

2.4.1 Anthropometry

Height and weight were recorded, and BMI calculated. BMI ≥40 kg/m^2 were excluded from the study.

2.4.2 Blood Pressure

Blood pressure was recorded after history taking as an average of 3 supine measures taken over 10 minutes (DINAMAP-1846-SX, Critikon Corp).

2.4.3 ECG

A 12-lead ECG was recorded and analysed by a physician. Most patients had high voltage criteria in keeping with LVH on the ECG.

2.4.4 Bloods

Fasting venous blood was drawn for glucose, lipid profile, free fatty acids (FFA), liver and renal function and NT-proBNP. Bloods were also drawn for metabolomics assessment which is explained in the next section below.

2.4.4.1 Metabolomics

Metabolomics is the study of complete profile of small-molecule metabolites providing metabolic overview. PPARα downregulation and substrate shift in AS, unlike other pathological states such as in diabetes, is maladaptive and interpretation of the metabolome ideally paired with measurement of energy flux rates can help elucidate and identify whether manipulation of metabolism can improve or rescue the HF phenotype in AS.

For this study, I collected blood samples from all AS participants including mild, moderate and severe disease to understand the timing of changes in cardiac metabolism across the spectrum of the disease. For OxFAST study participants, samples were collected both at baseline and 6 months to study the effect of PPARα agonist on fatty acid metabolism in the heart. These results would help in evaluating the rates of FAO and correlate with the results from CMR and blood tests in the study.

Samples are, however, awaiting to be analysed by Prof Jules Griffin and his team in Aberdeen. Unfortunately, due to the impact of COVID-19 pandemic and subsequent lockdowns, there have been delays with collaborator's lab set up and availability, hence these results were not available at the time of submission of this thesis.

2.5 Six-minute walk test

The test was undertaken as part of the study to define the baseline functional status of participants with asymptomatic moderate-severe AS. I further wanted to explore the relationship between cardiac metabolic state and exercise capacity in AS well as effect of altering the cardiac metabolism with PPARα agonist on functional status.

2.6 Cardiopulmonary exercise testing (CPET)

In this research, the main objective of performing CPET was to characterize the physiological effects of Fenofibrate in AS. In addition, I also sought to study the relationship between LV

metabolic, structural and functional parameters and CPET parameters across the spectrum of AS.

2.6.1 CPET protocol

Symptom-limited CPET was performed on an upright cycle ergometer in all cases (**Figure 2.2**). The workload protocol was chosen so that maximal effort was achieved within 10-20 minutes. Exercise workload was increased by a ramp protocol (10 W/min) after a 2-minute warm-up at 0 W. Patients were encouraged to exercise to exhaustion. A 12-lead electrocardiogram was continuously monitored during exercise and for at least 3 minutes during the post-test recovery phase. Blood pressure, oxygen saturation, modified Borg scale score and capillary blood lactate were measured at rest and every 3-4 minutes during exercise. Patients were allowed to take their usual medication on the day of the CPET. Ventilatory expired gas was analysed with a Metasoft CPET system (CORTEX Biophysik GmbH, Germany), calibrated with reference gases before each test. Breath-by-breath gas exchange data were recorded and then averaged over 30-second time periods. Peak VO_2 was defined as the highest consecutive 30-second averaged value obtained during exercise; it was normalized and expressed as a percentage of age-, sex- and body weight-predicted values. The VE/VCO_2 slope was calculated by linear regression. The respiratory exchange ratio (RER) was defined as VCO_2/VO_2. An abnormal exercise test (AET) was defined as a test with: the occurrence of symptoms, such as limiting breathlessness or fatigue at low workload, angina, dizziness or syncope; an abnormal blood pressure response (defined as a peak systolic blood pressure at or below the baseline level); or complex ventricular arrhythmia. The maximum workload was recorded and the percentage of maximum age- and sex-predicted workload was calculated.[201] Each patient was carefully questioned and observed during the recovery phase, in order to differentiate between abnormal and normal breathlessness. Abnormal breathlessness appeared early (i.e., at a low level of exercise relative to predicted

performance) and prevented the patient from speaking for several minutes. Normal breathlessness appeared at an expected time point during CPET and disappeared quickly during the post-exercise recovery phase.



Figure 2.2: Upright bicycle ergometer used for CPET testing

2.6.2 CPET results

Peak VO_2 was used where participants achieved maximal exercise effort. Peak VO_2 is, however, influenced by non-cardiac factors such as age, gender, and muscle mass[202] therefore, peak VO_2 values normalized to age, gender, and weight-based normative values generated by Metasoft software were used.[203] The Wasserman-Hansen percent-predicted equation offers optimal HF prognostication among peak VO_2 percent-predicted equations, with a peak VO_2 <47% of predicted serving as an optimal cut-point for determining mortality risk in HF.

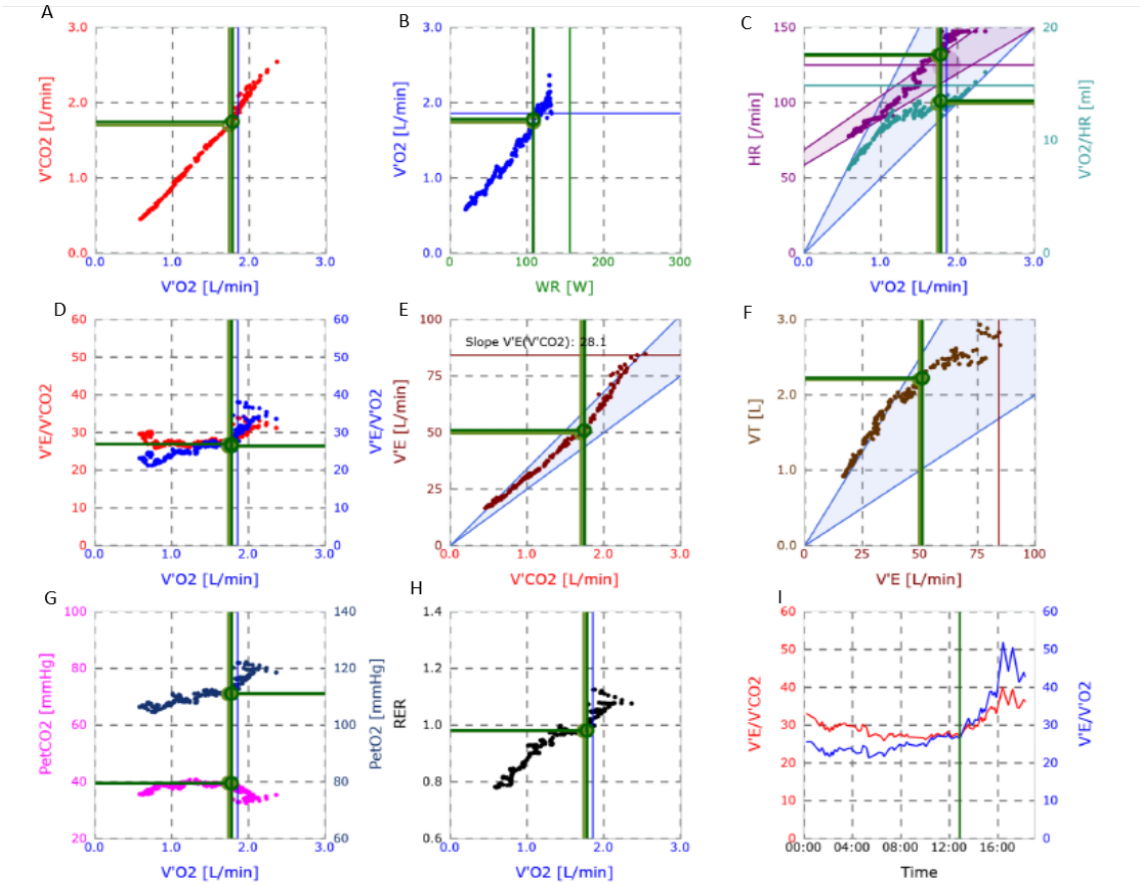


Figure 2.3: 9-panel CPET plot result from a patient with AS. *Panels A, B and C represent circulation. A) Illustration of VCO_2 vs. VO_2 relationship used to derive the VT by the V-slope method. VO_2 and VCO_2 increase proportionately during early aerobic exercise. Upon onset of anaerobic metabolism and lactate buffering by bicarbonate, there is a disproportionate increase in VCO_2 relative to VO_2 that is responsible for the steeper slope of the VCO_2-VO_2 relationship. (B) The aerobic efficiency panel reflects the relationship of utilization of oxygen (i.e., VO_2) to amount of work performed. A normal VO_2-work rate relationship during the incremental ramp portion of CPET is 10 ± 1.5 ml/min/W. (C) The ratio of VO_2 and heart rate (termed oxygen pulse) is equal to the product of stroke volume and $CaVO_2$ and most often reflects dynamic conditions that cause premature levelling or decrease in stroke volume in response to exercise (e.g., myocardial ischemia or ventricular-vascular uncoupling). Panels D – I represent ventilation and ventilatory efficiency. (D) Correlation between ventilatory equivalent for CO_2 ($V'E/VCO_2$) and O_2 ($V'E/VO_2$) and peak oxygen uptake (VO_2) (E) $V'E/VCO_2$ slope is a measure of the amount of ventilation required to exchange 1 L/min of CO_2. It reflects ventilation-perfusion matching during exercise as well as neural reflexes controlling dyspnoea and hyperventilation. (F) Ventilatory threshold plotted as function of V'E (G) End-tidal partial pressures of CO_2 ($petCO_2$) and O_2 ($petO_2$) plotted over VO_2 (H) Respiratory exchange ratio (RER) reflects general metabolic changes. (I) $V'E/VO_2$ and $V'E/VCO_2$ plotted over time. The ratio of $V'E/VO_2$, as well as $PETO_2$, decreases during exercise and reaches a nadir value just below the VT. After the onset of anaerobic metabolism, the $V'E/VO_2$ ratio and $PETO_2$ start increasing from their nadir values. The VT is expressed as the VO_2 value at the time point of VE/VO_2 or $PETO_2$ increase.*

2.7 Imaging assessment

2.7.1 Echocardiography

Echocardiography was not undertaken as part of the study. Participants' latest clinical echocardiogram findings were used to screen them against the eligibility criteria. For the correlation study, patients with confirmed mild, moderate or severe AS were recruited. For the Ox-FAST arm, out of those in the correlation arm only moderate-severe AS meeting the inclusion criteria were enrolled.

2.7.2 CMR scan protocol

All participants underwent a comprehensive CMR protocol using a Siemens 3T MR system as follows:

1. Myocardial Phosphorus Spectroscopy (^{31}P-MRS) at rest
2. Cine imaging for cardiac anatomy, mass and function
3. Myocardial tagging for LV strain assessment
4. Myocardial Proton Spectroscopy (^{1}H-MRS) at rest
5. Aortic valve and left ventricular outflow tract (LVOT) assessment
6. Pre-contrast T1 mapping of the heart
7. Late gadolinium enhancement (LGE) imaging
8. Post-contrast T1 mapping of the heart

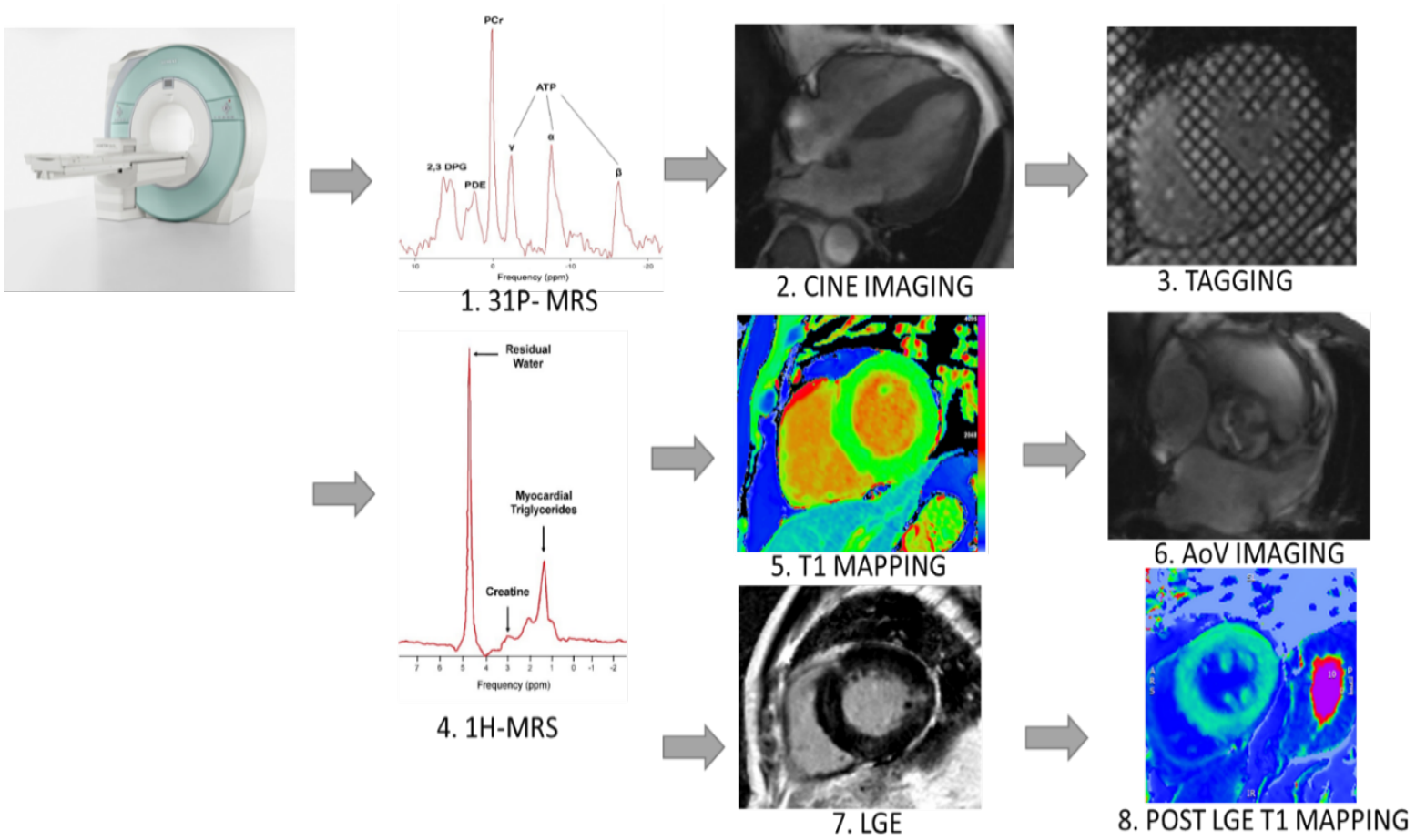


Figure 2.4: CMR scan protocol

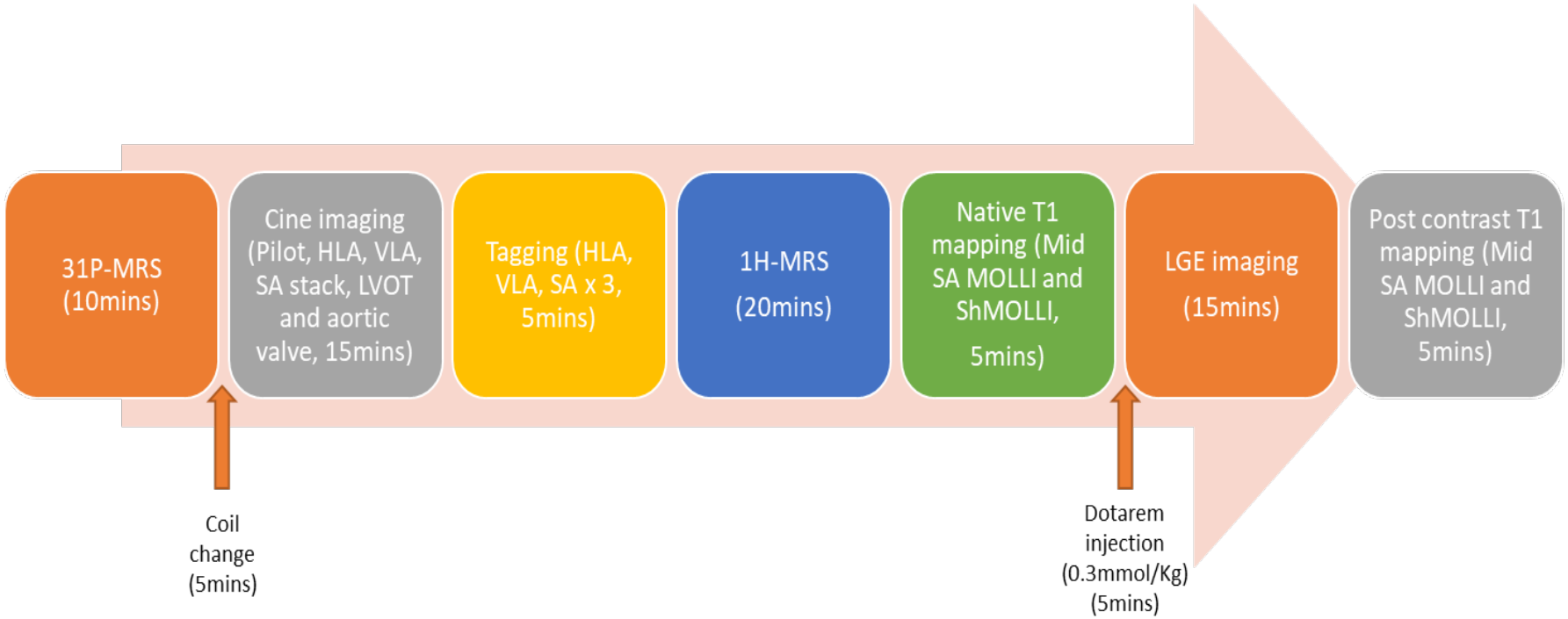


Figure 2.5: Timeline for CMR protocol

2.7.2.1 Phosphorus Magnetic Resonance Spectroscopy (^{31}P-MRS)

^{31}P-MRS allows the *in vivo* quantification of several important aspects of high-energy phosphate metabolism, from metabolite concentrations, such as PCr and ATP to metabolic fluxes through ATP-generating enzymes, including the PCr/ATP ratio and forward CK flux.[206]

Cardiac ^{31}P-MRS requires the localization of the signal (typically to the septum) to minimize contamination from signal outside the voxel of interest, especially from ribs, skeletal muscle and liver. Several localization sequences have been developed, but free induction decay (FID) localization is most commonly used, in which FID is measured immediately after excitation to compensate for the shorter T2 relaxation times of ATP and Pi.[207] Other widely used localization sequences for ^{31}P-MRS are 3D chemical shift imaging (3D-CSI) and 1D depth-resolved spectroscopy (DRESS). The simplest is depth resolved surface coil spectroscopy (DRESS) where a single slice parallel to the surface coil is selected by applying a gradient.[208] Image selected in-vivo spectroscopy (ISIS) selects a single voxel in three dimensions using inversion pulses applied with MR gradients but can be very sensitive to respiratory motion. Chemical shift imaging, or CSI uses frequency or phase encoding to differentiate signals from different areas in space. One-dimensional chemical shift imaging (1D-CSI) uses a stepped gradient to encode multiple sections parallel to the coil, acquiring a 'stack' of spectra along the axis of the gradient. In 2D or 3D CSI, gradient and phase encoding are used to build up a matrix of individual voxels.[209] (**Figure 2.6**). While CSI could be considered the method of choice for selecting an area of myocardium, it has downsides: it can lead to very long acquisition times and/or a small matrix size (i.e., a small total number of voxels), and where there is a small number of voxels, each voxel may have contributions from neighbouring tissues.[210]

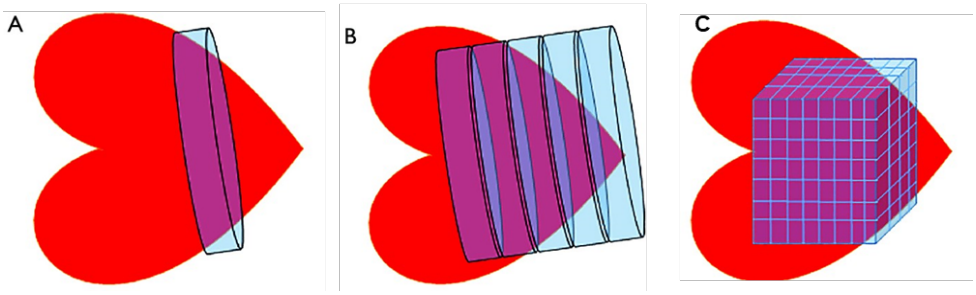


Figure 2.6: Comparison of ^{31}P-MRS Spectroscopy techniques A. DRESS; B. 1D CSI; C. 3D CSI (figure adapted with permission).[227]

The relative MR sensitivity (abundance) of phosphorus is 15 times lower than that of a proton. However, the spectroscopic peaks of interest are not hidden by other dominant signals (such as the water signal in ^{1}H-MRS) that require suppression, so they can be identified. The dominant signal is from phosphocreatine (PCr), which is usually assigned a chemical shift of 0 ppm due to its relative stability and prominence. Inorganic phosphates (Pi) and the phospholipids are located to the left of PCr. Resonant peaks from the three phosphate groups of ATP (γ-, α-, and β-ATP from left to right) are located to the right of PCr. (**Figure 2.7**).

Cardiac ^{31}P-MRS in humans is typically performed at higher magnetic field strengths of 1.5–3 T and takes 10-30 minutes to acquire. Use of high field scanners in recent years has significantly improved SNR (signal-to-noise ratio) for imaging ^{31}P metabolites with high spatial resolution. The literature average PCr/ATP ratio in a healthy human heart is 2.03 ± 0.38[206] but the absolute value is dependent on the sequence used.[176,211, 212] Modern MRS

techniques typically yield a variability of 13% for PCr/ATP ratios, which is in the same range as LV volumes and functional assessment on CMR scanning and echocardiography.[213, 214, 215]

2.7.2.1.1 Method used for PCr/ATP estimation

Spectra were obtained on a multinuclear 3T MRI scanner (Prisma; Siemens Healthcare, Erlangen, Germany). Participants were positioned supine with chest centered over a 3-element dual-tuned $^{1}H/^{31}P$ surface coil placed in the isocentre of the MRI system. Free induction decay (FID) inversion recovery curves (ten 1000μs) hard inversion pulses, inversion delay 100–3000 ms) and locations of phenyl phosphonic acid (PPA) fiducial and cod liver oil phantoms were acquired together with a 3D stack of short axis localizers. The middle of the acquisition matrix is placed over the basal-mid interventricular septum (**Figure 2.5 A**). A FID (free induction decay) acquisition based 1D localisation sequence, called depth-resolved surface coil MRS (DRESS) using slice-selective excitation pulse was used with saturation bands placed over liver and skeletal muscle. The PCr/ATP ratio reported is the blood- and saturation-corrected PCr/average ATP ratio, averaged over the 2 most basal septal voxels. Our non-gated 3D acquisition-weighted ultra-short echo time (TE) DRESS sequence takes about 3 min. The centre frequency is set 250 Hz left of (lower than the resonant frequency of) PCr, i.e. between ϒ- and α-ATP, so that the excitation bandwidth covers from β-ATP on one side to phospho-monoesters on the other. Sequence parameters included: acquisition matrix size 16 x 16 x 8,field of view 240 x 240 x 200 mm3, nominal voxel size 5.6 ml, 10 averages at the centre of k-space, repetition time (TR) = fixed with some inter-participant variability (910–1010 ms) dependent on specific absorption rate (SAR).

Spectral analysis was performed using OXSA, an open-source MATLAB implementation of the Advanced Method for Accurate, Robust and Efficient Spectral fitting (AMARES) algorithm.

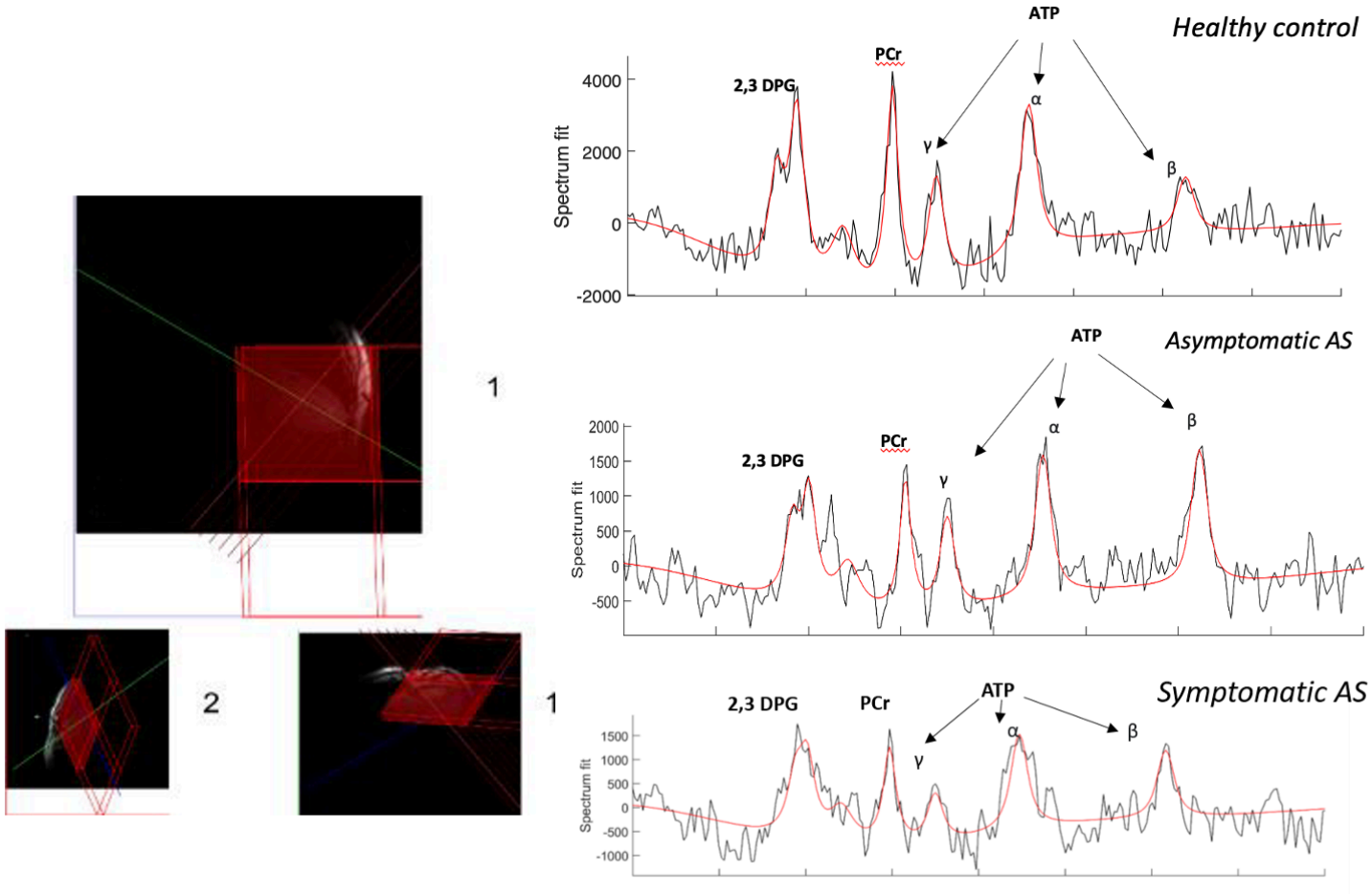


Figure 2.7: Examples cardiac energetics data from a healthy control, and patients with asymptomatifc and symptomatic Aortic stenosis. Left panel shows voxel placement (red) and right panel shows spectrum fit with labelled peaks

The resulting PCr/ATP ratio presented here is the blood- and saturation-corrected PCr/average ATP ratio, averaged over the two most basal septal voxels (each separated by a half-voxel shift). Measures of data quality include the signal-noise ratio (SNR) of the PCr peak and the coefficient of variation in the measured PCr/ATP ratio. Apart from selection of voxels on anatomic criteria and visual confirmation of correct peak fitting, analysis is fully automated.

2.7.2.2 Left ventricular function and mass

CMR is accurate, reproducible and well validated for measuring LV volumes and mass.[216] Cine images including pilot, horizontal long axis, vertical long axis, LVOT and short axis (SA) stack images were acquired for cardiac volume and function analysis using a 3T MR System using steady state free precession cine imaging[217] with slice thickness 8 mm, gap 2 mm, retrospective gating, TE 1.5 ms, TR 46 ms, flip-angle 50°, field-of-view (FOV) 400 mm, matrix size 256 in frequency encode direction.[236] Scans were performed supine in end-expiration. A 24-channel spine matrix and 18 channel body matrix were used. LV endocardial and epicardial contours in end-diastole and end-systole, as shown in figure, were contoured using cvi42 version 5.10.1 (Circle Cardiovascular Imaging Inc, Calgary, Alberta, Canada). SSFP sequences were gated prospectively when the participant was in atrial fibrillation otherwise retrospective gating was used.

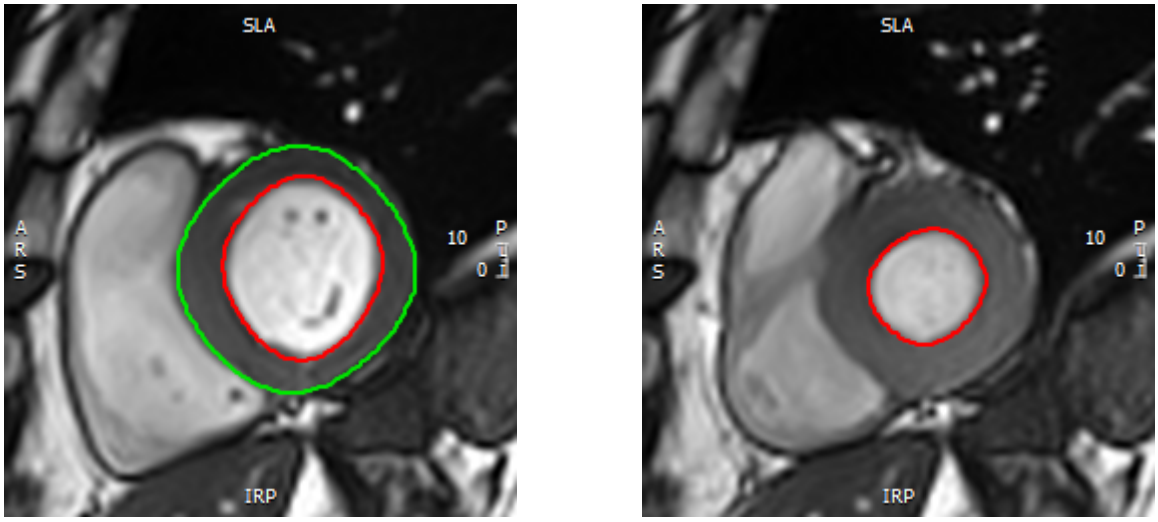


Figure 2.8: Left ventricular (LV) epicardial (green) and endocardial (red) contours for volume and function assessment performed on cvi42 version 5.10.1 in a patient with AS.

End-systolic (ESV) and end-diastolic (EDV) volumes were used to calculate stroke volume (SV) as SV = EDV – ESV. Ejection fraction (EF) was calculated as EF = SV/EDV. Papillary muscles were included as part of the LV volume but excluded from LV mass. LV mass is calculated as the difference between the total epicardial volume (sum of epicardial cross-sectional areas multiplied by the sum of the slice thickness and interslice gap) minus the total endocardial volume, multiplied by myocardial density (1.05 gcm^3).

For LV wall thickness analysis, LV epicardial and endocardial contours were identified in end-diastole and end-systole, and planimetry performed using semi-automated analysis software tools (cmr42 version 5.10.1; Circle Cardiovascular Imaging Inc.). The maximum LV wall thickness was curated from the basal short axis views of the left ventricle in end-diastole. Right and left ventricular trabeculations were excluded from wall thickness measurements.

2.7.2.3 Myocardial tagging

CMR is well validated tool for measurement of multidirectional strain using myocardial tagging sequence. A gradient echo-based tagging pulse sequence was performed with a segmented k-space, multi-shot sequence (TR 4.47ms, echo time 7.4ms, and flip angle 25). Spatial modulation of magnetisation (SPAMM) produced images with a grid-based pattern of horizontally and vertically modulated stripes 7mm apart acquired during singe breath hold, using a prospectively gated sequence.[218, 219] The temporal resolution (TR X no. of segments, 9) was 40.23 ms in all data sets and 15-35 frames per cardiac cycle were recorded, depending on heart rate. Two long axis (HLA and VLA) and three short axis cine images (basal, mid-ventricular, and apical) were chosen for tagging imaging sequences. The basal slice was carefully chosen to avoid the LV outflow tract in systole using the LVOT view; the mid-ventricular slice was chosen to include the papillary muscles; the apical slice was carefully selected to ensure that it contained sufficient myocardium to minimise partial volume effects. Tagged images were analysed using CIM TAG 2D version 9.1 (Auckland Medical Research, Auckland, New Zealand). Outcome parameters measured in this study were global mid-ventricular peak systolic circumferential strain, global peak systolic longitudinal strain, circumferential diastolic strain rate and longitudinal diastolic strain rate.

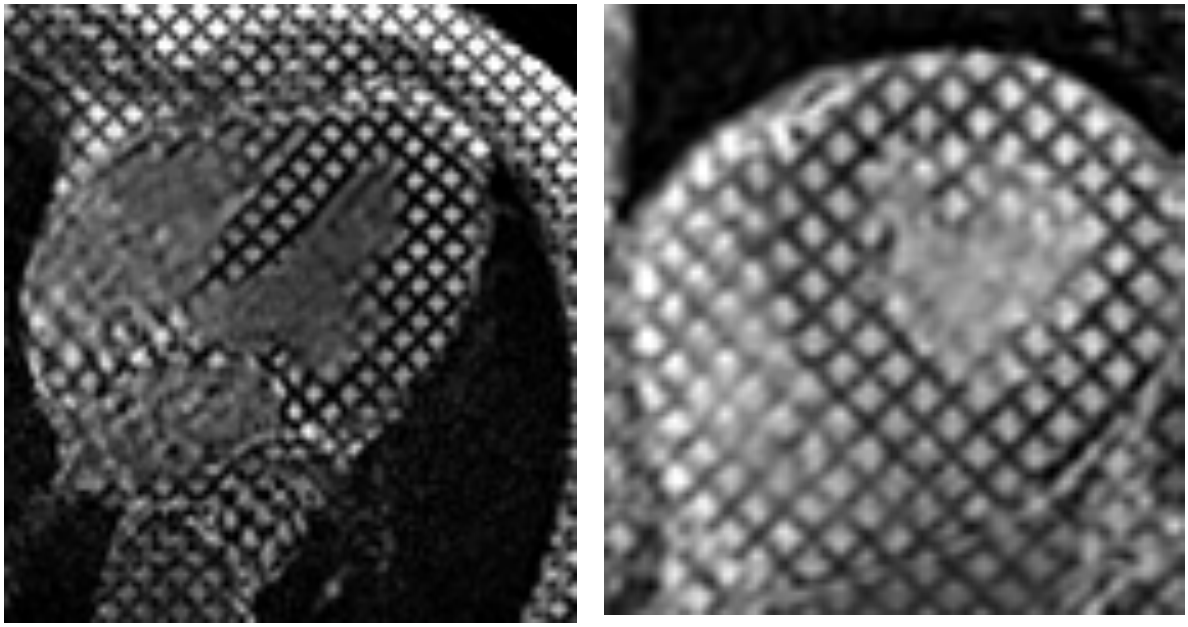


Figure 2.9: CMR tagging images of a long (left) and short axis (right) views in early diastole.

2.7.2.4 Proton Magnetic Resonance Spectroscopy (^{1}H-MRS)

Proton magnetic resonance spectroscopy (^{1}H MRS) is a powerful tool to gain insight into cardiac lipid and creatine metabolism.[174] Myocardial triglycerides (MTG) can be assessed using cardiac ^{1}H-MRS, which utilises the abundant hydrogen (^{1}H) protons. Cardiac ^{1}H MR spectra contain a number of peaks associated with triglycerides (TG) and peaks associated with taurine, choline/carnitine, and creatine.[220] The metabolite concentration can be quantified by calculating the peak area, expressed for example relatively to the water concentration.

Various clinical studies have assessed the presence of myocardial steatosis using ^{1}H-MRS and examined its functional associations in obesity, type 2 diabetes mellitus (T2DM), and in normal individuals when subjected to prolonged exercise and diet restrictions.[221, 222] These studies have shown that myocardial triglyceride (MTG) content is an independent correlate of both systolic and diastolic function, suggesting a potential causal relationship between

steatosis and such functional changes. Our group has previously demonstrated that in severe AS, steatosis is pronounced in both symptomatic and asymptomatic patients with AS (fat .proportion 0.89±0.42% in symptomatic AS; 0.75±0.36% in asymptomatic AS versus controls 0.45±0.17, both $p<0.05$) and is independently associated with impaired strain.[163] Furthermore the spectroscopic measurements of MTG have also been validated against histological analysis of lipid from myocardial biopsies of the same patients obtained during valve replacement.

Cardiac ^{1}H-MRS uses abundant hydrogen (^{1}H) protons, primarily for the detection of myocardial triglycerides (MTG) and total Cr content. However, the ^{1}H spectrum contains a dominant water signal which is several orders of magnitude stronger, and which needs to be sufficiently suppressed to detect the weak metabolite signals.[172] For ^{1}H-MRS, data are typically acquired at breath hold during diastole from a single voxel (14-16mL) localized in the myocardial septum (**Figure 2.10 A**) and take 10-15 minutes to acquire. The most frequently used single-voxel sequences for cardiac 1 H-MRS are stimulated echo acquisition mode (STEAM)[223] and point-resolved spectroscopy (PRESS).[224] An advantage of the STEAM pulse sequence is that a shorter TE can be achieved than when using the PRESS pulse sequence. Consequently, using STEAM, the signal intensities of spectral peaks are less affected by T2 decay, which makes STEAM advantageous for the detection of metabolites with short T2 relaxation times. During a 10 s breath-hold, water unsuppressed and suppressed spectra can be acquired by two phased array coils using STEAM sequence with electrocardiogram-triggered to mid-diastole. ^{1}H-MRS has been performed at our centre in only 6-7 breath-holds at 3T using STEAM sequence, allowing reliable and quick quantification of myocardial lipids.[172] Other metabolites (e.g. creatine and choline) are clinically relevant but more challenging to quantify because of their relatively low concentrations (approximately 10 mmol/L) and because of cardiac motion.[225] ^{1}H-MRS is

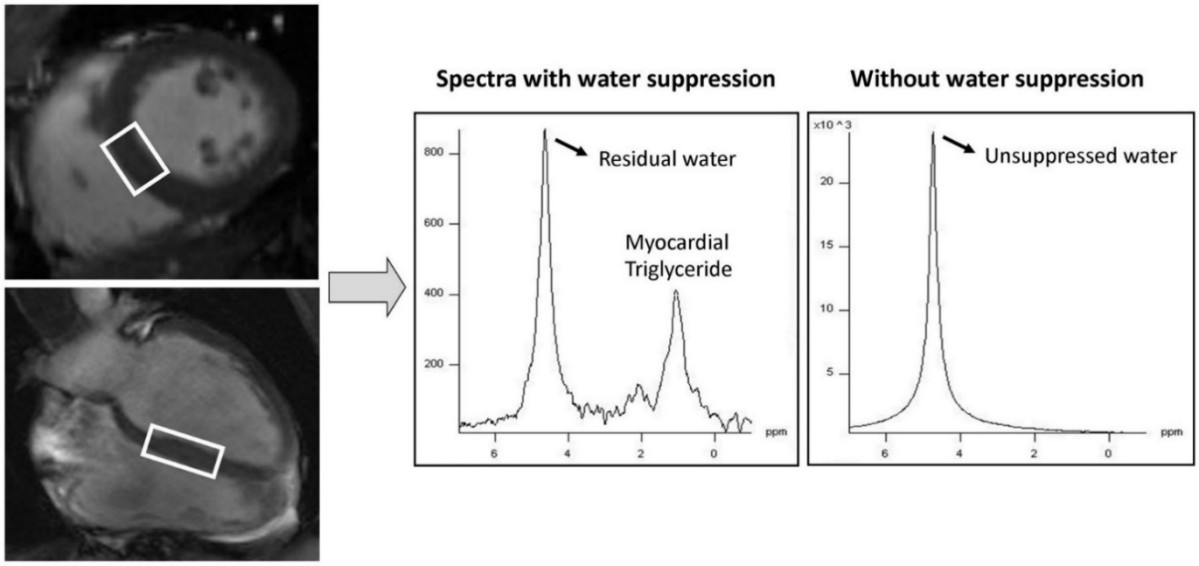
increasingly used in research studies but has not yet been adopted into clinical cardiology due to technical challenges include longer scan times to obtain sufficient signal-to-noise ratio (SNR) for detection of low concentration metabolites, and other considerations with data acquisition, post-processing and analysis.

2.7.2.4.1 ^{1}H- MRS method used

^{1}H- MRS was performed on a 3T Siemens Prisma using the 18-channel body and 24 channel spine coil for signal receiving. Mid ventricular long and SA cine were used to determine the trigger delay for mid diastole. A calibration pulse sequence was implemented to evaluate the optimal water suppression pulse scaling factor. Cardiac gated spectra were acquired using different water correction scaling factors and the one yielding the most effective water-suppression was chosen. A 22 x 18 x 32 mm stimulated echo acquisition mode (STEAM) voxel was planned on the corresponding cine frame. A water spectrum (3 averages, TR of at least 4s) was acquired in a single breath-hold to use as an internal reference. Next, five to six water-suppressed scans (5 averages each, TR of at least 2s) were acquired are mid-diastole in a series of single breath-holds.

Individual coil signals were combined within Matlab using specially written modules. The water-suppressed scans were constructively averaged, including frequency correction. Spectra were quantified using the Advanced Method of Accurate, Robust and Efficient Spectroscopic (AMARES) fitting algorithm. Metabolite peaks (including lipids/TGs) were analysed, and prior knowledge was used for all peak locations by using soft constraints. All peaks were fitted using Lorentzian line shapes. MTG is then calculated as the sum of detected lipid signal amplitudes (=CH-CH2-CH= @ 2.2 ppm, -CH2- @ 1.3 ppm, -CH3 @ 0.9 ppm) / water signal amplitude X 100. As ^{1}H-MRS analysis has no subjective element to it and is not operator dependent, inter observer and intra-observer variability test was not performed.

A.



B.

PDFF %	L/W CRLB %	Residual/Water %	R/W CRLB %	Fit Residual (Unsup)	Fit Residual (Sup)
0.87	± 6.77	0.48	± 5.33	0.00	0.34

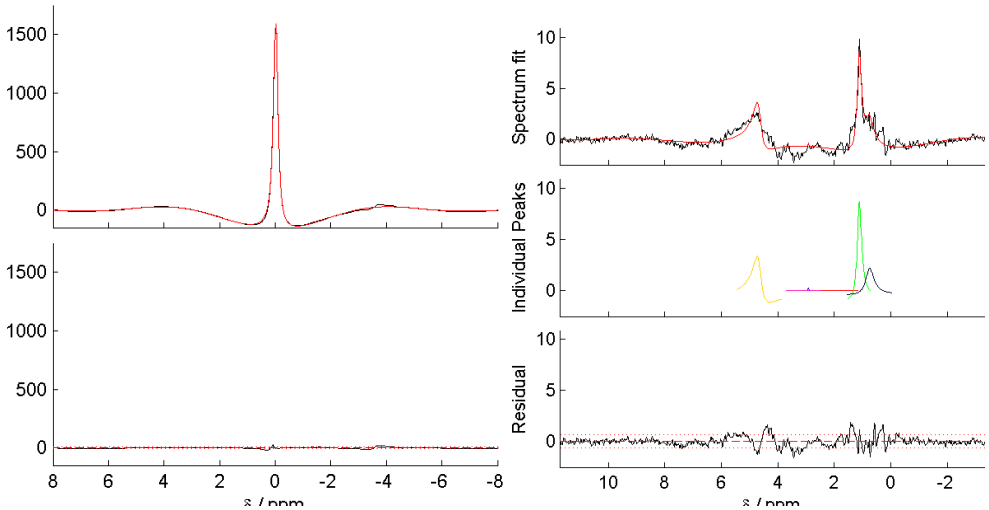


Figure 2.10: A) [1]H-MRS voxel position and graphic representation B) Results from a patient with AS.

2.7.2.5 Aortic valve cine and through-plane flow

Planning a plane perpendicular to both the LVOT long-axis LV cine and the coronal LVOT cine, aortic valve (AV) anatomy and AV area in mid-systole were captured at the AV leaflet tips using a breath-hold radial readout sequence (slice thickness 5 mm, TR 45 ms). Through-plane flow sequences (both breath-hold and free-breathing) were planned just distal to the AV leaflet tips. Typical parameters for breath-hold sequences were TE 2.3 ms TR 50 ms, flip angle 30, slice thickness 5.5 mm, FOV 450 mm in frequency encode direction, and aliasing velocity set (in severe AS) at 400-450cm/s and increased in increments until no aliasing was seen, or (in cases without AS) at 200cm/s.

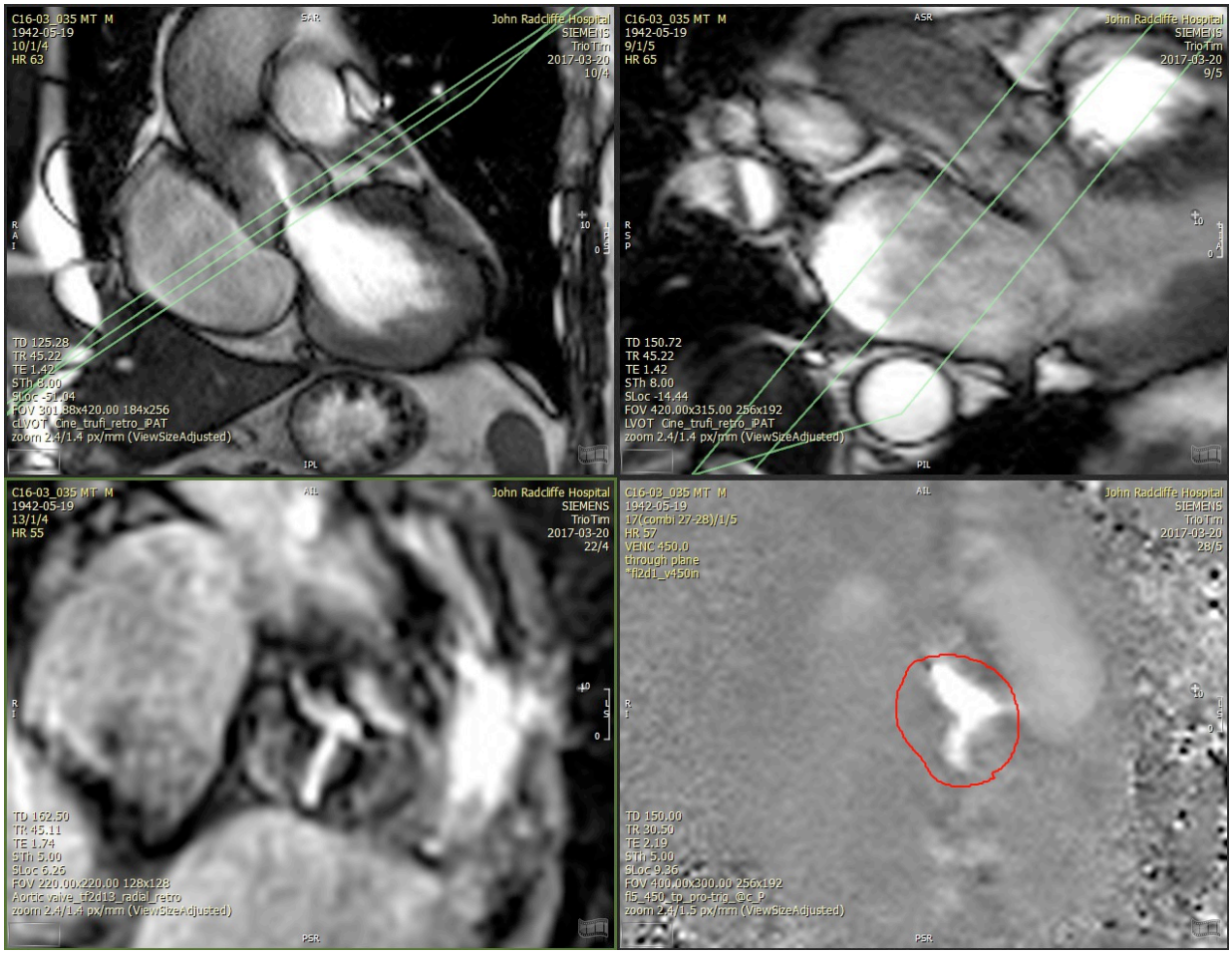


Figure 2.11: CMR acquisition of aortic valve images. *The plane planned through the AV leaflet tips (middle of the three green lines (upper two panels) used for AV cine (bottom right) and through-plane flow (bottom left).*

2.7.2.6 Late gadolinium enhancement imaging (LGE)

Late gadolinium enhancement (LGE) images were acquired using a free-breathing respiratory-triggered 2D inversion-recovery sequence approximately 3-5 minutes after administration of a bolus injection of an intravenous gadolinium-based contrast agent (0.3 mmol/kg; Dotarem) given manually, immediately followed by a 15-20 ml saline flush. The inversion time (TI) was adjusted for optimal nulling of remote normal myocardium. LGE images were acquired in standard long and short axis slices covering the whole LV. Initial study scans were performed using 2D segmented inversion-recovery gradient echo sequence with typical scan parameters: TR/TE = 750/3.38 ms, flip angle = 25°, FOV read = 380 mm, FOV phase = 75%, voxel size = 1.5 x 1.5 x 8.0 mm, slice thickness = 8.0 mm, GRAPPA = 2, reference lines = 24, measurements = 1, segments = 25, phases = 1, concatenations = 1, bandwidth = 130 Hz/Px.

However, after first 10 patients due to time constraint and length of scan protocol, images were instead acquired using 2D single-shot inversion-recovery sequence. Thus, only a qualitative assessment of gadolinium enhancement was done using cvi42 post-processing software (version 5.10.1, Circle Cardiovascular Imaging Inc., Calgary, Canada) for the presence or absence of LGE by two independent operators. LGE suspected on short axis imaging was confirmed with additional imaging in long axis views or perpendicular to the lesion (**Figure 2.12**). None of the patients had any evidence of infarction. Most patients with LGE enhancement had basal inferolateral fibrosis. Patients with non-specific LV/RV junction enhancement alone were considered to have no significant fibrosis and were reported as negative on LGE assessment.

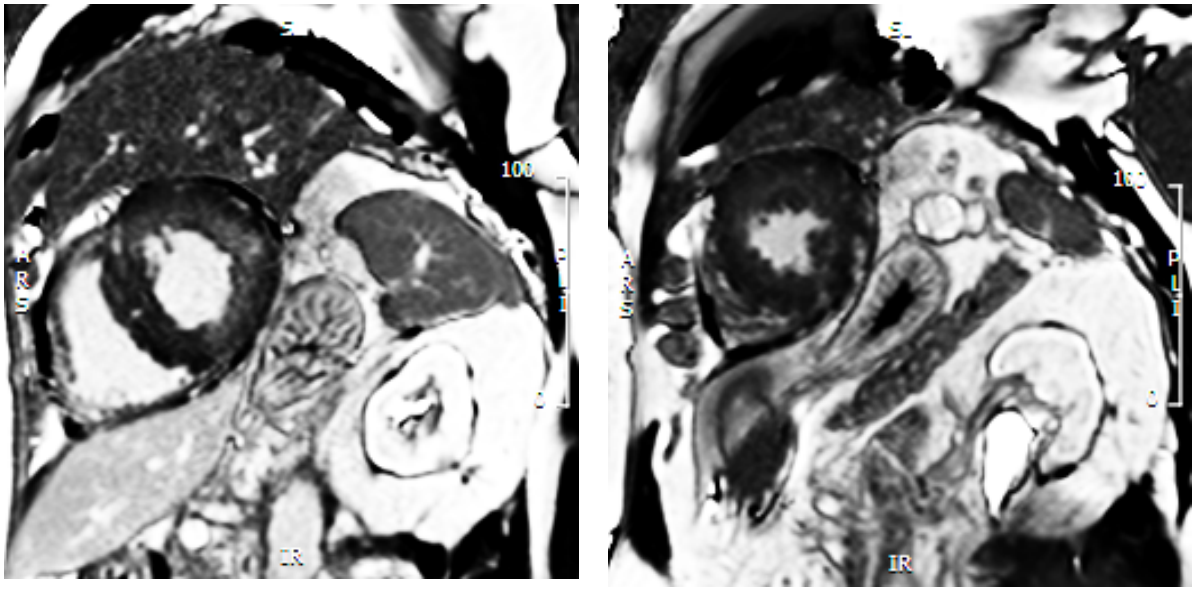


Figure 2.12: Late gadolinium acquisition images showing myocardial fibrosis in an AS patient. *Patchy late gadolinium enhancement seen on short axis images in the inferolateral wall in a patient with severe aortic stenosis.*

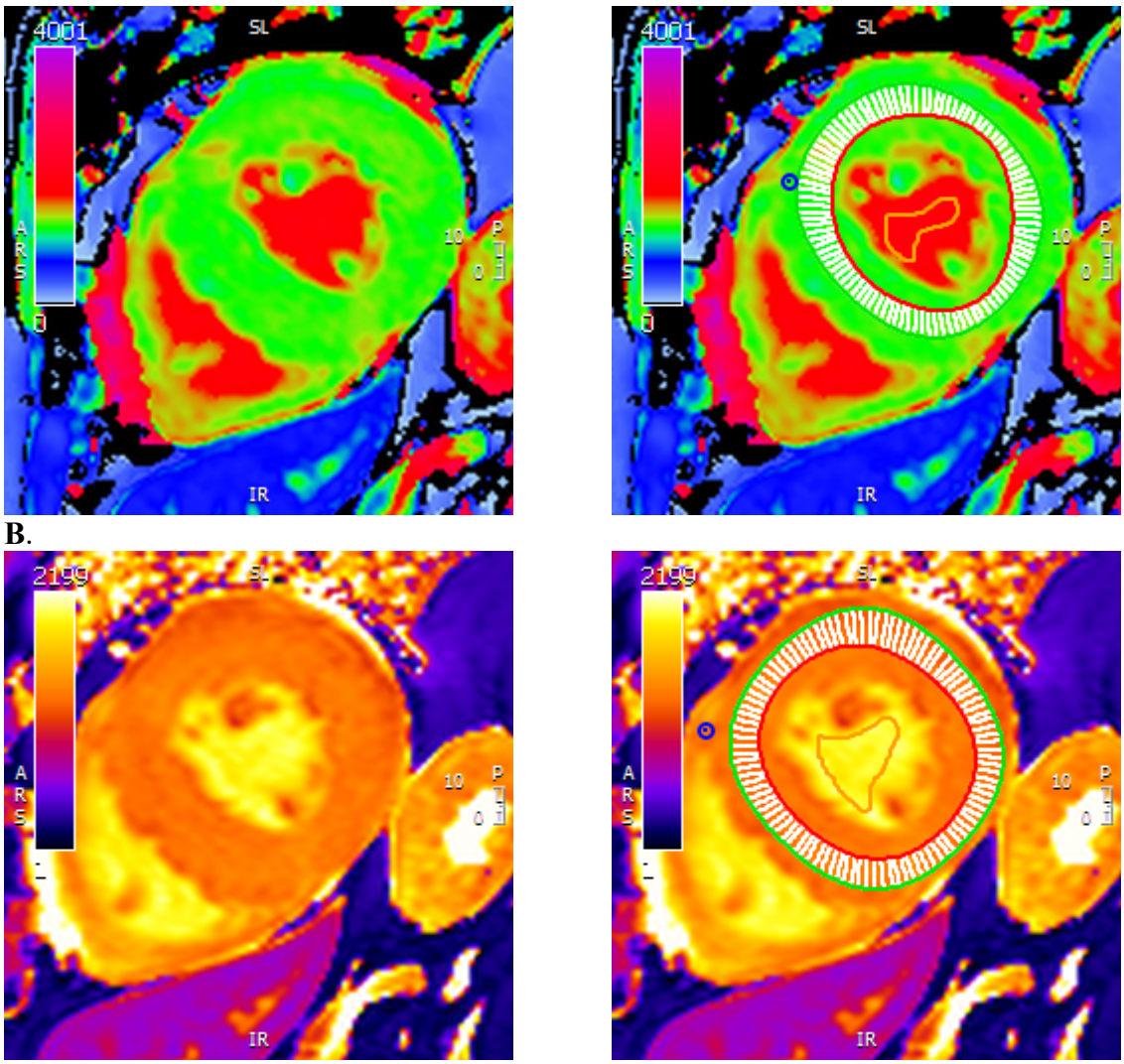
2.7.2.7 Native T1 mapping (Both MOLLI and ShMOLLI)

Myocardial T1-mapping was performed using the ShMOLLI 5(1)1(1)1 sequence as previously published.[226] Typical scan parameters were: TR/TE = 378.98/1.07 ms, flip angle 35°, FOV read 360 mm, FOV phase 75%, interpolated voxel size 0.9 x 0.9 x 8.0 mm, slice thickness 8.0 mm, trigger delay (TD) 260 ms, TI 260 ms, measurements 1, concatenations 1, bandwidth 898 Hz/Px. T1-maps were acquired in one mid-ventricular short axis slice matched to cine image.

MOLLI 5(3)3 (MyoMaps, Siemens Healthcare, Erlangen, Germany) T1-maps were acquired from vendor-provided product protocols including “Low HR” (256 matrix) and “High HR” (192 matrix) variants. Typical scan parameters for MOLLI “Low HR” were: TR/TE 279.84/1.13 ms, flip angle 35°, FOV read 360 mm, FOV phase 85.2%, voxel size 1.4 x 1.4 x 8.0 mm, slice thickness 8.0 mm, resolution 256, measurements 1, concatenations 1, bandwidth 1085 Hz/Px. Typical scan parameters for MOLLI “High HR” were: TR/TE 263.55/1.01 ms, flip angle 35°, FOV read 360 mm, FOV phase 85.4%, voxel size 1.9 x 1.9 x 8.0 mm, slice thickness 8.0 mm, resolution 192, measurements 1, concatenations 1,

bandwidth 1085 Hz/Px. Shimming and centre frequency adjustments were performed to generate images free from off- resonance artefacts. For the analysis of both MOLLI and ShMOLLI T1 maps, the LV myocardium of the short axis slice acquired at baseline was contoured using dedicated software as previously described providing a single average myocardial T1 value per each individual (**Figure 2.11**). Care was taken to minimise contamination of the myocardium by blood-pool and extra-myocardial structure partial volume effects.

A.



B.

Figure 2.13: T1-map analysis from a mid-ventricular slice. *Endocardial (red) and epicardial (green) contours are placed within the myocardium so as to avoid contamination from extra-myocardial tissues. A. ShMOLLI T1 maps (acquired and contoured image). B. MOLLI long T1 maps (acquired and contoured image).*

2.7.2.8 Post contrast T1 mapping and extracellular volume (ECV) estimation

Post-contrast T1-maps were acquired following administration of an intravenous gadolinium-based contrast agent. Slice position and sequence parameters were essentially unchanged to those used for native T1-mapping. Offline post-processing of post-contrast T1-maps was conducted using the same methods as outline for native T1-maps (section 2.8.6). R1 of blood and myocardium was calculated as R1 = 1/T1 for both native and post-contrast maps. Haematocrit was measured on a blood sample drawn on the same day, immediately prior to the CMR scan. Extracellular volume (ECV) (140):= (1−haematocrit) × ($\Delta R1\ myo$ / $\Delta R1\ blood$)

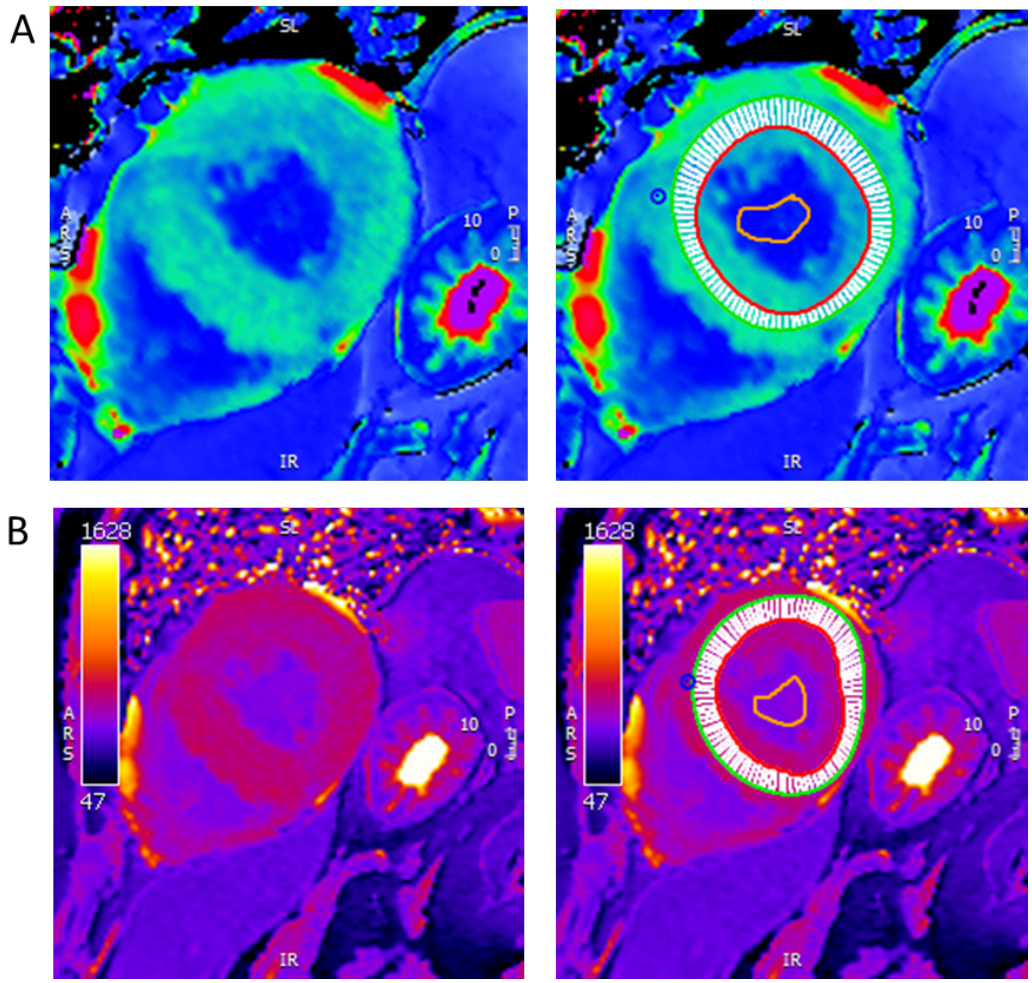


Figure 2.14 A. ShMOLLI T1 maps (acquired and contoured image). B. MOLLI long T1 maps (acquired and contoured image). *Endocardial (red) and epicardial (green) contours are placed within the myocardium so as to avoid contamination from extra-myocardial tissues. Blood pool contour (orange) used for ECV estimation.*

2.8 Summary

The methods described above provide the backbone for the work conducted in this thesis. Each individual chapter provides further details and clarification on how these techniques and methods used help obtain the relevant information for the research.

3 Chapter Three

Role of metabolic phenotyping in Aortic stenosis

3.1 Abstract

3.1.1 Background

There is wide individual heterogeneity in degree of hypertrophy and progression to myocardial fibrosis and heart failure in patients with AS. It yet remains unanswered why some with same degree of stenosis may develop greater hypertrophy and decline sooner compared to others. Impaired myocardial energetics and presence of myocardial steatosis has been shown in severe AS. An underlying interplay of metabolic interactions might explain this variability.

3.1.2 Purpose

To understand this, I first sought to investigate the metabolic remodelling in AS, at what stage of the disease does it begin, how it impacts on cardiac physiology and whether it precedes structural remodelling. I additionally sought to understand whether the cardinal metabolic features of myocardial steatosis and impaired energetics were differentially related to LV hypertrophy or pressure load in AS.

3.1.3 Methods

74 asymptomatic AS patients with varying degree of stenosis and 13 healthy volunteers were recruited to the study. Participants were divided into quartile groups based on their maximal LV wall thickness, a measure of structural remodelling, as measured on CMR and peak aortic valve gradient, marker of pressure overload, as measured on echocardiography. Comparison of various metabolic and structural parameters were made to understand the relationship between metabolic and structural remodelling in AS. Myocardial lipid content was measured

using ^{1}H-MRS and cardiac energetics were assessed using ^{31}P-MRS. Cardiac volumes and function including strain and aortic valve imaging were assessed by cardiovascular magnetic resonance (CMR) cine imaging.

3.1.4 Results

Here, I have shown for the first time that metabolic changes occur as early as mild- moderate stage of AS, including impaired cardiac energetics (Phosphocreatine/ATP [PCr/ATP] measured using ^{31}P-MRS): Q2 1.43±0.13 vs Q1 1.80±0.14, p=0.05 with worse energetic state seen in the severe stage of the disease, Q4 (PCr/ATP 1.39±0.14, p=0.02 vs Q1 1.80±0.14. Presence of myocardial steatosis is also seen early in AS, mean myocardial triglyceride content (MTG) in Q2 1.52±0.84 vs Q1 1.25±0.70, p 0.032 overall. Despite normal LV ejection fraction, there is substantial evidence of subclinical LV dysfunction in moderate-severe AS measured by LV strain parameters. In this study, all AS groups had impaired global systolic longitudinal strain [GLS] ($p<0.0001$) and diastolic circumferential strain rate (p 0.0007). Impaired systolic longitudinal strain in AS was linked not only to the degree of hypertrophy but also to the degree of energetic impairment (p 0.03). In addition, PCr/ATP was strongly associated with the presence of myocardial fibrosis (p 0.01). These novel findings suggest that adverse metabolic changes occur early and may have a causal relationship in subsequent decompensation in AS.

3.1.5 Conclusions

A gradient of myocardial energetic deficit and steatosis exists across the spectrum of hypertrophied AS hearts, notably I have shown in this study that this happens prior to the development of irreversible structural changes and is related to subclinical LV dysfunction. Thus, targeting myocardial metabolism may be a sensible strategy to risk stratify as well as potentially prevent and treat systolic failure in AS.

3.2 Introduction

AS is characterized by both progressive valve obstruction as well as LV remodelling response. Conventional thinking holds that hypertrophic growth of the myocardium is a "compensatory" response of the heart to increases in workload demand, serving to minimize wall stress and maintain contractile function. However, several lines of evidence – preclinical and epidemiological – highlight the maladaptive features of chronic ventricular hypertrophy.[227, 228] It is not yet fully known why there is wide individual variation in the myocardial response to the same degree of pressure overload. Where do metabolic changes fit into this picture of hypertrophy, subsequent irreversible myocardial fibrosis and decompensation, and the cause and effect relationship, if any, behind these structural and metabolic alterations in AS. The prominent metabolic changes due to pressure overload force a shift of reliance on glucose instead of fatty acids to provide energy for the heart.[229, 125] resulting in impaired cardiac energetics, which according to animal studies precedes manifestation of cardiac dysfunction and LV hypertrophy.[230] Similar metabolic changes are, however, also seen in established hypertrophy. LV hypertrophy, independent of pressure overload, is inherently associated with impaired myocardial metabolism; uncoupling of glycolysis and glucose metabolism, shift away from free fatty acid use and a depressed energetic state [231] and is a well-known risk factor for increased morbidity and mortality.[14] The PCr/ATP ratio, an index of cardiac bio-energetic state, is reduced in both animal and models of myocardial hypertrophy[142] and in HF.[134] It correlates not only with the degree of cardiac hypertrophy and accompanying LV dysfunction, but has also been shown to be a superior predictor of mortality.[133, 232] Thus, both pressure overload and LVH seem to contribute to the metabolic changes in AS but their relative contributions are unknown. Given the direct coupling of adenosine triphosphate (ATP) metabolism and contractile function,

metabolic alterations could represent an early and specific marker of vulnerability to failure in AS.

The knowledge of the timing of metabolic changes in relation to structural ventricular remodelling, including development of irreversible myocardial fibrosis a known prognostic marker, in AS is important. The annual rate of sudden death for asymptomatic AS patients, who are not yet offered surgery as per current guidelines, remains 1%.[233] Metabolic phenotyping may well help identify more sensitive markers of myocardial remodelling to characterise high-risk population among asymptomatic cohort as well as help identify a niche population that may benefit from an earlier intervention.

As such, I sought to determine the relative contribution of each - pressure overload i.e., severity of stenosis per se and degree of LVH in relation to metabolic remodelling. I, further, hypothesised that not only a gradient of myocardial energetic impairment and steatosis exists across the spectrum of AS but also these changes precede irreversible structural remodelling i.e., LVH and fibrosis as well as relate to the subclinical LV dysfunction predisposing to decompensation.

To investigate this, I used a combination of proton (^{1}H) and phosphorus (^{31}P) MRS, as detailed in Chapter 2, to measure myocardial energetics and triglyceride content (MTG) and cine CMR to assess cardiac function. To study the effect of myocardial fibrosis on metabolism, I also measured myocardial T1, ECV and late gadolinium enhancement (LGE). My goal was to study the relationship between metabolic and structural changes in asymptomatic AS patients throughout the spectrum of the disease.

3.3 Methods

The study received approval from a Research Ethics Committee (South London, 18/LO/1981). Research was conducted in accordance with institutional procedures and Declaration of Helsinki. Participants were prospectively recruited from clinical activity

across three sites in the UK: Oxford University hospital NHS trust, Oxford, Great Western hospital NHS trust, Swindon, and Royal Berkshire hospital, Reading. All participants provided written informed consent.

3.4 Study Design

Seventy-four AS participants and 13 healthy volunteers were recruited to the study. All AS recruits fulfilled the inclusion and exclusion criteria as briefly described below and detailed in Chapter 2.

Inclusion Criteria: Asymptomatic AS with varying degree of stenosis and meeting two of the three criteria (Mild AS: Peak velocity, Vmax <3m/sec, peak gradient, PG <30mmHg or Mean gradient, MG <20mmHg, AVA >1.5cm2; Moderate AS: Vmax 3-4m/sec, PG 30-60mmHg or MG 20- 40mmHg, AVA>1but <1.5cm2; Severe AS: Vmax >4m/sec, PG >60mmHg or MG >40mmHg, AVA <1cm2), not planned for AVR or TAVI, no other significant valvular pathology, no contraindication to magnetic resonance imaging. *Exclusion Criteria*: Known coronary artery disease, presence of other underlying cardiomyopathy, LVEF<50%, uncontrolled hypertension, type 1 or type 2 diabetes mellitus, liver impairment, BMI >40 kg/m2, significantly impaired renal function (eGFR<30ml/min). only underwent CMR assessment.

All study subjects underwent CMR scanning using a 3T MRI scanner (Magnetom Prisma; Siemens Healthineers) as below and represented in **Figure 3.1**.

1. ^{31}P-MRS to assess PCr/ATP as a measure of myocardial energetic status at rest.
2. ^{1}H-MRS to quantify myocardial steatosis.
3. Cine imaging to measure LV function, mass and volumes and assess aortic valve.
4. Tagging CMR to assess LV strain.

5. ShMOLLI T1 mapping to assess tissue characterisation.
6. Late gadolinium enhancement to evaluate myocardial fibrosis.

All methods used are as described in Chapter 2.



Figure 3.1: Pictorial representation of the participant groups and CMR protocol for the study.

3.5 Statistical Analysis

To investigate the relationship between myocardial metabolism and LV hypertrophy participants were divided into quartile groups based on their LV wall thickness (LVWT). To investigate the relationship between myocardial metabolism and LV pressure overload secondary to AS participants were divided into quartile groups based on peak aortic valve gradient. I, further investigated the effect of overall LV pressure overload in AS by dividing participants into quartile groups based on their total LV pressure gradient (i.e. aortic valve gradient + systolic blood pressure).

All data are expressed as mean ± SD depending on normality using Kolmogorov–Smirnov test. Categorical data are presented as numbers and percentages. Comparisons between the quartile groups were performed by 1-way ANOVA with post hoc Bonferroni correction. Ordered medians were compared using the Jonckheere-Terpstra test, according to the study design(i.e. using wall thickness, AV gradient or total LV pressure loading). Bivariable correlations were performed using the Pearson or Spearman method as appropriate. A $P<0.05$ was considered significant. All statistical analyses were performed with IBM SPSS Statistics, version 28 and GraphPad Prism (version 9.0.2 for Windows; GraphPad Software, San Diego, CA).

3.6 Results

3.6.1 Study population

Seventy-four patients (70% male, mean age 70±14 years, body mass index (BMI) 27±4.5 Kg/m^2) with varying degrees of AS as described above and thirteen normal controls (54% male, mean age 47±8 years and BMI 25±5 Kg/m^2) were studied.

Healthy volunteer population: The healthy volunteers were included to a) check whether the metabolic changes seen in mild AS group with relatively normal wall thickness were

secondary to AS and b) to add power to the study. Table below represents the healthy volunteer data in comparison with mild/moderate/severe AS participants.

Table 3.0: Baseline characteristics of study groups.
Values are mean ± SD or frequency (percentages). *BMI, Body mass index**; SBP,** systolic blood pressure; DBP, Diastolic blood pressure; FFA, Free fatty acids; TC, Total Cholesterol; TG, Triglycerides; AF, Atrial Fibrillation; AV, aortic valve; AVG, Aortic valve gradient;LV, left ventricle; WT, wall thickness; EDV, End diastolic volume; ESV, End systolic volume; SV, Stroke volume; GLS, Global longitudinal strain; GCS, Global circumferential strain; DLSR, Diastolic longitudinal strain rate; CSR, circumferential strain rate; LA, left atrium; RV, right ventricle; LA, left atrium; RV, right ventricle; MTG, myocardial triglyceride content; PCr/ATP, Phosphocreatine/adenosine triphosphate. P values are for 1-way ANOVA for all groups († significant), except cardiac metabolism where ordered medians were compared using Jonckheere-Terpstra test (* significant).*

Groups	**Normal (n=13)**	**Mild AS (n=30)**	**Mod AS (n=22)**	**Sev AS (n=22)**	**P value**
Age (yrs)	51 ± 8	74 ± 8	66 ± 14	73 ± 13	<0.001
Male (%)	9 (69)	17 (56)	16 (73)	17 (77)	0.33
BMI (kg/m2)	25 ± 4.7	26 ± 4.2	28 ± 3.6	26 ± 5.1	0.26
SBP (mmHg)	121 ± 8	137 ± 16	136 ± 18	145 ± 18	0.84
DBP (mmHg)	66 ± 5	73 ± 9	75 ±11	72 ± 16	0.78
HR (bpm)	55 ± 7	63 ± 13	65 ± 17	60 ± 11	0.38
Glucose (mmol/L),	-	5.0 ± 0.2	5.4 ± 0.9	5.8 ± 1.5	0.16
FFA (mmol/L)	-	0.53 ± 0.1	0.69 ± 0.3	0.66 ± 0.4	0.27
Butyrate (mmol/L)	-	0.11 ± 0.0	0.13 ± 0.1	0.15 ± 0.1	0.14
TC (mmol/L),	-	4.6 ± 0.8	4.7 ± 0.9	4.4 ± 0.7	0.77
TG (mmol/L),	-	0.98 ± 0.3	1.1 ± 0.6	0.96 ± 0.2	0.91
NT-pro BNP(pg/ml)	-	248 ± 108	442 ± 388	584 ± 829	0.30
AF, %	0 (0)	2 (7)	3 (14)	1(4)	0.51
Hypertension, %	2 (15)	9 (30)	8 (36)	9 (41)	0.65
Peak AVG, mmHg	9.2 ± 4.3	31.8 ± 6.8	50.4 ± 7.3	81.6 ± 13.3	<0.001
LVWT, mm	9.0 ± 1.1	13.3 ± 2.8	13.8 ± 2.3	15.9 ± 2.7	<0.001
AVA, cm2	3.7 ± 0.63	1.31 ± 0.26	1.16 ± 0.22	0.85 ± 0.19	<0.0001

Vmax, m/sec	1.5 ± 0.29	2.6 ± 0.19	3.2 ± 0.19	4.1 ± 0.53	<0.0001
LVEDV(ml)	143 ± 32	156 ± 52	150 ± 31	156 ± 33	0.71
LVESV(ml)	54 ± 18	65 ± 32	53 ± 15	55 ± 17	0.49
LV SV(ml)	90 ± 17	91 ± 22	97 ± 22	98 ± 23	0.67
LVMI (g/m2)	59 ± 14	56 ± 11	68 ± 13	75 ± 15	0.0003
LVEF (%)	59 ± 14	60 ± 8	64 ± 6.5	67 ± 8	0.02
GLS (%)	-15 ± 1.7	-13 ± 2.4	-12 ± 2.8	-11 ± 2.4	0.003
GCS(%)	-18 ± 2.4	-16 ± 2.5	-16 ± 4.1	-16 ± 4.0	0.53
DLSR (100/s)	33 ± 11	32 ± 9	27 ± 10	22 ± 8	0.003
CSR (100/s)	76 ± 14	51 ± 18	54 ± 22	47 ± 19	0.001
LA volume (ml)	61 ± 13	70 ± 33	71 ± 24	85 ± 30	0.08
RV EF (%)	60 ± 4	59 ± 6.2	61 ± 6	62 ± 5	0.30
PCr/ATP	1.77 ± 0.28	1.53 ± 0.47	1.49 ± 0.51	1.46 ± 0.43	0.03*
MTG (%)	1.17 ± 0.19	1.50 ± 0.87	1.66 ± 0.63	1.79 ± 1.11	0.05*

Healthy volunteer and mild AS group data were combined and then whole data divided into quartiles based on LVWT and pressure gradients to understand the relationship between wall thickness, pressure gradient and metabolic parameters.

Overall, mean age of the population in quartile 1 (Q1), which included normal controls was younger (mean age ~ 55 years) than the rest of the quartiles with AS participants (mean age ~ 71 years). This seems a fair representation of the real-world population with those characteristics.

All results were separated into the three groups and each discussed in detail below.

3.6.2 The Relationship between hypertrophy and metabolism

This analysis involved 87 participants separated into quartiles based on LV wall thickness.(Table 3.2 and Figure 3.2). LV wall thickness was measured as the maximal basal diameter in SA slice in end-diastole.

3.6.2.1 Demographic and clinical characteristics of LVWT quartiles

Patients in Q1 were relatively younger (mean age 53 ± 15 years) compared to Q2 (mean age 71 ± 10 years), p <0.001. There was no significant difference in age between Q2 to Q4. Similarly, systolic blood pressure was lower in Q1 (126 ± 11 mmHg) compared to rest of the quartiles (p<0.001). No significant difference in BP was noted between Q2 to Q4. All quartiles had more number of males than females.

All quartiles (Q1 to Q4) were matched in rest of the characteristics with no significant difference in blood glucose, free fatty acids, total cholesterol and triglyceride levels. Refer to **Table 3.1** below:

Table 3.1: ***Demographics, clinical and biochemical characteristics in group based on LVH. Values are expressed as mean ± SD for continuous data and frequency (percentages) for categorical data. P values are for 1-way ANOVA for all groups unless specified. † Significant.*** *AS indicates aortic stenosis; BMI, body mass index; BP, blood pressure; FFA, free fatty acids; HDL, high density lipoprotein; BNP, brain natriuretic peptide; ARB, Angiotensin Receptor Blockers; ACE-I, Angiotensin Converting Enzyme Inhibitors.*

Quartiles based on LVH	**Q1 (n=23)**	**Q2 (n=21)**	**Q3 (n=22)**	**Q4 (n=21)**	**P value**
LV wall thickness (mm)	9.6 ± 0.8	12.5 ± 0.5	14.5 ± 0.7	17.6 ± 1.3	**<0.001†**
Demographics data					
Age (years)	53 ± 15	71 ± 10	69 ± 14	74 ± 11	***<0.001†***
Male, n (%)	9 (39)	16 (76)	15 (68)	21(100)	***<0.001†***
BMI(kg/m^2)	25 ± 5	27 ± 5	27 ± 4	28 ± 4	0.15
Clinical data					
Systolic BP (mmHg)	126 ± 11	147 ± 16	139 ± 21	140 ± 14	***<0.001†***
Diastolic BP (mmHg)	75 ± 12	72 ± 9	75 ± 8	72 ± 8	0.67
Heart rate (bpm)	63 ± 11	63 ± 11	66 ± 12	64 ± 9	0.80
Hypertension, n (%)	4 (17)	6 (29)	4 (18)	14 (66)	***<0.001†***
Atrial Fibrillation	1 (4)	1 (5)	4 (18)	2 (10)	0.36
Biochemical parameters					
Blood glucose (mmol/L)	5.0 ± 0.6	5.2 ± 0.5	5.3 ± 0.8	5.8 ± 1.5	0.12
FFA (mmol/L)	0.80 ± 0.5	0.55 ± 0.2	0.70 ± 0.3	0.62 ± 0.3	0.21
Butyrate (mmol/L)	0.15 ± 0.1	0.09 ± 0.0	0.14 ±0.1	0.15 ± 0.1	0.12
Total cholesterol (mmol/L)	4.4 ± 0.8	4.6 ± 0.8	4.5 ± 0.9	4.4 ± 1.0	0.80
Triglycerides (mmol/L)	1.0 ± 0.4	0.96 ± 0.2	1.1 ± 0.5	0.93 ± 0.4	0.80
NT-pro BNP (ng/L)	140 ± 104	245 ± 327	442 ± 603	537 ± 868	0.24
Medications					
Beta blockers	3 (13)	1 (5)	1 (5)	4 (19)	0.44
ARB/ACE-I	4 (17)	6 (29)	4 (18)	14 (66)	0.004
Diuretics	0	1 (5)	2 (9)	3 (14)	0.81
Statins	3 (13)	11 (52)	6 (27)	10 (48)	0.26

3.6.2.2 Left ventricular structure and function (LVWT quartiles)

LV wall thickness increased across the quartiles (9.6 mm in Q1 vs 17.6mm in Q4, p <0.001). LV mass index (LVMI; 50 ± 12.5 kg/m^2 in Q1 vs 81 ± 13 kg/m2 in Q4, p <0.001) and LV end-diastolic volumes (LVEDV; 135 ± 33 ml in Q1 vs 163 ± 28 ml Q4, p = 0.04) also showed a step wise increase across the quartiles. LV ejection fraction was normal throughout the quartiles and not changed.

Peak systolic longitudinal strain (LS; normal range -15 to -20 %) whilst normal in Q1 (-15 ± 0.97 %) was reduced across the increasing wall thickness quartiles (-10 ± 1.8 % in Q4; p <0.001). LS also correlated positively with LVMI (R = 0.39, p<0.001). Peak systolic circumferential strain (CS) despite reducing numerically across the quartiles (Q1 -18.6 ± 1.8 % vs Q4 -15.7 ± 2.9%; p = 0.03), overall remained in the normal range (-15 to -20%).[234] LV diastolic function assessed by early diastolic longitudinal strain rate (normal range 41 to 136 %/s), and early diastolic circumferential strain rate normal range 22 to 145 %/s)[235] showed a significant step-wise reduction across the increasing LVWT quartiles as shown in **Table 3.2**. Overall, this shows that in asymptomatic AS with normal LVEF, early diastolic and subclinical LV systolic dysfunction occurs early even in the presence of modest hypertrophy (12mm in Q2). When controlled for AV gradient, there was significant correlation between LVWT and peak systolic longitudinal strain (r = -0.53, p<0.001), peak systolic circumferential strain (r = -0.37, p = 0.003) and diastolic circumferential strain (r = -0.29, p = 0.02), **Table 3.3**.

Table 3.2: Cardiac structure and function in groups based on LVH.
Values are mean ± SD or frequency (percentages). *AV, aortic valve; LV, left ventricle; LA, left atrium; RV, right ventricle; LGE, late gadolinium enhancement; ECV, extracellular volume; LA, left atrium; RV, right ventricle; MTG, myocardial triglyceride content; PCr/ATP, Phosphocreatine/adenosine triphosphate. P values are for 1-way ANOVA for all groups († significant), except cardiac metabolism where ordered medians were compared using Jonckheere-Terpstra test (* significant).*

Quartiles based on WT	**Q1(n=23)**	**Q2(n=21)**	**Q3 (n=22)**	**Q4(n=21)**	**P value**
LV wall thickness (mm)	9.6 ± 0.8	12.5 ± 0.5	14.5 ± 0.7	17.6 ± 1.3	**<0.001†**
AV parameters					
AV gradient, mmHg	24 ± 22	42 ± 17	47 ± 16	69 ±25	**<0.001†**
Aortic valve area, cm^2	2.5 ± 1.5	1.3 ± 0.5	1.0 ± 0.3	0.96 ± 0.3	**<0.001†**
Peak velocity, m/sec	2.2 ± 0.98	3.2 ± 0.7	3.3 ± 0.6	3.9 ± 0.8	**<0.001†**
LV parameters					
LV end-diastolic volume (ml)	135 ± 33	145 ± 31	157 ± 40	163 ± 28	**0.04†**
LV end-systolic volume (ml)	51 ± 16	51 ± 14	59 ± 22	58 ± 17	0.30
LV stroke volume (ml)	83 ± 18	95 ± 24	98 ± 22	101 ± 21	**0.04†**
LV mass index (kg/m^2)	50 ± 12.5	63 ± 9.6	73 ±11	81 ± 13	**<0.001†**
LV ejection fraction (%)	63 ± 4	65 ± 7	63 ± 7	65 ± 8	0.57
Longitudinal strain (%)	-15 ± 0.97	-12.6 ± 2.9	-12.3 ± 2.6	-10 ± 1.8	**<0.001†**
Circumferential strain (%)	-18.6 ± 1.8	-17 ± 4.3	-17.4 ± 3.7	-15.7 ± 2.9	**0.03†**
Diastolic long strain rate (/s)	26 ±13	28 ± 13	24 ± 8	21 ± 7	**0.02†**
Diastolic circ strain rate (/s)	69 ± 17	50 ± 24	48 ± 17	45 ± 19	**0.0007†**
LGE present, n (%)	0	5 (24)	9 (40)	17 (81)	**<0.001†**
ECV (%)	28 ± 4.1	27 ± 2.5	29 ± 7.2	30 ± 7.9	**<0.001†**
Native T1 (ms)	1130 ± 28	1119 ± 32	1142 ± 83	1157 ± 56	0.28
Other parameters					
LA volume (ml)	60 ± 22	66 ± 19	100 ± 45	74 ± 28	**<0.001†**
RV ejection fraction (%)	60 ± 5	62 ± 6	62 ± 6	61 ± 5	0.41
Cardiac metabolism					
MTG, %	1.38 ± 0.18	1.60 ± 0.15	1.70 ± 0.24	1.54 ± 0.16	0.29
PCr/ATP	1.80 ± 0.10	1.43 ± 0.09	1.54 ± 0.08	1.39 ± 0.09	**0.02***

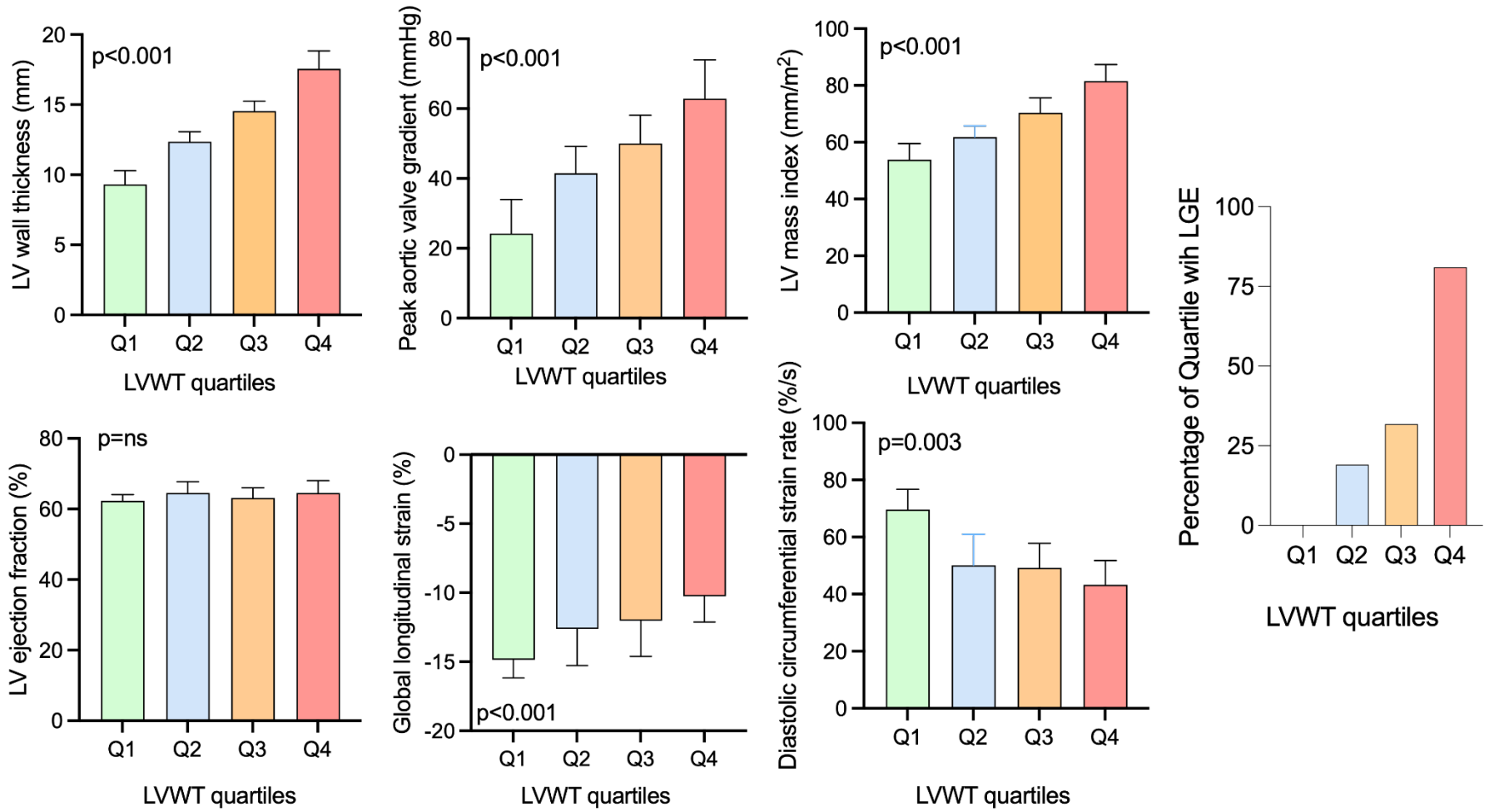


Figure 3.2: Graphic representation of LV structure and function in relation to LV wall thickness quartiles*. Green represents quartile (Q) 1 with wall thickness 9.6 ± 0.8 mm, Blue represents Q2, wall thickness 12.5 ± 0.5 mm, Orange represents Q3, wall thickness 14.5 ± 0.7 mm, Red represents Q4, wall thickness 17.6 ± 1.3 mm. All p values are from 1-way ANOVA comparison of means. P <0.05 is significant.*

3.6.2.3 Myocardial metabolism (LVWT quartiles)

Myocardial PCr/ATP was reduced 23% across the LVWT quartiles (ordered medians JT test, p = 0.02) suggesting that as WT is increased PCr/ATP is lower. However, the vast majority of the reduction in the PCr/ATP (20%) occurred between Q1 and Q2, (Q1 PCr/ATP 1.8 ± 0.51 vs Q2 1.43 ± 0.39; p = 0.01). In addition, when controlled for AV gradient, Age and BMI, the significant relationship between LVWT quartiles and PCr/ATP remained (r = -0.20, p = 0.04).

Myocardial triglyceride content was numerically higher in Q2 (1.60 ± 0.15%) compared to Q1 (1.38 ± 0.18%) which again highlights the presence of early metabolic changes represented by steatosis with values remaining higher across Q2-4 compared to Q1. The numerical reduction in myocardial lipid content between Q3 and Q4 (1.70 ± 0.24% vs 1.54 ± 0.08%) may be explained by higher prevalence of replacement fibrosis with disease severity. The important finding, however, is that steatosis occurs early and is not progressively related to WT as indicated by the absence of a stepwise increase in MTG across the quartiles (JT ordered medians p=0.29). Refer to **Table 3.2** and **Figure 3.3.** On partial correlation, controlling for AVG, Age and BMI, there was a significant association between MTG and LVWT (r = -0.27, p = 0.03).

On multivariate regression analysis with LVWT as dependent variable and LV gradient, MTG, Age, BMI and PCr/ATP as independent variables, only LV gradient (β = 0.44, p = <0.001), BMI (β = 0.26, p = 0.006) and PCr/ATP (β = -0.20, p = 0.03) were independent predictors of LVWT. Thus, myocardial energetics may play an important role in the hypertrophic process.

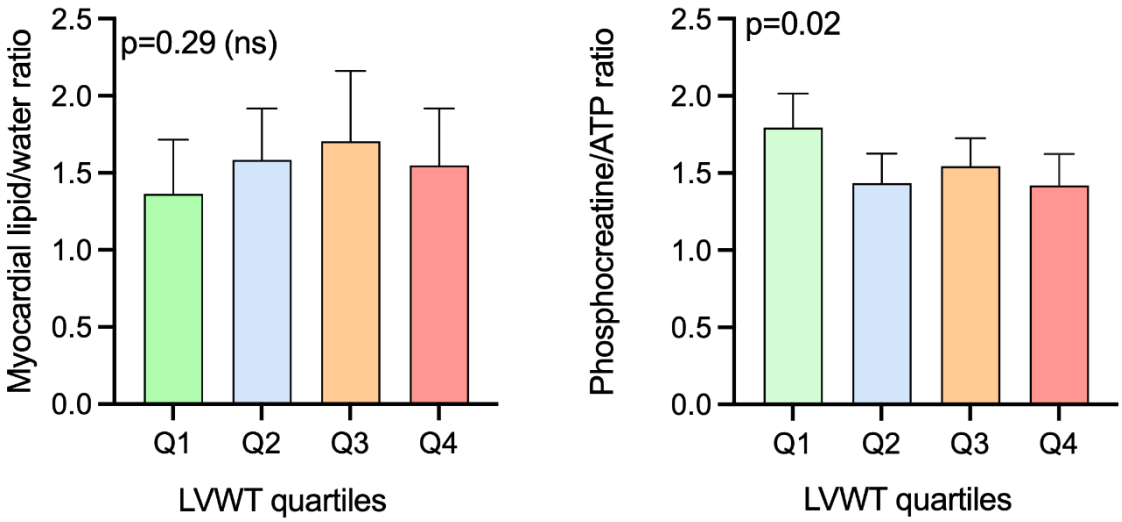


Figure 3.3: ***Graphic representation of cardiac metabolism characteristics in relation to LV wall thickness quartiles****. Green represents quartile (Q) 1 with wall thickness 9.6 ± 0.8 mm, Blue represents Q2, wall thickness 12.5 ± 0.5 mm, Orange represents Q3, and wall thickness 14.5 ± 0.7 mm, Red represents Q4, wall thickness 17.6 ± 1.3 mm. All p values are from Jonckheere-Terpstra test comparison of ordered medians. P <0.05 is significant.*

3.6.2.4 Myocardial Fibrosis on T1 mapping, extracellular volume (ECV) quantification and Late Gadolinium Enhancement (LGE) Imaging

T1 and ECV: Myocardial native T1 values were not changed across the quartiles (**Table 3.2**, p = 0.29), and remained within normal limits (normal range 1096-1212ms at 3T for our centre). In contrast, ECV progressively increased across the quartiles (Q1 28 ± 4.1% vs Q4 30 ± 7.9%, p<0.001), being abnormally high in Q3 and Q4, as shown in **Table 3.2**; normal ECV range (20.5%– 34.5%).[250]

LGE: The presence of late gadolinium enhancement was also seen to increase progressively across the quartiles, with highest % of cases in Q4 (81% in Q4 vs 0% in Q1, p <0.001). None of the patients had any evidence of infarction. Most patients with LGE enhancement had basal inferolateral fibrosis. Patients with non-specific LV/RV junction enhancement alone were considered to have no significant fibrosis and were reported as negative on LGE assessment. These findings are consistent with previous studies which have shown that replacement fibrosis appears to occur later and is irreversible. [251]

There was significant correlation between wall thickness and myocardial fibrosis on LGE (Rs = 0.61, p <0.001). There was also significant group difference between LVWT and LGE, with presence of LGE as grouping variable (p<0.001) . Presence of LGE was negatively associated with cardiac energetics, PCr/ATP (p =0.011), **Figure 3.4.** There was no significant relationship seen between steatosis and myocardial fibrosis (diffuse or replacement).

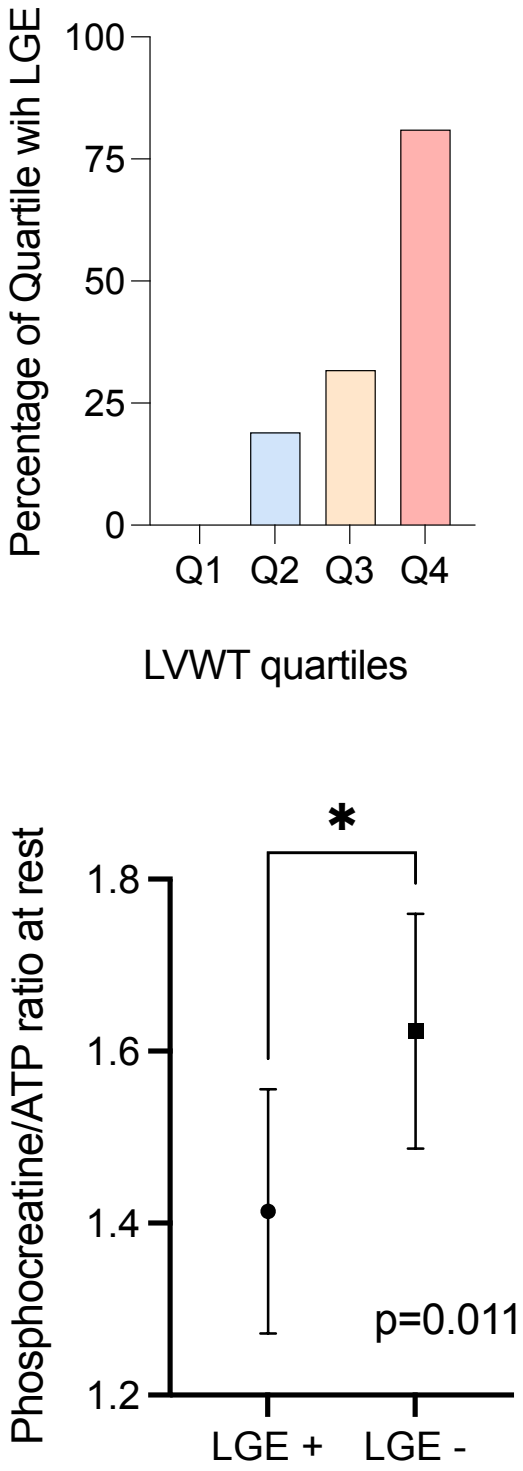


Figure 3.4: *Upper panel shows the relationship between replacement fibrosis (presence of late gadolinium enhancement) and LV wall thickness quartiles. Lower panel shows myocardial replacement fibrosis and cardiac energetics (Phosphocreatine/ATP ratio).*

Table 3.3: Correlation between LV wall thickness and LV specific functional and metabolic parameters when controlled for both AV and LV gradient. *Results from partial correlation when controlled for AVG and LVG. P<0.05 significant. LV, left ventricle; long, longitudinal; circ, circumferential; LGE, late gadolinium enhancement; MTG, myocardial triglyceride content; PCr/ATP, Phosphocreatine/Adenosine triphosphate ratio.*

Correlation with WT	r	P value
LV function and fibrosis		
Global long. strain (%)	-0.53	**<0.001***
Global circ. strain (%)	-0.37	**0.003***
Diastolic circ. strain rate (100/s)	-0.29	**0.02***
Presence of LGE	0.43	**<0.001***
Cardiac metabolism		
MTG (lipid/water ratio)	-0.12	0.33
PCr/ATP	-0.29	**0.02***

3.6.3 AS related pressure overload quartiles

3.6.3.1 Demographic and clinical characteristics

Participants in Q1 were relatively younger (mean age 58 ± 16 years) with lower average systolic BP (136 ± 18 mmHg) compared to rest of the quartiles (p<0.001). Q2 to Q4 were matched in age and BP. All quartiles (Q1 to Q4) were matched in rest of the characteristics with no significant difference in blood glucose, free fatty acids, total cholesterol and triglyceride levels. Refer to **Table 3.4** below

Table 3.4: ***Demographics, clinical and biochemical characteristics in group based on peak AV gradient: Values are mean ± SD for continuous data and frequency (percentages) for categorical data. P values are for 1-way ANOVA for all groups unless specified. † Significant.*** *AVG indicates aortic valve gradient; BMI, body mass index; BP, blood pressure; HDL, high density lipoprotein; BNP, brain natriuretic peptide; ARB, Angiotensin receptor blocker; ACE-I, Angiotensin converting enzyme inhibitors.*

Quartiles based on AVG	Q1 (n=21)	Q2 (n=22)	Q3 (n=21)	Q4 (n=21)	P value
AV gradient (mmHg)	16 ± 8	36 ± 4	49 ± 6	79 ± 14	**<0.001†**
Demographics data					
Age (years)	58 ± 16	68 ± 11	67 ± 17	74 ± 14	**0.005†**
Male, n (%)	9 (39)	16 (76)	15 (68)	21(100)	**<0.001†**
BMI (kg/m^2)	26 ± 5	27 ± 4	28 ± 5	26 ± 5	0.74
Clinical data					
Systolic BP (mmHg)	136 ± 18	135 ± 14	141 ± 20	141 ± 17	0.53
Diastolic BP (mmHg)	77 ± 11	72 ± 9	72 ± 8	72 ± 8	0.14
Heart rate (bpm)	65 ±12	64 ±11	63 ± 11	64 ± 9	0.95
Hypertension, n (%)	6 (23)	8 (36)	5 (24)	9 (43)	0.51
Atrial Fibrillation, n (%)	2 (1)	1 (4)	3 (14)	2 (10)	0.75
Biochemical parameters (mmol/L)					
Blood glucose	5 ± 0.5	5.1 ± 0.9	5.4 ± 0.4	5.5 ± 1.1	0.27
Free fatty acids	0.59 ± 0.2	0.58 ± 0.2	0.65 ± 0.2	0.74 ± 0.4	0.46
Betahydroxy-butyrate	0.11 ± 0.0	0.14 ± 0.1	0.11 ± 0.1	0.15 ± 0.1	0.48
Total Cholesterol	4.7 ± 0.9	4.3 ± 0.8	4.6 ± 0.7	4.3 ± 0.8	0.19
Triglycerides	1.2 ± 0.5	0.99 ±0.4	1.1 ± 0.3	0.89 ± 0.4	0.19
NT-pro BNP (ng/L)	199 ± 252	221 ± 216	327 ± 578	608 ± 838	0.17
Medications					
Beta blocker, n (%)	2 (1)	3 (14)	1 (5)	3 (14)	0.72
ARB/ACE-I, n (%)	6 (23)	8 (36)	5 (24)	9 (43)	0.51
Diuretics, n (%)	0	3 (14)	0	3 (14)	0.08
Statins, n (%)	5 (22)	8 (36)	7 (33)	10 (48)	0.36

3.6.3.2 LV structure and function

This analysis involved 87 participants separated into quartiles based on peak AV gradient, measure of degree of pressure overload secondary to AS (**Table 3.5** and **Figure 3.5**).

With increasing pressure load secondary to AS, there was an increase in LV wall thickness (Q1 10.4 ± 2.3 vs 15.8 ± 2.6 mm; p <0.001). As expected, LVMI and LVEF was higher in Q 2-4 compared to Q1, with the difference across the groups being significant (p = 0.009 and p = 0.034, respectively).

Global systolic longitudinal strain reduced across the increasing pressure gradient quartiles (-13.8±2.2% in Q1 vs -10.6±2.5% in Q4; p <0.001) along with impairment in diastolic function, including early diastolic circumferential strain rate (Q1 66 ± 21 vs Q4 43 ± 19 100/s; p <0.001) with a step wise reduction across the ordered groups.

On partial correlation controlling for LV wall thickness, only peak systolic circumferential strain had an association with AVG. See **Table 3.6**.

Table 3.5: Cardiac structure and function in groups based on peak AV gradient. Values are mean ± SD or frequency (percentages). *AVG indicates aortic valve gradient; LV, left ventricle; LA, left atrium; RV, right ventricle; LGE, late gadolinium enhancement; ECV, extracellular volume. P values are for 1-way ANOVA for all groups unless specified (<0.05 significant). † Significant.*

Groups based on AVG	Q1 (n=23)	Q2 (n=22)	Q3 (n=21)	Q4 (n=21)	P value
Peak AV gradient, mmHg	16 ± 8	36 ± 3.8	49 ± 6	79 ± 14	<0.001†
AV parameters					
AV gradient, mmHg	10.4 ± 2.3	13.8 ± 3.0	13.6 ± 2.3	15.8 ± 2.6	<0.001†
Aortic valve area, cm^2	2.6 ± 1.3	1.2 ± 0.23	1.0 ± 0.3	0.8 ± 0.2	<0.001†
Peak velocity, m/sec	1.9 ± 0.5	2.9 ± 0.17	3.4 ± 0.2	4.3 ± 0.5	<0.001†
LV Parameters					
LV end-diastolic volume (ml)	139 ± 32	155 ± 39	146 ± 34	160 ± 30	0.21
LV end-systolic volume (ml)	53 ± 17	60 ± 22	49 ± 13	58 ± 18	0.13
LV stroke volume (ml)	86 ± 17	94 ± 23	98 ± 27	98 ± 20	0.27
LV mass index (kg/m^2)	53 ± 16	70 ± 14	64 ±15	77 ± 14	0.009†
LV WT (mm)	10.4 ± 2.3	13.8 ± 3.0	13.6 ± 2.3	15.8 ± 2.6	<0.001
LV ejection fraction (%)	63 ± 5	61 ± 6	66 ± 7	64 ± 7	0.034†
Longitudinal strain (%)	-13.8 ± 2.2	-12.6 ± 2.6	-12.5 ± 2.6	-10.6 ± 2.5	<0.001†
Circumferential strain (%)	-17.4 ± 2.5	-15.7 ± 2.6	-17.3 ± 4.5	-16.8 ± 3.1	0.20
Diastolic long strain rate (/s)	25 ± 12	29 ± 13	25 ± 8	21 ± 8	0.18
Diastolic circ strain rate (/s)	69 ± 19	45 ± 18	57 ± 21	46 ± 21	<0.001†
LGE present, n (%)	3 (13)	7 (32)	5 (24)	15 (71)	<0.001†
ECV (%)	30±5.8	28±7.2	27±4.9	29±5.7	<0.001†
Native T1 (ms)	1164±54	1125±40	1112±71	1173±16	0.003
Other parameters					
LA volume (ml)	67 ± 27	74 ± 43	80 ± 33	78 ± 29	0.63
RV ejection fraction (%)	60 ± 4	61 ± 7	63 ± 6	61 ± 5	0.60
Cardiac metabolism					
MTG (%)	1.27±0.7	1.53±0.84	1.64±0.64	1.79±1.03	0.034 *
PCr/ATP	1.65±0.34	1.55±0.52	1.49±0.55	1.47±0.40	0.056

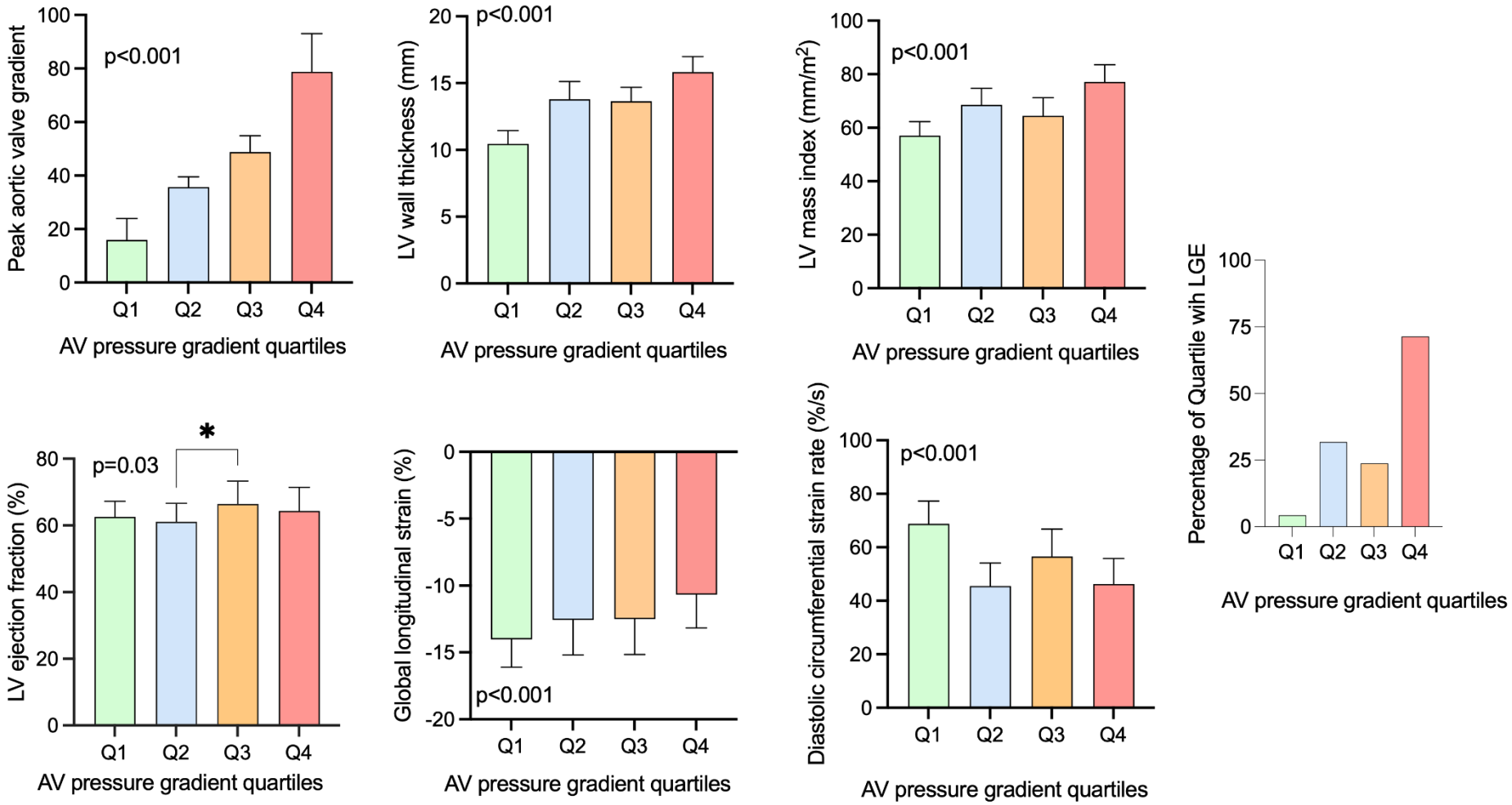


Figure 3.5: ***Graphic representation of LV structure and function in relation to AV pressure gradient quartiles.*** *Green represents quartile (Q) 1 with peak aortic valve gradient (AVG) 16 ± 8 mmHg, Blue represents Q2, AVG 36 ± 3.8 mmHg, Orange represents Q3, AVG 49 ± 6 mmHg, Red represents Q4, AVG 79 ± 14 mmHg. All p values are from 1-way ANOVA comparison of means. P <0.05 is significant.*

3.6.3.3 Myocardial metabolism

Myocardial PCr/ATP was numerically reduced across the increasing AV pressure gradient quartiles (ordered medians JT test, p=0.056). In contrast, myocardial triglyceride content increased significantly (by 40%) across the increasing AVG quartiles (JT ordered medians p=0.03, **Table 3.5**). However, on partial correlation analysis once controlled for LVWT, there was no significant relationship between AVG quartiles and PCr/ATP (r = -0.02, p = 0.99), but that with MTG content remained borderline significant (r = 0.17, p = 0.07).

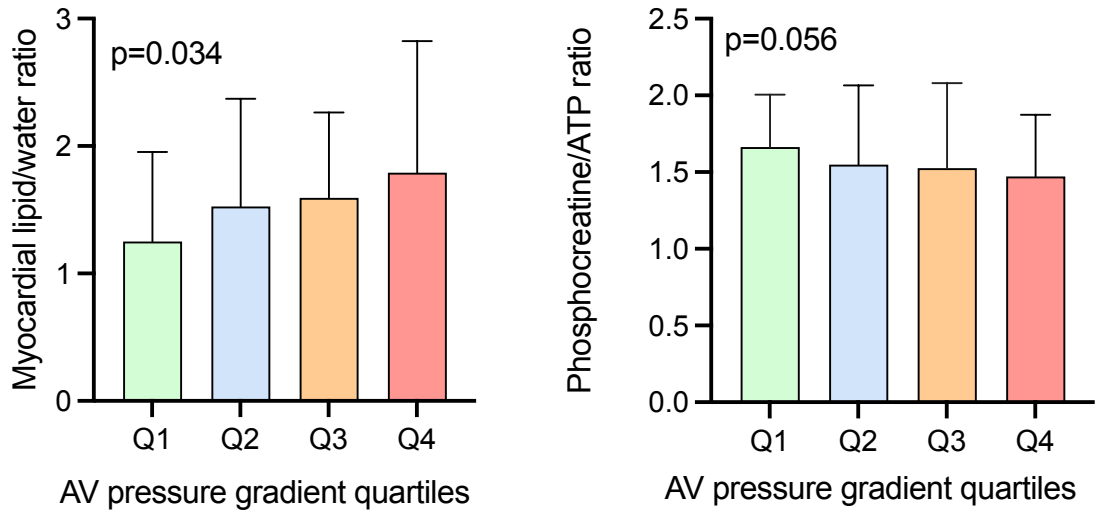


Figure 3.6: Graphic representation of cardiac metabolism characteristics in relation to AV pressure gradient. *Green represents quartile (Q) 1 with peak aortic valve gradient (AVG) 16 ± 8 mmHg, Blue represents Q2, AVG 36 ± 3.8 mmHg, Orange represents Q3, AVG 49 ± 6 mmHg, Red represents Q4, AVG 79 ± 14 mmHg. All p values are from Jonckheere-Terpstra test comparison of ordered medians. P <0.05 is significant.*

3.6.3.4 Myocardial Fibrosis on T1 mapping, extracellular volume (ECV) quantification and late Gadolinium Enhancement Imaging

T1 and ECV: Native T1 and ECV overall remained within normal range within the quartiles. But were numerically lower in Q2-3 and then increased in Q4. The difference between the quartiles was statistically significant ($p<0.001$).**Table 3.5**.

Late gadolinium imaging: Areas of LGE were identified in overall 34% of patients with increasing prevalence across the quartiles, highest in Q4. The predominant pattern of LGE was patchy, involving mainly the basal inferior and inferolateral wall.

On controlling for LVWT, there was no significant relationship between presence of LGE and AVG ($r = 0.18$, $p = 0.15$).See **Table 3.6 below.**

Table 3.6: Partial correlation between AV gradient and main LV function and metabolism parameters when controlled for LVWT. *LV, left ventricle; long, longitudinal; circ, circumferential; LGE, late gadolinium enhancement; MTG, myocardial triglyceride content; PCr/ATP, Phosphocreatine/Adenosine triphosphate ratio.*

AVG Variables (controlled for LVWT)	r	P value
LV function and fibrosis		
Global long strain (%)	-0.08	0.49
Global circ strain (%)	-0.27	**0.03**
Diastolic circumferential strain rate (/s)	-0.05	0.69
Presence of LGE	0.18	0.15
Cardiac metabolism		
MTG (lipid/water ratio)	0.17	0.07
PCr/ATP	-0.01	0.99

3.6.4 LV pressure gradient quartiles

As the LV is subject to the combination of afterload from both systemic arterial blood pressure and aortic valve obstruction I next sought to investigate the relationship between total LV pressure load and metabolic remodelling. For this analysis all 87 participants were divided into quartiles based on total LV gradient (i.e. AVG + SBP).

3.6.4.1 Demographic and clinical characteristics

Participants in Q1 were relatively younger (mean age 55 ± 13 years) with lower average systolic BP (124 ± 10 mmHg) compared to rest of the quartiles (both $p<0.001$ on group ANOVA). Age and systolic BP increased across Q2 to Q4. All quartiles (Q1 to Q4) were matched in rest of the characteristics with no significant difference in blood glucose, free fatty acids, total cholesterol and triglyceride levels. See **Table 3.7**.

Table 3.7: Demographics, clinical and biochemical characteristics in group based on total LV gradient*. Values are mean ± SD for continuous data and frequency (percentages) for categorical data. P values are for 1-way ANOVA for all groups unless specified. † Significant. AS indicates aortic stenosis; BMI, body mass index; BP, blood pressure; HDL, high density lipoprotein; BNP, brain natriuretic peptide; ARB, Angiotensin receptor blocker; ACE-I, Angiotensin converting enzyme inhibitors.*

Groups based on LVG	**Q1 (n=22)**	**Q2 (n=23)**	**Q3 (n=20)**	**Q4 (n=22)**	**P value**
Total LV gradient (mmHg)	142 ± 14	170 ± 6	193 ± 8	223 ± 18	<0.001†
Demographics data					
Age (years)	55 ± 13	65 ± 17	70 ± 12	77 ± 10	<0.001†
Male, n (%)	12 (55)	17 (74)	16 (80)	16(73)	0.30
BMI(kg/m2)	25 ± 4	28 ± 4	26 ± 5	27 ± 5	0.42
Clinical data					
Systolic BP (mmHg)	124 ± 10	134 ± 11	143 ± 17	152 ± 18	<0.001†
Diastolic BP (mmHg)	73 ± 12	74 ± 8	73 ± 9	74 ± 7	0.95
Heart rate (bpm)	64 ± 13	66 ± 10	60 ± 10	65 ± 9	0.21
Hypertension, n (%)	5 (23)	8 (35)	6 (30)	9 (41)	0.63
Atrial Fibrillation, n (%)	2 (9)	1 (4)	2 (10)	3 (14)	0.76
Biochemical parameters					
Blood glucose (mmol/L)	5.1 ± 0.6	5.1 ± 0.8	5.2 ± 0.5	5.5 ± 1.0	0.23
FFA (mmol/L)	0.53 ± 0.2	0.62 ± 0.2	0.78 ± 0.4	0.64 ± 0.2	0.18
Total cholesterol (mmol/L)	4.5 ± 0.9	4.6 ± 0.7	4.4 ± 0.8	4.6 ± 0.9	0.85
Triglycerides (mmol/L)	1.1 ± 0.3	1.1 ± 0.4	0.98 ± 0.4	1.03 ± 0.6	0.94
NT-pro BNP (ng/L)	228 ± 281	313 ± 587	263 ± 432	521 ± 727	0.46
Medications					
Beta blockers, n (%)	3 (14)	2 (9)	2 (10)	2 (9)	0.95
ARB/ACE-I, n (%)	5 (23)	4 (18)	6 (30)	9 (41)	0.63
Diuretics, n (%)	1 (4)	2 (9)	2 (10)	1 (5)	0.86
Statins, n (%)	5 (23)	6 (26)	9 (45)	10 (45)	0.25

3.6.4.2 LV structure and function

With increasing total LV pressure overload, there was an increase in LV wall thickness (Q1 10.1 ± 2.1 vs 15.3 ± 2.5 mm; p <0.001). LVMI also increases with increasing gradient (60 ± 18 kg/m^2, Q1 vs 75 ± 16, Q4; p = 0.03). LVEF remained within normal limits in all the quartile groups, **Table 3.8.**

Pattern of strain measurement was similar to AVG gradients with global systolic longitudinal strain being reduced across the increasing LV gradient quartiles (-14.7 ± 1.4% in Q1 vs -10.6 ± 2.5% in Q4; p <0.001) along with evidence of diastolic dysfunction, mainly early diastolic circumferential strain rate (Q1 66 ± 19 vs Q4 46 ± 22 100/s; p <0.02) with a step wise reduction across the ordered groups.

When controlled for LVWT, there was no relationship between strain parameters and total LV gradient. See **Table 3.9**.

Table 3.8: Cardiac structure and function in groups based on total LV gradient. Values are mean ± SD or frequency (percentages). *LVG indicates total left ventricular gradient; LV, left ventricle; AVA, aortic valve area; LA, left atrium; RV, right ventricle; LGE, late gadolinium enhancement; ECV, extracellular volume. P values are for 1-way ANOVA for all groups unless specified (<0.05 significant). † Significant.*

Groups based on LVG	Q1 (n=22)	Q2 (n=23)	Q3 (n=20)	Q4 (n=22)	P value
Total LV gradient, mmHg	142 ± 14	170 ± 6	193 ± 8	223 ± 18	<0.001†
AV parameters					
AVA, cm^2	2.5 ± 1.3	1.3 ± 0.7	1.0 ± 0.3	0.9 ± 0.3	<0.001†
Peak velocity, m/sec	2.1 ± 0.8	2.9 ± 0.4	3.4 ± 0.7	4.0 ± 0.6	<0.001†
LV parameters					
LV wall thickness, mm	10.1 ± 2.1	13.9 ± 3.2	14.1 ± 2.3	15.3 ± 2.5	<0.001†
LV end-diastolic volume (ml)	147 ± 45	144 ± 30	152 ± 26	156 ± 35	0.67
LV end-systolic volume (ml)	56 ± 24	55 ± 14	55 ± 13	53 ± 18	0.95
LV stroke volume (ml)	91 ± 23	88 ± 21	98 ± 21	99 ± 22	0.27
LV mass index	63 ± 22	67 ± 13	69 ±12	75 ± 16	0.16
LV ejection fraction	62 ± 5	61 ± 5	64 ± 7	67 ± 7	0.032†
Systolic longitudinal strain (%)	-14.7 ± 1.4	-11.7 ± 2.6	-12.7 ± 2.5	-10.6 ± 2.5	<0.001†
Systolic circumferential strain (%)	-17.9 ± 2.4	-15.5 ± 3.1	-17.2 ± 3.3	-16.9 ± 3.6	0.11
Diastolic long strain rate (/s)	25 ± 11	25 ± 11	29 ±11	21 ± 8	0.13
Circumferential strain rate (/s)	66 ± 19	51 ± 24	52 ± 16	46 ± 22	0.02†
LGE present, n (%)	1 (5)	10 (44)	5 (25)	14 (64)	<0.001†
ECV (%)	28 ± 4.2	29 ± 8.3	28 ± 6.9	29 ± 3.3	0.81
Native T1(ms)	1120 ± 29	1126 ± 47	1120 ± 39	1176 ± 74	0.003
Other parameters					
LA volume (ml)	74 ± 45	68 ± 25	72 ± 26	86 ± 34	0.29
RV ejection fraction (%)	60 ± 5	60 ± 7	63 ± 6	63 ± 4	0.12
Cardiac metabolism					
MTG, %	1.29 ± 0.76	1.49 ± 0.73	1.72 ± 0.66	1.72 ± 1.1	0.08*
PCr/ATP	1.71 ± 0.34	1.53 ± 0.56	1.40 ± 0.42	1.52 ± 0.45	0.07*

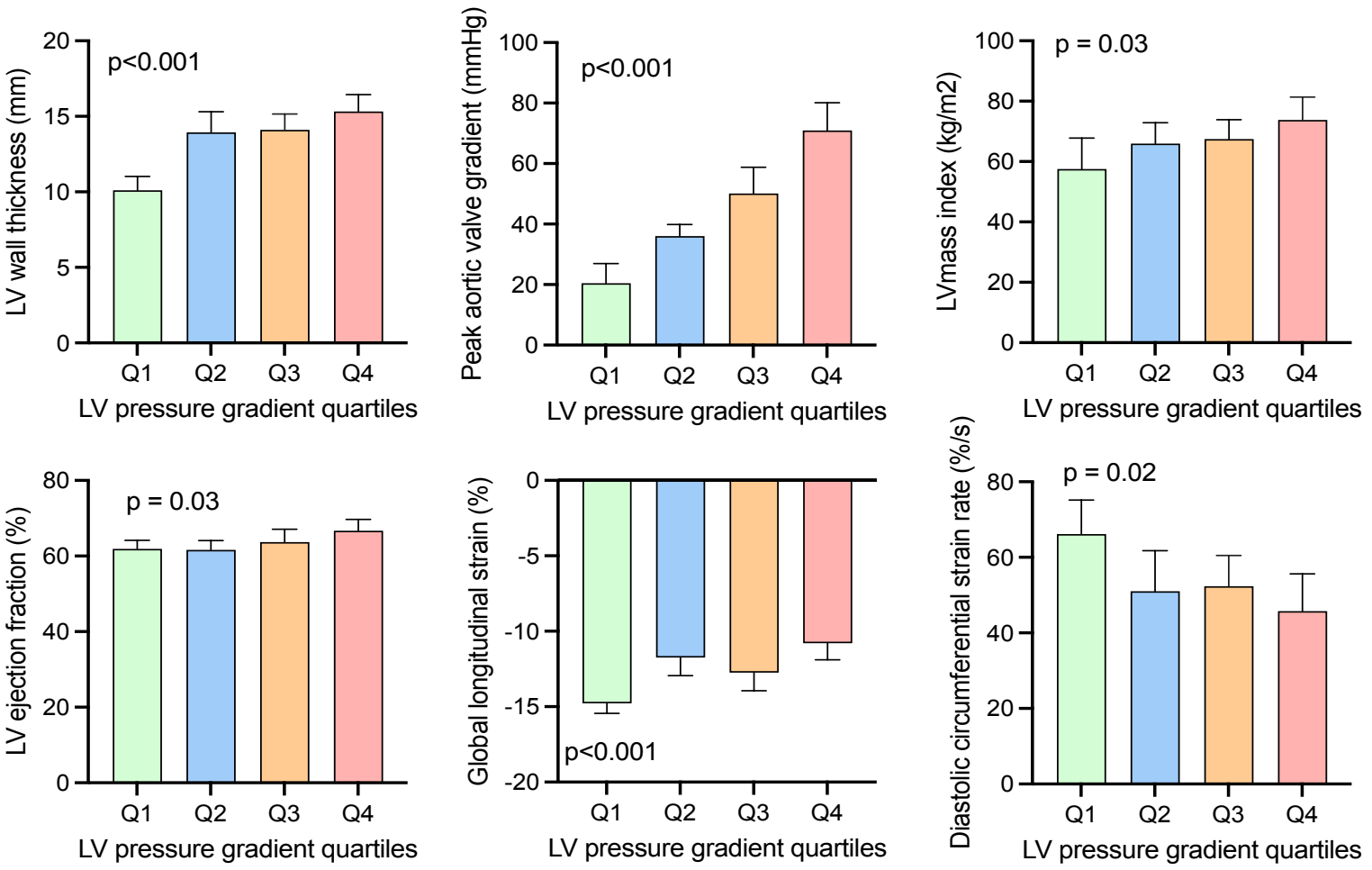


Figure 3.7: Graphic representation of main LV structure and function findings in relation to total LV gradient quartiles. *Green represents quartile (Q) 1 with peak LV gradient (LVG) 142 ± 14 mmHg, Blue represents Q2, LVG 176 ± 6 mmHg, Orange represents Q3, LVG 193 ± 8 mmHg, Red represents Q4, LVG 223 ± 18 mmHg. All p values are from 1-way ANOVA comparison of means. P <0.05 is significant*

3.6.4.3 Myocardial metabolism

Myocardial PCr/ATP reduced from Q1-Q3 before plateauing in Q4. The reduction from Q1 to Q3 was statistically significant (1.71 ± 0.34, Q1 vs 1.40 ± 0.42, Q3; p = 0.03) but the change was overall not statistically significant (ordered medians JT test, p=0.08, **Table 3.8, Figure 3.8**).

Myocardial triglyceride content increased numerically (by 35%) across the increasing AVG quartiles (JT ordered medians p=0.08, **Table 3.8**) with a 47% increase between Q1 and Q2 (1.29 ± 0.76, Q1 vs 1.49 ± 0.73, Q2).

When controlled for LVWT variable, LVG correlated significantly to MTG (r = 0.21, p = 0.03), but not to PCr/ATP (p = 0.70). This relationship was not significant when controlled for both LVWT and AVG. See **Table 3.9**

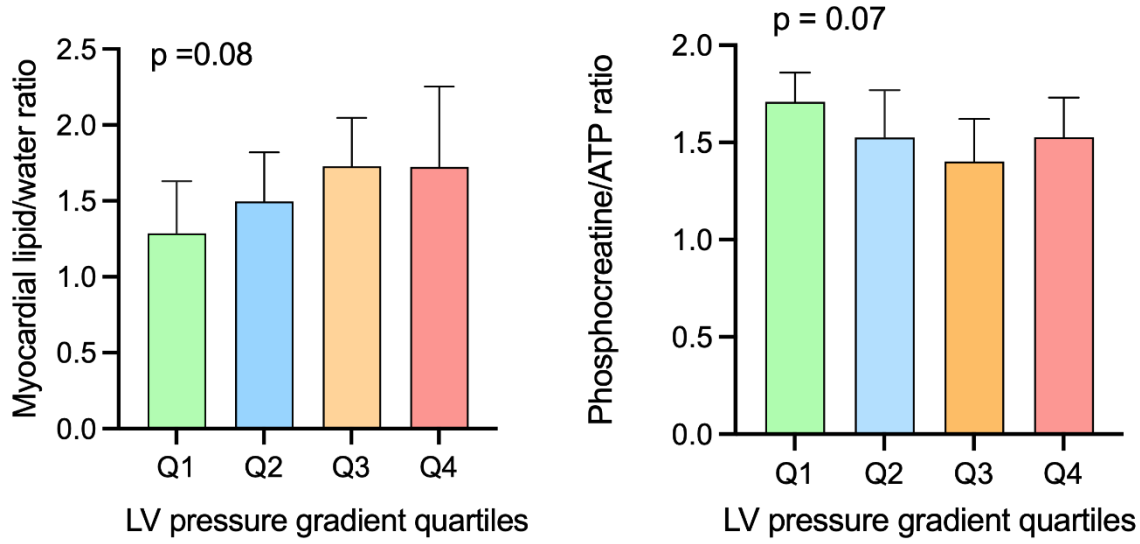


Figure 3.8: Graphic representation of cardiac metabolism characteristics in relation to LV pressure gradient. *Green represents quartile (Q) 1 with peak LV gradient (LVG) 142 ± 14 mmHg, Blue represents Q2, LVG 176 ± 6 mmHg, Orange represents Q3, LVG 193 ± 8 mmHg, Red represents Q4, LVG 223 ± 18 mmHg. All p values are from ordered medians JT test, p <0.05 significant.*

3.6.4.4 Myocardial Fibrosis on T1 mapping, extracellular volume (ECV) quantification and late Gadolinium Imaging

The relationship between myocardial fibrosis and LV pressure gradient was similar to that seen for AV gradient and as described below:

T1 and ECV: No significant trend was seen in myocardial T1 values and ECV across the LVG groups. Native T1 and ECV were low normal in Q1-3 and then increased in Q4 (1176 ± 74 ms, Q4 vs 1120 ± 29 ms, Q1). All values remained within normal range (**Table 3.8**).

Late gadolinium imaging: Percentage of those with LGE i.e. evidence of myocardial replacement fibrosis was highest in Q4 (64% Q4 vs 5% Q1). No correlation was seen between LVG and presence of LGE ($r = 0.06$, $p = 0.56$).

Table 3.9: Partial correlation between LV gradient and main LV function and metabolism parameters when controlled for LVWT.

LVG Variables (controlled for LVWT)	r	P value
LV function and fibrosis		
Global long strain (%)	0.04	0.73
Global circ strain (%)	-0.19	0.13
Diastolic circ strain rate (100/s)	-0.13	0.29
Presence of LGE	0.07	0.56
Cardiac metabolism		
MTG (lipid/water ratio)	0.24	**0.03***
PCr/ATP	0.05	0.70

3.7 Discussion

The main novel findings from this study are A) Impaired energetics and myocardial steatosis occur early in the AS disease process, this has not been studied previously. B) What initiates these changes is still unclear but there seems to be a relationship between LV hypertrophy and impairment of cardiac energetics. AV/LV gradient is more related to development of steatosis. C) In this study, the effect of LV gradient on cardiac physiology or metabolism was mainly driven by AV gradient than SBP.

3.7.1 Effect of LV hypertrophy

3.7.1.1 LV structure/function and LV hypertrophy

Whilst all LVH quartiles maintained normal EF, there was strong evidence of subclinical LV impairment in both systolic and diastolic strain parameters early in Q2 in LVH groups, which worsened with disease severity. LV peak systolic and diastolic strain impairment was driven mainly by LV hypertrophy (peak systolic longitudinal strain $p < 0.001$; peak systolic circumferential strain $p = 0.003$; Diastolic circumferential strain rate $p = 0.02$). Longitudinal contraction was impaired in Q2 whilst circumferential systolic strain was affected in Q3 and Q4. This is in keeping with previous studies which have demonstrated LVH to cause impaired longitudinal function in pressure overload despite normal EF. Circumferential and radial strain impairment occurs later and is also related to hypertrophy.[236, 237]

3.7.1.2 Cardiac metabolism and LV hypertrophy

Alterations in cardiac metabolism were seen before the development of significant LVH. In this study, abnormal myocardial lipid and energetics were present as early as Q2 in LVH group. Myocardial steatosis, measured as myocardial lipid/water ratio on ^{1}H-spectroscopy (average normal values from 10 healthy volunteers 1.20 ± 0.30%) was higher in Q2-4 but did not have a significant relationship with degree of LVH based on wall thickness. PCr/ATP, on the other hand was reduced in Q2 with only modest hypertrophy (~12mm) and worsened

overall as LVH increased, independent of AV gradient (p = 0.02). It is plausible that early metabolic changes with reduced energetics causes compensatory increase in cardiac myocyte size early in the disease process exacerbating the hypertrophic response to pressure overload. Thus, degree of metabolic impairment potentially guides the hypertrophic response and could explain the individual heterogeneity in degree of hypertrophy for same pressure overload. Another novel finding in this study was the significant relationship between impaired cardiac energetics and the presence of myocardial fibrosis (p = 0.01).

3.7.1.3 Myocardial fibrosis and LV hypertrophy

Presence of myocardial replacement fibrosis as seen on LGE was related significantly to degree of LV hypertrophy (p <0.001) than pressure overload (p = 0.15). This is in keeping with previous studies that have shown that LV hypertrophy is associated with myocyte apoptosis that result in focal sites of replacement fibrosis which may be important in the transition from compensated hypertrophy to heart failure.[238] This study has shown for the first time that presence of LGE is also accompanied by lower PCr/ATP, which in turn is related to LVH. This may explain findings from previous histological studies that have demonstrated an association between myocardial fibrosis at the time of valve replacement and both impaired recovery of LV systolic function and poor long-term outcomes following valve replacement.[239] Considering impaired energetics are seen in the group where AVG and LVH are only modestly increased, and that PCr/ATP is significantly lower in those with fibrosis on LGE, it is plausible that there may be a causal relationship between these metabolic changes that precede myocardial fibrosis and overall prognosis in AS.

Myocardial steatosis did not have any relationship with presence or absence of myocardial fibrosis in the study.

3.7.2 Effect of pressure overload (both AVG and LVG)

3.7.2.1 LV structure and function and pressure overload

The changes in LV structure and function in this study were mainly secondary to AV pressure overload. Despite both AVG and SBP being related to LVH, on regression analysis only AVG was independent predictor of LVH (r = 0.59, p <0.001). Hence the discussion for LV structure and function is limited to AV gradient quartiles only.

Both LV wall thickness and LVMI increased with increasing AV gradient quartiles. LVEF remained normal across the AV gradient quartiles, however, there was evidence of subclinical LV dysfunction with impaired longitudinal and circumferential systolic strain and strain rate with increasing disease severity. The impairment in strain was driven by LVH than AVG on regression analysis, which is expected as LV strain impairment in AS is driven by geometrical changes secondary to hypertrophy than AV gradient itself. [37, 240]

3.7.2.2 Cardiac metabolism and pressure overload

Cardiac metabolism was altered in Q2 with abnormal pressure overload (peak AVG 36 ± 18 mmHg). Myocardial lipid content increased progressively across the pressure overload quartiles (both AVG and LVG) with significant difference between the quartile groups. Moreover, on correlation analysis, myocardial steatosis was driven by both total pressure overload (r = 0.24, p = 0.03) and AV pressure overload alone (r = o.22, p = 0.05), independent of LV hypertrophy. Thus, highlighting the importance of blood pressure control in AS in preventing cardiac lipotoxicity.[241, 242] PCr/ATP ratio reduced significantly across the increasing pressure overload quartiles but this reduction did not correlate to the degree of pressure overload.

3.7.2.3 Myocardial fibrosis and pressure overload

Myocardial fibrosis was present in all pressure overload quartiles and % cases increased across the quartiles.

3.8 Blood parameters and cardiac metabolism

Circulating fatty acid levels correlated significantly with both myocardial lipid content and PCr/ATP ratio.

Rest of the analysis is represented in the correlation matrix below.

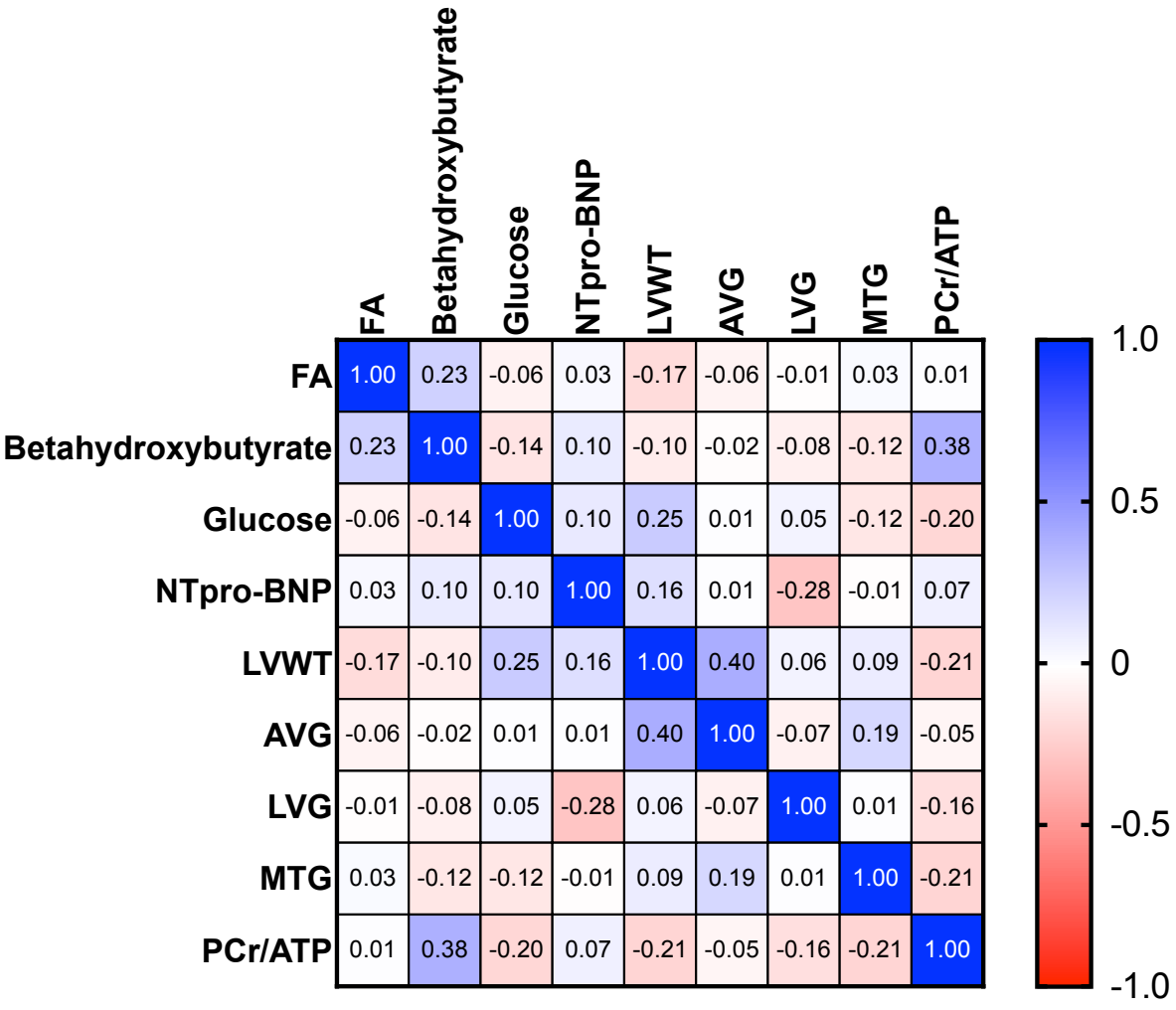


Figure 3.9: Correlation matrix representing Pearson correlation between main blood parameters and structural and metabolic parameters. FA, fatty acids, BNP, Brain natriuretic peptide; LVWT, left ventricular wall thickness; AVG, Aortic valve gradient; LVG, Left ventricular pressure gradient; MTG, myocardial lipid content; PCr/ATP, Phosphocreatine/ATP ratio.

3.9 Conclusions

This study findings suggest that metabolic changes start in mild-moderate stage of AS and could potentially drive or accelerate structural remodelling in the disease process. The particular metabolic changes described in this study i.e. reduced PCr/ATP and myocardial lipid accumulation have previously been studied in moderate - severe AS and believed to occur secondary to metabolic reconfiguration with perturbations in FAO. [142,163,164] These adaptations improve myocardial oxygen efficiency but are associated with depletion of energy reserve the compound, Phosphocreatine (PCr) whilst maintaining ATP levels until decompensation ensues.[133,164] I have shown that low PCr/ATP levels precede the development of significant hypertrophy and potentially exacerbate the hypertrophic response and subsequent myocardial fibrosis in AS. This could explain the individual variability in response to similar pressure overload conditions. Also, the myocardial steatosis which is more related to the degree of pressure overload than hypertrophy can accelerate myocardial damage by generating toxic intermediates such as diacylglycerols and ceramides which further compromise ATP production and overall cell viability. These findings corroborate with previous studies in experimental models of LV pressure overload supporting a causal role for cardiac metabolic dysregulation in structural and functional impairment.[193, 243,232]
In conclusion from the study findings, LV hypertrophy in pressure overload could potentially be driven by premature metabolic dysregulation resulting in impaired energetics, but once significant hypertrophy develops, it may be driving further deterioration in myocardial structure, function and energy production.

3.10 Rationale for metabolic therapy in AS

AS poses a significant healthcare burden and still lacks pharmacological therapeutic option, despite them being a focus of significant interest for many years. No drug has yet shown to

improve cardiac function/cardiovascular outcomes. The understanding of cardiac energy metabolism has improved dramatically in recent decades, and the importance of metabolic signalling in adaptive and maladaptive responses to pressure overload as well as ATP generation is now appreciated. AS has particular promise for metabolic therapy, where down regulation of PPARα signalling pathway appears to be an important causal factor in the alterations in cardiac substrate metabolism and sequential decreased myocardial efficiency and cardiac functional impairment. The successful translation of therapies upregulating PPARα requires deeper understanding of the interplay between cardiac substrate metabolism, lipid deposition, energy generation and cardiac function in AS. This has now become possible with state-of-the-art MR metabolic imaging techniques: ^{1}H-Spectroscopy for myocardial triglyceride content and ^{31}P-Spectroscopy for ATP metabolism. These techniques have provided insight into the metabolic phenotype of AS, and may become useful for disease monitoring, identifying the most promising drugs and assessing response in AS.

We explore the potential of PPARα agonist, Fenofibrate as a metabolic modulator to augment cardiac physiology in AS using MRS techniques further in Chapter 5 and 6.

4 Chapter Four

Effect of cardiac metabolism on exercise capacity in AS

4.1 Abstract

4.1.1 Introduction

Aortic stenosis (AS) results in obstruction of blood flow through the aortic valve. The ventricular response to chronic pressure overload and other consequences of AS are important to understand. Determining how the ventricular remodelling in AS affects functional capacity in AS is not always straightforward especially in an elderly population. Around one-third of asymptomatic AS patients' develop cardiac symptoms on exertion.[244] Cardiopulmonary exercise testing (CPET) is an objective assessment of patients' exercise tolerance.[245] It can not only help identify asymptomatic at-risk individuals with hemodynamically compromising AS but also to help assess the efficacy of potential disease–modifying therapies in AS. The objective assessment of maximal exercise capacity using peak oxygen consumption (VO_2) measurement in asymptomatic AS patients can help understand the relationship between exercise capacity and cardiac physiology and metabolism in AS, which has been relatively unexplored previously. In this experiment, I sought to identify which CMR parameters of cardiac function and metabolism could predict exercise capacity in asymptomatic AS.

4.1.2 Methods

74 asymptomatic AS patients across the spectrum of the disease {Total 74; Mild-moderate AS (n=18), moderate AS (n=38), severe AS (n=18)} were recruited to the study. Comparison of exercise and myocardial parameters was made to understand the relationship between exercise capacity and LV remodelling in AS. Cardiac volumes, function and aortic valve

were assessed using cardiac magnetic resonance (CMR) cine imaging. Myocardial lipid content and cardiac energetics were assessed using ^{1}H and ^{31}P MR spectroscopy. Functional capacity was measured using six-minute walk test (6MWT) and CPET. Spirometry was performed on all participants prior to CPET in order to exclude underlying significant lung pathology.

According to the mean peak VO_2, patients with reduced exercise capacity were significantly older ($p = 0.025$) and more frequently females ($p = 0.001$). There were significant correlations between peak VO_2 and age ($r = -0.314$, $p = 0.006$), LV end-diastolic volume ($r = 0.310$, $p = 0.006$), LV stroke volume ($r = 0.30$, $p = 0.01$), and LV mass, both absolute and indexed ($r = 0.31$, all $p = 0.002$). Parameters of AS severity and LVEF did not correlate with peak VO_2 (p = ns for all). Among LV deformation parameters, circumferential strain was significantly associated with peak VO_2 ($r = 0.43$, $p = 0.005$, and $r = 0.32$, $p = 0.04$, respectively). With multivariate analysis, age ($\beta = 0.50$; $p = 0.03$) and body mass index were the only independent determinants ($r^2 = 0.423$) of peak VO_2. Cardiac MTG and energetics did not correlate to exercise capacity.

4.1.3 Conclusion

In asymptomatic AS, LV volumes, LV mass and impaired LV myocardial circumferential strain relate to reduced exercise capacity. Age and BMI were the only independent determinants of exercise capacity.

4.2 Introduction

Management of AS currently relies on symptoms. However, symptom reporting is an objective assessment and perhaps not the best for guiding treatment in AS. This has led LV ejection fraction.[246] An assiduous search for parameters that could help identify patients who may benefit from early or alternative therapeutic intervention has begun in recent years. There is evidence that LVEF is not an accurate estimator of myocardial contractility in patients with AS.[247] LV hypertrophy by compensating for the increased wall stress pseudo normalises LVEF values creating a false impression of normal LV systolic performance. Having studied the paradigm of myocardial structural and metabolic remodelling in AS and its deleterious effect on myocardial function which begin at the mild-moderate stage of the disease process, as shown in Chapter 3, I wanted to study how these changes impact aerobic capacity in AS.

The heart has to keep contracting to provide the body with the oxygen and nutrients it needs. Under normal physiological conditions, due to the small storage of high energy phosphate in cardiac myocytes, normal heart function depends on the tight coupling of intracellular ATP production and myocardial contraction [142], and ATP is mainly derived from the catabolism of glucose and fatty acids. In healthy adults, the heart obtains about 50%-70% of myocardial acetyl CoA derived ATP from fatty acids. When endogenous fatty acid supply is reduced, intracellular triacylglycerol hydrolyses the fatty acid back through specific lipases including adipose triglyceride lipase (ATGL)[248,249] for fatty acid oxidation and subsequent ATP generation. The efficient absorption and recycling of fatty acids by the heart is the key to ensuring ATP supply and systolic function[250] and glycolysis produces less than 10% of total ATP in healthy hearts. The main pathway for ATP resynthesis is mitochondrial oxidative phosphorylation (>98%), which is driven by the reduction equivalent NADH and FADH2 produced by fatty acid oxidation, pyruvate oxidation, and Krebs cycle. In a healthy heart, the

hydrolysis rate of ATP matches the rate of ATP resynthesis, and the tissue content of ATP is very constant, even though the conversion rate of ATP is greatly raised.[251] The elevated acute load during exercise has a strong effect on myocardial metabolism. In the heart, exercise boosts contractility and oxygen consumption, which is 10 times higher than the resting rate Although the heart can take advantage of substrates including carbohydrates, lipids, amino acids, and ketone bodies, to provide energy, while its substrate preference vary under both physiological and pathological stress.[196] The changes of substrate utilization and mitochondrial adaptation induced by exercise in physiological cardiomyocytes are effective guarantees to maintain the normal myocardial cells function.

Cardiopulmonary exercise testing offers an assessment of individuals' functional capacity through evaluation of gas exchange during exercise and thus an assessment of systems involved in both oxygen transport and utilization.[252] Cardiopulmonary exercise testing allows for measurement of the volume of tissue oxygen uptake, which is a key parameter that offers insights into cardiac and pulmonary function, as expressed by Fick's principle, according to which equates to cardiac output multiplied by the arterio-venous gradient [$C(a\text{-}v)O_2$].[253, 254] During ramp-like exercise, VO_2 increases exponentially up to a steady state corresponding to peak exercise, and will adopt different patterns in patients with different cardiac conditions. Moderate to severe AS can interfere with the body's normal physical responses to increased work, and thus affect the peak VO_2.[254]

From a metabolic perspective, one primary focus is the time and intensity dependent contributions of the three major energy pathways.[255] First, the phosphagen system, the PCr to ATP reaction regulated by creatine kinase (CK), resynthesizes ATP during immediate, high intensity work. Second, the short-term lactic acid system, relies on glycogen-dependent glycolysis to fuel intermediate, moderate to high intensity activity.[256] Third, the long-term

aerobic system requires efficient oxidative metabolism to support moderately intense, long-duration exercise. We know from our earlier knowledge in AS that all these major energy pathways undergo remodelling in AS with early reduction of PCr pool and impaired PCr/ATP ratio, switch to glucose metabolism with more reliance on glycolysis.

In parallel to the energy systems, careful consideration of the oxygen demand and time course of oxygen uptake are also necessary. In the early course of exercise, an increase in the cellular energetic demand occurs, requiring increased oxygen uptake. However, despite constant intensity, there is a slight delay (up to several minutes) in oxygen uptake to match the steady-state metabolic demands. This phenomenon deemed the "oxygen deficit," represents the mismatch between total oxygen uptake and the steady-state oxygen requirement.[257] During this time, ATP re-synthesis is supported by both the immediate and short-term energy systems (i.e., PCr and glycolysis). In time, the oxygen uptake matches the oxygen demand and the steady-state metabolic needs are met primarily by long-term aerobic metabolism. Research has shown that exercise-trained individuals have a reduced "oxygen deficit" and reach steady-state, aerobic metabolism at a faster rate compared to sedentary counterparts.[258] The enhanced metabolic capacity of the system is furnished by a combination of augmented oxygen delivery and improved biochemical processes.

The effects of exercise on the heart with AS are not completely understood. Pressure overload in AS contributes to the heart's dysfunctional status. Accelerated glycolysis is a hallmark of the pathological hypertrophied myocardium[259] and alterations in the PCr/ATP ratio have been reported.[181] LV hypertrophy is characterized by derangements in cardiac energy metabolism including lower PCr/ATP, abnormal creatine kinase kinetics and deranged substrate utilization. The PCr/ATP is significantly decreased at rest in hearts with LVH and the severity of this abnormality is proportional to the degree of cardiac hypertrophy

and accompanying LV dysfunction. It is plausible that the capacity to augment ATP delivery with stress might be compromised in pressure overload hearts as the energetic shuttle may essentially be operating at maximal capacity at rest, with no reserve like other cardiomyopathy states such as obesity.

Cardiopulmonary exercise testing (CPET) with measurement of gas exchange provides quantitative, objective, and more accurate non-invasive evaluation of maximal exercise capacity.[204] However, very few studies have focused on evaluating exercise capacity in AS [260] and studying its relationship with myocardial function and metabolism. In the present study, I sought to explore the relationship between exercise capacity as assessed by peak VO2 with CMR derived indices of LV size/function and metabolism in patients with asymptomatic AS. I hypothesise that in those with higher MTG content on ^{1}H-MRS will have lower peak VO_2 potentially due to perturbations in FAO and inability to augment FAO at peak exercise.

4.3 Methods

4.3.1 Study population

Seventy-four participants including mild-moderate AS (n=30; aortic valve area, mean AVA 1.2±0.23cm^2, peak velocity 2.9±0.17m/sec, peak valve gradient 36±4mmHg), moderate AS (n=22; AVA 1.0 ± 0.3cm^2, peak velocity 3.4±0.2 m/sec, peak valve gradient 49±6 mmHg) and severe AS (n=22; AVA 0.8 ± 0.2 cm^2, peak velocity 4.3±0.5 m/sec, peak valve gradient 79±14 mmHg) were prospectively included in the study. All participants met the inclusion and exclusion criteria as described in Chapter 2. All participants gave informed consent and the local ethics committee approved the protocol.

4.3.2 Study assessments

All participants underwent blood tests (including full blood count, renal and liver function, lipid profile, NT-proBNP, glucose and free fatty acids) followed by CMR assessment at 3T MRI scanner (Magneton Prisma; Siemens Healthineers) as per the following protocol:

- ^{31}P-MRS to assess PCr/ATP as a measure of myocardial energetic status at rest.
- ^{1}H-MRS to quantify myocardial steatosis.
- Cine imaging to measure LV function, mass and volumes and assess aortic valve.
- Tagging CMR to assess LV strain.
- ShMOLLI T1 mapping to assess tissue characterisation.
- Late gadolinium enhancement to evaluate interstitial fibrosis.

Participants then underwent 6MWT and CPET as detailed in Chapter 2, sections 2.6 and 2.7. CPET bike protocol was designed with three distinct stages: a warm-up stage, an exercise stage with progressive increase in workload, and recovery stage. Patients were encouraged to exercise until exhaustion and discouraged from talking during the test. All assessments were performed in fasted state.

4.3.3 Statistical analysis

Patients were divided into two groups according to the mean peak VO_2 distribution. The results were expressed as mean ± standard deviation or percentages unless otherwise specified. The statistical differences between groups were assessed using student t-test or Fisher's exact test as appropriate. The relationship between CMR data and peak VO_2 was evaluated using linear regression model. Values of $p<0.05$ were considered significant. All statistical analysis were performed with SPSS, version 28 and GraphPad Prism (version 9.0.2 for Windows; GraphPad Software, San Diego, CA).

4.4 Results

4.4.1 Characteristics of the population

Among the 74 patients included in the study (age 70 ± 14 years, 72% men), 44 (59%) had moderate - severe AS. None of the patients had known peripheral artery disease or intermittent claudication during CPET. For the purpose of analysis, patients were divided into groups of preserved maximal exercise capacity (MEC) >22ml/kg/min and reduced MEC <22ml/kg/min.

Patients' clinical and demographic characteristics and main CPET data are summarized in **Table 4.1**.

The CMR characteristics of the studied population are depicted in **Table 4.2.**

Table 4.1: Demographic, clinical and cardiopulmonary exercise test (CPET) data
Data are presented as mean ± SD or n (%). MEC, maximal exercise capacity; SBP, systolic blood pressure; DBP, diastolic blood pressure; HR, heart rate; ACE-I, Angiotensin converting enzyme inhibitors; ARB, Angiotensin receptor blockers; Hb, Haemoglobin; TC, Total cholesterol; TG, triglycerides; Peak VO_2, peak oxygen capacity; VE/VCO2; Minute ventilation/carbon dioxide production; VT, Ventilatory threshold; RER, Respiratory exchange ratio; 6MWT, six minute walk test; BNP, Brain natriuretic peptide; Hb, haemoglobin

Characteristics	**Total n=74**	**Preserved MEC, n=36 (VO_2 >22 ml/min/kg)**	**Reduced MEC, n=38 (VO_2 <22 ml/min/kg)**	**P value**
Age (years)	70±14	69±14	73±11	**0.025**
Female, n (%)	21 (28)	4 (11)	17 (45)	**0.001**
BMI (Kg/m^2)	27±5	25±4	31±4	**<0.001**
HR (bpm)	64±11	63±10	64±11	0.76
SBP (mmHg)	140±18	137±18	146±17	0.05
DBP (mmHg)	72±9	72±9	71±7	0.4
Co-morbidities				
Atrial fibrillation	8 (11)	1 (3)	7 (18)	
Hypertension	26 (35)	13 (36)	13(34)	
Medications				
ACE-i/ARB	26 (35)	13 (36)	13(34)	
Beta blockers	9 (12)	2 (6)	7 (18)	
Statins	29 (39)	11 (31)	18 (47)	
Diuretics	6 (8)	3 (8)	3 (8)	
Bloods (°mmol/L)				
NT-proBNP (ng/ml)	354±570	191±121	498±750	**0.03**
FFA°	0.65±0.3	0.62±0.32	0.69±0.24	0.35
Beta-hydroxybutyrate°	0.13±0.07	0.13±0.70	0.14±0.06	0.68
Glucose°	5.2±0.8	5.5±1.0	5.0±0.7	0.03
Hb (mg/dl)	138 ±13	137±12	140±13	0.25
Total Cholesterol°	4.5±0.8	4.5±0.89	4.6±0.69	0.84
Triglycerides°	1.04±0.4	1.11±0.52	0.99±0.34	0.31
CPET data				
Peak VO_2 (ml/min/kg)	21.6±5.8	24.3±4.8	16.2±3.5	**<0.001**
VE/VCO_2 slope	38±5	39±5	37±4	0.12
VT (kg/ml/min)	26±7	30±5	18±3	**<0.001**
RER	1.3±0.14	1.32 ± 0.12	1.21±0.14	**<0.001**
Test duration (mins)	16±4	17±4	13±3	**0.003**
Max. workload (watts)	111±40	123±38	86±33	**<0.001**
Peak HR (bpm)	139±22	144±22	134±21	0.06
Peak SBP (mmHg)	174±22	170±23	180±17	0.09
6MWT distance (m)	417±93	436±72	390±114	0.17

Table 4.2: CMR parameters

Data are expressed as mean ± SD. LV, left ventricle; EDV, end diastolic volume; ESV, end systolic volume;LVM, left ventricular mass; WT, wall thickness; LGE, late gadolinium enhancement; EF, ejection fraction; long, longitudinal; circ, circumferential;SR, strain rate; MTG, myocardial triglyceride content; PCr/ATP, phosphocreatine/adenosine triphosphate ratio; AS, aortic stenosis; AV, aortic valve; AVA, aortic valve area

Characteristics	Overall (n=74)	Preserved MEC n=36 (VO_2 >22 ml/min/kg)	Reduced MEC n=38 (VO_2<22 ml/min/kg)	P value
LV structure				
LVEDV (ml)	151 ± 35	160 ± 29	141 ± 37	**0.02**
LVESV (ml)	55 ± 18	59 ± 14	51 ± 20	0.06
Indexed LVM (kg/m^2)	70 ± 15	74 ± 13	65 ± 16	**0.02**
Absolute LVM (kg)	134 ± 41	143 ± 33	125 ± 46	**0.04**
LVWT (mm)	13 ± 3	14 ± 3	14 ± 3	0.73
Presence of LGE (%)	28 (38)	18 (50)	10 (26)	0.54
Native T1 (ms)	1140 ± 59	1129 ± 61	1150 ± 55	0.17
LV function				
Stroke volume (ml)	95 ± 23	101 ± 19	88 ± 24	**0.009**
LVEF (%)	64 ± 7	63 ± 5	64 ± 8	0.54
Global long strain (%)	-12 ± 3	-11.9 ± 2.3	-12.2 ± 3	0.64
Global circ strain (%	-16.6 ± 3	-17.2 ± 2.6	-15.9 ± 3.9	0.10
Diastolic circ SR (1/s)	50 ± 20	52 ± 21	46 ± 19	0.18
Cardiac metabolism				
MTG (lipid/water ratio)	1.62 ± 0.86	1.49 ± 0.8	1.74 ± 0.9	0.23
PCr/ATP	1.50 ± 0.47	1.48 ± 0.4	1.53 ± 0.5	0.72
AS severity				
Peak AV gradient (mmHg)	50 ± 22	51 ± 22	49 ± 21	0.73
AVA (cm$^{2)}$	1.1 ± 0.3	1.1 ± 0.3	1 ± 0.3	0.90
Peak velocity (m/sec)	3.4 ± 0.7	3.5 ± 0.7	3.3 ± 0.7	0.23

4.4.2 Functional capacity in AS

4.4.2.1 Relationship with LV structure and function

Mean peak VO_2 was 21.6 ± 5.8 mL/kg/min (range 10–36 mL/kg/min, *Figure* **4.1***)* for the whole cohort. Six patients (8%) could not exercise to maximal volitional effort and had an RER of <1.1. Of note, none of them developed abnormal/clinically significant symptoms during the test. Patients with reduced maximal exercise capacity, MEC (peak VO_2 < mean) were significantly older, more frequently females and had higher BMI (**Table 4.1***)*. Reduced MEC group had lower LV end-diastolic and end-systolic volumes, LV stroke volume and LV mass, both absolute and indexed (**Table 4.2***)*. There were no other significant differences between the two groups regarding clinical, demographic, and conventional CMR data.

There was a significant correlation between absolute peak VO_2 and age (r = −0.31, p = 0.006), LV end-diastolic volume; LVEDV (r = 0.32, p = 0.006), LV end-systolic volume; LVESV (r = 0.29, p = 0.01), LV stroke volume; LVSV (r = 0.29, p = 0.01), absolute LV mass (r = 0.27, p = 0.02) and LV mass index (r = 0.31, p = 0.002, Table 4.3). In contrast, there was no significant correlation between peak VO_2 and resting LVEF.

Among LV myocardial deformation parameters, only global systolic circumferential strain (GCS) was significantly associated with peak VO_2 (r = 0.30, p 0.01), **Table 4.3**. When divided into groups based on mean peak VO_2, patients with reduced MEC had numerically reduced GCS (−17.2 ± 2.6% vs. −15.9 ± 3.9%) as well as circumferential diastolic strain rate (52 ± 21/sec vs 46 ± 19/sec) when compared to those with preserved MEC, but the difference between the groups was not significant (all p = ns, **Table 4.2**).

Among all LV structure and function parameters derived by CMR, the strongest univariate determinant of peak VO_2 were LV volumes and global circumferential strain (GCS, **Table 4.3).**

However, on multivariate regression after mean centering for LVEDV in the model including age, BMI, LVEDV, LVSV, LVMI and GCS, the main determinants of peak VO_2 ($r^2 = 0.38$) were only age (B 0.06, SE 0.29, p 0.002) and BMI (B 0.29, SE 0.09, P <0.001)

Table 4.3: Relationship between peak VO_2, age, BMI and CMR parameters.

LV, left ventricle; EDV, end diastolic volume; ESV, end systolic volume; SV, stroke volume; MI, mass index; EF, ejection fraction; long, longitudibal; circ, circumferential; MTG, myocardial triglyceride content; PCr/ATP, phosphocreatine/adenosine triphosphate ratio; AS, aortic stenosis; AV, aortic valve; AVA, aortic valve area; long, longitudinal; circ, circumferential.

Variables	r	P value
Age (years)	-0.31	**0.006**
BMI (kg/m^2)	-0.40	**<0.001**
LV structure and function		
LVEDV (ml)	0.32	**0.006**
LVESV (ml)	0.29	**0.01**
LVSV (ml)	0.29	**0.01**
LVMI (kg/m^2)	0.31	**0.002**
LVEF (%)	-0.14	0.24
Global long strain (%)	-0.12	0.34
Global circ strain (%)	0.30	**0.01**
Diastolic circ SR (1/s)	0.24	0.05
Cardiac metabolism		
MTG (lipid/water ratio)	-0.10	0.42
PCr/ATP	0.00	0.99
AS severity		
Peak AV gradient (mmHg)	-0.08	0.49
AVA (cm^2)	0.04	0.74
Vmax (m/sec)	0.03	0.80

4.4.2.2 Relationship with Aortic valve parameters

There was no significant relationship between valve parameters and peak oxygen capacity in this cohort (Refer to **Table 4.2 and 4.3**)

4.4.2.3 Relationship between cardiac metabolism and exercise capacity

Two main cardiac metabolic parameters – MTG and PCr/ATP, were compared with parameters of exercise capacity.

As described in Chapter 3, this research had shown that metabolic changes occur early in AS and I wanted to understand if these changes had any effect on exercise capacity before the development of symptoms or irreversible structural remodelling.

Overall, whilst the exercise capacity correlated to LV volumes, no significant relationship was seen with resting MTG or cardiac energetics (PCr/ATP). When divided into groups based on mean MEC, MTG content was much higher in those with reduced MEC compared to preserved MEC (MTG content 1.74 ± 0.9% in reduced MEC vs 1.49 ± 0.8 % in preserved MEC) but the difference was not significant. However, on removing one extreme outlier from the MTG data, the medians JT across VO_2 quartiles shows that those with lower MTG have better VO_2 (p 0.058). There was no significant difference between cardiac energetics in the two groups (1.53 ± 0.5 in reduced MEC vs 1.48± 0.4 in preserved MEC).

4.5 Discussion

The major findings of the present study are (i) MEC varies widely in asymptomatic patients with moderate to severe AS and is often lower than expected average. 45% of the study population had peak VO_2 lower than the cut-off (peak VO_2 <20ml/min/Kg) for favourable outcomes from heart failure studies,[261] (ii) classical parameters of AS severity do not influence MEC, (iii) MEC is modestly related to the degree of LV end-diastolic volume and LV stroke volume, (iv) LVEF does not affect MEC in AS patients with apparently preserved

LV systolic function, and (vi) Global longitudinal strain was impaired significantly throughout the cohort, but only LV circumferential strain correlated to MEC; a cut-off value of −16% could be used to predict reduced MEC in asymptomatic patient with moderate to severe AS.

4.5.1 LV structure and exercise capacity in AS

Several small studies have shown that exercise capacity is frequently altered in patients with AS. In a study by Clyne *et al* asymptomatic patients with AS had a reduced exercise tolerance when compared with controls.[262] Moreover, Rajani *et al s*howed that peak indexed LV stroke volumes and peak VO_2 values were lower in patients who developed symptoms during the test. In the present study, peak VO_2 varied widely from normal to markedly reduced values (mean: 16.2 ± 3.5 mL/kg/min).[263] Peak VO_2 values were significantly lower in older patients and in females with asymptomatic AS in this study, in agreement with data obtained in the general population.[202, 245] It is worth emphasizing that the present study included only patients without history of self-reported exertional dyspnoea, angina, or syncope, and no symptom development during the CPET test. Yet, 45% of the included patients had a suboptimal exercise capacity.

4.5.2 LV function and exercise capacity in AS

Peak VO_2 is related to peak exercise cardiac output through the Fick equation. Cardiac output is related to heart rate and stroke volume, both at rest and during exercise. In the study cohort, resting LV stroke volume was associated with peak VO_2, patients with lower MEC had smaller LV stroke volume, suggesting that an LV with a low stroke volume at rest does not have sufficient resources to adapt to exercise. Hence, patients with lower LV stroke volumes at rest tend to have reduced MEC. We did not measure LVSV at stress in this study.

Despite the LV wall thickness being similar in both the groups, high absolute LV mass was associated with reduced peak VO_2 on multivariate analysis. This suggests that potential loss of LV filling volume related to ventricular remodelling can be deleterious on MEC in AS.

Interestingly, from all conventional parameters of LV systolic function shown in Table 4.3, only LV stroke volume showed a significant relationship with peak VO_2, while LVEF was neither associated with lower MEC, nor different between groups. The lack of association between LVEF and peak VO_2 suggests that LVEF is a not a good estimator of exercise performance in patients with concentric remodelling and increased LV haemodynamic afterload. In the current guidelines, LVEF is the only LV function parameter used to recommend AVR in asymptomatic patients with severe AS. . In AS, the presence of LV hypertrophy, through a simple geometrical effect, can generate a confusing impression of 'normal' LV systolic performance, despite a progressive decline in cardiac output.

In contrast to global LVEF, LV longitudinal systolic function is impaired earlier in conditions with high afterload, as in AS indicated by impaired longitudinal deformation. Though the LV longitudinal strain was depressed overall (average -12 %),[234] in all AS participants in this study, it did not show a relationship with peak VO_2. Only the decrease in circumferential strain (cut off -16%), [234,235]related to differences in peak VO_2 in this study. It is not clear why the study did not detect a relationship of peak VO_2 with longitudinal strain as shown in previous studies[45] but only with circumferential strain. These study patients were in an advanced stage of the disease where the myocardial dysfunction is likely to be progressed from subendocardial to transmural fibres, therefore affecting both longitudinal and circumferential function.

4.5.3 Cardiac metabolism and exercise capacity

In this study, there was no direct association between cardiac metabolic parameters and peak VO_2. It is well known that in a normal heart, an increase in myocardial workload is accompanied by increases in the catabolism of multiple substrates, in particular, fatty acids and lactate. During steady state sub-maximal exercise, when lactate production (influx) equals lactate removal (outflux), the lactate concentration in the lactate pool stays constant and the rate of oxygen consumption is the measure of the whole body energy expenditure regardless of the magnitude of lactate production and removal or the absolute blood lactate concentration. At exercise intensities above steady state, a rise in the concentration could be attributed to an increase in the rate of lactate production or result from a decrease in the rate of lactate removal.[264]

PCr is an energy buffer that supports the transient failure of other metabolic pathways to support ATP. The equilibrium constant of the CK reaction is around 20 and the slightest drop in ATP allows the reaction to proceed to ATP. Thus, the ATP concentration stays nearly constant until almost all the PCr is utilized. The PCr levels follow an exponential time course after changes in work rate before approaching a steady state condition at moderate exercise intensities. However, for exercise intensities above lactate threshold, the anaerobic glycolytic energy supply becomes significant and the association between PCr and O_2 rate has not yet been systematically reported. During recovery, the level of PCr must be recovered mostly through oxidative metabolism in a normal heart, the pH must be re-established and ADP removed.

The majority of these patients were able to exercise to maximal volitional effort with increase in lactate production as measured on capillary blood lactate. Average values for

lactate were higher in the preserved MEC group (4.7 ± 1.7 mmol/L vs 2.9 ± 1.2 mmol/L in the reduced MEC group). We know that oxidative metabolism is reduced in. hypertrophied AS hearts, hence it is plausible from this data that those with preserved MEC must have been able to increase rates of anaerobic glycolysis (as indicated by higher lactate values in this cohort) to replenish PCr pools.

It is also known that PPARα-mediated control of cardiac metabolic gene expression is activated in response to exercise training.[64] During exercise, hormone-activated lipolysis in adipose tissue increases circulating FFA, which enhances FFA uptake and utilization.[265] However, heightened levels of circulating FFAs are only partially responsible for increasing fatty acid oxidation because higher cardiac workloads appear sufficient to increase fat oxidation in the heart. Cardiac TAG (triacylglycerol) utilization rates also increase considerably with exercise and appear to be further stimulated by lactate availability, suggesting that lactate may stimulate TAG turnover. Furthermore, after exercise adaptation, genes responsible for fatty acid transport and catabolism are elevated, which may help optimize fat utilization in the heart.[255]

Thus, in the preserved MEC group, whether the lactate production stimulated TAG turnover and augmented FAO with improved energetics is not known as this was not investigated .

Overall, a complex interplay of metabolic interactions resulting from alterations in PPARα signalling and fat metabolism in AS are likely to affect overall exercise performance, but any such effect may not have been detected in this study due to (i) limited assessment of metabolism measuring only two parameters, and (ii) small sample size for studying such effect. Further assessment with metabolomics before and after exercise in future studies may elicit a relationship between cardiac metabolic changes and exercise performance in AS.

Metabolomics analysis measuring rates of glycolysis, pyruvate oxidation and lactate production pre and at peak exercise would provide useful information. The two CMR metabolic parameters measured at rest in this study did not show a relationship with exercise capacity. However, perhaps future studies could explore measuring stress PCr/ATP and MTG in this cohort to see if they are able to augment energy production in the myocardium at peak exercise.

4.6 Conclusions

Degenerative AS usually affects elderly population, where increased age, female sex and high BMI reduce overall exercise performance. In addition, in asymptomatic patients with moderate to severe AS and preserved LVEF, lower LV volumes and higher absolute LV mass reduce myocardial efficiency during increase workload and predispose to heart failure. Global longitudinal strain is impaired early in AS and relates to subclinical LV dysfunction and reduced exercise capacity as shown in previous studies. But this study suggests that in advanced stages of the disease, perhaps global circumferential strain relates better with reduced exercise capacity. Future studies with larger cohort of mild, moderate and severe AS are required to establish cut-off for both longitudinal and circumferential strain that may affect exercise capacity.

4.7 Limitations

The sample size of the present study is relatively small but all patients included had a CPET. Peak VO_2 may be affected by pulmonary diseases, neuromuscular, or musculoskeletal disease, anaemia or any other pathology that decreases the oxygen transport capacity of blood. However, none of the patients included in the present study had symptoms or any of the above-mentioned pathologies and all underwent spirometry prior to CPET to exclude occult respiratory disease. Exercise-induced myocardial ischaemia may be a limiting factor of

MEC. However, none of our patients had a history of coronary artery disease, or presented angina or significant ST changes suggestive of active myocardial ischaemia during exercise

5 Chapter Five

A prospective double blinded randomised controlled trial of metabolic modulation therapy in Aortic stenosis

5.1 Abstract

5.1.1 Background

Aortic stenosis (AS) is associated with metabolic changes that cause a progressive impairment of cardiac metabolism and high-energy phosphate production. As a consequence of the impaired cardiac metabolism, other processes are activated in the hypertrophied heart that further exacerbate the progression to HF. Myocardial lipid accumulation and reduced production of high-energy phosphates has important implications for both systolic and diastolic heart function in AS. Metabolic agents, mainly PPARα agonist, have the potential to optimise cardiac substrate metabolism. This approach may be effective in improving subclinical dysfunction and functional capacity in AS.

5.1.2 Methods

In this prospective, randomized, double-blind, placebo-controlled trial, patients with moderate-to-severe asymptomatic AS (n=72) were recruited and randomly assigned to Fenofibrate 200 mg daily or matched placebo for 6 months (mean treatment duration 180 ± 7 days). Of the total 72, 59 received Fenofibrate and 13 received Placebo. All subjects underwent cardiac magnetic resonance and exercise testing at 0 and 6 months, with follow-up data available in 47 patients. The primary end point was change in myocardial triglyceride content (MTG) from baseline to 6 months determined by proton magnetic resonance spectroscopy (^{1}H-MRS). Secondary outcome measures included change in cardiac energetics

(PCr/ATP) determined by phosphorus magnetic resonance spectroscopy (^{31}P-MRS), left ventricular strain determined by myocardial tagging and exercise capacity i.e. peak VO_2 assessment via cardiopulmonary exercise testing. (See Methods chapter for details on these assessments).

5.1.3 Results

There was a statistically significant reduction in myocardial triglyceride content (the primary end point) in the Fenofibrate group (-0.40 ± 0.97; 95% CI -0.74, -0.06; p 0.022). MTG content also reduced in the placebo group (mean change -0.46 ± 0.69, 95% CI -1.11, 0.17, p 0.13), but the reduction was not statistically significant. Whilst in the treatment group there is evidence to support that this reduction in MTG was a consequence of significant activation of in vivo fatty acid oxidation with substantial change in blood beta hydroxy butyrate levels (0.08 ± 0.21; 95% CI -0.003, 0.17; p 0.028), the cause of reduction in placebo group is unclear. Fenofibrate treatment group also showed significant reduction in total cholesterol (-0.61 ± 1.2; 95%CI -1.2, 0.02; p 0.04) and non-HDL cholesterol (-0.6 ± 0.64; 95% CI -0.85, -0.35; p <0.0001) as expected compared to placebo, where there was no significant change. Cardiac energetics (PCr/ATP) showed modest, but statistically significant improvement in the Fenofibrate treatment group (0.14 ± 0.48; CI: - 0.03, 0.30; p = 0.05) vs Placebo group (0.11 ± 0.75; CI -0.42, 0.65; p 0.64). Parameters of AS severity worsened in both arms with time. Measures of LV function including global circumferential and longitudinal strain did not show any change with treatment in either of the groups.

5.1.4 Discussion

Fenofibrate works as a metabolic modulator upregulating fatty acid metabolism in pressure overload AS hearts. However, such modulation does not modify cardiac physiology or halt disease progression in moderate-severe AS.

Introduction

Pressure overloaded hypertrophy is inherently associated with impaired myocardial metabolism with uncoupling of glycolysis and glucose metabolism, and shift away from free fatty acid use resulting in a depressed energetic state. Hypertrophied myocardium is metabolically vulnerable. It is yet not fully known if such metabolic derangements plays a causative role in myocardial decompensation in hypertrophied hearts or is a result of extensive structural remodelling. Lower rates of FAO are associated with cardiomyopathies and HF.[58, 81] I have shown in this research that the metabolic changes occur early in patients with AS preceding structural changes (Chapter 3) and are related to subclinical dysfunction. Furthermore, in AS patients with established structural remodelling i.e. marked hypertrophy and myocardial fibrosis, there is an associated increased mortality and morbidity especially when undergoing aortic valve surgery.[266] Thus, it would be plausible to hypothesise that altering metabolism favourably towards FAO in AS may potentially prepare the myocardium well to deal with the structural changes that ensue with chronic pressure overload. To that effect, metabolic therapies have been proposed as a targeted therapy for improving the tolerance of the myocardium which may delay or prevent progression of disease together with improving outcomes post valve replacement.

The central role of peroxisome proliferator-activated receptors (PPARs) in heart metabolism, particularly fatty acid oxidation (FAO) and mitochondrial bioenergetics, makes them a promising therapeutic target for the treatment of cardiac diseases including cardiac hypertrophy and HF.[267] Due to high expression and the beneficial role of PPARα and PPARβ/δ in the heart, numerous studies have been conducted to study the efficiency of PPARα and PPARβ/δ agonists on various animal models with HF. Fenofibrate is a dual activator of PPARα and PPARγ, with 10-fold selectivity for PPARα.[268] Oral intake of

fenofibrate (100 mg/kg body weight) significantly attenuated end-diastolic and end-systolic LV dimensions and cardiac fibrosis in aldosterone-induced hypertrophy model independently of an effect of the drug on blood pressure.[269] Similar effects were observed in porcine and canine tachycardia-induced cardiomyopathy models.[270] Fenofibrate attenuated hypertrophy, inhibited the inflammatory response, improved the survival of Dahl salt-sensitive rats and decreased fibrosis in the rat model with the pressure overload-induced HF.[113] Likewise, fenofibrate prevented the development of cardiac hypertrophy in spontaneously hypertensive rats by decreasing LV mass index, cardiomyocyte trans diameter, cardiomyocyte area, collagen volume fraction and perivascular circumferential area.[271] Additionally, fenofibrate has shown to attenuate isoproterenol-induced acute myocardial ischemic injury.[268]Apoptosis plays a key role in the pathophysiology of diabetic cardiomyopathy, and fenofibrate showed a cardio protective role against diabetic cardiomyopathy by virtue of its ability to prevent cardiac fibrosis and inhibit myocardial apoptotic signals.[167] These studies indisputably suggest the cardio protective pleiotropic actions of fenofibrate, besides its lipid lowering effects.

Another important thought when considering pharmacological therapy is the timing of such a therapy in diseases like AS. Metabolic modulation is most likely to be beneficial at a stage when the changes are still reversible and before the development of gross structural changes. To ascertain this, however, remains a challenge and no study till date has looked at the timing of metabolic remodelling or the relationship between metabolic and structural remodelling in AS.I have for the first time shown in this research that metabolic derangement occurs as early as mild-moderate stage of AS but this study has not been designed to predict the reversible or irreversible nature of these changes in the presence of a constant pressure overload state. Of note and to the best of my knowledge, all interventional studies in AS, be it drug or surgical intervention have looked at more severe spectrum of the disease. There have been no studies

to date investigating metabolic modulation using PPARα agonists in asymptomatic moderate-severe AS. Consequently, Ox-FAST is the first prospective, randomised, double-blind, placebo-controlled trial assessing the effects of Fenofibrate treatment on cardiac lipid metabolism and physiology.

5.2 Methods

A prospective, single centre, double-blind, randomised, placebo-controlled study of Fenofibrate (200mg once daily if eGFR >60ml/min and 67mg once daily in those with eGFR <60ml/min) was conducted in patients with asymptomatic moderate-severe AS. The study was approved by the South London Research Ethics Committee (18/LO/1981) but was exempt from the Medicines and Healthcare products Regulatory Agency as this was a mechanistic study to study metabolic modulator effect of Fenofibrate in moderate-severe AS. The study was registered with ClinicalTrials.gov (NCT05256758), and patients were enrolled between May 2018 and October 2021 from the John Radcliffe hospital in Oxford, Royal Berkshire hospital in Reading and Great western hospital in Swindon. Informed consent was obtained from each participant and all research was performed in accordance with the Declaration of Helsinki and the UK Human Tissue Act 2004 within a research governance framework.

5.2.1 Study drug dose, duration and randomisation

During the baseline visit (Visit 2), eligible patients were randomly assigned to either 200 mg of Fenofibrate (67mg dose for those with eGFR<60ml/min) or matching Placebo per day for a period of 180 days.

This dose of Fenofibrate 200 mg once daily was chosen as it is effective in reducing levels of triglycerides, total cholesterol, and LDL-C and increasing levels of HDL-C in patients with dyslipidaemias. Its efficacy and tolerability in the treatment of hypertriglyceridemia and combined hyperlipidaemia have been demonstrated in numerous clinical trials.[272, 273] As a

PPARα agonist, it has been shown to regulate cellular lipid metabolism and have protective cardiovascular effects.[274] These modes of action support the scientific rationale of using fenofibrate in this study and 200mg once daily is the recommended initial adult dose. In elderly patients without renal impairment, the normal adult dose is recommended. In renal dysfunction, the dose of Fenofibrate may need to be reduced.

Study duration of 6 months (180 ± 7 days) was considered sufficient based on evidence from previous studies. Previous human[275] and animal studies[165, 167] have shown that the effect of Fenofibrate on cellular lipid metabolism becomes evident within six to fourteen weeks after treatment. In the pilot study by Mahmod et al, eight months post AVR, both myocardial steatosis and strain were found to be significantly reduced.[163] Based on this evidence, a study duration of 6 months as expected to exert expected physiological effect.

Randomisation occurred in a 4:1 fashion and the drug randomisation was carried out using flagged label method. Nottingham University hospital (NUH) pharmacy supplied both the active drug and placebo bottles, with annex 13 (EU guidelines to Good Manufacturing Practice) compliant labels containing a sequential pack number according to randomisation list, to the site pharmacy. The small tear off section on the bottle stating whether the product is active or placebo was removed at the point of dispensing by the site pharmacy and attached to an accountability log as proof of which product the patient has been administered. The local pharmacy was also made aware of patient's eGFR thus enabling them to dispense the correct dose of the active drug. Hence, with the exception of the site pharmacy, all patients, investigators and everyone else involved in study conduct/analysis in this double-blind study remained blinded with regard to the randomised treatment cohort until all patients had completed the study and database had been locked.

5.2.2 Study visit schedule

After screening patients' records of potentially eligible participants, those interested were invited for visit 1, which included consent, baseline assessments and randomisation (See chapter 2 Methods, section 2.3). Participants took study medication in total for 180 ± 7days once a day. Participants were then invited for safety and compliance visit (visit 2, 90 ± 7 days), which was done face-to-face pre-covid (until March 2020) and through telephone (March 2020 onwards), before their end of study assessment (Visit 3, 180 ± 7 days). To ensure safety, an additional phone call or contact through email (Visit 4, 7-10 days after Visit 3) was conducted to ensure uncomplicated withdrawal from the study drug. **Figure 5.1** provides an overview of the visit schedule and timeline for Ox-FAST.



Figure 5.1: Visit Timeline Ox-FAST. *Schematic overview of study design: After screening and determination of their eligibility, participants will be invited for randomisation and baseline assessments (Visit 1; Day 1). A safety/ compliance assessment will be conducted after 90 days (± 7) of treatment (Visit 2; Day 90 ±7). Following treatment for 180 days, baselines assessments were repeated (Visit 3; Day 180 ± 7). A final follow-up was carried* out *via telephone/email (Visit 4; Day 187 ± 7).*

5.2.3 Study population

Patients were considered eligible if they had moderate-severe AS with no symptoms and left ventricular ejection fraction (LVEF) ≥ 50%. Patients with concomitant other cardiac pathology including known coronary artery disease, cardiomyopathy or other significant valve disease were excluded. Other conditions that could affect cardiac fatty acid and

carbohydrate metabolism like Diabetes mellitus and high BMI (≥ 40 Kg/m^2) were also excluded. A comprehensive list of inclusion and exclusion criteria is presented below in **Figure 5.2.**

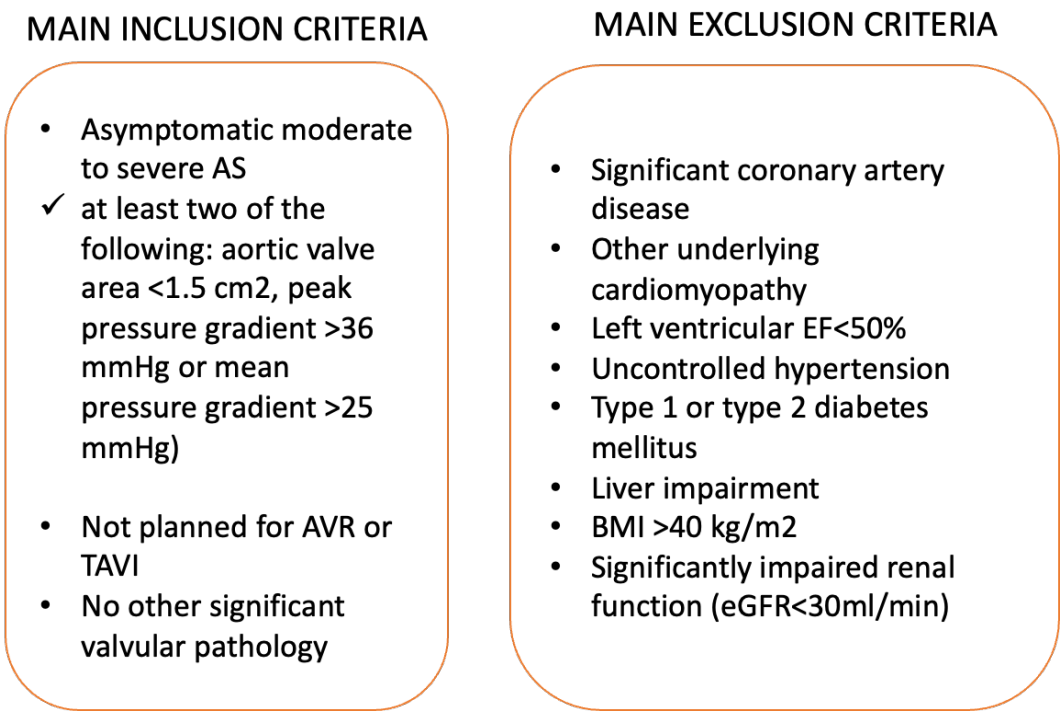


***Figure 5.2: Detailed inclusion and exclusion criteria for Ox-FAST**; AVR, Aortic valve replacement; TAVI, Trans catheter aortic valve intervention; EF, ejection fraction; BMI, body mass index; eGFR, estimated glomerular filtration rate.*

5.2.4 Study end points

The primary end-point was change in myocardial triglyceride/lipid content (MTG) as measured by proton MR spectroscopy, ^{1}H-MRS after 6 months (180 ± 7 days) of Fenofibrate or Placebo.

Secondary end-points were change in LV strain, an indicator of LV subclinical function, as measured by CMR tagging CIM TAG 2D version 9.1 (Auckland Medical Research, Auckland, New Zealand) and change in cardiac energetics, measured as phosphocreatine/ATP ratio on phosphorus MR spectroscopy (^{31}P-MRS). These end-point

results are discussed in this chapter. We also looked at changes in exercise capacity, measured as peak VO_2 on cardiopulmonary exercise testing. CPET results are discussed in chapter 6.

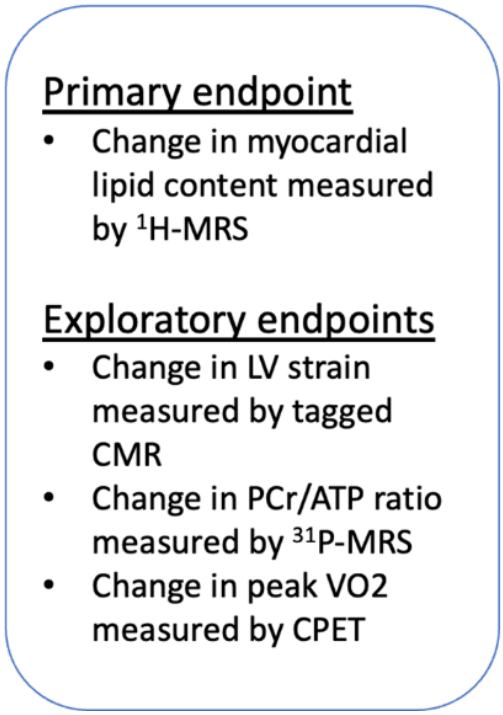


Figure 5.3 Pictorial representation of the end-points.

5.2.5 Data acquisition and analysis

5.2.5.1 Blood/Laboratory tests

A variety of biomarkers of safety and efficacy (**Table 5.1**) were measured in venous blood samples from patients fasting for at least 6 hours (refer to chapter 2, section 2.3).

Table 5.1: Safety and efficacy bloods and laboratory tests Ox-FAST.

Haematology (blood sample) • Full blood count Clinical Chemistry (fasting blood samples) • Liver function tests (Albumin, ALP, ALT, bilirubin) • Renal function profile (Sodium, potassium, urea, creatinine) • Creatinine Phosphokinase (CK) – only where clinically indicated Lipid Profile (fasting blood samples) • Total cholesterol • HDL cholesterol • Calculated LDL cholesterol • Triglycerides • Free fatty acids Pregnancy test in women of child bearing potential (WOCP) • Urine sample for pregnancy test

Fasting venous bloods for efficacy and safety analyses were sent and analysed at the local laboratory (Oxford university hospital NHS trust).

5.2.5.2 Cardiac Magnetic Resonance imaging

CMR imaging was performed using 3-Tesla MRI scanner (Magnetom PRISMA, Siemens Healthineers, Erlangen, Germany). **Figure 5.4** shows the CMR sequences used to acquire data. Cardiac indices, valve parameters, late gadolinium imaging and T1-mapping analysis were performed in an anonymised fashion offline in accordance with SCMR guidelines,[276] using cvi42version 5.10.1 (Circle Cardiovascular Imaging Inc, Calgary, Alberta, Canada) by an independent operator who was blinded to patient treatment status. Tagged images were analysed using CIM TAG 2D version 9.1 (Auckland Medical Research, Auckland, New Zealand). Spectroscopy analysis and quantification for both ^{1}H-MRS and ^{31}P-MRS were done using specially written modules in Matlab and AMARES fitting algorithm. Image analysis is explained in detail in Chapter 2, section 2.8. **Figure 5.4** below shows a schematic overview of CMR sequences used.

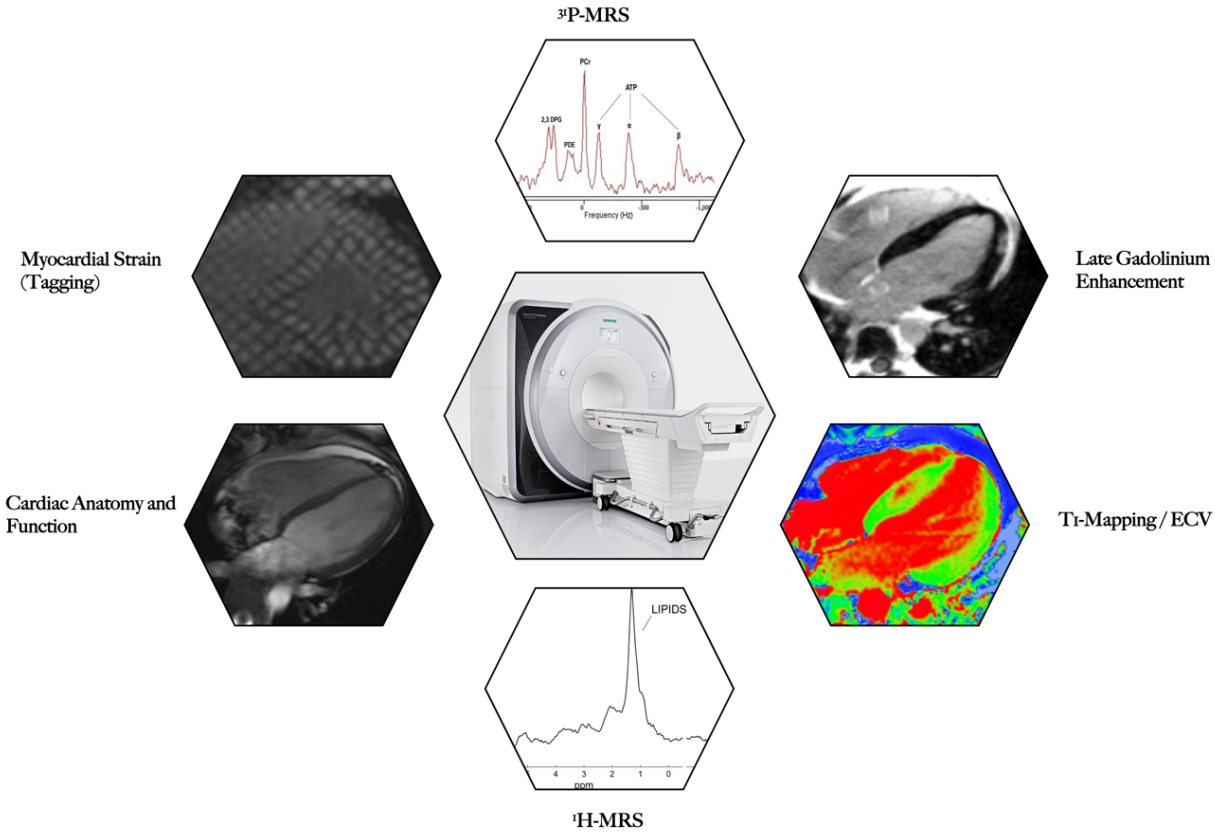


Figure 5.4: Overview of CMR Sequences Ox-FAST*. Cardiovascular magnetic resonance (CMR) sequences used for the Ox-FAST trial. All sequences were performed on scanners by the same vendor and identical field strength (3 Tesla). ^{1}H-MRS=proton magnetic resonance spectroscopy; ^{31}P MRS=phosphorus magnetic resonance spectroscopy; ECV=extracellular volume.*

5.2.5.3 Cardiopulmonary exercise testing and six-minute walk test

This part of the study is discussed in detail in the next chapter (Chapter 6).

5.2.5.4 Statistical Analysis

Due to lack of significant data describing the impact of PPARα agonists on measures of cardiac metabolism in patients with AS, the power calculations were based on previous data on asymptomatic AS[163] with MTG of 0.75 ± 0.36% vs 0.45 ± 0.17% in normal controls. In this study, my primary focus was to detect physiological effect i.e. change in MTG before and after Fenofibrate in the treatment group. Thus, the power calculations were aimed at detecting expected changes from baseline in the treatment group alone, and the comparison between treatment group and placebo is not included in the calculation. The purpose of

including the placebo group was a) to have a control group in terms of disease progression b) to further blind the study team during the data analysis process. Hence, there were higher number of patients in the treatment group compared to placebo. To detect a mean difference in MTG of 0.15% in the treatment group (i.e. half the difference to normal when compared to the previous study) with a SD of 0.36, power of 80% and a $p < 0.05$, a minimum sample size of 38 was required. Allowing for 23% dropouts as calculated from previous projects with similar study population, the total number of subjects anticipated for recruitment in the treatment group was 49. The placebo group had 13 patients (dropouts included) in total. Thus, taking the total number to be recruited to 62 (n=49 for treatment group and n=13 for placebo). Of the 62 patients, only 48 were expected to have both baseline and follow-up tests. Due to the unforeseen impact of global COVID-19 pandemic and subsequent effects on healthcare systems as well as restrictions implemented, 12 participants recruited from December 2019 - January 2020 were unable to complete their end-of treatment visit, and thus, had to be excluded. Recruitment target was, henceforth, revised based on power calculations. To achieve 48 complete datasets, the revised recruitment target of 67 participants (13 to the placebo group and 54 in the treatment group) was calculated. This was calculated taking into consideration the 17% dropout rate in pre-covid recruitment to the study.

All analysis was performed on complete datasets of patients using descriptive statistics or analysis of variance (ANOVA). All summaries were produced for both cohorts (treatment and placebo) using all available data. For primary and secondary end-points analysis, the analysis was done separately in the Placebo and treatment group. Baseline and 6-month follow-up data in each completed dataset was analysed using paired t-test. All analysis was performed on SPSS, version 28 and GraphPad Prism (version 9.0.2 for Windows; GraphPad

Software, San Diego, CA). Pearson and Spearman correlation analysis was also used where applicable.

5.3 Results

A total of 72 participants were enrolled into the study and randomised to treatment

5.3.1 Study population

Overall, 47 (85%) participants successfully completed the study, see Consort chart for the study below.

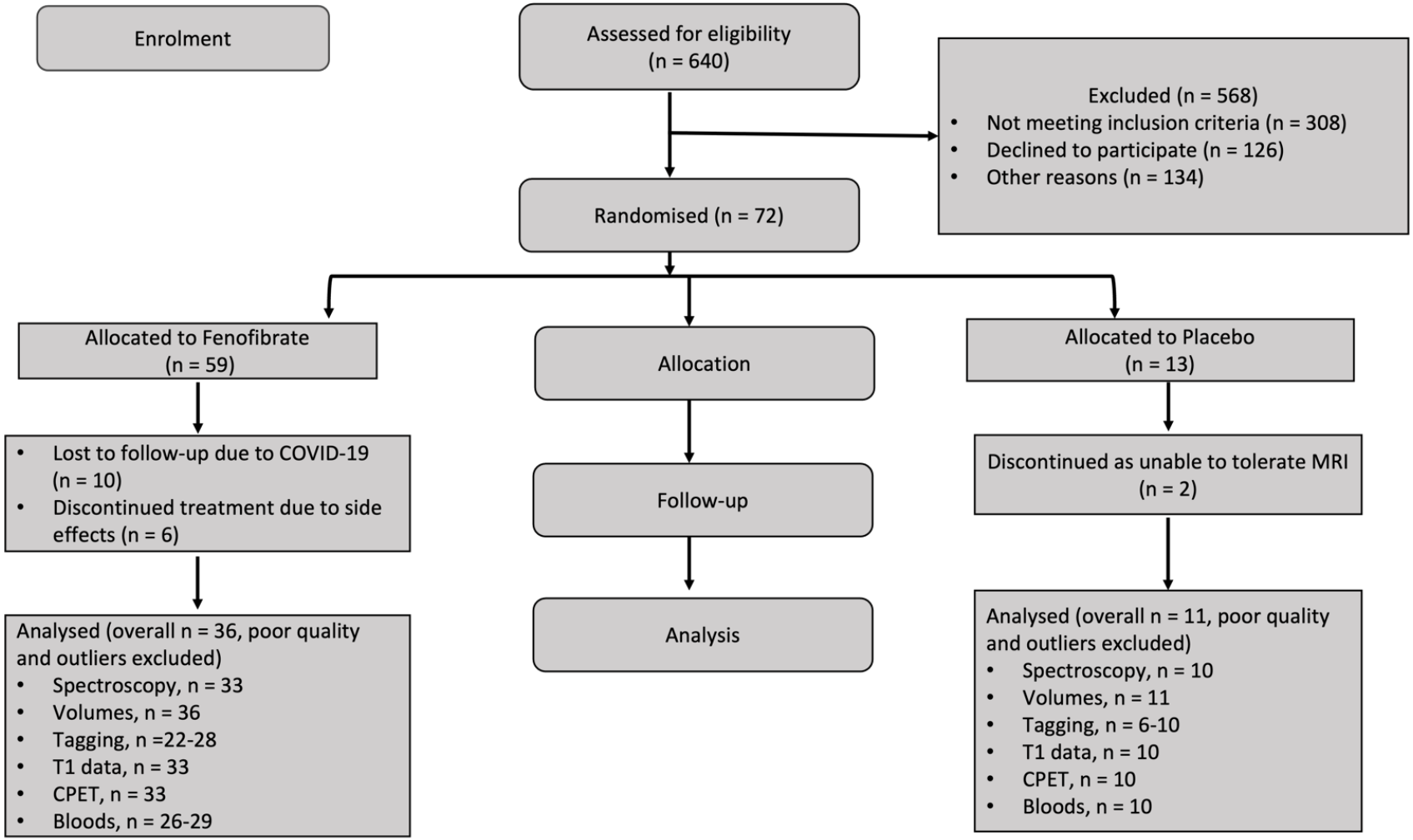


Figure 5.5 : CONSORT flow chart of the randomised controlled trial

The mean duration of exposure to treatment was 176.4 ± 7.8 days for the Fenofibrate group with treatment compliance of 98.6 ± 2.21 %. The mean duration of treatment in the placebo group was 173 ± 11.6 days and overall treatment compliance of 99.6 ± 0.44%. 82% of patients were male, all patients were White (100%) and their mean age was 70 ± 14 years. All subject characteristics were similar in both groups including age, BMI, blood pressure and heart rate. Bloods including free fatty acids, butyrate levels, glucose and cholesterol levels were also similar in both groups (p = ns). Mean NT- proBNP was higher in the placebo group but the difference between the two groups was not significant. **Table 5.2** summarises selected general baseline characteristics and **Table 5.3** CMR characteristics at baseline.

***Table 5.2**: **Baseline characteristics Ox-FAST**: **Characteristics at baseline for all patients randomised to treatment.** BMI, body mass index; SBP, systolic blood pressure; DBP, diastolic blood pressure; HR, heart rate; ACE-i, angiotensin converting enzyme inhibitor; ARB, angiotensin receptor blocker.*

Characteristics	**Fenofibrate (n= 59)**	**Placebo (n=13)**	**P-value**
Age, mean ± SD, years	70 ± 14	72 ± 17	0.67
Sex, %			0.95
Male	71.7	72.7	
Female	28.3	27.3	
Race, n (%)			
White	59 (100)	13 (100)	
BMI (Kg/m2), mean ± SD	27.3 ± 4.7	25.7 ± 4.3	0.29
SBP (mmHg), mean ± SD	138 ± 17	145 ± 21	0.22
DBP(mmHg), mean ± SD	72 ± 9	75 ± 6	0.29
HR (bpm), mean ± SD	63 ± 11	64 ± 9	0.76
Bloods (mean ± SD)			
NT-proBNP (pg/ml)	239 (383, 114)	431 (373, 122)	0.40
Glucose (mmol/L)	5.27 ± 0.68	5.56 ± 1.33	0.34
Free fatty acids (mmol/L)	0.66 ± 0.28	0.64 ± 0.31	0.89
Butyrate levels (mmol/L)	0.14 ± 0.07	0.10 ± 0.02	0.17
Total cholesterol(mmol/L)	4.54 ± 0.83	4.23 ± 0.72	0.28
Triglycerides (mmol/L)	1.02 ± 0.40	0.97 ± 0.34	0.73
Comorbidities & medications (%)			
Atrial Fibrillation	13.2	9.1	0.88
Hypertension	34	36.4	0.71
ACE-i/ARB	34	36.4	0.88
Beta blockers	13.2	0	0.21
Statins	34	63.6	0.07
Diuretics	9.4	0	0.29

Table 5.3: Baseline CMR characteristics Ox-FAST. All values expressed as mean ± SD. *AV, aortic valve; LV, left ventricle; EDV, end-diastolic volume; ESV, end-systolic volume; SV, stroke volume; EF, ejection fraction; ECV, extra-cellular volume; LGE, late gadolinium enhancement; RV, right ventricle; LA, left atrium.*

	Fenofibrate	**Placebo**	**P value**
Randomised patients, n (%)	59 (100)	13 (100)	
Valve parameters (mean ± SD)			
Aortic valve area (cm2)	1.01 ± 0.26	0.93 ± 0.14	0.37
Peak aortic velocity (m/sec)	3.4 ± 0.6	4.1 ± 0.74	0.001
Peak AV gradient (mmHg)	50 ± 18.5	70 ± 24.7	0.004
Primary endpoint (mean ± SD)			
MTG (lipid/water %)	1.58 ± 0.85	2.09 ± 1.04	0.17
Secondary endpoints (mean ± SD)			
PCr/ATP ratio	1.51 ± 0.51	1.58 ± 0.39	0.66
Peak systolic strain (%)			
Longitudinal	-11.9 ± 2.8	-12.2 ± 2.3	0.75
Circumferential	-16.2 ± 3.3	-19.4 ± 2.6	0.006
Peak diastolic strain rate (%/sec)			
Longitudinal	24.5 ± 10.7	23.2 ± 7.2	0.73
Circumferential	46.4 ± 18.8	62.2 ± 23	0.02
LV parameters (mean ± SD)			
LVEDV (ml)	153.6 ± 34.8	153.1 ± 33.6	0.97
LVESV (ml)	56.3 ± 8.3	51.5 ± 17.9	0.43
SV (ml)	95.9 ± 22.9	101.5 ± 19.4	0.46
LVEF (%)	63.4 ± 6.6	67 ± 6.5	0.11
LV mass index (g/m2)	69.1 ± 14.8	71.9 ± 18.4	0.59
Average native T1 (ms)	1140 ± 57.3	1137 ± 67.7	0.86
ECV (%)	28.4 ± 6.3	26.1 ± 2.2	0.30
Presence of LGE (%)	28.2	36.3	0.12
Other parameters (mean ± SD)			
RVEF (%)	61.3 ± 5.5	61.8 ± 5.9	0.80
LA volume (mls)	81 ± 38.4	71 ± 18.3	0.44

5.3.2 Primary Outcome

5.3.2.1 Myocardial triglyceride content (^{1}H-MRS)

In this study, I observed a significant reduction in the myocardial triglyceride content (MTG) in the Fenofibrate group. The mean difference was -0.40 (SE 0.17, 95% CI: -0.74, -0.06; p = 0.0224) following 180 days of treatment with Fenofibrate. However, the mean drop was comparable to that in the placebo group where the mean difference was -0.41 (SE 0.26, 95% CI: -1.10, 0.18; p = 0.1255). When I further evaluated the ΔMTG in both groups with a t-test, results remained similar with the mean difference being significant in the treatment group only (mean difference -0.43, SE 0.18, 95% CI:-0.79, -0.08; p = 0.018) – likely due to the smaller numbers in the placebo group. **Figure 5.6** below compares the change in MTG in the two groups

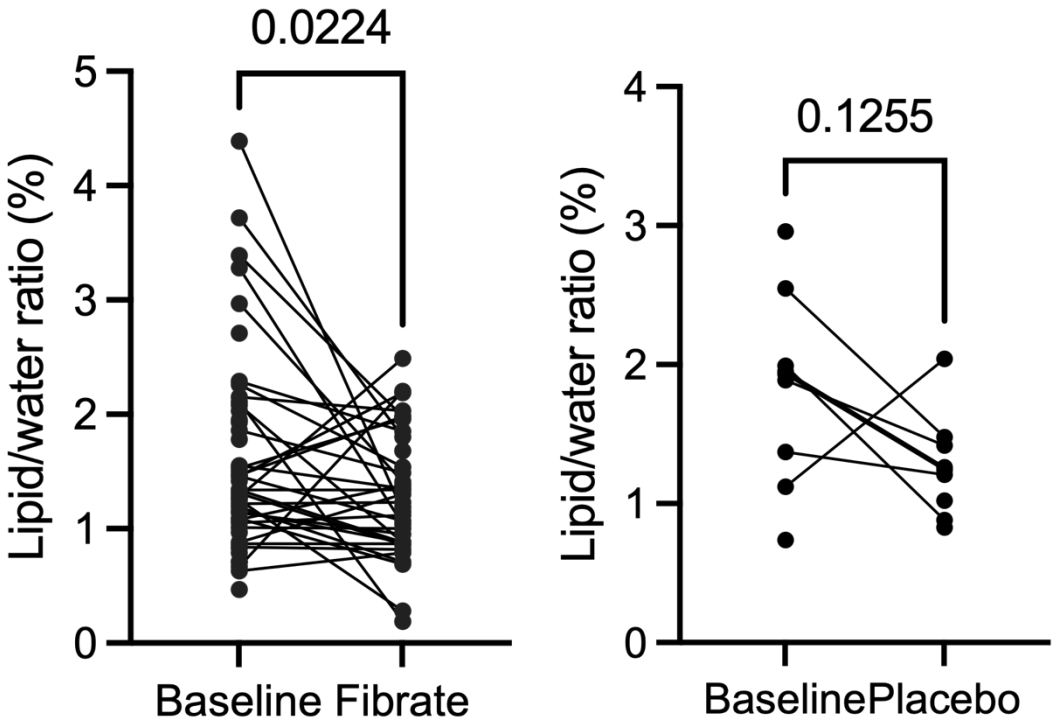


***Figure 5.6**: **Changes in MTG levels from baseline to 6 months treatment with Fenofibrate and placebo**. Results from paired t-test showing change in individual values in both groups. Lipid/water ratio, % is representative of myocardial triglyceride content.*

Of note, the study was not powered to detect a difference between the two groups but to only study the effect of Fenofibrate on MTG content.

5.3.3 Secondary outcomes

5.3.3.1 Cardiac energetics (PCr/ATP on ^{31}P-MRS)

There was no considerable change in cardiac energetics as indicated by PCr/ATP ratio derived using ^{31}-PMRS, in either of the groups. However the small increase in the treatment group was statistically significant. The mean difference in the Fenofibrate group was 0.12 (SE 0.08, 95% CI: - 0.05, 0.29; p = 0.04) and in the placebo group the mean difference was 0.11 (SE 0.24, 95% CI: - 0.42, 0.65; p = 0.64). On further analysis of the ΔPCr/ATP in both groups, the results were unchanged with no considerable change in PCr/ATP.

Figure 5.7 shows the mean change in PCr/ATP in the two groups and **Figure 5.8** shows the ΔPCr/ATP in both the groups]

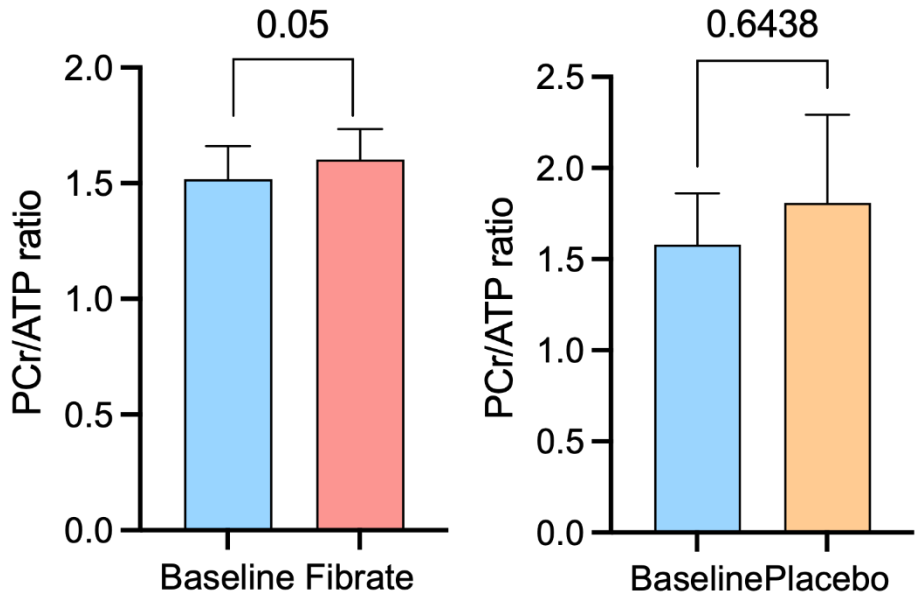


Figure 5.7: Change in PCr/ATP Ox-FAST: Change in Phosphocreatine/ATP ratio from baseline to 6 months treatment with Fenofibrate and Placebo*. Results from paired t-test showing mean values with 95% confidence interval s in both groups. PCr/ATP, Phosphocreatine/adenosine triphosphate ratio.*

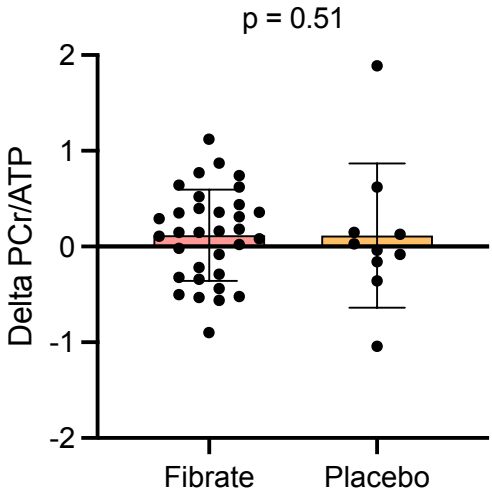


Figure 5.8: Delta PCr/ATP OxFAST: Scatter plot with bars with mean and 95% confidence intervals of delta PCr/ATP ratio for individual patients in respective cohorts*.*

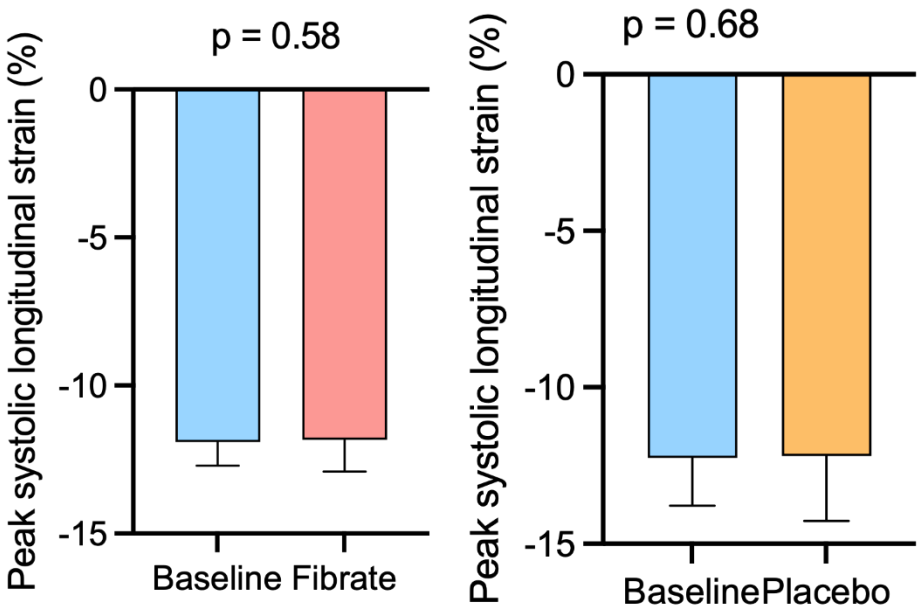
5.3.3.2 Left ventricular structure and function

As outlined above, the study was powered to detect change in the fibrate group only.

5.3.3.2.1 LV systolic strain parameters

This study did not show any significant improvement in LV strain parameters. Comparison was made from baseline to 6 months' treatment values in both groups separately. There was no statistically significant improvement in peak systolic longitudinal strain (0.26, 95% CI: -1.22, 0.70, p = 0.58) or circumferential strain (0.15, 95% CI: -1.38, 1.08, p = 0.81) in the fibrate group. Similarly in the placebo group, no statistically significant change was observed in these parameters. However, in the placebo group there was a trend towards deterioration in peak systolic circumferential strain over 6 months duration (See **Figure 5.9** and **Table 5.4** below).

(A)



(B)

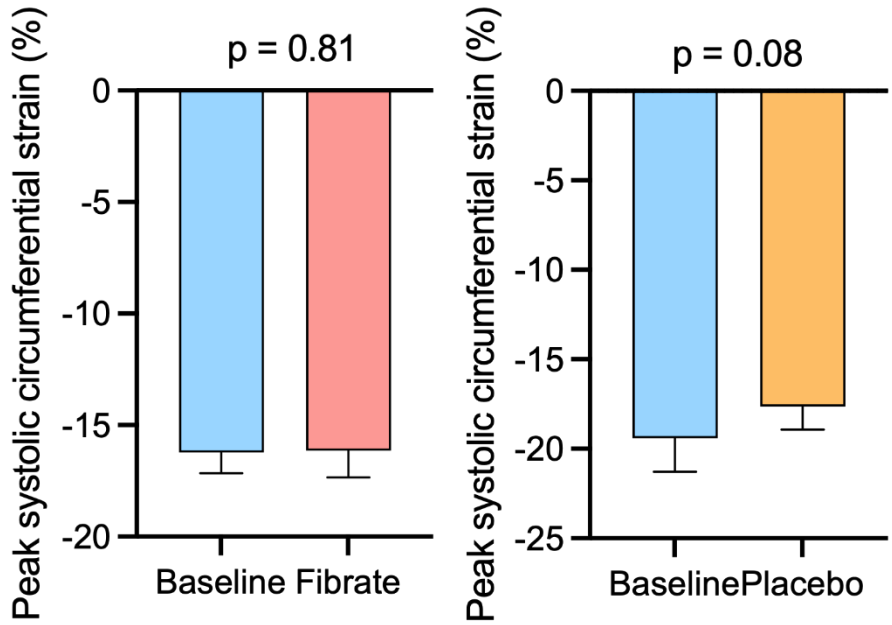


Figure 5.9 (A) and (B) represent the mean with 95% CI values of LV strain parameters as measured by MR tagging from baseline to 6 months in both groups.

Table 5.4 summarises the change in CMR parameters of LV structure and function from baseline to 6 month in both groups. *Results from paired t-test of both groups showing mean values at baseline of all parameters ± standard deviation (SD), followed by mean difference between baseline and post- treatment values in each group. * represent statistically significant values. Long; longitudinal; circ, circumferential; SR, strain rate; LV, left ventricle; LA, left atrium; RV, right ventricle.*

Parameter	N recruited	N analysed	Mean±SD (baseline)	Mean±SD (post treatment)	Mean difference (95% CI)	P value
Peak systolic long strain (%)						
Fenofibrate	*59*	*28*	*-12.2 ± 2.4*	*-11.9 ± 2.92*	*0.26 (-1.22, 0.70)*	*0.58*
Placebo	*13*	*10*	*-11.9 ± 1.9*	*-12.2 ± 2.9*	*0.32 (-1.97,1.35)*	*0.68*
Peak systolic circ strain (%)						
Fenofibrate	*59*	*28*	*-16.1 ± 2.82*	*-16.3 ± 3.12*	*0.15 (-1.38, 1.08)*	*0.80*
Placebo	*13*	*10*	*-19.4 ± 2.61*	*-17.7 ± 2.00*	*-1.71 (-0.23, 3.65)*	*0.07*
Peak diastolic long SR (/s)						
Fenofibrate	*59*	*22*	*23.8 ± 10.8*	*33.8 ± 11.2*	*9.6 (1.13, 18.1)*	*0.028**
Placebo	*13*	*6*	*24.6 ± 7.5*	*25.8 ± 7.9*	*1.17 (13.7, -11.3)*	*0.67*
LV end-diastolic volume (ml)						
Fenofibrate	*59*	*36*	*161 ± 35*	*157 ± 40*	*-3.4 (-9.4, 2.5)*	*0.25*
Placebo	*13*	*11*	*153 ± 34*	*153 ± 46*	*-0.09 (-14.4, 14.2)*	*0.99*
LV Stroke volume (ml)						
Fenofibrate	*59*	*36*	*98.5 ± 22*	*88.9 ± 22*	*-9.5 (-15, -4)*	*0.001**
Placebo	*13*	*11*	*101.5 ± 19.3*	*83.9 ± 16.7*	*-17.6 (-24.9, -10.3)*	*0.0003**
LV ejection fraction (%)						

Fenofibrate	*59*	*36*	*62.3 ± 6.6*	*57.4 ± 5.1*	*-4.9 (-6.9, -2.9)*	*<0.001**
Placebo	*13*	*11*	*67 ± 6.5*	*59.3 ± 4.3*	*-7.7 (-11.9, -3.5)*	*0.002**
LV mass index (Kg/m2)						
Fenofibrate	*59*	*36*	*71.6 ± 15.2*	*72.6 ± 18.3*	*0.86 (-2.6, 4.34)*	*0.62*
Placebo	*13*	*11*	*71.9 ± 18.4*	*74.4 ± 26.1*	*2.5 (-8.6, 13.6)*	*0.63*
LV wall thickness (mm)						
Fenofibrate	*59*	*36*	*14.5 ± 2.9*	*14.8 ± 2.9*	*0.23 (-0.36, 0.82)*	*0.44*
Placebo	*13*	*11*	*14.8 ± 2.8*	*14.8 ± 3.8*	*-0.06 (-1.48, 1.35)*	*0.92*
LA volume (ml)						
Fenofibrate	*59*	*36*	*86.8 ± 41.2*	*104.6 ± 49.7*	*17.8 (28.5, 7.12)*	*0.002**
Placebo	*13*	*11*	*71.3 ± 18.4*	*90.1 ± 30.5*	*18.8 (34.8, 2.77)*	*0.026**
RV ejection fraction (%)						
Fenofibrate	*59*	*36*	*61.6 ± 5.4*	*61.4 ± 5.3*	*-0.28 (-2.4, 1.81)*	*0.78*
Placebo	*13*	*11*	*61.8 ± 5.9*	*60.8 ± 7.4*	*-1.0 (-4.7, 2.75)*	*0.56*

5.3.3.2.2 LV volumes and systolic function

All patients, both in fibrate and placebo groups, had normal LV ejection fraction (LVEF) at baseline. There was deterioration in LVEF compared to baseline in both the groups over 6 months' period. Despite the values remaining above the normal range (>55%), the drop in EF was statistically significant in both groups (**Table 5.4** and **Figure 5.10**)

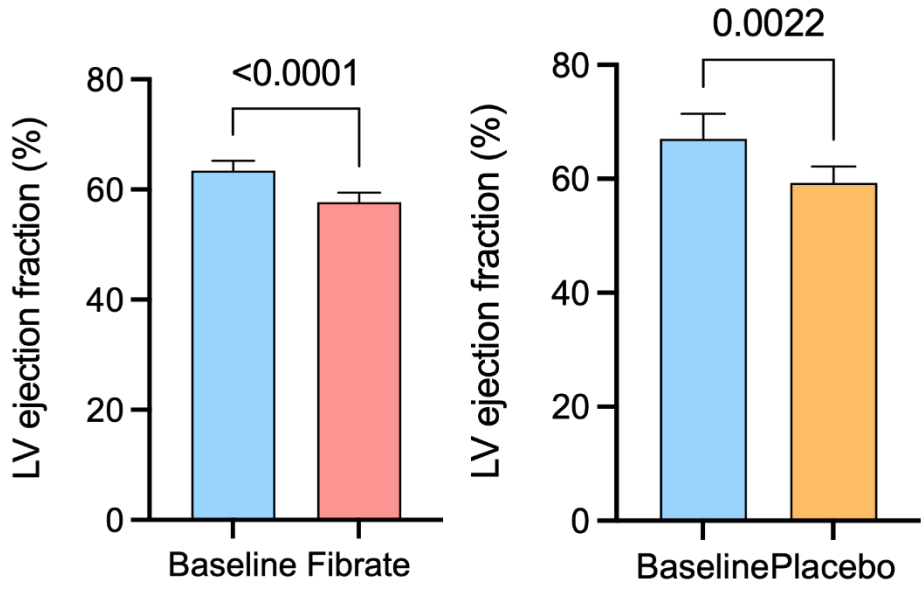


Figure 5.10: Bar graph of paired t-test for LVEF in each group showing mean values with 95% confidence intervals*. LV, left ventricle.*

In keeping with reduced LVEF, there was significant reduction in LV stroke volume (-9.5, 95% CI:-15, -4; p = 0.001) in the fibrate group as well as the placebo group (-17.6, 95% CI: -24.9, -10.3; p = 0.0003). This deterioration in SV was much worse in the placebo group. See **Figure 5.11.**

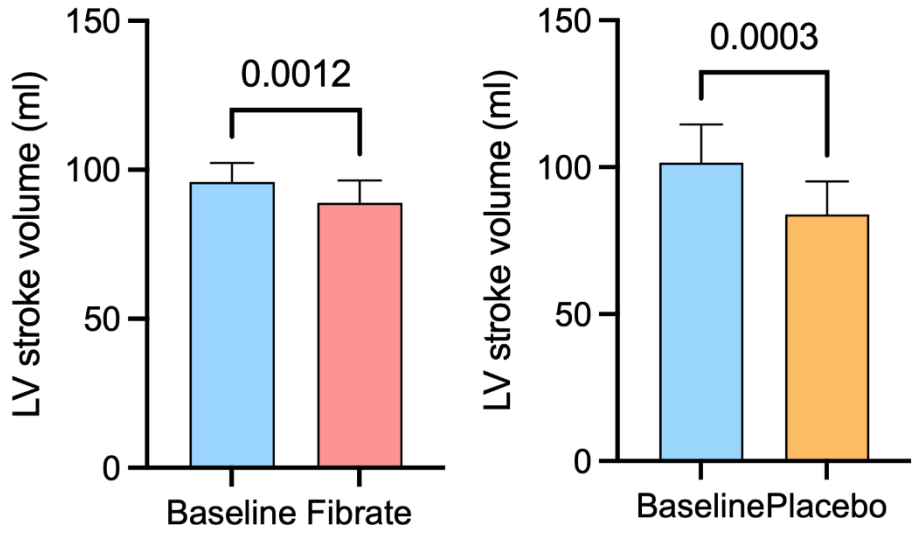
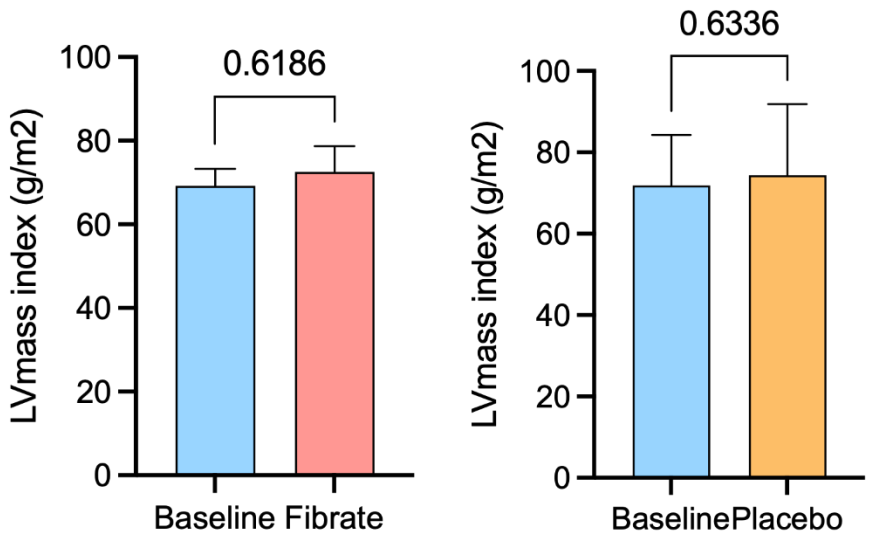


Figure 5.11: Bar graph of paired t-test for LV stroke volume (ml) in each group showing mean values with 95% confidence intervals. *LV, left ventricle.*

In terms of LV structural remodelling, assessment of degree of hypertrophy was done by measuring wall thickness and mass index. There was no considerable change in LV mass index in either of the groups (0.86, 95% CI: -2.6, 4.34, p = 0.62 in fibrate vs 2.5, 95% CI: -8.6, 13.6, p = 0.63 in placebo), but numerically the mass index was higher at post treatment, more so in the placebo group. No significant change in LV wall thickness was observed. **See Figure 5.12.**

(A)



(B)

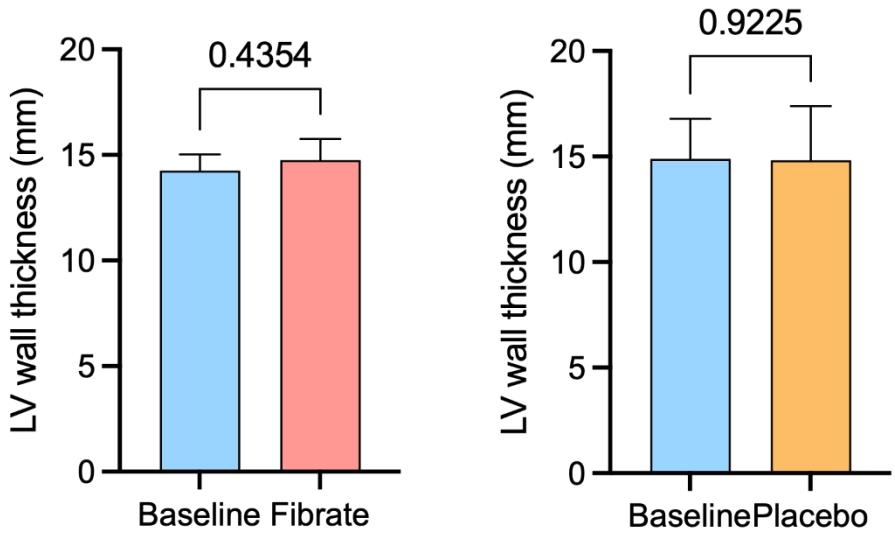
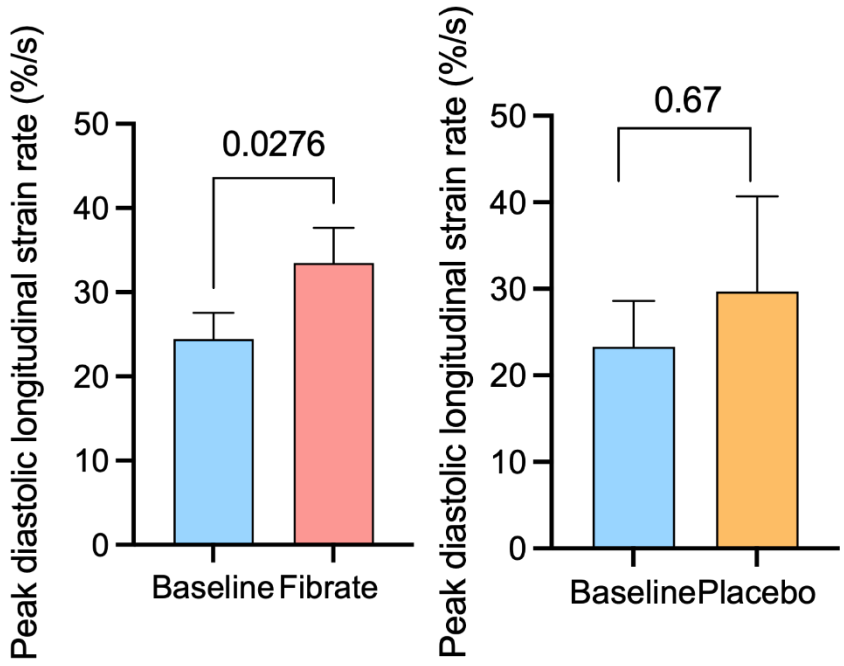


Figure 5.12: Bar graph of paired t-test for (A) LV mass index (Kg/m^2) and (B) LV wall thickness (mm) in each group showing mean values with 95% confidence intervals*. LV, left ventricle.*

5.3.3.2.3 Diastolic parameters

In this study, we also looked at the parameters of diastolic function, namely strain rate and LA volume. When peak diastolic longitudinal strain rate values pre and post- treatment with Fenofibrate were studied, there was a significant improvement (9.6, 95% CI: 1.13, 18.1; p = 0.028). There was improvement of peak diastolic longitudinal strain rate in the placebo group as well, but the change was not statistically significant (**Table 5.4**). LA volume, conversely, significantly increased in the Fenofibrate group after 6 months' treatment (17.8, 95% CI: 28.5, 7.12; p = 0.002) and this increase was similar to that in the placebo group (18.8, 95% CI: 34.8, 2.77; p = 0.03). **Figure 5.13 (A) and (B)** show the results for peak diastolic longitudinal strain rate and LA volume respectively in both the groups.

(A)



(B)

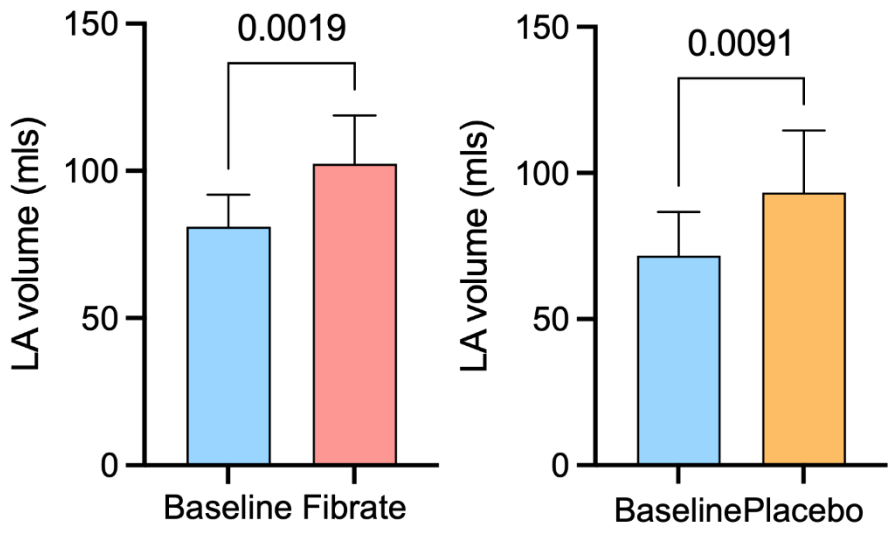


Figure 5.13: ***Bar graph of paired t-test for (A) peak diastolic longitudinal strain rate (%/s) and (B) LA volume (ml) in each group showing mean values with 95% confidence intervals.*** *LA, left atrium.*

5.3.3.2.4 Native T1 mapping, Extracellular volume (ECV) estimation and late gadolinium enhancement (LGE)

There were no significant change in the native T1 values, extracellular volume, myocardial matrix and cellular volume in either of the groups. See **Table 5.5** for details. 35% (19/53) patients in fibrate group and 64% (7/11) patients in the placebo groups had evidence of late gadolinium enhancement at baseline. The absolute numbers of patients with evidence of replacement fibrosis increased in the treatment group in the 6 months' duration to 24/35 patients compared to placebo, where the number of patients with LGE enhancement remained the same (7/9).

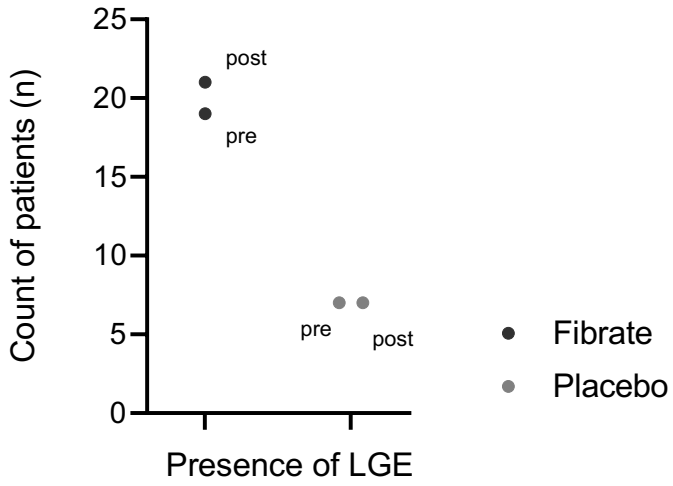


Figure 5.14 shows count of patients with late gadolinium enhancement (LGE) in both the groups pre and post 6 months' treatment.

Table 5.5: Summary of the paired t-test results for the change in native T1 values, extra- cellular volume fraction, myocardial matrix and cellular volume concentrations pre and post treatment in both fibrate and placebo groups. *Vol, volume*

Parameter	N recruited	N analysed	Mean ± SD (baseline)	Mean ± SD (post treatment)	Mean difference (95% CI)	P value
Native T1 (ms)						
Fenofibrate	*59*	*33*	*1149 ± 65*	*1151 ± 68*	*-1.9 (-22.6, 18.72)*	*0.85*
Placebo	*13*	*10*	*1137 ± 68*	*1139 ± 74*	*2.0 (-24.1, 28.14)*	*0.87*
Extracellular volume (%)						
Fenofibrate	*59*	*33*	*28.9 ± 6.4*	*28.9 ± 5.3*	*-0.0 (-0.032, 0.032)*	*0.99*
Placebo	*13*	*10*	*26.1 ± 2.2*	*27 ± 2.5*	*0.82 (-0.66, 2.3)*	*0.24*
Myocardial matrix vol (ml)						
Fenofibrate	*59*	*33*	*19.4 ± 4.4*	*20.2 ± 4.6*	*0.83 (-0.35, 2.0)*	*0.16*
Placebo	*13*	*10*	*22.9 ± 5.2*	*20.7 ± 5.1*	*-2.2 (-8, 3.6)*	*0.40*
Myocardial cellular vol (ml)						
Fenofibrate	*59*	*33*	*54.5 ± 9.3*	*55.1 ± 8.7*	*0.62 (-2.4, 3.6)*	*0.62*
Placebo	*13*	*10*	*53 ± 14.4*	*49.7 ± 15.1*	*-3.2 (-20.2, 13.9)*	*0.67*

5.3.3.3 Blood markers analysis

Fasting venous blood samples were analysed for different blood parameters (as listed in **Table 5.6**).

There was a significant increase in the serum beta-hydroxybutyrate levels in the fibrate group post treatment 0.08 (95% CI: -0.002, 0.17; p = 0.028) with no significant change in the serum free fatty acid levels 0.00 (95% CI: -0.10, 0.10; p = 0.98). No notable change was seen in beta- hydroxybutyrate levels in the placebo group. See **Table 5.6** for details.

As expected, serum total cholesterol dropped considerably in the Fenofibrate group -0.61 (95% CI: -1.2, -0.02; p = 0.04). Non-HDL levels also followed the same trend in the fibrate group reducing by -0.60 (95% CI: -0.85, -0.35; p = <0.0001). No significant change was seen in the cholesterol levels in the placebo group.

NT-pro BNP levels worsened in both fibrate and placebo groups over the duration of the study with the change being statistically significant in the fibrate group (MD 87.6; 95% CI: 41.8, 133.3; p = 0.006).

(A)

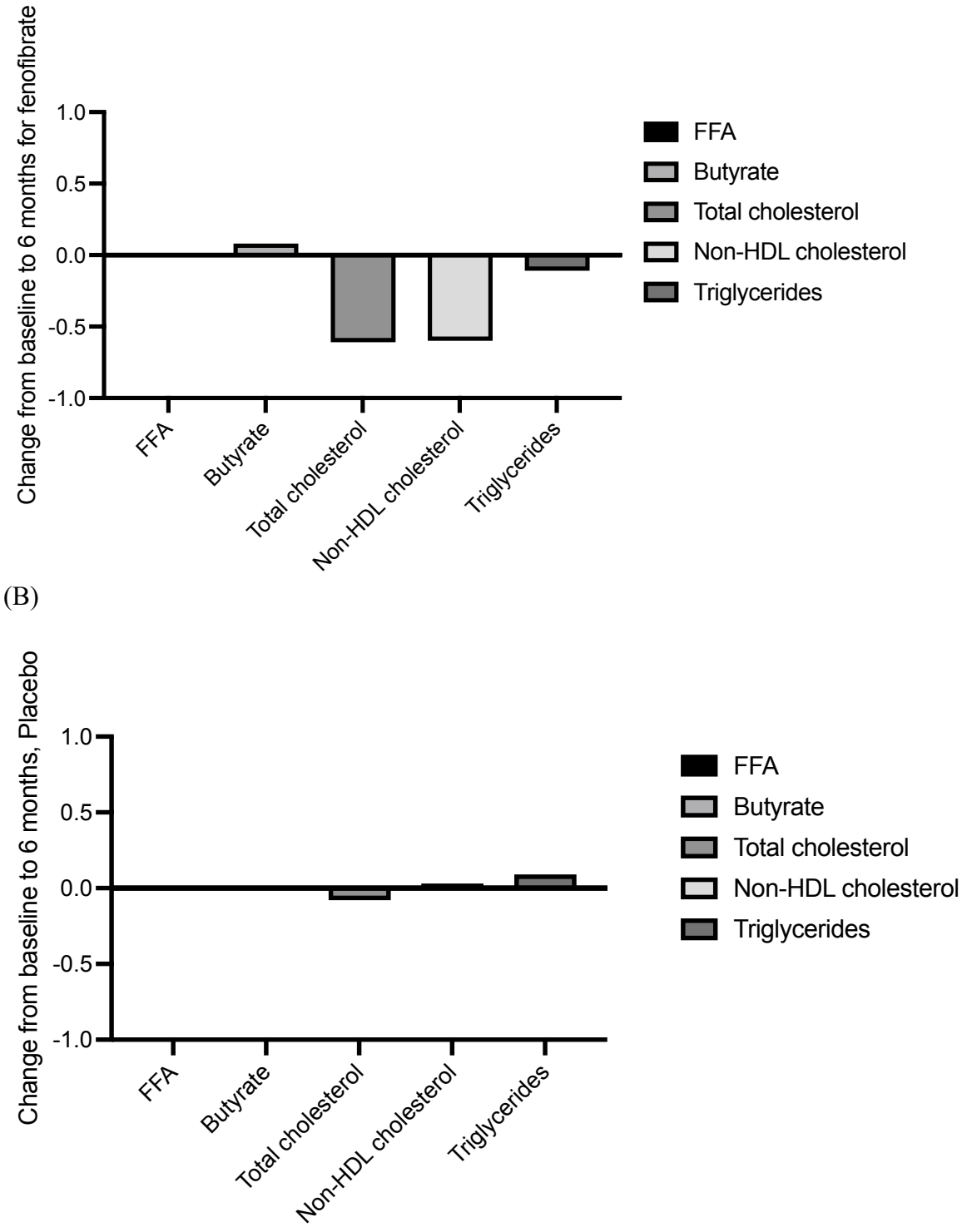


Figure 5.15: Summary of the main changes in free fatty acids and lipid profile in the (A) Fenofibrate and (B) Placebo group.

***Table 5.6: Summary of the paired t-test results for blood markers post 6 months treatment with Fenofibrate and placebo**. HDL, high density lipoprotein; BNP, Brain natriuretic peptide.*

Parameter	N recruited	N analysed	Mean ± SD (baseline)	Mean ± SD (post treatment)	Mean difference (95% CI)	P value
Free fatty acids (mmol/L)						
Fenofibrate	*59*	*27*	*0.66 ± 0.33*	*0.66 ± 0.36*	*0.00 (-0.10, 0.10)*	*0.98*
Placebo	*13*	*9*	*0.69 ± 0.34*	*0.69 ± 0.29*	*-0.00 (-0.48, 0.48)*	*0.99*
Beta-hydroxybutyrate levels (mmol/L)						
Fenofibrate	*59*	*26*	*0.13 ± 0.07*	*0.22 ± 0.21*	*0.08 (-0.002, 0.17)*	*0.028**
Placebo	*13*	*9*	*0.10 ± 0.02*	*0.10 ± 0.01*	*0.0 (-0.046, 0.046))*	*0.50*
Serum cholesterol (mmol/L)						
Fenofibrate	*59*	*26*	*4.6 ± 0.82*	*4.0 ± 0.76*	*-0.61 (-1.2, -0.02)*	*0.04**
Placebo	*13*	*9*	*4.2 ± 0.76*	*4.1 ± 0.68*	*-0.08 (-0.85, 0.67)*	*0.79*
Serum triglycerides (mmol/L)						
Fenofibrate	*59*	*26*	*0.95 ± 0.34*	*0.84 ± 0.39*	*-0.11 (-0.39, 0.16)*	*0.40*
Placebo	*13*	*9*	*0.96 ± 0.37*	*1.06 ± 0.47*	*0.09 (-0.46, 0.67)*	*0.69*
Non-HDL cholesterol (mmol/L)						
Fenofibrate	*59*	*27*	*3.3 ± 0.85*	*2.7 ± 0.80*	*-0.6 (-0.85, -0.35)*	*<0.0001**
Placebo	*13*	*10*	*2.88 ± 0.71*	*2.91 ± 0.55*	*0.03 (-0.12, 0.18)*	*0.67*
HDL cholesterol (mmol/L)						
Fenofibrate	*59*	*27*	*1.42 ± 0.29*	*1.40 ± 0.27*	*-0.02 (-0.08, 0.036)*	*0.4427*
Placebo	*13*	*10*	*1.28 ± 0.33*	*1.30 ± 0.43*	*0.02 (-0.09, 0.13)*	*0.70*

NT-pro BNP (pmol/L)						
Fenofibrate	*59*	*27*	*289.5 ± 382.7*	*377.1 ± 447.4*	*87.6 (41.8, 133.3)*	*0.006**
Placebo	*13*	*9*	*201 ± 207*	*268 ± 253*	*67.6 (-6.9, 142.2)*	*0.07*
Glucose (mmol/L)						
Fenofibrate	*59*	*26*	*5.0 ± 0.63*	*4.7 ± 0.69*	*-0.30 (-0.66, 0.05)*	*0.09*
Placebo	*13*	*8*	*5.7 ± 1.43*	*5.1 ± 1.37*	*-0.55 (-1.4, 0.34)*	*0.19*
Haemoglobin levels (mg/dl)						
Fenofibrate	*59*	*29*	*140 ± 12.7*	*136 ± 13.3*	*-4.1 (-6.8, -1.36)*	*0.005**
Placebo	*13*	*9*	*136 ± 13.5*	*135.3 ± 15.3*	*-1.36 (-5.6, 2.9)*	*0.49*

5.4 Discussion

This is the first randomised controlled study investigating the effects of PPARα agonist, Fenofibrate on cardiac fatty acid metabolism (myocardial lipid content) and energetics (PCr/ATP). Additionally, the exploratory outcomes including CMR markers of cardiac structure and function as well as blood markers discussed in this chapter strengthen our mechanistic understanding of treatment effects with Fenofibrate on cardiac physiology in moderate-severe AS.

Use of Fenofibrate considerably reduced the myocardial triglyceride content ($p<0.05$) in 6 months' duration. There was a modest improvement in cardiac energetics in both the fenofibrate and placebo groups, but this was statistically significant in the fenofibrate group only ($p=0.05$, one-tailed). There was no significant change in measures of LV subclinical dysfunction (peak systolic longitudinal and circumferential strain) in either the fibrate or placebo groups. However, there was some improvement in measures of diastolic function (peak longitudinal strain rate) in the fibrate group.

Blood markers showed a significant increase in the beta-hydroxybutyrate levels ($p<0.05$) with no change in free fatty acid levels in the fibrate group. Conceivably, there was also a notable change in the blood cholesterol levels in the fibrate group.

5.4.1.1 Changes in myocardial triglyceride content

Myocardial lipid accumulation is observed in tissues with high turnover/metabolism of FFAs, such as the heart, when utilization of FFAs is impaired in the face of continued FFA import or production. While long-chain FFAs are the major source of energy in the normal adult mammalian heart, pressure overload in AS is associated with a switch in energy substrate utilization from FFAs to glucose,[129] and decreased FFA oxidation is associated with triglyceride accumulation.[168] Transcriptionally, long-chain fatty acid oxidation is regulated by

PPARα, a nuclear receptor that binds to peroxisome proliferator response element (PPRE) to up-regulate the transcription and translation of genes for all the enzymes involved in the β-oxidation of fatty acids.[277] Importantly, these metabolic changes appear to precede structural alterations and hence, might be better suited to risk stratify and guide treatment in AS. Thus, metabolic modulation with PPARα is a promising target for metabolic precision therapy in AS.

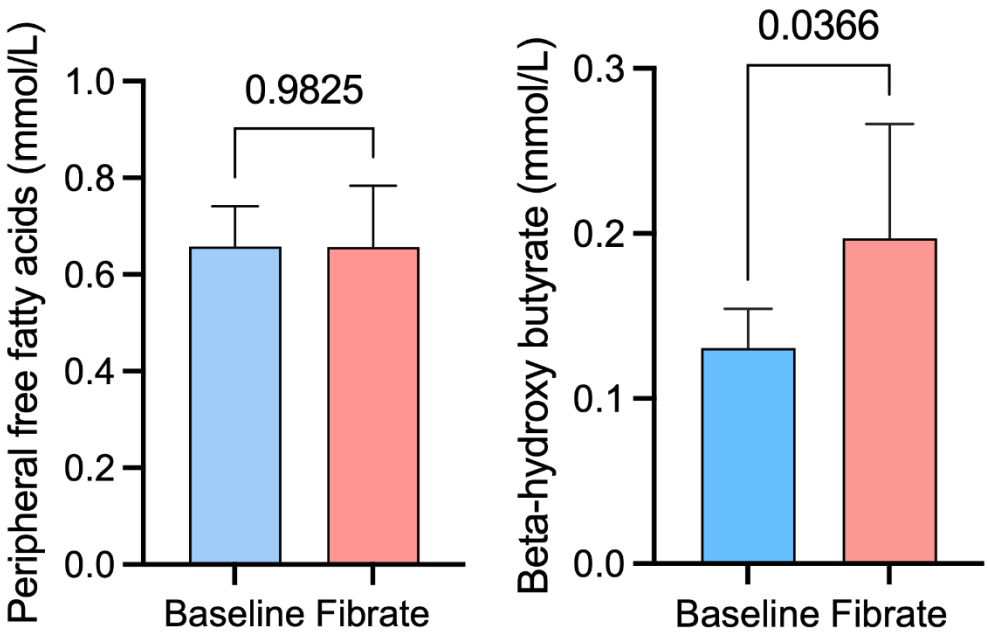
However, it is worth mentioning that the placebo group also showed a considerable drop in myocardial triglyceride content, though the change was not significant.

There is clear evidence from the blood markers that there was increased FAO in vivo as indicated by increased beta-hydroxy butyrate levels but no change in circulating FA levels. I appreciate that these results were from venous blood samples and represent increased FAO in the liver. However, taking this and reduced MTG on MRS together, it is plausible that similar increased FAO occurred in the myocardium as well.as a result of action of Fenofibrate (explained in the section 5.4.4.2 below). The mechanism underlying the reduction in MTG content in the placebo group remains unclear.

5.4.1.2 Change in blood markers

The changes in blood markers in the fibrate group in this study have shown that the reduction in MTG content occurred through increased fatty acid oxidation rates as evidenced by the increase in beta-hydroxybutyrate levels in the blood (**Figure 5.16**). There was no change in peripheral (fasting venous) free fatty acid levels implying there was no increased uptake of FA. Increased beta-hydroxybutyrate levels post fibrate indicate increased FAO in the liver with more production of acetyl Co-A and subsequent beta-hydroxybutyrate. **Figure 5.17**). No such change in beta-hydroxybutyrate levels were seen in the placebo group despite a drop in MTG.

(A)



(B)

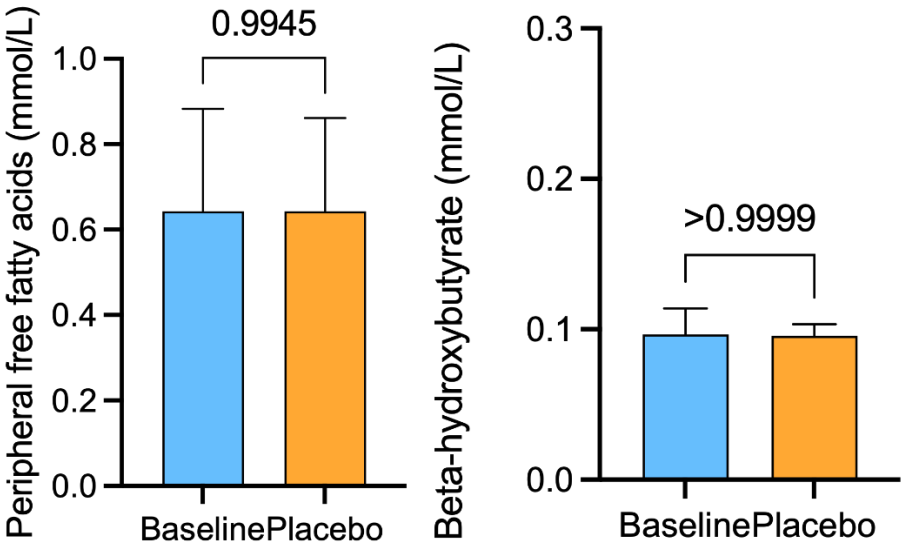


Figure 5.16: Change in free fatty acid and beta-hydroxybutyrate levels in the (A) Fibrate group (B) Placebo group as assessed by paired t-test from baseline to 6 months.

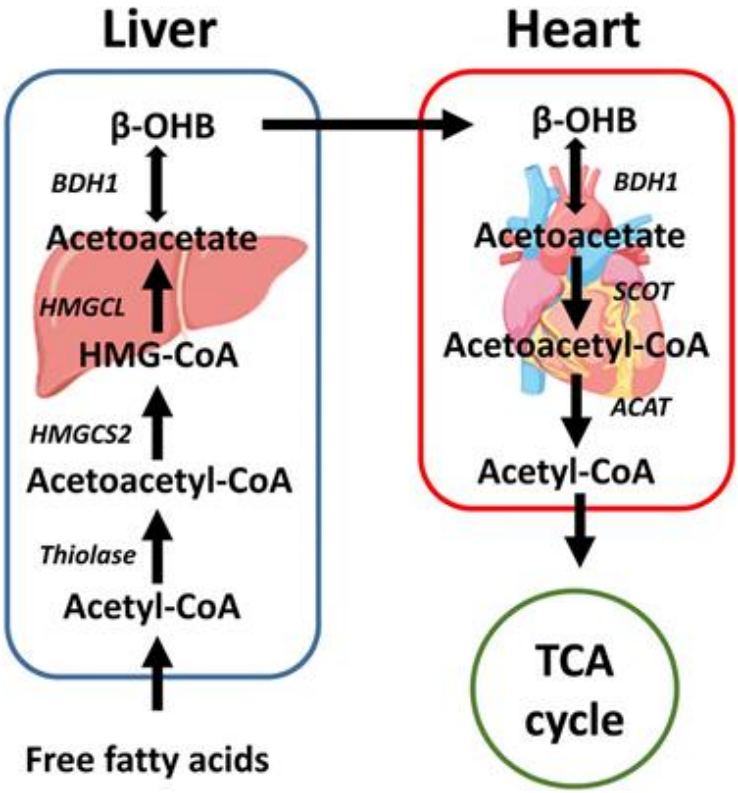


Figure 5.17: A brief schematic of the ketone body production and oxidation in the liver and heart. *Ketone bodies are mainly produced in the liver with fatty acid oxidation. After being transported through the circulatory system, β-OHB can be oxidized in extrahepatic organs, such as the heart. In the heart, β-OHB can generate acetyl-CoA that can enter the TCA cycle.*[278] *β-OHB: β-hydroxybutyrate, HMGCS2: 3-hydroxy-3-methylglutaryl-CoA synthase 2, HMG-CoA: 3-hydroxy-3-methylglutary-CoA, HMGCL: 3-hydroxy-3-methylglutaryl-CoA lyase, BDH1: β-hydroxybutyrate dehydrogenase 1, SCOT: Succinyl-CoA: 3-oxoacid-CoA transferase, ACAT: Acetyl-CoA acetyltransferase, TCA cycle: Tricarboxylic acid cycle.*

Of note, there was no corresponding change in circulating free fatty acid levels in the fibrate group. Thus, this suggests that the reduction in MTG the fibrate group was secondary to upregulation of fatty acid oxidation rates without altering the free fatty acid supply.

5.4.1.3 Change in cardiac energetics (PCr/ATP)

There was only a modest increase in PCr/ATP in the Fibrate group ($p = 0.05$). However, as we are measuring a ratio i.e. PCr/ATP, the results are influenced by two variables, PCr and ATP. It is well known that PCr pools decrease early in non-failing pressure overload whilst the heart is still able to maintain the ATP production.[182, 184]

As the disease progresses and the heart transitions from compensated stage towards failure, the ATP production may start getting affected.[135] Myocardial ATP levels have shown to fall in HF and longitudinal studies in animals have shown that the ATP loss is slow and progressive.[279] Hence, it's plausible that there is perhaps reduction in both PCr and ATP levels in the transition phase before the development of overt HF. As the disease advances, the fall in ATP can result in pseudo-normalization of PCr-to-ATP ratios from being reduced, thus making even a small improvement post treatment much more impactful.

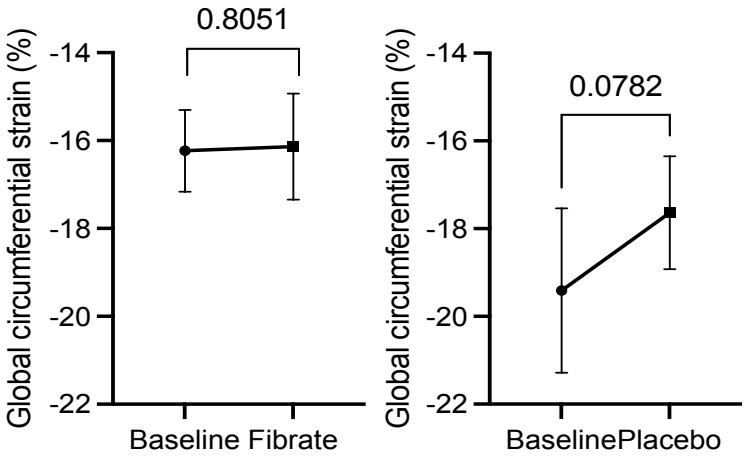
5.4.1.4 Change in left ventricular function and structure

There was no significant effect on cardiac physiology despite the changes in cardiac metabolism, described above, in the fibrate group. No change was seen in the placebo group either.

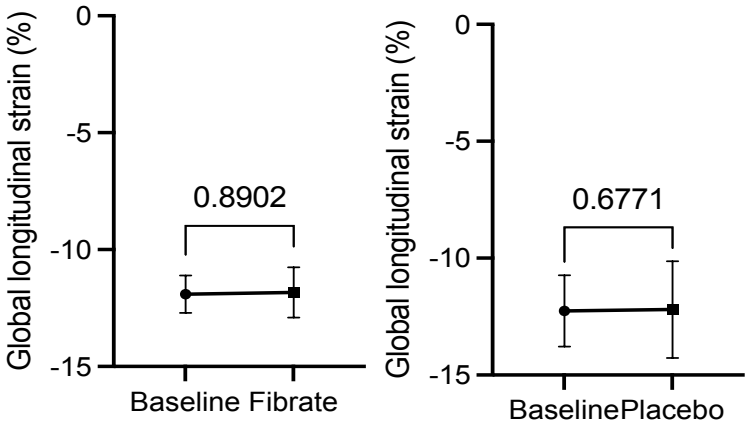
Whilst there was evidence of subclinical dysfunction with impaired peak systolic longitudinal and borderline normal circumferential strain (normal range -15 to -20%) at baseline. There was no significant improvement in either of these parameters in the fibrate group post-treatment. It is, however, noteworthy that the peak systolic circumferential strain fell considerably in the placebo group during the study (**Figure 5.18**). Hence, it is plausible that Fenofibrate potentially prevented such deterioration in the fibrate group. There was also a

modest improvement in peak diastolic longitudinal strain rate in the fibrate group (p = 0.028). Overall, there was a deterioration in LV ejection fraction, despite the values remaining in the normal range, as the disease progressed over the 6 months duration in both the groups.

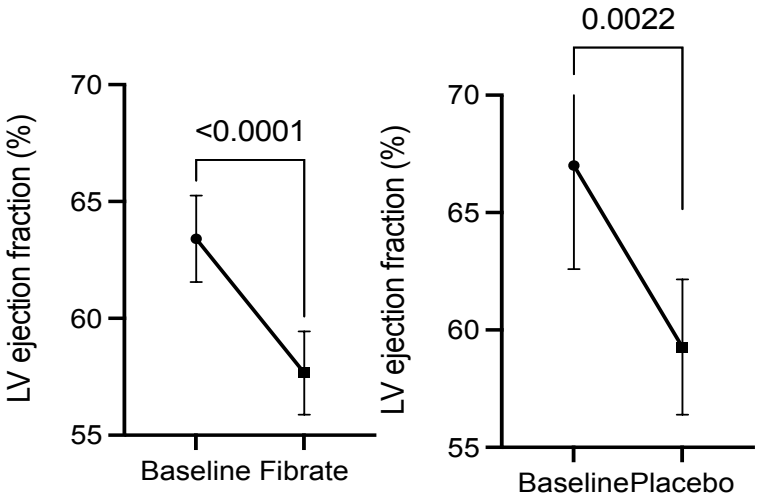
(A)



(B)



(C)



(D)

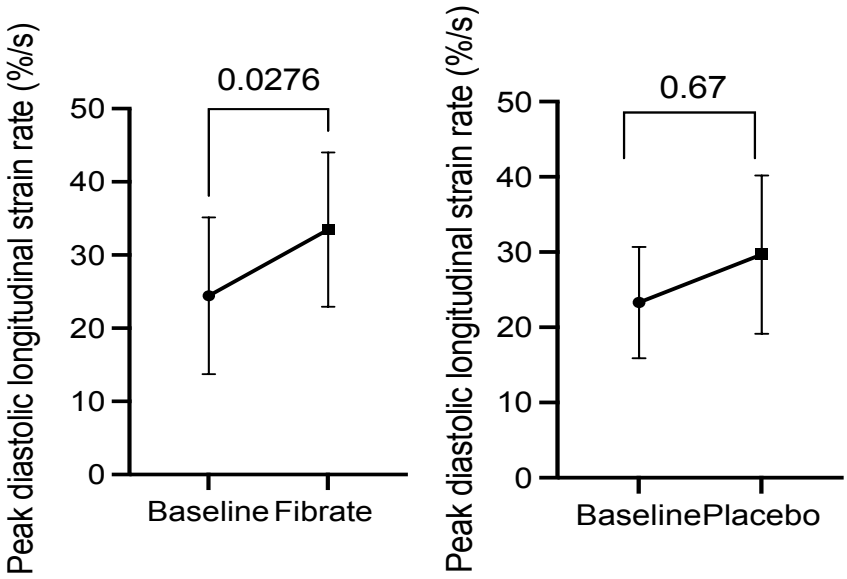


Figure 5.18: Summary of the changes in left ventricular (A) circumferential strain, (B) longitudinal strain and (C) ejection fraction (D) Diastolic longitudinal strain rate in both the groups.

Myocardial hypertrophy, high LV mass index and myocardial fibrosis in pressure overload AS state are known to predict future events and indicate high risk population.[14, 44] In this study, I investigated measures of LV structure and function via CMR. Fenofibrate did not result in reduced hypertrophy or reverse remodelling of the myocardium.

5.5 Limitations and future directions

The main limitation of the study is that the placebo groups was not powered to detect a difference between the placebo and fibrate group but was only there to allow blinding during randomisation. The study was not powered to make comparison between Fibrate and Placebo groups which would have required much larger number of subjects and funds. Due to funding limitation of BHF CRTF, the options were to either underpower both arms for direct 1:1 comparison or power one arm adequately. Also, this study was a proof-of-concept study to determine if cardiac metabolism was modifiable using PPARα agonist, Fenofibrate.

Hence, we powered the Fibrate arm adequately to detect change from baseline to 6 months' treatment.

The study was affected by the global COVID-19 pandemic and subsequent national lockdowns which led to loss of follow-ups. As a result, in the fibrate group we ended up with only 34 complete datasets instead of 48. Whilst this did not affect the primary outcome, the other outcomes might have been affected by the smaller sample size.

The study treatment was provided for 6 months (180 ± 7 days) and in a single dose 200mg OD (in those with eGFR >90ml/min) and 67 mg OD (in those with eGFR 60-90ml/min). One does wonder whether a longer treatment duration might have provided different results, and perhaps a chance for the metabolic changes seen in this study to exert effect on cardiac physiology.

Due to limitations to funding, I did not assess creatine kinase flux in this study, which may have been a better marker for cardiac ATP delivery than PCr/ATP.

Finally, another possible limitation could be the selection of AS cohort. In this study, I recruited participants with the more severe spectrum of the disease where the advanced pressure overload perhaps masks the beneficial impact of myocardial metabolic changes. And whether such metabolic modulation in mild-moderate disease may be more beneficial.

Also, it would be quite interesting to follow-up the participants in this trial to see if treatment with Fenofibrate affected their outcomes or LV remodelling post valve replacement.

Serum metabolomics results would have improved our understanding of the study results and perhaps explain why the drop in MTG in fibrate group did not have a physiological effect. The most plausible explanation is that Fenofibrate did modulate cardiac metabolism, as evidenced by serum FFA and butyrate levels, but the study was underpowered to detect physiological effect. However, other possibility could be that though Fenofibrate was able to

modulate cardiac metabolism but not to an extent to influence physiology, secondary to a sub therapeutic dose or duration of drug.

Change in MTG in the placebo group cannot be fully elucidated.

5.6 Conclusions

This study is the first proof-of-concept imaging trial of metabolic therapy in AS. It has shown that it is feasible to reduce myocardial lipid content with a PPARα agonist, Fenofibrate in moderate-severe progressive AS. Such a modulation does improve myocardial energetics as well as diastolic function . However, there was no improvement in systolic strain parameters or regression of LVH.

This study has also highlighted the role of cardiac magnetic resonance imaging, in particular magnetic resonance spectroscopy[280] in assessing changes in myocardial metabolism in pressure-overload LVH, which are important for understanding the pathophysiologic processes, identifying those most at risk of decompensation and for developing new therapeutic targets.

Future mechanistic trials investigating the effect of metabolic therapy in early stages of AS would be useful. The results from this study could be taken as a blueprint in generating further, large scale evidence.

6 Chapter Six

The effect of metabolic modulation on cardio-respiratory fitness and exercise capacity in AS

6.1 Abstract

6.1.1 Background

Hypertrophied AS hearts exhibit myocardial steatosis and energetic impairment, but the pathophysiological impact of such metabolic alterations is not fully understood. I, hypothesised, that the metabolic modulator, Fenofibrate would ameliorate myocardial steatosis and energy deficit and thereby improve cardiac function and exercise capacity in moderate-severe AS.

6.1.2 Methods

Seventy-two patients with asymptomatic moderate-severe AS were randomised to Fenofibrate (n = 59) or Placebo (n = 13). Myocardial lipid content and PCr/ATP ratio, LV strain parameters, myocardial fibrosis, peak VO_2 and six-minute walking distance were assessed at baseline and study end (180± 7 days).

6.1.3 Results

Despite reducing myocardial steatosis and modestly improving energetics, Fenofibrate did not have any significant effect on peak VO_2 (MD 0.09, 95% CI: -1.09, 1.27; p = 0.87) or 6MWT (MD -7.2, 95% CI: 7.9, -22.2; p = 0.33) or markers of diastolic function and LV strain. Peak VO_2 related significantly to LV systolic strain and diastolic strain rate in the Fibrate group.

6.1.4 Conclusions

In asymptomatic moderate-severe AS stage, Fenofibrate a modulator of substrate metabolism did not influence aerobic capacity despite reducing myocardial lipid content and improving cardiac energetics.

6.2 Introduction

Pressure overload hypertrophy leads to LV remodelling, encompassing increases in LV mass and end-diastolic volumes as well as changes in functional parameters. Physiological abnormalities of the LV with impaired relaxation, decreased diastolic filling and increased myocardial stiffening is well-known in moderate-severe AS.[281] Patients with moderate-severe AS are also known to have impaired longitudinal and circumferential strain with evidence of diastolic dysfunction despite a normal ejection fraction.[247, 282] These changes in strain and diastolic function appear either to be more sensitive for detection of abnormal LV function in patients with AS or to precede systolic dysfunction or both.[240, 283, 284]

The effects of myocardial steatosis on cardiac structure and function has been investigated in both animal and human models showing contributing to significant decline in cardiac function.[152, 162, 285] Accumulation of myocardial triglycerides is one of the causal factors associated with ventricular stiffening and impairments in strain and diastolic function.[286]

Peroxisome proliferator-activated receptor (PPAR)α is the main transcriptional factor controlling lipid homeostasis in the heart, and its down regulation is linked to perturbations in FAO and myocardial lipid accumulation.[64,65] Fenofibrate, a PPARα agonist has the potential to alter this imbalance of FAO and may help modulate myocardial fatty acid metabolism and subsequently reduce myocardial steatosis.[165] This could potentially have a beneficial effect on cardiac physiology and may further improve functional capacity in patients with moderate-severe AS.

Functional capacity is commonly quantified using peak oxygen consumption (VO_2), which is a product of cardiac output (heart rate x stroke volume) multiplied by arterial venous oxygen difference. Thus, the complex interplay of cardiac, pulmonary, peripheral muscle and cellular function determines the overall ability to exercise. Various factors contribute to functional capacity including age, sex, body mass index, and comorbid medical conditions, which are known to be associated with a decrement in exercise capacity, as reflected by a decrease in maximal workload achieved or peak VO_2 on cardio-pulmonary exercise testing (CPET).[287, 288, 198] Abnormalities of LV diastolic dysfunction, however, are shown to be associated with exercise capacity, independent of age, sex and body mass index.[289, 290, 291] Increased left atrial (LA) volume has been suggested to reflect longstanding. pressure overload and thus a valuable parameter reflecting both the duration and severity of the diastolic dysfunction in cardiac conditions.[260] Impaired longitudinal strain is associated with abnormal exercise response and increased risk of cardiac events in asymptomatic patients with severe AS.[48] Both diastolic and subclinical systolic dysfunction can be measured using CMR imaging. LV peak systolic longitudinal strain, LV peak systolic circumferential strain and LV late diastolic longitudinal strain rate can be measured using CMR tagging, which is the gold standard for measurement of myocardial strain.[218]

The aim of the present study was therefore to evaluate the effect of reducing myocardial lipid content on parameters of exercise capacity in moderate-severe AS and whether any change in exercise capacity was related to the CMR parameters of systolic and diastolic function.

6.3 Methods

In this prospective, randomized, double-blind, placebo-controlled study, patients with moderate-to-severe asymptomatic AS (n=72) were randomly assigned to Fenofibrate 200 mg daily (n = 59) or matched placebo (n = 13) for 6 months (mean treatment duration 180 ± 7 days). All subjects underwent cardio-pulmonary exercise testing using ergometer bike at 0

and 6 months, with follow-up data in 43 participants. The secondary outcome was change in peak oxygen consumption (VO_2) measured using CPET and six-minute walk distance on 6MWT.

Details of the randomisation process and study population have already been described in Chapter 5, section 5.3.1

6.3.1 Data acquisition

6.3.1.1 Cardio-pulmonary exercise test (CPET)

Patients were seated on a stationary exercise bike (Ergoline GmbH, Bitz, Germany) for resting spirometry and a cardiopulmonary exercise test (CPET) using breath-by-breath respiratory gas analysis (Metalyzer 3B, Cortex Biophysik, Leipzig, Germany). A standardised incremental exercise protocol was used, and patients encouraged to exercise until a RER of ≥1.1 was reached. Peripheral oxygen saturation (SpO_2), capillary lactate and subjective exertion (Borg Scale) were assessed every 3-4 minutes and peak VO_2 measured at maximal exhaustion.

6.3.1.2 Six-minute walk test

Participants performed a six-minute walk test (6-MWT) at their own pace along a 20-meter corridor. Total distance covered, rating of perceived exertion as well as SpO_2 were recorded prior to and after the test (see Chapter 2)

6.3.2 Data analysis

6.3.2.1 CPET and spirometry

Breath-by-breath respiratory gas analysis to calculate peak VO_2 and other indices as well as spirometry analysis of FEV1 and FVC was conducted on a workstation after every individual exercise test (see Chapter 2).

6.3.2.2 Statistical analysis

Statistical analysis was performed on complete datasets using descriptive statistics or analysis of variance (ANOVA) or Pearson correlation. The secondary end-point analysis was done separately in the placebo and treatment group. Baseline and 6-month follow-up data in each completed dataset was

analysed using paired t-test. All analysis was performed using SPSS, version 28 and GraphPad Prism (version 9.0.2 for Windows; GraphPad Software, San Diego, CA). All data is presented as mean ± SD (standard deviation) unless stated otherwise. Determination of statistical significance between pre and post treatment tests was assessed by paired t-test. Values of $p < 0.05$ were considered as statistically significant.

6.4 Results

A total of 72 participants were enrolled in the study and randomised to receive either Fenofibrate or Placebo treatment.

6.4.1 Study population

Overall, 47 (65%) participants successfully completed the study, of which 11 were on placebo and 36 were assigned to Fenofibrate. The mean duration of exposure to treatment was 176.4 ± 7.8 days for the Fenofibrate group with treatment compliance of 98.6 ± 2.21 %. The mean duration of treatment in the placebo group was 173 ± 11.6 days and overall treatment compliance of 99.6 ± 0.44%. 82% of patients were male, all patients were White (100%) and their mean age was 70 ± 14 years. All subject characteristics were similar in both groups including age, BMI, blood pressure and heart rate.

Chapter 5, Table 5.2 summarises the baseline characteristics of the cohorts. **Reproduced again** below:

Table 5.2: Baseline characteristics Ox-FAST: Characteristics at baseline for all patients randomised to treatment. *BMI, body mass index; SBP, systolic blood pressure; DBP, diastolic blood pressure; HR, heart rate; ACE-i, angiotensin converting enzyme inhibitor; ARB, angiotensin receptor blocker.*

Characteristic	Fenofibrate (n= 59)	Placebo (n=13)	P-value
Age, mean ± SD, years	70 ± 14	72 ± 17	ns
Male, %	71.7	72.7	
Female, %	28.3	27.3	
BMI (Kg/m2), mean ± SD	27.3 ± 4.7	25.7 ± 4.3	ns
SBP (mmHg), mean ± SD	138 ± 17	145 ± 21	ns
DBP(mmHg), mean ± SD	72 ± 9	75 ± 6	ns
HR (bpm), mean ± SD	63 ± 11	64 ± 9	ns
Bloods, mean ± SD			
NT-proBNP (pg/ml)	342 ± 491 (38.5, 2611.6)	529 ± 1046 (10.3, 3272.9)	ns
Glucose (mmol/L)	5.27 ± 0.68	5.56 ± 1.33	ns
Free fatty acids (mmol/L)	0.66 ± 0.28	0.64 ± 0.31	ns
Beta-hydroxybutyrate levels (mmol/L)	0.14 ± 0.07	0.10 ± 0.02	ns
Total cholesterol(mmol/L)	4.54 ± 0.83	4.23 ± 0.72	ns
Triglycerides (mmol/L)	1.02 ± 0.40	0.97 ± 0.34	ns
Comorbidities and medications			
Atrial Fibrillation, %	13.2	9.1	

Hypertension, %	34	36.4
ACE-i/ARB, %	34	36.4
Beta blockers, %	13.2	0
Statins, %	34	63.6
Diuretics, %	9.4	0

6.4.2 Cardiopulmonary exercise testing parameters

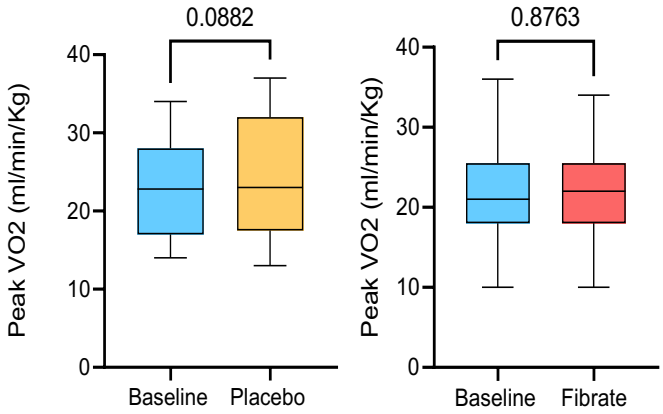
Mean peak VO_2 in the fibrate group post 6 months' treatment was 22.1 ± 5.8 ml/kg/min, which was lower than that in the placebo group (24.1 ± 8.1ml/kg/min, $p<0.001$). After 6 months of study duration and treatment, 53% (18/34) participants in the Fibrate group and 55% (6/11) had peak VO_2 < 85% predicted value, compared to 74% (25/34) and 45% (5/11) at baseline respectively.

Mean VE/VCO_2 slope was overall elevated (Table 4.1, chapter 4), >35 ml/kg/min – prognostic cut-off from heart failure studies[292] but was similar in both groups post treatment (40.2 ± 4.9 ml/min in Fibrate vs 40.5 ± 6.1 ml/min in Placebo). VO_2 at ventilatory threshold (VT) was higher in the Placebo group vs Fibrate post treatment (31 ± 7.2 kg/ml/min in Placebo vs 26.8 ± 6.2 kg/ml/min in Fibrate group).

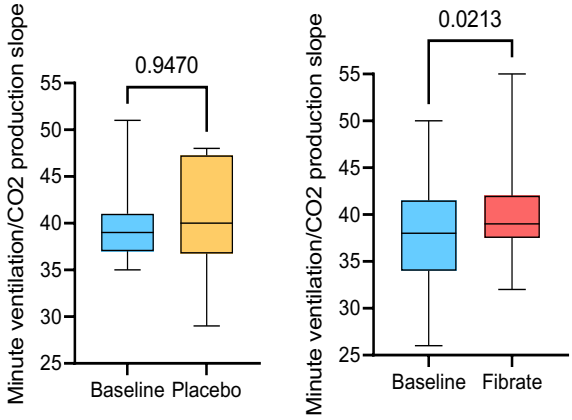
On multivariate regression analysis of both the post treatment groups, age, BMI, gender, LVMI and LVSV were predictors of peak VO_2. However, on univariate analysis only age, BMI and female sex were independent predictors of peak VO_2. These were like that in baseline results as detailed in Chapter 4.

Rest of the analysis was focussed on the change in CPET parameters and its relationship with other parameters. See **Figure 6.1** below.

(A)



(B)



(C)

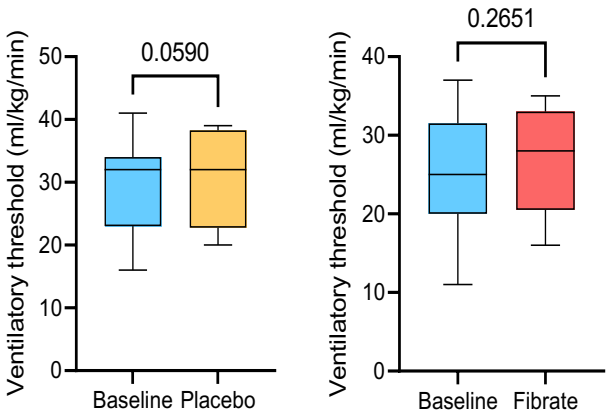


Figure 6.1: Mean values for the main CPET parameters in the two groups both pre and post treatment and paired t-test results for these parameters i.e. (A) peak VO_2, (B) VE/VCO2 and (C) VT. *Peak VO_2, maximal oxygen capacity; VE/VCO2, minute ventilation/carbon dioxide production; VT, ventilatory threshold*

Pre and post treatment: There was no significant change from baseline to 6 months in peak VO_2 (mean difference 0.09, 95% CI: -1.09, 1.27; p = 0.88) or ventilatory threshold, VT (mean difference 0.58, 95% CI: -0.46, 1.61; p = 0.27) in the fibrate group. The minute ventilation/carbon dioxide production (VE/VCO_2) slope however worsened significantly in the Fenofibrate group post 6 months treatment (mean difference 2.2, 95% CI: 0.34, 3.96; p = 0.02). In the Placebo group, no significant improvement or deterioration was seen in any of these parameters. Two participants in the fibrate group were not able to reach the required RER in the post treatment tests, rest all were able to exercise to maximal volitional effort (RER 1.27 ± 0.11) in the Fibrate group as well as in the Placebo group (RER 1.29 ± 0.12).

6.4.3 Spirometry results

Spirometry assessment did not show any significant change in the Fibrate group. However, in the Placebo group there was slight improvement in the forced vital capacity, FVC from baseline to 6 months (mean difference 0.92, 95% CI: 0.61, 1.21; p = 0.0001). No improvement was seen in FEV1 in the placebo group

Table 6.1 presents a summary of the CPET and spirometry results.

***Table 6.1*: Summary of the paired t-test results for spirometry, CPET and 6MWT parameters in both the fibrate and placebo groups.** *FEV1, forced expiratory volume; FVC, forced vital capacity; CPET, cardiopulmonary exercise test; VO_2, maximal oxygen consumption; VT, ventilatory threshold; VE/VCO2, minute ventilation/carbon dioxide production; RER, respiratory quotient; 6MWT, six minute walk test.*

Parameter	N recruited	N analysed	Mean ± SD (baseline)	Mean difference (95% CI)	P value
Spirometry, FEV1					
Fenofibrate	59	33	2.5 ± 0.97	0.37 (-0.15, 0.88)	0.15
Placebo	13	10	3.8 ± 1.3	-0.46 (-1.15, 0.24)	0.15
Spirometry, FVC					
Fenofibrate	59	33	4.1 ± 0.48	-1.16 (-7.8, 5.5)	0.27
Placebo	13	10	3.43 ± 0.96	0.92 (0.61, 1.21)	**0.0001***
CPET parameters					
Peak VO_2 (ml/min/Kg)					
Fenofibrate	59	33	21.9 ± 5	0.09 (-1.09, 1.27)	0.87
Placebo	13	10	22.1 ± 6.9	2.0 (-0.37, 4.41)	0.09
VT (ml/kg/min)					
Fenofibrate	59	33	26.3 ± 5.8	0.58 (-0.46, 1.61)	0.27
Placebo	13	10	28.5 ± 7.4	2.5 (-0.12, 5.12)	0.06
VE/VCO2 slope					
Fenofibrate	59	33	38 ± 5.4	2.2 (0.34, 3.96)	**0.02***
Placebo	13	10	40.4 ± 4.7	0.10 (-3.2, 3.41)	0.95

RER					
Fenofibrate	59	33	1.27 ± 0.11	0.002 (-0.03, 0.03)	0.90
Placebo	13	10	1.29 ± 0.12	-0.03 (-0.11, 0.04)	0.35
Maximum workload (W)					
Fenofibrate	59	33	117 ± 34	-1.63 (-10.8, 7.6)	0.72
Placebo	13	10	118.7 ± 46.7	-2.4 (-12.3, 7.4)	0.59
Capillary lactate (mmol/L)					
Fenofibrate	59	33	3.6 ± 1.4	-0.30 (1.43, 0.25)	0.24
Placebo	13	10	4.3 ± 2.0	-0.37 (-1.06, 0.32)	0.25
6MWT distance (m)					
Fenofibrate	59	33	435 ± 103	-7.2 (7.9, -22.2)	0.33
Placebo	13	10	409 ± 111	7.5 (-29, 44)	0.64

6.4.4 Six-minute walk test

Patients in the Fibrate group had higher baseline distance walked on 6MWT (435 ± 103 metres) compared to placebo (409 ± 111 metres). Post 6 months treatment, there was no significant change in the 6MWT distance for either of the groups. Numerically, those in fibrate group had slightly lower post treatment values (mean difference -7.5) than at baseline but the actual distance covered remained overall higher in the Fibrate group when compared to Placebo (430 ± 73 m vs 417 ± 86 m). See Figure 6.2.

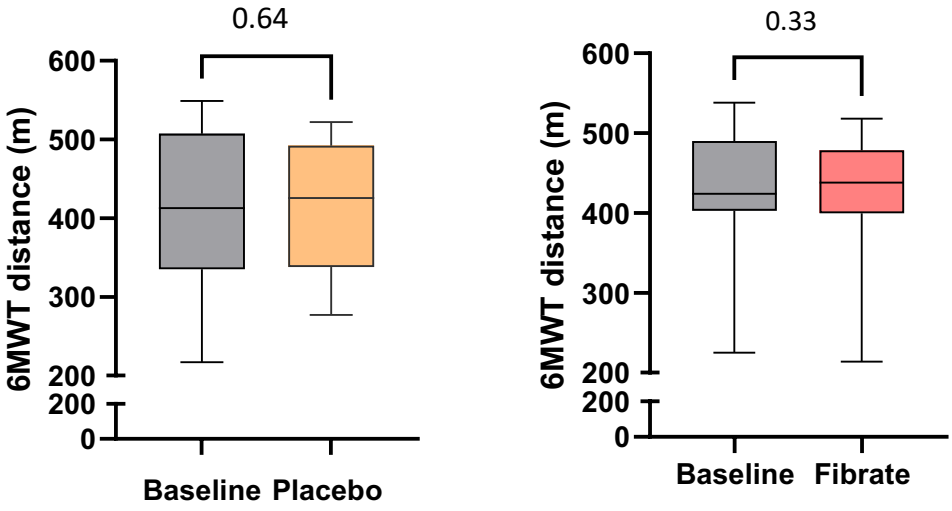


Figure 6.2: Graphic representation of pre and post treatment values of 6MWT distance in both the Fenofibrate and Placebo groups *(6MWT, six-minute walk test, ns = not significant).*

6.4.5 Exercise parameters and CMR measures of LV structure and function

6.4.5.1 LV systolic and diastolic strain

There was no significant correlation between delta change in LV peak systolic longitudinal and circumferential strain and delta change in measures of peak VO_2, VT or VE/VCO_2 in either the Placebo or Fibrate groups. Similar results were seen when delta change in longitudinal diastolic strain rate was compared to the delta of CPET parameters. (**Table 6.2**) However, on examining the post treatment values in the Fibrate group, peak VO_2 were moderately associated with both peak systolic longitudinal strain rate (r = -0.39, 95% CI:-0.68, -0.0068; p = 0.047) and peak systolic circumferential strain (r = -0.44, β = -0.92, 95% CI: -1.73, -0.13; p = 0.03). No significant correlation was seen between peak VO_2 and longitudinal diastolic strain rate (r = -0.36, p = 0.16). VT and VE/VCO2 did not correlate to any measured strain parameters.

In the placebo group, no significant relationship was seen between any of the CPET and strain parameters.

Table 6.2: Relationship between peak VO_2, maximal oxygen capacity and left ventricular strain parameter results post 6 months treatment for both Fenofibrate and Placebo groups. (P < 0.05 is considered significant). LV, left ventricle; long, longitudinal; circ, circumferential.

Variables	N recruited	N analysed	Pearson r	P value
LV strain parameters				
Peak systolic long strain (%)				
Fenofibrate	59	26	-0.44	0.023*
Placebo	13	10	0.47	0.17
Peak systolic circ strain (%)				
Fenofibrate	59	26	-0.39	0.047*
Placebo	13	10	0.22	0.57
Diastolic long strain rate (100/s)				
Fenofibrate	59	26	-0.36	0.16
Placebo	13	10	0.15	0.78

6.4.5.2 LV structure and function

Changes in the measures of LV structure and function, mainly LV end-diastolic volume (ΔLVEDV), LV stroke volume (ΔLVSV), LV mass index (ΔLVMI), LV wall thickness (ΔLVWT), and ejection fraction (ΔLVEF) were compared to changes in main CPET parameters i.e., peak VO_2 (ΔVO_2), ventilatory threshold (ΔVT) and minute ventilation/ carbon dioxide production slope ($\Delta VE/VCO_2$) pre and post treatment in the Fibrate group. LVEDV, LVSV and LVMI were chosen for analysis as these parameters had shown significant correlation with CPET parameters in the baseline data as explained in Chapter 4. In the Fibrate group, there was unexpectedly a significant negative correlation seen between ΔLVSV and Δ_{VO2} which may represent adaptive LV remodelling in well-compensated AS. However, no significant correlation was seen with other LV parameters. Details in **Table 6.3** below:

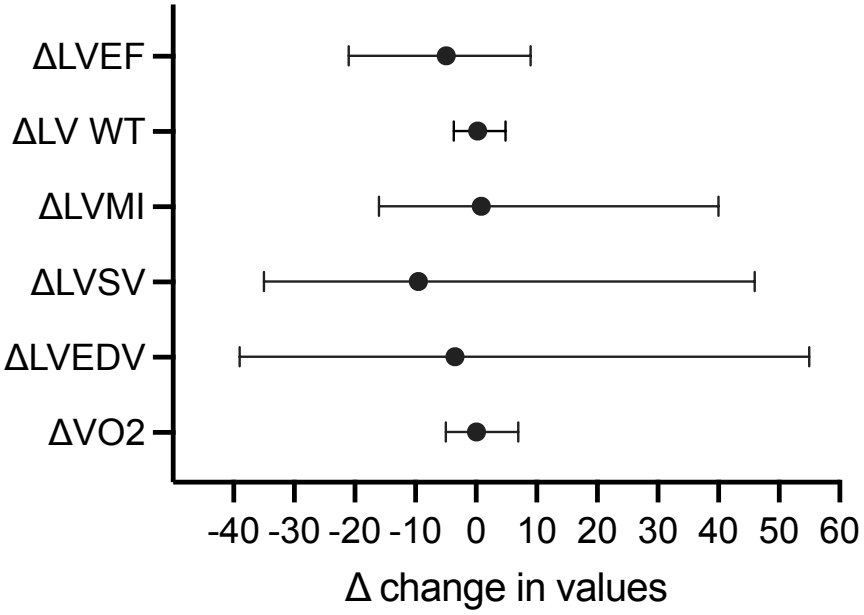
Table 6.3: Pearson correlation results between delta change in main LV parameters and peak VO_2 in the Fibrate group. *ΔVO_2, peak oxygen capacity (ml/Kg/min); LV, Left ventricular; ΔLVEDV, delta LV end-diastolic volume (mls); ΔLVSV, LV stroke volume; (mls) ΔLVMI, LV mass index (Kg/m^2); ΔLVWT, LV wall thickness (mm); ΔLVEF, LV ejection fraction (%). P < 0.05 considered significant.*

Parameter	N recruited	N analysed	Pearson r	95% CI	P value
ΔVO2	*59*	*33*			
ΔLVEDV	59	33	-0.29	-0.64, 0.17	0.21
ΔLVSV	59	33	-0.49	-0.77, -0.06	0.03*
ΔLVMI	59	33	0.18	-0.29, 0.58	0.45
ΔLVWT	59	33	-0.37	-0.69, 0.09	0.11
ΔLVEF	59	33	-0.40	-0.71, 0.05	0.77

Comparable results were seen in the placebo group with only the LVSV correlating with CPET measurements. See **Figure 6.3** below:

\

(A) Fibrate group



(B) Placebo group

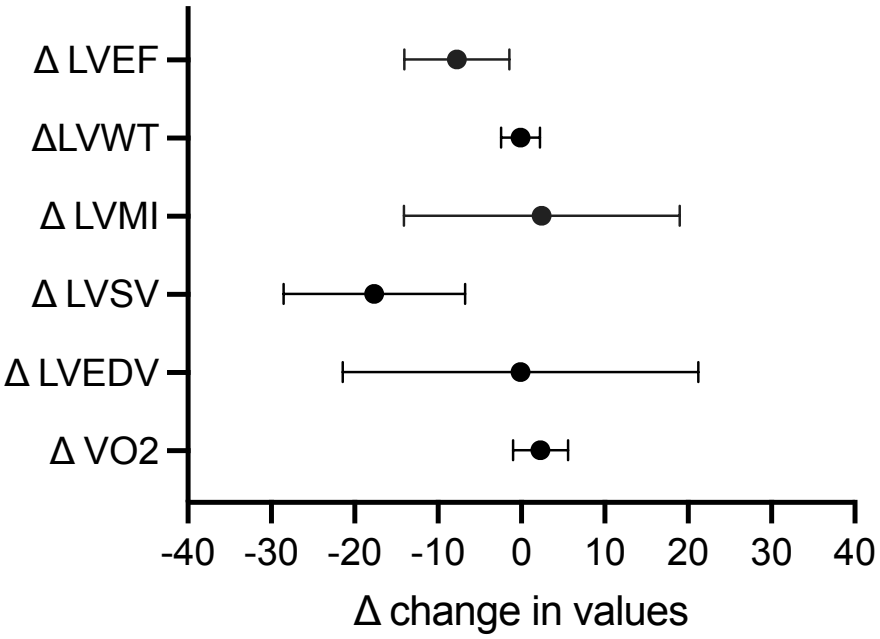


Figure 6.3: Correlation results for comparison between delta change in main LV parameters and peak VO_2 in both the Fibrate and Placebo groups. *ΔVO_2, peak oxygen capacity(ml/Kg/min); LV, Left ventricular; ΔLVEDV, delta LV end-diastolic volume (ml); ΔLVSV, LV stroke volume (ml); ΔLVMI, LV mass index (Kg/m^2); ΔLVWT, LV wall thickness (mm); ΔLVEF, LV ejection fraction (%)*

On comparison of the post-treatment values alone for LV parameters and exercise capacity in the Fibrate group, no significant correlation was seen between any of the parameters. See Table 6.4.

Table 6.4: Results of correlation analysis between post treatment values of peak VO_2 and chosen LV parameters in the Fibrate group. *Peak VO_2, maximal oxygen capacity (ml/Kg/min); LVSV, LV stroke volume (mls); LVEDV, LV end-diastolic volume (mls); LVMI, LV mass index (Kg/m^2); LVWT, LV wall thickness (mm); LVEF, LV ejection fraction (%).*

	Peak VO_2 vs. LVSV	**Peak VO_2 vs. LVEDV**	**Peak VO_2 vs. LVMI**	**Peak VO_2 vs. LVWT**	**Peak VO_2 vs. LVEF**
N analysed	33	33	33	33	33
Pearson r	0.22	0.22	-0.02	-0.18	-0.10
95% confidence interval	-0.13, 0.52	-0.13, 0.52	-0.36, 0.33	-0.49, 0.16	-0.43, 0.25
R squared	0.049	0.047	0.0004	0.03	0.01
P value	0.21	0.22	0.91	0.30	0.55

6.4.5.3 LA volume

Patients in both Fibrate and placebo groups had abnormal LA volumes at baseline (86.8 ± 41.2 mls in Fibrate vs 71.3 ± 18.4 mls in Placebo) which worsened over the study duration irrespective of whether they received Fibrate or Placebo (mean change Fibrate 17.8mls, p =0.002 vs mean change Placebo 18.8, p = 0.02) as detailed in chapter 5.

LA volumes at baseline as well as post treatment did not predict peak VO_2. Similarly, Δ LA volumes did not predict Δ peak VO_2 in Fibrate (r = -0.29, p = 0.21) or Placebo groups (r = 0.54, p = 0.13).

6.4.5.4 Valve parameters

No significant relationship was seen between peak VO_2 and change in aortic valve area (r = 0.18, p = 0.44 in fibrate vs r = 0.29, p = 0.40 in placebo) or aortic valve gradient (r = 0.29, p = 0.22 in fibrate vs r = 0.21, p = 0.56 in placebo) post 6 months' treatment in the Fibrate or Placebo groups.

6.4.5.5 Myocardial fibrosis

Native T1 values and extra-cellular volume were compared pre and post treatment in both the Fibrate and Placebo groups separately. No significant correlation was found between myocardial fibrosis and exercise parameters obtained from both 6MWT and CPET. These findings are consistent with previous such studies. [293]

Table 6.5: Correlation between delta change in main CPET parameters and markers of myocardial fibrosis, specifically Native T1 values (ms) and Extracellular volume fraction (%) in (A) Fenofibrate, and (B) Placebo group. *ΔVO₂, peak oxygen capacity (ml/Kg/min); ΔVT, VO₂ at ventilatory threshold (ml/Kg/min); Δ VE/VCO2, minute ventilation/carbon dioxide production slope; 6MWT, six-minute walk test distance (metres).*

(A) Fenofibrate

Parameter	N Fenofibrate	Pearson r	P value
ΔVO2	33		
Δ Native T1 (ms)		0.16	0.55
ΔECV (%)		-0.17	0.56
ΔVT	33	ΔVT vs	
Δ Native T1 (ms)		0.47	0.06
ΔECV (%)		0.11	0.73
ΔVE/VCO2	33		
Δ Native T1 (ms)		0.26	0.31
ΔECV (%)		0.24	0.41
6MWT distance	33		
Δ Native T1 (ms)		0.35	0.13
ΔECV (%)		0.16	0.55

(B) Placebo

Parameter	N Placebo	Pearson r	P value
ΔVO₂	11		
Δ Native T1 (ms)		-0.37	0.32
ΔECV (%)		0.39	0.29
ΔVT	11		
Δ Native T1 (ms)		-0.60	0.09
ΔECV (%)		0.39	0.29
ΔVE/VCO2	11		
Δ Native T1 (ms)		-0.43	0.24
ΔECV (%)		0.09	0.81
6MWT distance	11		
Δ Native T1 (ms)		-0.78	0.93
ΔECV (%)		-0.05	0.07

6.4.6 Exercise parameters and CMR parameters of cardiac metabolism

The reduction in myocardial triglyceride content (MTG) did not have any influence on maximal oxygen capacity, Peak VO_2 during exercise in both the Fibrate ($r = 0.37$, $p = 0.08$) and Placebo group ($r = -0.39$, $p = 0.38$).

Similarly, change in PCr/ATP ratio did not show any correlation to peak VO_2 ($r = -0.10$, $p = 0.65$ Fibrate vs $r = -0.54$, $p = 0.13$ Placebo) in any of the groups.

6.4.7 Main predictors of peak VO_2

Despite the correlation between LV systolic strain parameters and peak VO2 values, only Age, BMI and LVMI remain the main predictors of peak VO2 at baseline on multivariate regression analysis. BMI and LVMI consistently predicted peak VO_2 post 6 months treatment (See Table 6.6)

Table 6.6: Main predictors of peak VO_2 in the study. *LVMI: Indexed left ventricular mass (Results from multivariate linear regression, $p < 0.05$ significant).*

Predictors of Peak VO_2	r	Unstandardised B	P value
Baseline			
Age	-0.39	-0.16	0.006*
BMI	-0.50	-0.58	<0.001*
LVMI (kg/m^2)	0.34	0.11	0.02*
Post treatment (either Fibrate or Placebo)			
Age	-0.22	-0.1	0.23
BMI	-0.60	-0.86	<0.001*
LVMI (kg/m^2)	0.43	0.11	0.02*

6.5 Discussion

To my knowledge, this is the first interventional study exploring the effect of changes in cardiac metabolism and physiology on exercise capacity in AS. In addition, this study again establishes the feasibility, reproducibility and safety of CPET in this AS population. The major findings from this comparison between pre and post treatment values in both groups

and delta change in parameters indicate : (i) Peak VO_2 did not improve or significantly deteriorate in either the Fibrate or Placebo groups; (ii) There was no relationship between the change in cardiac metabolism and the exercise parameters (iii) Peak VO_2/ exercise capacity in AS was only related to LV strain parameters and LV stroke volume, both of which again did not significantly improve or deteriorate in either the Fibrate or Placebo groups. This is discussed in detail in the sections below.

This study, importantly, reiterates findings from previous studies in asymptomatic moderate-severe AS that despite being asymptomatic a major proportion of these patients have a peak $_{VO2}$ <85% predicted with an abnormal VE/VCO2 slope (>32), which are both predictors of outcome.[204, 294] Impaired strain parameters on CMR relate to lower peak VO_2 values.[295] Thus, LV strain assessment and CPET together have the ability to detect a high proportion of false asymptomatic patients that is not predicted by resting or exercise echocardiography alone, an investigation routinely used for surveillance of these patients. CPET also has a potential role in surgical selection of asymptomatic AS patients.

6.5.1 Effect of LV peak systolic strain parameters and stroke volume on peak VO_2

Circumferential strain: In this study, we saw a significant correlation between peak systolic circumferential strain and peak $VO_{2;}$ reduced circumferential strain was related to lower peak VO_2 in line with pre-treatment analysis as detailed in Chapter 4. This relationship was significant in the Fibrate group only. Placebo group was not powered to detect change in cardiac physiology or exercise capacity and was only there for blinding purposes in this study.

The reduction in circumferential strain and its significant relationship with peak VO_2 seen in this study could be explained by its impact on LV stroke volume and ejection fraction. It has been shown previously that circumferential shortening has a relatively greater contribution to

stroke volume (i.e., two-thirds) and ejection fraction than longitudinal shortening, independent of wall thickness.[296]

Stroke volume is a known predictor of peak VO_2 on CPET.[204]

Peak VO_2 = HR (max) X SV (max) X (CaO_2-CVO_2)

where HR is maximum heart rate, SV is maximum stroke volume and CaO_2-CVO_2 is net oxygen extraction.

Despite normal LVEF, significant relationship was seen between change in peak VO_2 and change in stroke volume in both pre and post treatment groups as explained in Chapter 4 and section 6.4.5.2 above.

Longitudinal strain*:* Impaired longitudinal and circumferential strain are seen in progressive moderate-severe AS[297] and longitudinal strain is known to be independently associated with exercise capacity.[48] Impaired longitudinal strain was present in both the groups pre and post treatment but correlated to reduced peak VO_2 on exercise to the post treatment values in the fibrate group only. The delta change in longitudinal strain and peak VO_2 did not correlate in our study. A possible explanation could be that the longitudinal strain values were low to start with in our study groups (-11.9 ± 2.8 in the fibrate group vs -12.2 ± 2.3% in the placebo group) with no significant change (Fibrate mean change 0.26 vs Placebo mean change 0.32) post treatment as detailed in chapter 5. The study was perhaps underpowered to detect any relationship with that small degree of change in values.

6.5.2 LV diastolic function and Peak VO_2

Peak diastolic longitudinal strain rate, LA volume, and myocardial fibrosis are known CMR estimates of diastolic dysfunction.[298]

Diastolic dysfunction is known to precede systolic impairment and progression to heart failure in AS and is also an important predictor of prognosis.[49] All these parameters of diastolic dysfunction were evident in this study cohort at baseline and at the end of 6 months

study duration as detailed in Chapter 3 and 5. However, no significant relationship of these diastolic parameters including strain rate, LA volume and myocardial fibrosis was seen with parameters of exercise capacity. Myocardial fibrosis and its relationship with exercise capacity in this cohort has been studied before and similarly found no association. Change in diastolic parameters was not the main end-point of the study and only an exploratory one, for which the study was perhaps underpowered.

6.5.3 Main predictors of Peak VO_2

Age, BMI and LVMI were the main predictors of peak VO_2 in the study. Age and BMI are non-modifiable, and LVMI did not show any significant improvement in either of the groups. Consequently, there was no change in peak VO2

6.6 Limitations

The main limitation of the study was that it was not adequately powered to detect any change in exercise capacity pre and post treatment in the Fibrate group or for comparison between Fibrate and placebo groups. Also, the CMR data collected was at rest so we were unable to correlate CPET parameters with stress CMR parameters (at similar level of exercise as CPET).

This would have undoubtedly provided more accurate information on changes in cardiac physiology and metabolism in these patients on exercise and whether the ability to increase cardiac output differed in the two treatment groups (Fibrate vs placebo).

6.7 Conclusions

In summary, there was no significant improvement or change in exercise capacity in either the Fibrate or Placebo group. In the Fibrate group, despite a significant alteration in cardiac metabolism with reduced steatosis and modest improvement in energetics, this effect did not translate to any favourable change in cardiac physiology and consequently exercise capacity.

This study also highlights that the selected moderate-severe AS population in this trial was at an advanced stage of the disease with evidence of significant diastolic and subclinical systolic dysfunction. Even though 94% of patients were able to achieve maximal volitional effort (RER >1.15), overall majority of the population had lower average peak VO_2 and VE/VCO2 values despite the absence of symptoms and normal spirometry. Perhaps this was due to attenuation of the cardiac output response during exercise secondary to abnormal LV haemodynamics.

Despite its limitations, this study does make an important argument that altering cardiac metabolism in face of constantly increasing pressure overload at such advanced stage of disease is unlikely to have a significant beneficial effect on cardiac function or exercise capacity. In this study, patients did not complete any quality of life or symptom improvement questionnaire so it is difficult to comment if there was any subjective improvement in patients' symptoms in any of the groups.

7 Chapter Seven

General conclusions and Future directions

7.1 General Conclusions

This thesis was dedicated to understanding the role of metabolic remodelling in AS and its impact on overall disease progression, cardiac function and exercise capacity in these patients.

Here, I investigated changes in cardiac metabolism, in particular myocardial steatosis and energetic deficit, across the spectrum of AS to precisely understand the timing of such changes in AS, whether they have a cause or effect relationship with the structural and functional changes seen in AS using gold standard, cutting edge techniques (^{1}H-MRS, ^{31}P-MRS and myocardial tagging).

Once I had established that these metabolic changes do occur at early stage of AS and worsen as disease progresses, I further explored with a randomised placebo-controlled double blind study design whether it was possible to alter cardiac metabolism in the heart with a PPARα agonist in moderate-severe AS stage when these metabolic changes are well-established and how such modulation would affect cardiac physiology and functional capacity in AS.

1. In ***Chapter 1***, I discussed the pathophysiology and disease progression in AS highlighting that the disease process in AS affects both the valve and the myocardium. Much research has previously explored the valve mechanisms and potential targets to alter the disease process with no significant results. Myocardial response to pressure overload in AS has been a subject of interest in recent years and a potential target for disease modulation. Many studies have discussed myocardial structural and functional changes, and most of the metabolic data to date is from animal models of aortic

banding rather than real world insulin resistant chronic AS population. Pressure overload in AS encompasses both structural and metabolic remodelling, and increases the risk of decompensation into heart failure. In the healthy human heart, fat and glucose are responsible for the majority of ATP production, approximately 60-90% coming from fat and 40-10% from glucose, although these ratios change depending upon the prevailing mix of metabolic substrates in the blood stream, in addition to changes in conditions of the heart such as stress or ischaemia. A major component of metabolic derangement in AS is abnormal cardiac substrate use, with downregulation of fatty acid oxidation, increased reliance on glucose metabolism and subsequent myocardial lipid accumulation. Altered cardiac substrate utilisation and consequent myocardial steatosis and reduced energy efficiency has been implicated in the transition from compensated hypertrophy to heart failure in AS. These changes can be assessed using cardiac magnetic resonance spectroscopy (MRS). Proton (^{1}H) MRS allows the assessment of myocardial triglyceride content and creatine concentration, while phosphorus (^{31}P) MRS allows non-invasive *in vivo* quantification of the phosphocreatine to adenosine-triphosphate ratio (PCr/ATP), a measure of cardiac energy status which is reduced in patients with severe AS.

This substantial metabolic reconfiguration in AS is partly driven by nuclear receptor and transcriptional co-regulator signalling circuits orchestrating fuel selection and mitochondrial oxidative capacity, of which peroxisome proliferator-activated receptor α (PPARα), a fatty-acid ligand binding master transcription factor promoting FAO, plays a critical role along with interacting regulators of oxidative metabolism like PPARγ coactivator-1α (PGC-1α). PPARα not only plays a key role in the transcriptional control of substrate switching but artificial ligands for PPARα, such as fenofibrate, also protect against endothelin-induced cardiac hypertrophy and failure,

and cardiac function is seen to be severely damaged in PPARα null mice during pressure overload.

Thus, a therapeutic approach that alters myocardial substrate selection may target both the cardiac metabolic and structural effects of pressure overload, and is likely to be effective in treating cardiac dysfunction in AS. PPAR agonists are one such group of drugs especially, PPARα, which play a central role in FAO signalling system and also control lipid homeostasis. The ability of PPARα receptors to respond to distinct metabolic cues provides a potential mechanism to maintain a balance between FA breakdown and storage and their downregulation in pressure overload hypertrophy state has shown to have deleterious effects. Fibrates (PPARα agonists), thus, are a promising therapeutic option with their ability to upregulate FAO in cardiac myocytes and reduce lipotoxicity in pressure overload hypertrophy. MRS has the ability to provide fundamental insights into cardiac metabolism as well as monitor response to therapeutic intervention, thus, dramatically advancing our understanding of the pathophysiology and metabolic nature of AS.

2. In ***Chapter 2***, the combined methods for the thesis are summarised. Magnetic resonance spectroscopy (MRS) is the only non-invasive, non-radiation exposure technique for the. investigation of cardiac metabolism in vivo. Myocardial triglycerides (MTG) can be assessed using cardiac ^{1}H-MRS, which utilises the abundant hydrogen (^{1}H) protons. Various previous clinical studies have assessed the presence of myocardial steatosis using ^{1}H-MRS and examined its functional associations in obesity, type 2 diabetes mellitus (T2DM), and in normal individuals when subjected to prolonged exercise and diet restrictions. In severe AS, our group had demonstrated pronounced steatosis (two-fold higher when compared to controls) in both symptomatic and asymptomatic patients. ^{31}P-MRS allows the *in vivo*

quantification of phosphorus (^{31}P)-containing metabolites involved in energy metabolism, such as PCr and ATP. Pressure-overload LVH increases the energetic cost of mechanical work and when this is at the severe end of the spectrum the resulting mismatch in myocardial energy supply and demand may contribute to the development of HF. The PCr/ATP ratio, an index of cardiac bio-energetic state, is reduced in animal models of myocardial hypertrophy, in human LVH, and in HF. It correlates not only with the degree of cardiac hypertrophy and accompanying LV dysfunction, but has also been shown to be a superior predictor of mortality. CMR is a well-established technique to assess cardiac function, morphology, valve anatomy and function in patients with AS. It is a well validated tool for measurement of multidirectional strain using myocardial tagging sequence. Late gadolinium enhancement (LGE) and T1 mapping techniques are able to assess myocardial fibrosis that occurs as a result of structural remodelling in AS and could offer prognostically important information. Cardiopulmonary exercise testing (CPET) provides assessment of the integrative exercise responses involving the pulmonary, cardiovascular and skeletal muscle systems, which are not adequately reflected through the measurement of individual organ system function. CPET is being used increasingly in a wide spectrum of clinical applications for evaluation of undiagnosed exercise intolerance and for objective determination of functional capacity and impairment. In this research, the main objective of performing CPET was to characterize the physiological effects of Fenofibrate in AS well as study the relationship between cardiac metabolic and CPET parameters across the spectrum of AS. Blood samples were taken for safety as well as to investigate whether fatty acid oxidation was upregulated in the Fenofibrate group.

3. In ***Chapter 3***, metabolic remodelling across the spectrum of AS is investigated hypothesising that it occurs early in the disease process preceding structural changes. This would potentially explain the wide individual heterogeneity when it comes to degree of hypertrophy and progression to myocardial fibrosis and heart failure in AS. Why some with same degree of stenosis develop greater hypertrophy and decline sooner compared to others. To investigate this, 74 asymptomatic AS patients with varying degree of stenosis and 13 healthy volunteers were assessed using CMR imaging methods. Participants were divided into quartile groups based on their LV wall thickness, a measure of structural remodelling, as measured on CMR and peak aortic valve gradient, marker of pressure overload, as measured on echocardiography. Comparison of various metabolic and structural parameters were made to understand the relationship between metabolic and structural remodelling in AS. This concluded that a gradient of myocardial energetic deficit and steatosis exists across the spectrum of hypertrophied AS hearts, notably I showed in this study that this happens prior to the development of irreversible structural changes and is related to subclinical LV dysfunction. Thus, targeting myocardial metabolism may be a sensible strategy to risk stratify as well as potentially prevent and treat systolic failure in AS.
4. In ***Chapter 4***, I sought to investigate if the metabolic remodelling which occurs early in the disease process affects functional capacity in AS well as study the relationship between structural changes and functional capacity in AS. Another aim was to identify CMR parameters of cardiac function and metabolism that may predict exercise capacity in AS. For this, 74 asymptomatic AS patients with varying degree of stenosis and 13 healthy volunteers who underwent CMR assessment (Chapter 3) were further evaluated with six-minute walk test (6MWT) and cardio-pulmonary exercise test (CPET). This concluded that reduced exercise capacity in asymptomatic AS was

not related to changes in cardiac metabolism. Impaired LV strain, LV stroke volume and mass index were the only predictors of peak VO_2 when controlled for age and BMI.

5. ***Chapter 5*** improved our understanding of the perturbations in cardiac metabolism and the timing and nature of such changes in AS. I set to experiment if the cardiac metabolism can be modulated with a PPARα agonist, Fenofibrate in AS and what effect, if any, would such modulation have on cardiac physiology. Fenofibrate was selected for the study as PPARα has a vital role in controlling lipid metabolism and homeostasis in the heart. Also, its downregulation and resulting dysregulated FAO in AS has been well-studied previously. Thus, making it a promising therapeutic target. For this, I enrolled 72 moderate-severe AS patients into a prospective, randomised, double-blind, placebo controlled trial. The placebo group was assigned for blinding purposes only. After 6 months of treatment with Fenofibrate, there was a significant reduction in myocardial steatosis and modest favourable change in energetics with blood marker evidence of fatty acid upregulation. However, such metabolic modulation did not modify cardiac physiology or halt disease progression in moderate-severe AS.
6. In ***Chapter 6***, it was hypothesised that favourable alteration of cardiac metabolism mainly reduction in myocardial lipid content with PPARα agonist, Fenofibrate and possible upregulation of FAO may improve overall exercise performance in moderate-severe AS patients. Even though no significant change in cardiac physiology was seen in Chapter 5, it was plausible that if there was an improvement in the ability of the myocardium to generate energy, this may translate to less attenuation of cardiac output on exercise and better overall aerobic capacity. In addition, I wanted to re-evaluate the relationship between CMR parameters of LV

structure and function with exercise capacity in asymptomatic moderate-severe AS patients post 6 months' treatment with Fenofibrate. It would also highlight the feasibility and safety of CPET in advanced asymptomatic AS. This was an extension of the prospective, randomised, double-blind, placebo controlled trial. Cardio-respiratory fitness of the participants who completed the 6 months' treatment was measured using CPET and 6MWT. Whilst majority of these patients had a low average peak VO_2 (<85% predicted), this did not improve or significantly deteriorate in either the Fibrate or Placebo groups. No significant effect of change in cardiac metabolism on the exercise parameters was seen. Peak VO_2 in this cohort of AS only related to LV strain parameters and LV stroke volume, both of which again did not significantly improve or deteriorate in either the Fibrate or Placebo groups.

To conclude, this research has provided novel insights into the presence and impact of metabolic remodelling in AS, which has been a matter of great interest in this area in recent years. Metabolic modulation has lately been anticipated as a potential cure or option to modify disease processes in number of cardiac conditions including pressure overload hypertrophy such as in AS. In this first proof-of-concept study, it has been shown that cardiac metabolism can be modulated in AS with metabolic modulator therapy, specifically PPARα agonist, Fenofibrate. More importantly, this study argues that such metabolic modulation at moderate-severe stage with established diastolic and subclinical systolic dysfunction is unlikely to refashion the myocardial response in a way to alter the disease process significantly. The impact of a constantly increasing pressure overload in moderate-severe AS perhaps overpowers any significant gain from changes in cardiac metabolism.

7.2 Future directions

This research has laid foundation as a pilot study for future studies of metabolic therapy in pressure overload disorders. Future studies, perhaps targeting the disease process early may

elicit more favourable results in AS. Secondly, the long term effect of metabolic modulation on surgical outcomes or mortality in these patients could be studied to establish if upregulating FAO in AS offered any prognostic benefit. This study, due to lack of metabolomics data , could not establish the effect of increasing fatty acid metabolism with PPARα agonist on use of alternative substrates and intermediate metabolism. This may be another future avenue for research to help elucidate more precise relationship between metabolic changes and hypertrophy.

8. **References**

1. Iung B, Vahanian A. Degenerative calcific aortic stenosis: a natural history. *Heart*. 2012;98(Suppl 4):iv7-iv13. doi:10.1136/heartjnl-2012-302395
2. Lindman BR, Clavel MA, Mathieu P, et al. Calcific aortic stenosis. *Nat Rev Dis Primers*. 2016;2:16006.
3. DAVIES SW, GERSHLICK AH, BALCON R. Progression of valvar aortic stenosis: a long-term retrospective study. *Eur Heart J*. 1991;12(1):10-14. doi:10.1093/oxfordjournals.eurheartj.a059815
4. Baumgartner H, Falk V, Bax JJ, et al. 2017 ESC/EACTS Guidelines for the management of valvular heart disease. *Eur Heart J*. 2017;38(36):2739-2791. doi:10.1093/eurheartj/ehx391
5. Arsenault BJ, Boekholdt SM, Mora S, et al. Impact of High-Dose Atorvastatin Therapy and Clinical Risk Factors on Incident Aortic Valve Stenosis in Patients With Cardiovascular Disease (from TNT, IDEAL, and SPARCL). *Am J Cardiol*. 2014;113(8):1378-1382. doi:10.1016/j.amjcard.2014.01.414
6. Francis JM, Joseph J, Loudon M, et al. A prospective, double-blind, randomized controlled trial of the angiotensin-converting enzyme inhibitor Ramipril In Aortic Stenosis (RIAS trial). *Eur Heart J Cardiovasc Imaging*. 2015;16(8):834-841. doi:10.1093/ehjci/jev043
7. Innasimuthu AL, Katz WE. Effect of Bisphosphonates on the Progression of Degenerative Aortic Stenosis. *Echocardiography*. 2011;28(1):1-7. doi:https://doi.org/10.1111/j.1540-8175.2010.01256.x
8. Osnabrugge RLJ, Mylotte D, Head SJ, et al. Aortic Stenosis in the Elderly. *J Am Coll Cardiol*. 2013;62(11):1002-1012. doi:10.1016/j.jacc.2013.05.015
9. Rosenhek R, Klaar U, Schemper M, et al. Mild and moderate aortic stenosis: Natural history and risk stratification by echocardiography. *Eur Heart J*. 2004;25(3):199-205. doi:10.1016/j.ehj.2003.12.002
10. Rosenhek R, Binder T, Porenta G, et al. Predictors of Outcome in Severe, Asymptomatic Aortic Stenosis. *New England Journal of Medicine*. 2000;343(9):611-617. doi:10.1056/NEJM200008313430903
11. Lorell BH, Carabello BA. Left ventricular hypertrophy: Pathogenesis, detection, and prognosis. *Circulation*. 2000;102(4):470-479. doi:10.1161/01.CIR.102.4.470
12. Lorell BH, Carabello BA. Left Ventricular Hypertrophy . *Circulation*. 2000;102(4):470-479. doi:10.1161/01.CIR.102.4.470
13. Chin CWL, Everett RJ, Kwiecinski J, et al. Myocardial Fibrosis and Cardiac Decompensation in Aortic Stenosis. *JACC Cardiovasc Imaging*. 2017;10(11):1320-1333. doi:10.1016/j.jcmg.2016.10.007
14. Cioffi G, Faggiano P, Vizzardi E, et al. Prognostic effect of inappropriately high left ventricular mass in asymptomatic severe aortic stenosis. *Heart*. 2011;97(4):301-307. doi:10.1136/hrt.2010.192997
15. Cote C, Pibarot P, Despres JP, et al. Association between circulating oxidised low-density lipoprotein and fibrocalcific remodelling of the aortic valve in aortic stenosis. *Heart*. 2008;94(9):1175-1180. doi:10.1136/hrt.2007.125740
16. Novo G, Fazio G, Visconti C, et al. Atherosclerosis, Degenerative Aortic Stenosis and Statins. *Curr Drug Targets*. 2011;12(1):115-121. doi:10.2174/138945011793591545

17. Mathieu P, Boulanger MC, Bouchareb R. Molecular biology of calcific aortic valve disease: towards new pharmacological therapies. *Expert Rev Cardiovasc Ther*. 2014;12(7):851-862. doi:10.1586/14779072.2014.923756
18. Cowell SJ, Newby DE, Prescott RJ, et al. A Randomized Trial of Intensive Lipid-Lowering Therapy in Calcific Aortic Stenosis. *New England Journal of Medicine*. 2005;352(23):2389-2397. doi:10.1056/NEJMoa043876
19. Rossebø AB, Pedersen TR, Boman K, et al. Intensive Lipid Lowering with Simvastatin and Ezetimibe in Aortic Stenosis. *New England Journal of Medicine*. 2008;359(13):1343-1356. doi:10.1056/NEJMoa0804602
20. Chan KL, Teo K, Dumesnil JG, Ni A, Tam J. Effect of Lipid Lowering With Rosuvastatin on Progression of Aortic Stenosis. *Circulation*. 2010;121(2):306-314. doi:10.1161/CIRCULATIONAHA.109.900027
21. Poggio P, Songia P, Cavallotti L, et al. PCSK9 Involvement in Aortic Valve Calcification. *J Am Coll Cardiol*. 2018;72(24):3225 LP - 3227. doi:10.1016/j.jacc.2018.09.063
22. David MZ, Marie-Christine A, Delphine D, et al. Evaluation and Clinical Implications of Aortic Valve Calcification Measured by Electron-Beam Computed Tomography. *Circulation*. 2004;110(3):356-362. doi:10.1161/01.CIR.0000135469.82545.D0
23. Clavel MA, Messika-Zeitoun D, Pibarot P, et al. The Complex Nature of Discordant Severe Calcified Aortic Valve Disease Grading: New Insights From Combined Doppler Echocardiographic and Computed Tomographic Study. *J Am Coll Cardiol*. 2013;62(24):2329-2338. doi:https://doi.org/10.1016/j.jacc.2013.08.1621
24. Peeters FECM, Meex SJR, Dweck MR, et al. Calcific aortic valve stenosis: hard disease in the heart: A biomolecular approach towards diagnosis and treatment. *Eur Heart J*. 2017;39(28):2618-2624. doi:10.1093/eurheartj/ehx653
25. Pawade TA, Doris MK, Bing R, et al. Effect of Denosumab or Alendronic Acid on the Progression of Aortic Stenosis: A Double-Blind Randomized Controlled Trial. *Circulation*. 2021;143(25):2418-2427. doi:10.1161/CIRCULATIONAHA.121.053708
26. Schurgers LJ, Teunissen KJF, Hamulyák K, Knapen MHJ, Vik H, Vermeer C. Vitamin K–containing dietary supplements: comparison of synthetic vitamin K₁ and natto-derived menaquinone-7. *Blood*. 2007;109(8):3279 LP - 3283. doi:10.1182/blood-2006-08-040709
27. Lindholt JS, Frandsen NE, Fredgart MH, et al. Effects of menaquinone-7 supplementation in patients with aortic valve calcification: study protocol for a randomised controlled trial. *BMJ Open*. 2018;8(8):e022019. doi:10.1136/bmjopen-2018-022019
28. Peeters EF, Van Mourik JM, Meex JS, et al. Bicuspid Aortic Valve Stenosis and the Effect of Vitamin K2 on Calcification Using 18F-Sodium Fluoride Positron Emission Tomography/Magnetic Resonance: The BASIK2 Rationale and Trial Design. *Nutrients* . 2018;10(4). doi:10.3390/nu10040386
29. Nadir MA, Wei L, Elder DHJ, et al. Impact of Renin-Angiotensin System Blockade Therapy on Outcome in Aortic Stenosis. *J Am Coll Cardiol*. 2011;58(6):570-576. doi:10.1016/j.jacc.2011.01.063
30. Chambers J. The left ventricle in aortic stenosis: evidence for the use of ACE inhibitors. *Heart*. 2005;92(3):420-423. doi:10.1136/hrt.2005.074112
31. O'Brien KD, Probstfield JL, Caulfield MT, et al. Angiotensin-Converting Enzyme Inhibitors and Change in Aortic Valve Calcium. *Arch Intern Med*. 2005;165(8):858. doi:10.1001/archinte.165.8.858

32. Rosenhek R, Rader F, Loho N, et al. Statins but Not Angiotensin-Converting Enzyme Inhibitors Delay Progression of Aortic Stenosis. *Circulation*. 2004;110(10):1291-1295. doi:10.1161/01.CIR.0000140723.15274.53
33. Di Pasquale G, Vassiliki' Coutsoumbas G, Zagnoni S, Filippini E, Resciniti E. Aortic stenosis in the elderly can be prevented: old risk factors and a new pathological condition. *European Heart Journal Supplements*. 2019;21(Supplement_B):B52-B53. doi:10.1093/eurheartj/suz017
34. Krayenbuehl HP, Hess OM, Monrad ES, Schneider J, Mall G, Turina M. Left ventricular myocardial structure in aortic valve disease before, intermediate, and late after aortic valve replacement. *Circulation*. 1989;79(4):744-755. doi:10.1161/01.CIR.79.4.744
35. Monrad ES, Hess OM, MuRAKAMI T, Nonogi H, Corin WJ, Krayenbuehl HP. Time course of regression of left ventricular hypertrophy after aortic valve replacement. *Circulation*. 1988;77(6):1345-1355.
36. Călin A, Roşca M, Beladan CC, et al. The left ventricle in aortic stenosis – imaging assessment and clinical implications. *Cardiovasc Ultrasound*. 2015;13(1):22. doi:10.1186/s12947-015-0017-4
37. Störk T, Möckel M, Danne O, Völler H, Eichstädt H, Frei U. Left ventricular hypertrophy and diastolic dysfunction: their relation to coronary heart disease. *Cardiovasc Drugs Ther*. 1995;9(3):533-537.
38. Hein S, Arnon E, Kostin S, et al. Progression From Compensated Hypertrophy to Failure in the Pressure-Overloaded Human Heart. *Circulation*. 2003;107(7):984-991. doi:10.1161/01.CIR.0000051865.66123.B7
39. Carroll JD, Carroll EP, Feldman T, et al. Sex-associated differences in left ventricular function in aortic stenosis of the elderly. *Circulation*. 1992;86(4):1099-1107. doi:10.1161/01.CIR.86.4.1099
40. Gunther S, Grossman W. Determinants of ventricular function in pressure-overload hypertrophy in man. *Circulation*. 1979;59(4):679-688. doi:10.1161/01.CIR.59.4.679
41. Kupari M, Turto H, Lommi J. Left ventricular hypertrophy in aortic valve stenosis: preventive or promotive of systolic dysfunction and heart failure? *Eur Heart J*. 2005;26(17):1790-1796. doi:10.1093/eurheartj/ehi290
42. F. AC, Marcelo N, L. HM, et al. Prognostic Significance of Myocardial Fibrosis Quantification by Histopathology and Magnetic Resonance Imaging in Patients With Severe Aortic Valve Disease. *J Am Coll Cardiol*. 2010;56(4):278-287. doi:10.1016/j.jacc.2009.12.074
43. Yarbrough WM, Mukherjee R, Ikonomidis JS, Zile MR, Spinale FG. Myocardial remodeling with aortic stenosis and after aortic valve replacement: Mechanisms and future prognostic implications. *J Thorac Cardiovasc Surg*. 2012;143(3):656-664. doi:10.1016/j.jtcvs.2011.04.044
44. Bing R, Cavalcante JL, Everett RJ, Clavel MA, Newby DE, Dweck MR. Imaging and Impact of Myocardial Fibrosis in Aortic Stenosis. *JACC Cardiovasc Imaging*. 2019;12(2):283-296. doi:10.1016/j.jcmg.2018.11.026
45. Dweck MR, Joshi S, Murigu T, et al. Midwall Fibrosis Is an Independent Predictor of Mortality in Patients With Aortic Stenosis. *J Am Coll Cardiol*. 2011;58(12):1271-1279. doi:https://doi.org/10.1016/j.jacc.2011.03.064
46. Pibarot P, Dumesnil JG. Longitudinal myocardial shortening in aortic stenosis: ready for prime time after 30 years of research? *Heart*. 2010;96(2):95-96. doi:10.1136/hrt.2009.177345

47. Henein MY, Priestley K, Davarashvili T, Buller N, Gibson DG. Early changes in left ventricular subendocardial function after successful coronary angioplasty. *Heart*. 1993;69(6):501-506. doi:10.1136/hrt.69.6.501
48. Douard H, Perlant M, Reant P, et al. Impact of impaired myocardial deformations on exercise tolerance and prognosis in patients with asymptomatic aortic stenosis. *European Journal of Echocardiography*. 2008;10(3):414-419. doi:10.1093/ejechocard/jen299
49. Kampaktsis PN, Kokkinidis DG, Wong SC, Vavuranakis M, Skubas NJ, Devereux RB. The role and clinical implications of diastolic dysfunction in aortic stenosis. *Heart*. 2017;103(19):1481-1487. doi:10.1136/heartjnl-2017-311506
50. Bruch C, Stypmann J, Grude M, Gradaus R, Breithardt G, Wichter T. Tissue Doppler imaging in patients with moderate to severe aortic valve stenosis: Clinical usefulness and diagnostic accuracy. *Am Heart J*. 2004;148(4):696-702. doi:10.1016/j.ahj.2004.03.049
51. Friedberg MK, Redington AN. Right Versus Left Ventricular Failure. *Circulation*. 2014;129(9):1033-1044. doi:10.1161/CIRCULATIONAHA.113.001375
52. Santamore WP, Dell'Italia LJ. Ventricular interdependence: Significant left ventricular contributions to right ventricular systolic function. *Prog Cardiovasc Dis*. 1998;40(4):289-308. doi:10.1016/S0033-0620(98)80049-2
53. Galli E, Mabo P, Donal E, et al. Prevalence and prognostic value of right ventricular dysfunction in severe aortic stenosis. *Eur Heart J Cardiovasc Imaging*. 2014;16(5):531-538. doi:10.1093/ehjci/jeu290
54. Rigolli M, Sivalokanathan S, Bull S, et al. A Hyperdynamic RV Is an Early Marker of Clinical Decompensation and Cardiac Recovery in Aortic Stenosis With Normal LV Ejection Fraction. *JACC Cardiovasc Imaging*. 2019;12(1):214-216. doi:10.1016/j.jcmg.2018.08.029
55. Marzia R, Sanjay S, Sacha B, et al. Abstract 16916: Right Ventricular Function in Aortic Stenosis: Early Marker of Decompensation and Left Ventricular Recovery. *Circulation*. 2017;136(suppl_1):A16916-A16916. doi:10.1161/circ.136.suppl_1.16916
56. Pibarot P, Dumesnil JG. Aortic Stenosis: Look Globally, Think Globally. *JACC Cardiovasc Imaging*. 2009;2(4):400-403. doi:10.1016/j.jcmg.2009.01.004
57. Neubauer S. The Failing Heart — An Engine Out of Fuel. *New England Journal of Medicine*. 2007;356(11):1140-1151. doi:10.1056/NEJMra063052
58. Lopaschuk GD, Ussher JR, Folmes CDL, Jaswal JS, Stanley WC. Myocardial Fatty Acid Metabolism in Health and Disease. *Physiol Rev*. 2010;90(1):207-258. doi:10.1152/physrev.00015.2009
59. Dzeja PP, Terzic A. Phosphotransfer networks and cellular energetics. *Journal of Experimental Biology*. 2003;206(12):2039-2047. doi:10.1242/jeb.00426
60. Mootha VK, Arai AE, Balaban RS. Maximum oxidative phosphorylation capacity of the mammalian heart. *American Journal of Physiology-Heart and Circulatory Physiology*. 1997;272(2):H769-H775. doi:10.1152/ajpheart.1997.272.2.H769
61. Wallimann T, Wyss M, Brdiczka D, Nicolay K, Eppenberger HM. Intracellular compartmentation, structure and function of creatine kinase isoenzymes in tissues with high and fluctuating energy demands: the 'phosphocreatine circuit' for cellular energy homeostasis. *Biochemical Journal*. 1992;281(1):21-40. doi:10.1042/bj2810021
62. Wallimann T, Tokarska-Schlattner M, Schlattner U. The creatine kinase system and pleiotropic effects of creatine. *Amino Acids*. 2011;40(5):1271-1296.
63. Irie H, Krukenkamp IB, Brinkmann JFF, et al. Myocardial recovery from ischemia is impaired in CD36-null mice and restored by myocyte CD36 expression or medium-

chain fatty acids. *Proceedings of the National Academy of Sciences*. 2003;100(11):6819-6824. doi:10.1073/pnas.1132094100
64. Barger PM, Kelly DP. PPAR Signaling in the Control of Cardiac Energy Metabolism. *Trends Cardiovasc Med*. 2000;10(6):238-245. doi:10.1016/S1050-1738(00)00077-3
65. Barger PM, Brandt JM, Leone TC, Weinheimer CJ, Kelly DP. Deactivation of peroxisome proliferator–activated receptor-α during cardiac hypertrophic growth. *Journal of Clinical Investigation*. 2000;105(12):1723-1730. doi:10.1172/JCI9056
66. Lehman JJ, Boudina S, Banke NH, et al. The transcriptional coactivator PGC-1α is essential for maximal and efficient cardiac mitochondrial fatty acid oxidation and lipid homeostasis. *American Journal of Physiology-Heart and Circulatory Physiology*. 2008;295(1):H185-H196. doi:10.1152/ajpheart.00081.2008
67. Taegtmeyer H, Young ME, Lopaschuk GD, et al. Assessing Cardiac Metabolism. *Circ Res*. 2016;118(10):1659-1701. doi:10.1161/RES.0000000000000097
68. Pereira RO, Wende AR, Olsen C, et al. GLUT1 deficiency in cardiomyocytes does not accelerate the transition from compensated hypertrophy to heart failure. *J Mol Cell Cardiol*. 2014;72:95-103.
69. Tian R, Abel ED. Responses of GLUT4-deficient hearts to ischemia underscore the importance of glycolysis. *Circulation*. 2001;103(24):2961-2966.
70. Chanda D, Luiken JJFP, Glatz JFC. Signaling pathways involved in cardiac energy metabolism. *FEBS Lett*. 2016;590(15):2364-2374.
71. Tran DH, Wang Z V. Glucose Metabolism in Cardiac Hypertrophy and Heart Failure. *J Am Heart Assoc*. 2019;8(12):e012673. doi:10.1161/JAHA.119.012673
72. Doenst T, Nguyen TD, Abel ED. Cardiac metabolism in heart failure: implications beyond ATP production. *Circ Res*. 2013;113(6):709-724.
73. Fernandez-Caggiano M, Eaton P. Heart failure—emerging roles for the mitochondrial pyruvate carrier. *Cell Death Differ*. 2021;28(4):1149-1158. doi:10.1038/s41418-020-00729-0
74. Kolwicz SC, Tian R. Glucose metabolism and cardiac hypertrophy. *Cardiovasc Res*. 2011;90(2):194-201. doi:10.1093/cvr/cvr071
75. Des Rosiers C, Labarthe F, Lloyd SG, Chatham JC. Cardiac anaplerosis in health and disease: food for thought. *Cardiovasc Res*. 2011;90(2):210-219.
76. Hue L, Taegtmeyer H. The Randle cycle revisited: a new head for an old hat. *Am J Physiol Endocrinol Metab*. 2009;297(3):E578-E591. doi:10.1152/ajpendo.00093.2009
77. Russell RR, Taegtmeyer H. Changes in citric acid cycle flux and anaplerosis antedate the functional decline in isolated rat hearts utilizing acetoacetate. *J Clin Invest*. 1991;87(2):384-390.
78. Pound KM, Sorokina N, Ballal K, et al. Substrate–Enzyme Competition Attenuates Upregulated Anaplerotic Flux Through Malic Enzyme in Hypertrophied Rat Heart and Restores Triacylglyceride Content. *Circ Res*. 2009;104(6):805-812. doi:10.1161/CIRCRESAHA.108.189951
79. Karwi QG, Uddin GM, Ho KL, Lopaschuk GD. Loss of Metabolic Flexibility in the Failing Heart. *Front Cardiovasc Med*. 2018;5:68. doi:10.3389/fcvm.2018.00068
80. Ingwall JS. *ATP and the Heart*. Vol 11. Springer Science & Business Media; 2002.
81. Ingwall JS. Energy metabolism in heart failure and remodelling. *Cardiovasc Res*. 2009;81(3):412-419. doi:10.1093/cvr/cvn301
82. Cooney GJ, Taegtmeyer H, Newsholme EA. Tricarboxylic acid cycle flux and enzyme activities in the isolated working rat heart. *Biochemical Journal*. 1981;200(3):701-703. doi:10.1042/bj2000701

83. Taegtmeyer H, Wilson CR, Razeghi P, Sharma S. Metabolic energetics and genetics in the heart. *Ann N Y Acad Sci*. 2005;1047(1):208-218.
84. Dzeja PP, Hoyer K, Tian R, et al. Rearrangement of energetic and substrate utilization networks compensate for chronic myocardial creatine kinase deficiency. *J Physiol*. 2011;589(Pt 21):5193-5211. doi:10.1113/jphysiol.2011.212829
85. Zhang J, Duncker DJ, Ya X, et al. Effect of left ventricular hypertrophy secondary to chronic pressure overload on transmural myocardial 2-deoxyglucose uptake: a 31P NMR spectroscopic study. *Circulation*. 1995;92(5):1274-1283.
86. Bittl JA, Ingwall JS. Reaction rates of creatine kinase and ATP synthesis in the isolated rat heart. A 31P NMR magnetization transfer study. *Journal of Biological Chemistry*. 1985;260(6):3512-3517.
87. Sahlin K, Harris RC. The creatine kinase reaction: a simple reaction with functional complexity. *Amino Acids*. 2011;40(5):1363-1367.
88. Weiss RG, Gerstenblith G, Bottomley PA. ATP flux through creatine kinase in the normal, stressed, and failing human heart. *Proceedings of the National Academy of Sciences*. 2005;102(3):808-813. doi:10.1073/pnas.0408962102
89. Balestrino M. Role of Creatine in the Heart: Health and Disease. *Nutrients*. 2021;13(4). doi:10.3390/nu13041215
90. Quigley AF, Kapsa RMI, Esmore D, Hale G, Byrne E. Mitochondrial respiratory chain activity in idiopathic dilated cardiomyopathy. *J Card Fail*. 2000;6(1):47-55. doi:https://doi.org/10.1016/S1071-9164(00)00011-7
91. Oka S ichi, Zhai P, Yamamoto T, et al. Peroxisome Proliferator Activated Receptor-α Association With Silent Information Regulator 1 Suppresses Cardiac Fatty Acid Metabolism in the Failing Heart. *Circ Heart Fail*. 2015;8(6):1123-1132. doi:10.1161/CIRCHEARTFAILURE.115.002216
92. Sihag S, Cresci S, Li AY, Sucharov CC, Lehman JJ. PGC-1α and ERRα target gene downregulation is a signature of the failing human heart. *J Mol Cell Cardiol*. 2009;46(2):201-212. doi:10.1016/j.yjmcc.2008.10.025
93. Schoonjans K, Watanabe M, Suzuki H, et al. Induction of the Acyl-Coenzyme A Synthetase Gene by Fibrates and Fatty Acids Is Mediated by a Peroxisome Proliferator Response Element in the C Promoter. *Journal of Biological Chemistry*. 1995;270(33):19269-19276. doi:10.1074/jbc.270.33.19269
94. Motojima K, Passilly P, Peters JM, Gonzalez FJ, Latruffe N. Expression of Putative Fatty Acid Transporter Genes Are Regulated by Peroxisome Proliferator-activated Receptor α and γ Activators in a Tissue- and Inducer-specific Manner. *Journal of Biological Chemistry*. 1998;273(27):16710-16714. doi:10.1074/jbc.273.27.16710
95. Reddy JK, Hashimoto T. Peroxisomal beta-oxidation and peroxisome proliferator-activated receptor alpha: an adaptive metabolic system. *Annu Rev Nutr*. 2001;21:193-230. doi:10.1146/annurev.nutr.21.1.193
96. Djouadi F, Brandt JM, Weinheimer CJ, Leone TC, Gonzalez FJ, Kelly DP. The role of the peroxisome proliferator-activated receptor α (PPARα) in the control of cardiac lipid metabolism. *Prostaglandins Leukot Essent Fatty Acids*. 1999;60(5-6):339-343. doi:10.1016/S0952-3278(99)80009-X
97. Brandt JM, Djouadi F, Kelly DP. Fatty Acids Activate Transcription of the Muscle Carnitine Palmitoyltransferase I Gene in Cardiac Myocytes via the Peroxisome Proliferator-activated Receptor α. *Journal of Biological Chemistry*. 1998;273(37):23786-23792. doi:10.1074/jbc.273.37.23786

98. Gulick T, Cresci S, Caira T, Moore DD, Kelly DP. The peroxisome proliferator-activated receptor regulates mitochondrial fatty acid oxidative enzyme gene expression. *Proc Natl Acad Sci U S A*. 1994;91(23):11012-11016.
99. Disch DL, Rader TA, Cresci S, et al. Transcriptional control of a nuclear gene encoding a mitochondrial fatty acid oxidation enzyme in transgenic mice: role for nuclear receptors in cardiac and brown adipose expression. *Mol Cell Biol*. 1996;16(8):4043-4051.
100. Zhang B, Marcus SL, Sajjadi FG, et al. Identification of a peroxisome proliferator-responsive element upstream of the gene encoding rat peroxisomal enoyl-CoA hydratase/3-hydroxyacyl-CoA dehydrogenase. *Proceedings of the National Academy of Sciences*. 1992;89(16):7541-7545. doi:10.1073/pnas.89.16.7541
101. van der Lee KAJM, Vork MM, De Vries JE, et al. Long-chain fatty acid-induced changes in gene expression in neonatal cardiac myocytes. *J Lipid Res*. 2000;41(1):41-47.
102. Mascaró C, Acosta E, Ortiz JA, Marrero PF, Hegardt FG, Haro D. Control of Human Muscle-type Carnitine Palmitoyltransferase I Gene Transcription by Peroxisome Proliferator-activated Receptor. *Journal of Biological Chemistry*. 1998;273(15):8560-8563. doi:10.1074/jbc.273.15.8560
103. Djouadi F, Weinheimer CJ, Saffitz JE, et al. A gender-related defect in lipid metabolism and glucose homeostasis in peroxisome proliferator- activated receptor alpha- deficient mice. *Journal of Clinical Investigation*. 1998;102(6):1083-1091. doi:10.1172/JCI3949
104. Leone TC, Weinheimer CJ, Kelly DP. A critical role for the peroxisome proliferator-activated receptor alpha (PPARalpha) in the cellular fasting response: the PPARalpha-null mouse as a model of fatty acid oxidation disorders. *Proc Natl Acad Sci U S A*. 1999;96(13):7473-7478.
105. Bougarne N, Weyers B, Desmet SJ, et al. Molecular Actions of PPARα in Lipid Metabolism and Inflammation. *Endocr Rev*. 2018;39(5):760-802. doi:10.1210/er.2018-00064
106. Muerhoff AS, Griffin KJ, Johnson EF. The peroxisome proliferator-activated receptor mediates the induction of CYP4A6, a cytochrome P450 fatty acid omega-hydroxylase, by clofibric acid. *Journal of Biological Chemistry* . 1992;267(27):19051-19053.
107. Smeets PJH, Planavila A, van der Vusse GJ, van Bilsen M. Peroxisome proliferator-activated receptors and inflammation: take it to heart. *Acta Physiologica*. 2007;191(3):171-188. doi:10.1111/j.1748-1716.2007.01752.x
108. Bansal T, Chatterjee E, Singh J, et al. Arjunolic acid, a peroxisome proliferator-activated receptor α agonist, regresses cardiac fibrosis by inhibiting non-canonical TGF-β signaling. *Journal of Biological Chemistry*. 2017;292(40):16440-16462. doi:10.1074/jbc.M117.788299
109. Diep Q. PPARα activator fenofibrate inhibits myocardial inflammation and fibrosis in angiotensin II-infused rats. *J Mol Cell Cardiol*. 2004;36(2):295-304. doi:10.1016/j.yjmcc.2003.11.004
110. Smeets PJH, Teunissen BEJ, Willemsen PHM, et al. Cardiac hypertrophy is enhanced in PPAR -/- mice in response to chronic pressure overload. *Cardiovasc Res*. 2008;78(1):79-89. doi:10.1093/cvr/cvn001
111. Abdurrachim D, Prompers JJ, Nicolay K, Nabben M, Glatz JFC, Luiken JJFP. Good and bad consequences of altered fatty acid metabolism in heart failure: evidence from mouse models. *Cardiovasc Res*. 2015;106(2):194-205. doi:10.1093/cvr/cvv105

112. Young ME, Laws FA, Goodwin GW, Taegtmeyer H. Reactivation of Peroxisome Proliferator-activated Receptor α Is Associated with Contractile Dysfunction in Hypertrophied Rat Heart. *Journal of Biological Chemistry*. 2001;276(48):44390-44395. doi:10.1074/jbc.M103826200
113. OGATA T, MIYAUCHI T, SAKAI S, IRUKAYAMA-TOMOBE Y, GOTO K, YAMAGUCHI I. Stimulation of peroxisome-proliferator-activated receptor α (PPAR α) attenuates cardiac fibrosis and endothelin-1 production in pressure-overloaded rat hearts. *Clin Sci*. 2002;103(s2002):284S-288S. doi:10.1042/CS103S284S
114. Lee SS, Pineau T, Drago J, et al. Targeted disruption of the alpha isoform of the peroxisome proliferator-activated receptor gene in mice results in abolishment of the pleiotropic effects of peroxisome proliferators. *Mol Cell Biol*. 1995;15(6):3012-3022.
115. Aoyama T, Peters JM, Iritani N, et al. Altered Constitutive Expression of Fatty Acid-metabolizing Enzymes in Mice Lacking the Peroxisome Proliferator-activated Receptor α (PPARα). *Journal of Biological Chemistry*. 1998;273(10):5678-5684. doi:10.1074/jbc.273.10.5678
116. Forman BM, Chen J, Evans RM. Hypolipidemic drugs, polyunsaturated fatty acids, and eicosanoids are ligands for peroxisome proliferator-activated receptors alpha and delta. *Proc Natl Acad Sci U S A*. 1997;94(9):4312-4317.
117. Chatham JC, Young ME. Metabolic Remodeling in the Hypertrophic Heart. *Circ Res*. 2012;111(6):666-668. doi:10.1161/CIRCRESAHA.112.277392
118. Sambandam N, Lopaschuk GD, Brownsey RW, Allard MF. Energy Metabolism in the Hypertrophied Heart. *Heart Fail Rev*. 2002;7(2):161-173. doi:10.1023/A:1015380609464
119. Taegtmeyer H, Sen S, Vela D. Return to the fetal gene program. *Ann N Y Acad Sci*. 2010;1188(1):191-198. doi:10.1111/j.1749-6632.2009.05100.x
120. He L, Kim T, Long Q, et al. Carnitine Palmitoyltransferase-1b Deficiency Aggravates Pressure Overload–Induced Cardiac Hypertrophy Caused by Lipotoxicity. *Circulation*. 2012;126(14):1705-1716. doi:10.1161/CIRCULATIONAHA.111.075978
121. Kolwicz SC, Olson DP, Marney LC, Garcia-Menendez L, Synovec RE, Tian R. Cardiac-Specific Deletion of Acetyl CoA Carboxylase 2 Prevents Metabolic Remodeling During Pressure-Overload Hypertrophy. *Circ Res*. 2012;111(6):728-738. doi:10.1161/CIRCRESAHA.112.268128
122. Carley AN, Taegtmeyer H, Lewandowski ED. Matrix Revisited. *Circ Res*. 2014;114(4):717-729. doi:10.1161/CIRCRESAHA.114.301863
123. Pal N, Acharjee A, Ament Z, et al. Metabolic Profiling of Aortic Stenosis and Hypertrophic Cardiomyopathy Identifies Mechanistic Contrasts in Substrate Utilisation. *bioRxiv*. Published online January 1, 2019:715680. doi:10.1101/715680
124. Abozguia K, Elliott P, McKenna W, et al. Metabolic Modulator Perhexiline Corrects Energy Deficiency and Improves Exercise Capacity in Symptomatic Hypertrophic Cardiomyopathy. *Circulation*. 2010;122(16):1562-1569. doi:10.1161/CIRCULATIONAHA.109.934059
125. Ritterhoff J, Young S, Villet O, et al. Metabolic remodeling promotes cardiac hypertrophy by directing glucose to aspartate biosynthesis. *Am Heart Assoc*. 2020;126:182-196. doi:10.1161/CIRCRESAHA.119.315483
126. Leong HS, Grist M, Parsons H, et al. Accelerated rates of glycolysis in the hypertrophied heart: are they a methodological artifact? *American Journal of Physiology-Endocrinology and Metabolism*. 2002;282(5):E1039-E1045. doi:10.1152/ajpendo.00507.2001

127. Schroeder MA, Lau AZ, Chen AP, et al. Hyperpolarized 13 C magnetic resonance reveals early- and late-onset changes to in vivo pyruvate metabolism in the failing heart. *Eur J Heart Fail*. 2013;15(2):130-140. doi:10.1093/eurjhf/hfs192
128. Natalia S, Michael OJ, D. MR, et al. Recruitment of Compensatory Pathways to Sustain Oxidative Flux With Reduced Carnitine Palmitoyltransferase I Activity Characterizes Inefficiency in Energy Metabolism in Hypertrophied Hearts. *Circulation*. 2007;115(15):2033-2041. doi:10.1161/CIRCULATIONAHA.106.668665
129. O'Donnell JM, Fields AD, Sorokina N, Lewandowski ED. The absence of endogenous lipid oxidation in early stage heart failure exposes limits in lipid storage and turnover. *J Mol Cell Cardiol*. 2008;44(2):315-322. doi:10.1016/j.yjmcc.2007.11.006
130. Zhang J, Merkle H, Hendrich K, et al. Bioenergetic abnormalities associated with severe left ventricular hypertrophy. *Journal of Clinical Investigation*. 1993;92(2):993-1003. doi:10.1172/JCI116676
131. Schulze PC. Myocardial lipid accumulation and lipotoxicity in heart failure. *J Lipid Res*. 2009;50(11):2137-2138. doi:10.1194/jlr.R001115
132. Schaffer JE. Lipotoxicity: when tissues overeat. *Curr Opin Lipidol*. 2003;14(3).
133. Conway MA, Allis J, Ouwerkerk R, Niioka T, Rajagopalan B, Radda GK. Detection of low phosphocreatine to ATP ratio in failing hypertrophied human myocardium by 31P magnetic resonance spectroscopy. *The Lancet*. 1991;338(8773):973-976. doi:10.1016/0140-6736(91)91838-L
134. Ye Y, Gong G, Ochiai K, Liu J, Zhang J. High-Energy Phosphate Metabolism and Creatine Kinase in Failing Hearts. *Circulation*. 2001;103(11):1570-1576. doi:10.1161/01.CIR.103.11.1570
135. Smith CS, Bottomley PA, Schulman SP, Gerstenblith G, Weiss RG. Altered Creatine Kinase Adenosine Triphosphate Kinetics in Failing Hypertrophied Human Myocardium. *Circulation*. 2006;114(11):1151-1158. doi:10.1161/CIRCULATIONAHA.106.613646
136. SHEN W, SPINDLER M, HIGGINS M, et al. The fall in creatine levels and creatine kinase isozyme changes in the failing heart are reversible: Complex post-transcriptional regulation of the components of the CK system. *J Mol Cell Cardiol*. 2005;39(3):537-544. doi:10.1016/j.yjmcc.2005.05.003
137. Ingwall JS, Atkinson DE, Clarke K, Fetters JK. Energetic correlates of cardiac failure: Changes in the creatine kinase system in the failing myocardium. *Eur Heart J*. 1990;11(suppl B):108-115. doi:10.1093/eurheartj/11.suppl_B.108
138. Nakae I, Mitsunami K, Omura T, et al. Proton magnetic resonance spectroscopy can detect creatine depletion associated with the progression of heart failure in cardiomyopathy. *J Am Coll Cardiol*. 2003;42(9):1587-1593. doi:10.1016/j.jacc.2003.05.005
139. Beer M, Seyfarth T, Sandstede J, et al. Absolute concentrations of high-energy phosphate metabolites in normal, hypertrophied, and failing human myocardium measured noninvasively with 31P-SLOOP magnetic resonance spectroscopy. *J Am Coll Cardiol*. 2002;40(7):1267-1274. doi:https://doi.org/10.1016/S0735-1097(02)02160-5
140. Ingwall JS, Weiss RG. Is the Failing Heart Energy Starved? *Circ Res*. 2004;95(2):135-145. doi:10.1161/01.RES.0000137170.41939.d9
141. Peterzan MA, Lygate CA, Neubauer S, Rider OJ. Metabolic remodeling in hypertrophied and failing myocardium: a review. *American Journal of Physiology-Heart and Circulatory Physiology*. 2017;313(3):H597-H616. doi:10.1152/ajpheart.00731.2016

142. Kolwicz SC, Purohit S, Tian R. Cardiac Metabolism and its Interactions With Contraction, Growth, and Survival of Cardiomyocytes. *Circ Res*. 2013;113(5):603-616. doi:10.1161/CIRCRESAHA.113.302095
143. Allard MF, Schonekess BO, Henning SL, English DR, Lopaschuk GD. Contribution of oxidative metabolism and glycolysis to ATP production in hypertrophied hearts. *American Journal of Physiology-Heart and Circulatory Physiology*. 1994;267(2):H742-H750. doi:10.1152/ajpheart.1994.267.2.H742
144. Akki A, Smith K, Seymour AML. Compensated cardiac hypertrophy is characterised by a decline in palmitate oxidation. *Mol Cell Biochem*. 2008;311(1-2):215-224. doi:10.1007/s11010-008-9711-y
145. Sack MN, Rader TA, Park S, Bastin J, McCune SA, Kelly DP. Fatty acid oxidation enzyme gene expression is downregulated in the failing heart. *Circulation*. 1996;94(11):2837-2842.
146. Lewandowski ED, O'donnell JM, Scholz TD, Sorokina N, Buttrick PM. Recruitment of NADH shuttling in pressure-overloaded and hypertrophic rat hearts. *American Journal of Physiology-Cell Physiology*. 2007;292(5):C1880-C1886.
147. Listenberger LL, Han X, Lewis SE, et al. Triglyceride accumulation protects against fatty acid-induced lipotoxicity. *Proceedings of the National Academy of Sciences*. 2003;100(6):3077-3082.
148. Chiu HC, Kovacs A, Ford DA, et al. A novel mouse model of lipotoxic cardiomyopathy. *Journal of Clinical Investigation*. 2001;107(7):813-822. doi:10.1172/JCI10947
149. Saburi Y. Changes in distinct species of 1,2-diacylglycerol in cardiac hypertrophy due to energy metabolic disorder. *Cardiovasc Res*. 2003;57(1):92-100. doi:10.1016/S0008-6363(02)00608-9
150. Shu H, Peng Y, Hang W, Li N, Zhou N, Wang DW. Emerging Roles of Ceramide in Cardiovascular Diseases. *Aging Dis*. 2022;13(1):232-245. doi:10.14336/AD.2021.0710
151. Goldberg IJ, Trent CM, Schulze PC. Lipid Metabolism and Toxicity in the Heart. *Cell Metab*. 2012;15(6):805-812. doi:10.1016/j.cmet.2012.04.006
152. Marfella R, Di Filippo C, Portoghese M, et al. Myocardial lipid accumulation in patients with pressure-overloaded heart and metabolic syndrome. *J Lipid Res*. 2009;50(11):2314-2323. doi:10.1194/jlr.P900032-JLR200
153. Stansfield WE, Charles PC, Tang R hang, et al. Regression of pressure-induced left ventricular hypertrophy is characterized by a distinct gene expression profile. *J Thorac Cardiovasc Surg*. 2009;137(1):232-238.e8. doi:https://doi.org/10.1016/j.jtcvs.2008.08.019
154. Schrepper A, Mohr FW, Färber G, et al. Decreased rates of substrate oxidation ex vivo predict the onset of heart failure and contractile dysfunction in rats with pressure overload. *Cardiovasc Res*. 2009;86(3):461-470. doi:10.1093/cvr/cvp414
155. Lang D. Cardiac hypertrophy and oxidative stress: a leap of faith or stark reality? *Heart*. 2002;87(4):316-317. doi:10.1136/heart.87.4.316
156. Rousset S, Alves-Guerra MC, Mozo J, et al. The Biology of Mitochondrial Uncoupling Proteins. *Diabetes*. 2004;53(suppl_1):S130-S135. doi:10.2337/diabetes.53.2007.S130
157. Murray AJ, Cole MA, Lygate CA, et al. Increased mitochondrial uncoupling proteins, respiratory uncoupling and decreased efficiency in the chronically infarcted rat heart. *J Mol Cell Cardiol*. 2008;44(4):694-700. doi:10.1016/j.yjmcc.2008.01.008
158. Boehm EA, Jones BE, Radda GK, Veech RL, Clarke K. Increased uncoupling proteins and decreased efficiency in palmitate-perfused hyperthyroid rat heart. *American*

Journal of Physiology-Heart and Circulatory Physiology. 2001;280(3):H977-H983. doi:10.1152/ajpheart.2001.280.3.H977

159. Murray AJ, Anderson RE, Watson GC, Radda GK, Clarke K. Uncoupling proteins in human heart. *The Lancet*. 2004;364(9447):1786-1788. doi:10.1016/S0140-6736(04)17402-3
160. YOUNG ME, PATIL S, YING JUN, et al. Uncoupling protein 3 transcription is regulated by peroxisome proliferator-activated receptor α in the adult rodent heart. *The FASEB Journal*. 2001;15(3):833-845. doi:https://doi.org/10.1096/fj.00-0351com
161. Ji XB, Li XR, Hao-Ding, et al. Inhibition of Uncoupling Protein 2 Attenuates Cardiac Hypertrophy Induced by Transverse Aortic Constriction in Mice. *Cellular Physiology and Biochemistry*. 2015;36(5):1688-1698. doi:10.1159/000430142
162. Zhou YT, Grayburn P, Karim A, et al. Lipotoxic heart disease in obese rats: Implications for human obesity. *Proceedings of the National Academy of Sciences*. 2000;97(4):1784 LP - 1789. doi:10.1073/pnas.97.4.1784
163. Mahmod M, Bull S, Suttie JJ, et al. Myocardial Steatosis and Left Ventricular Contractile Dysfunction in Patients With Severe Aortic Stenosis. *Circ Cardiovasc Imaging*. 2013;6(5):808-816. doi:10.1161/CIRCIMAGING.113.000559
164. Peterzan MA, Clarke WT, Lygate CA, et al. Cardiac Energetics in Patients With Aortic Stenosis and Preserved Versus Reduced Ejection Fraction. *Circulation*. 2020;141(24):1971-1985. doi:10.1161/CIRCULATIONAHA.119.043450
165. Zou J, Le K, Xu S, et al. Fenofibrate ameliorates cardiac hypertrophy by activation of peroxisome proliferator-activated receptor-α partly via preventing p65-NFκB binding to NFATc4. *Mol Cell Endocrinol*. 2013;370(1):103-112. doi:https://doi.org/10.1016/j.mce.2013.03.006
166. Goikoetxea MJ, Beaumont J, D??ez J. Peroxisome Proliferator-Activated Receptor ?? and Hypertensive Heart Disease. *Drugs*. 2004;64(Supplement 2):9-18. doi:10.2165/00003495-200464002-00003
167. Forcheron F, Basset A, Abdallah P, Del Carmine P, Gadot N, Beylot M. Diabetic cardiomyopathy: effects of fenofibrate and metformin in an experimental model – the Zucker diabetic rat. *Cardiovasc Diabetol*. 2009;8(1):16. doi:10.1186/1475-2840-8-16
168. van Ewijk PA, Schrauwen-Hinderling VB, Bekkers SCAM, Glatz JFC, Wildberger JE, Kooi ME. MRS: a noninvasive window into cardiac metabolism. *NMR Biomed*. 2015;28(7):747-766. doi:10.1002/nbm.3320
169. Tognarelli JM, Dawood M, Shariff MIF, et al. Magnetic Resonance Spectroscopy: Principles and Techniques: Lessons for Clinicians. *J Clin Exp Hepatol*. 2015;5(4):320-328. doi:10.1016/j.jceh.2015.10.006
170. Fragasso G, Perseghin G, De Cobelli F, et al. Effects of metabolic modulation by trimetazidine on left ventricular function and phosphocreatine/adenosine triphosphate ratio in patients with heart failure. *Eur Heart J*. 2006;27(8):942-948. doi:10.1093/eurheartj/ehi816
171. Beer M, Wagner D, Myers J, et al. Effects of Exercise Training on Myocardial Energy Metabolism and Ventricular Function Assessed by Quantitative Phosphorus-31 Magnetic Resonance Spectroscopy and Magnetic Resonance Imaging in Dilated Cardiomyopathy. *J Am Coll Cardiol*. 2008;51(19):1883-1891. doi:https://doi.org/10.1016/j.jacc.2007.09.075
172. Rial B, Robson MD, Neubauer S, Schneider JE. Rapid quantification of myocardial lipid content in humans using single breath-hold 1 H MRS at 3 Tesla. *Magn Reson Med*. 2011;66(3):619-624. doi:10.1002/mrm.23011

173. Ding B, Peterzan MA, Mozes FE, et al. Cardiac creatine quantified by cycled water-suppressed 1H-MRS at 3T. In: *ISMRM*. ; 2019.
174. Faller KME, Lygate CA, Neubauer S, Schneider JE. 1H-MR spectroscopy for analysis of cardiac lipid and creatine metabolism. *Heart Fail Rev*. 2013;18(5):657-668. doi:10.1007/s10741-012-9341-z
175. Wilson M, Andronesi O, Barker PB, et al. Methodological consensus on clinical proton MRS of the brain: Review and recommendations. *Magn Reson Med*. 2019;82(2):527-550. doi:10.1002/mrm.27742
176. Bottomley PA. NMR Spectroscopy of the Human Heart. In: *EMagRes*. Major Reference Works. John Wiley & Sons, Ltd; 1996. doi:10.1002/9780470034590.emrstm0345.pub2
177. Neubauer S, Horn M, Cramer M, et al. Myocardial Phosphocreatine-to-ATP Ratio Is a Predictor of Mortality in Patients With Dilated Cardiomyopathy. *Circulation*. 1997;96(7):2190-2196. doi:10.1161/01.CIR.96.7.2190
178. Crilley JG, Boehm EA, Blair E, et al. Hypertrophic cardiomyopathy due to sarcomeric gene mutations is characterized by impaired energy metabolism irrespective of the degree of hypertrophy. *J Am Coll Cardiol*. 2003;41(10):1776-1782. doi:https://doi.org/10.1016/S0735-1097(02)03009-7
179. Phan TT, Abozguia K, Nallur Shivu G, et al. Heart Failure With Preserved Ejection Fraction Is Characterized by Dynamic Impairment of Active Relaxation and Contraction of the Left Ventricle on Exercise and Associated With Myocardial Energy Deficiency. *J Am Coll Cardiol*. 2009;54(5):402-409. doi:10.1016/j.jacc.2009.05.012
180. Beer M, Sandstede J, Landschütz W, et al. Altered energy metabolism after myocardial infarction assessed by 31 P-MR-spectroscopy in humans. *Eur Radiol*. 2000;10(8):1323-1328. doi:10.1007/s003300000316
181. Neubauer S, Horn M, Pabst T, et al. Cardiac high-energy phosphate metabolism in patients with aortic valve disease assessed by 31P-magnetic resonance spectroscopy. *J Investig Med*. 1997;45(8):453—462.
182. Ye Y, Wang C, Zhang J, et al. Myocardial creatine kinase kinetics and isoform expression in hearts with severe LV hypertrophy. *American Journal of Physiology-Heart and Circulatory Physiology*. 2001;281(1):H376-H386. doi:10.1152/ajpheart.2001.281.1.H376
183. Ingwall JS, Kramer MF, Fifer MA, et al. The Creatine Kinase System in Normal and Diseased Human Myocardium. *New England Journal of Medicine*. 1985;313(17):1050-1054. doi:10.1056/NEJM198510243131704
184. Mahmod M, Francis JM, Pal N, et al. Myocardial perfusion and oxygenation are impaired during stress in severe aortic stenosis and correlate with impaired energetics and subclinical left ventricular dysfunction. *Journal of Cardiovascular Magnetic Resonance*. 2014;16(1):29. doi:10.1186/1532-429X-16-29
185. Beyerbacht HP, Lamb HJ, van der Laarse A, et al. Aortic Valve Replacement in Patients with Aortic Valve Stenosis Improves Myocardial Metabolism and Diastolic Function. *Radiology*. 2001;219(3):637-643. doi:10.1148/radiology.219.3.r01jn25637
186. Apps A, Lau J, Peterzan M, Neubauer S, Tyler D, Rider O. Hyperpolarised magnetic resonance for in vivo real-time metabolic imaging. *Heart*. 2018;104(18):1484 LP - 1491. doi:10.1136/heartjnl-2017-312356
187. Rider OJ, Tyler DJ. Clinical Implications of Cardiac Hyperpolarized Magnetic Resonance Imaging. *Journal of Cardiovascular Magnetic Resonance*. 2013;15(1):93. doi:10.1186/1532-429X-15-93

188. Agger P, Hyldebrandt JA, Hansen ESS, et al. Magnetic resonance hyperpolarization imaging detects early myocardial dysfunction in a porcine model of right ventricular heart failure. *Eur Heart J Cardiovasc Imaging*. 2020;21(1):93-101. doi:10.1093/ehjci/jez074
189. Lewis AJM, Tyler DJ, Rider O. Clinical Cardiovascular Applications of Hyperpolarized Magnetic Resonance. *Cardiovasc Drugs Ther*. 2020;34(2):231-240. doi:10.1007/s10557-020-06942-w
190. Schroeder MA, Atherton HJ, Ball DR, et al. Real-time assessment of Krebs cycle metabolism using hyperpolarized C magnetic resonance spectroscopy. *The FASEB Journal*. 2009;23(8):2529-2538. doi:https://doi.org/10.1096/fj.09-129171
191. Miller JJ, Lau AZ, Nielsen PM, et al. Hyperpolarized [1,4-13C2]Fumarate Enables Magnetic Resonance-Based Imaging of Myocardial Necrosis. *JACC Cardiovasc Imaging*. 2018;11(11):1594-1606. doi:10.1016/j.jcmg.2017.09.020
192. Gallagher FA, Kettunen MI, Day SE, et al. Magnetic resonance imaging of pH in vivo using hyperpolarized 13C-labelled bicarbonate. *Nature*. 2008;453(7197):940-943. doi:10.1038/nature07017
193. Seymour AML, Giles L, Ball V, et al. In vivo assessment of cardiac metabolism and function in the abdominal aortic banding model of compensated cardiac hypertrophy. *Cardiovasc Res*. 2015;106(2):249-260. doi:10.1093/cvr/cvv101
194. Lahey R, Carley AN, Wang X, et al. Enhanced Redox State and Efficiency of Glucose Oxidation With miR Based Suppression of Maladaptive NADPH-Dependent Malic Enzyme 1 Expression in Hypertrophied Hearts. *Circ Res*. 2018;122(6):836-845. doi:10.1161/CIRCRESAHA.118.312660
195. Wang T, Zhu XH, Li H, et al. Noninvasive assessment of myocardial energy metabolism and dynamics using in vivo deuterium MRS imaging. *Magn Reson Med*. 2021;86(6):2899-2909. doi:https://doi.org/10.1002/mrm.28914
196. Ritterhoff J, Tian R. Metabolism in cardiomyopathy: every substrate matters. *Cardiovasc Res*. 2017;113(4):411-421. doi:10.1093/cvr/cvx017
197. Mancini DM, Eisen H, Kussmaul W, Mull R, Edmunds LH, Wilson JR. Value of peak exercise oxygen consumption for optimal timing of cardiac transplantation in ambulatory patients with heart failure. *Circulation*. 1991;83(3):778-786. doi:10.1161/01.CIR.83.3.778
198. Enright PL. The Six-Minute Walk Test. *Respir Care*. 2003;48(8):783 LP - 785.
199. Ponikowski P, Voors AA, Anker SD, et al. 2016 ESC Guidelines for the diagnosis and treatment of acute and chronic heart failure: The Task Force for the diagnosis and treatment of acute and chronic heart failure of the European Society of Cardiology (ESC)Developed with the special contribution of. *Eur Heart J*. 2016;37(27):2129-2200. doi:10.1093/eurheartj/ehw128
200. Sigvardsen PE, Larsen LH, Carstensen HG, et al. Six-minute walking test and long term prognosis in patients with asymptomatic aortic valve stenosis. *Int J Cardiol*. 2017;249:334-339. doi:https://doi.org/10.1016/j.ijcard.2017.09.183
201. Gibbons RJ, Balady GJ, Beasley JW, et al. ACC/AHA Guidelines for Exercise Testing: A report of the American College of Cardiology/American Heart Association task force on practice guidelines (Committee on Exercise Testing). In: *Journal of the American College of Cardiology*. Vol 30. ; 1997:260-311. doi:10.1016/S0735-1097(97)00150-2
202. Wasserman K. *Cardiopulmonary Exercise Testing and Cardiovascular Health*. Wiley-Blackwell; 2002.

203. Hansen JE, Sue DY, Wasserman K. Predicted Values for Clinical Exercise Testing. *American Review of Respiratory Disease*. 1984;129(2P2):S49-S55. doi:10.1164/arrd.1984.129.2P2.S49
204. Malhotra R, Bakken K, D'Elia E, Lewis GD. Cardiopulmonary Exercise Testing in Heart Failure. *JACC Heart Fail*. 2016;4(8):607-616. doi:10.1016/j.jchf.2016.03.022
205. Tanabe Y, Nakagawa I, Ito E, Suzuki K. Hemodynamic basis of the reduced oxygen uptake relative to work rate during incremental exercise in patients with chronic heart failure. *Int J Cardiol*. 2002;83(1):57-62. doi:https://doi.org/10.1016/S0167-5273(02)00013-X
206. Bottomley PA. MRS Studies of Creatine Kinase Metabolism in Human Heart. In: *EMagRes*. Vol 5. John Wiley & Sons, Ltd; 2016:1183-1202. doi:10.1002/9780470034590.emrstm1488
207. Bottomley PA, Smith LS, Brazzamano S, Hedlund LW, Redington RW, Herfkens RJ. The fate of inorganic phosphate and pH in regional myocardial ischemia and infarction: A noninvasive 31P NMR study. *Magn Reson Med*. 1987;5(2):129-142. doi:10.1002/mrm.1910050205
208. Bottomley PA, Foster TB, Darrow RD. Depth-resolved surface-coil spectroscopy (DRESS) for in Vivo 1H, 31P, and 13C NMR. *Journal of Magnetic Resonance (1969)*. 1984;59(2):338-342. doi:https://doi.org/10.1016/0022-2364(84)90179-3
209. Bakermans AJ, Abdurrachim D, van Nierop BJ, et al. In vivo mouse myocardial 31P MRS using three-dimensional image-selected in vivo spectroscopy (3D ISIS): technical considerations and biochemical validations. *NMR Biomed*. 2015;28(10):1218-1227. doi:10.1002/nbm.3371
210. Watson W, Miller J, Lewis A, et al. Use of cardiac magnetic resonance to detect changes in metabolism in heart failure. *Cardiovasc Diagn Ther*. 2020;10:583-597. doi:10.21037/cdt.2019.12.13
211. Köstler H, Landschütz W, Koeppe S, et al. Age and gender dependence of human cardiac phosphorus metabolites determined by SLOOP 31P MR spectroscopy. *Magn Reson Med*. 2006;56(4):907-911. doi:https://doi.org/10.1002/mrm.21027
212. Okada M, Mitsunami K, Inubushi T, Kinoshita M. Influence of aging or left ventricular hypertrophy on the human heart: Contents of phosphorus metabolites measured by 31P MRS. *Magn Reson Med*. 1998;39(5):772-782. doi:https://doi.org/10.1002/mrm.1910390515
213. Barbier P, Mirea O, Cefalù C, Maltagliati A, Savioli G, Guglielmo M. Reliability and feasibility of longitudinal AFI global and segmental strain compared with 2D left ventricular volumes and ejection fraction: intra- and inter-operator, test–retest, and inter-cycle reproducibility. *Eur Heart J Cardiovasc Imaging*. 2015;16(6):642-652. doi:10.1093/ehjci/jeu274
214. Lamb HJ, Doornbos J, den Hollander JA, et al. Reproducibility of Human Cardiac 31P-NMR Spectroscopy. *NMR Biomed*. 1996;9(5):217-227. doi:10.1002/(SICI)1099-1492(199608)9:5<217::AID-NBM419>3.0.CO;2-G
215. Ellis J, Valkovič L, Purvis LAB, Clarke WT, Rodgers CT. Reproducibility of human cardiac phosphorus MRS (31 P-MRS) at 7 T. *NMR Biomed*. 2019;32(6):e4095. doi:10.1002/nbm.4095
216. Grothues F, Smith GC, Moon JCC, et al. Comparison of interstudy reproducibility of cardiovascular magnetic resonance with two-dimensional echocardiography in normal subjects and in patients with heart failure or left ventricular hypertrophy. *Am J Cardiol*. 2002;90(1):29-34. doi:10.1016/S0002-9149(02)02381-0

217. Hudsmith LE, Petersen SE, Francis JM, Robson MD, Neubauer S. Normal human left and right ventricular and left atrial dimensions using steady state free precession magnetic resonance imaging. VO - 7 RT - Journal Article. *Journal of cardiovascular magnetic resonance : official journal of the Society for Cardiovascular Magnetic Resonance OP - 775-782*. (5 WP-).
218. Shehata ML, Cheng S, Osman NF, Bluemke DA, Lima JAC. Myocardial tissue tagging with cardiovascular magnetic resonance. *Journal of Cardiovascular Magnetic Resonance*. 2009;11(1):1-12.
219. Stuber M, Spiegel MA, Fischer SE, et al. Single breath-hold slice-following CSPAMM myocardial tagging. *Magnetic Resonance Materials in Physics, Biology and Medicine*. 1999;9(1):85-91.
220. Griffin JL, Williams HJ, Sang E, Nicholson JK. Abnormal lipid profile of dystrophic cardiac tissue as demonstrated by one- and two-dimensional magic-angle spinning 1H NMR spectroscopy. *Magn Reson Med*. 2001;46(2):249-255. doi:https://doi.org/10.1002/mrm.1185
221. Bilet L, Weijer T, Hesselink MKC, et al. Exercise-induced modulation of cardiac lipid content in healthy lean young men. *Basic Res Cardiol*. 2011;106(2):307-315. doi:10.1007/s00395-010-0144-x
222. McGavock JM, Lingvay I, Zib I, et al. Cardiac Steatosis in Diabetes Mellitus. *Circulation*. 2007;116(10):1170-1175. doi:10.1161/CIRCULATIONAHA.106.645614
223. Frahm J, Merboldt KD, Hänicke W. Localized proton spectroscopy using stimulated echoes. *Journal of Magnetic Resonance (1969)*. 1987;72(3):502-508. doi:10.1016/0022-2364(87)90154-5
224. BOTTOMLEY PA. Spatial Localization in NMR Spectroscopy in Vivo. *Ann N Y Acad Sci*. 1987;508(1 Physiological):333-348. doi:10.1111/j.1749-6632.1987.tb32915.x
225. Ding B, Peterzan M, Mózes FE, Rider OJ, Valkovič L, Rodgers CT. Water-suppression cycling 3-T cardiac 1 H-MRS detects altered creatine and choline in patients with aortic or mitral stenosis. *NMR Biomed*. 2021;n/a(n/a):e4513. doi:10.1002/nbm.4513
226. Piechnik SK, Ferreira VM, Dall'Armellina E, et al. Shortened Modified Look-Locker Inversion recovery (ShMOLLI) for clinical myocardial T1-mapping at 1.5 and 3 T within a 9 heartbeat breathhold. *Journal of Cardiovascular Magnetic Resonance*. 2010;12(1):69. doi:10.1186/1532-429X-12-69
227. Levy D, Garrison RJ, Savage DD, Kannel WB, Castelli WP. Prognostic implications of echocardiographically determined left ventricular mass in the Framingham Heart Study. *New England Journal of Medicine*. 1990;322(22):1561-1566.
228. Frey N, Katus HA, Olson EN, Hill JA. Hypertrophy of the heart: a new therapeutic target? *Circulation*. 2004;109(13):1580-1589.
229. Lai L, Leone T, Keller M, … OMCH, 2014 undefined. Energy metabolic reprogramming in the hypertrophied and early stage failing heart: a multisystems approach. *Am Heart Assoc*.
230. Hamirani YS, Kundu BK, Zhong M, et al. Noninvasive Detection of Early Metabolic Left Ventricular Remodeling in Systemic Hypertension. *Cardiology*. 2016;133(3):157-162. doi:10.1159/000441276
231. Lehman JJ, Kelly DP. Transcriptional Activation Of Energy Metabolic Switches In The Developing And Hypertrophied Heart. *Clin Exp Pharmacol Physiol*. 2002;29(4):339-345. doi:10.1046/j.1440-1681.2002.03655.x
232. Jameel M, Zhang J. Myocardial Energetics in Left Ventricular Hypertrophy. *Curr Cardiol Rev*. 2009;5(3):243-250. doi:10.2174/157340309788970379

233. Minners J, Rossebo A, Chambers JB, et al. Sudden cardiac death in asymptomatic patients with aortic stenosis. *Heart*. 2020;106(21):1646 LP - 1650. doi:10.1136/heartjnl-2019-316493
234. Jeung MY, Germain P, Croisille P, ghannudi S el, Roy C, Gangi A. Myocardial Tagging with MR Imaging: Overview of Normal and Pathologic Findings. *RadioGraphics*. 2012;32(5):1381-1398. doi:10.1148/rg.325115098
235. Moreira HT, Nwabuo CC, Armstrong AC, et al. Reference Ranges and Regional Patterns of Left Ventricular Strain and Strain Rate Using Two-Dimensional Speckle-Tracking Echocardiography in a Healthy Middle-Aged Black and White Population: The CARDIA Study. *J Am Soc Echocardiogr*. 2017;30(7):647-658.e2. doi:10.1016/j.echo.2017.03.010
236. Manaka M, Tanaka N, Takei Y, Kurohane S, Takazawa K, Yamashina A. [Assessment of regional myocardial systolic function in hypertensive left ventricular hypertrophy using harmonic myocardial strain imaging]. *J Cardiol*. 2005;45(2):53-60.
237. Kosmala W, Plaksej R, Strotmann JM, et al. Progression of Left Ventricular Functional Abnormalities in Hypertensive Patients with Heart Failure: An Ultrasonic Two-Dimensional Speckle Tracking Study. *Journal of the American Society of Echocardiography*. 2008;21(12):1309-1317. doi:10.1016/j.echo.2008.10.006
238. Sabbah H. Apoptotic cell death in heart failure. *Cardiovasc Res*. 2000;45(3):704-712. doi:10.1016/S0008-6363(99)00348-X
239. Puls M, Beuthner BE, Topci R, et al. Impact of myocardial fibrosis on left ventricular remodelling, recovery, and outcome after transcatheter aortic valve implantation in different haemodynamic subtypes of severe aortic stenosis. *Eur Heart J*. 2020;41(20):1903-1914. doi:10.1093/eurheartj/ehaa033
240. Cramariuc D, Gerdts E, Davidsen ES, Segadal L, Matre K. Myocardial deformation in aortic valve stenosis: relation to left ventricular geometry. *Heart*. 2010;96(2):106-112. doi:10.1136/hrt.2009.172569
241. Li J, Kemp BA, Howell NL, et al. Metabolic changes in spontaneously hypertensive rat hearts precede cardiac dysfunction and left ventricular hypertrophy. *Am Heart Assoc*. 2019;8(4). doi:10.1161/JAHA.118.010926
242. Polak-Iwaniuk A, Harasim-Symbor E, Gołaszewska K, Chabowski A. How Hypertension Affects Heart Metabolism . *Frontiers in Physiology* . 2019;10.
243. Elezaby A, Sverdlov AL, Tu VH, et al. Mitochondrial remodeling in mice with cardiomyocyte-specific lipid overload. *J Mol Cell Cardiol*. 2015;79:275-283. doi:10.1016/j.yjmcc.2014.12.001
244. Bhattacharyya S, Khattar R, Chahal N, Moat N, Senior R. Dynamic Assessment of Stenotic Valvular Heart Disease by Stress Echocardiography. *Circ Cardiovasc Imaging*. 2013;6(4):583-589. doi:10.1161/CIRCIMAGING.113.000201
245. Balady GJ, Arena R, Sietsema K, et al. Clinician's Guide to Cardiopulmonary Exercise Testing in Adults. *Circulation*. 2010;122(2):191-225. doi:10.1161/CIR.0b013e3181e52e69
246. Carabello BA. Aortic valve replacement should be operated on before symptom onset. *Circulation*. 2012;126(1):112-117.
247. Ng ACT, Delgado V, Bertini M, et al. Alterations in multidirectional myocardial functions in patients with aortic stenosis and preserved ejection fraction: a two-dimensional speckle tracking analysis. *Eur Heart J*. 2011;32(12):1542-1550. doi:10.1093/eurheartj/ehr084
248. Kienesberger PC, Pulinilkunnil T, Sung MMY, et al. Myocardial ATGL Overexpression Decreases the Reliance on Fatty Acid Oxidation and Protects against

Pressure Overload-Induced Cardiac Dysfunction. *Mol Cell Biol*. 2012;32(4):740-750. doi:10.1128/MCB.06470-11
249. Haemmerle G, Moustafa T, Woelkart G, et al. ATGL-mediated fat catabolism regulates cardiac mitochondrial function via PPAR-α and PGC-1. *Nat Med*. 2011;17(9):1076-1085. doi:10.1038/nm.2439
250. Kim TT, Dyck JRB. The role of CD36 in the regulation of myocardial lipid metabolism. *Biochimica et Biophysica Acta (BBA) - Molecular and Cell Biology of Lipids*. 2016;1861(10):1450-1460. doi:10.1016/j.bbalip.2016.03.018
251. Stanley WC, Chandler MP. Energy metabolism in the normal and failing heart: potential for therapeutic interventions. *Heart Fail Rev*. 2002;7(2):115-130. doi:10.1023/A:1015320423577
252. Ross RM. ATS/ACCP statement on cardiopulmonary exercise testing. *Am J Respir Crit Care Med*. 2003;167(10):1451-author.
253. McArdle WD, Katch FI, Katch VL. *Essentials of Exercise Physiology*. Lippincott Williams & Wilkins; 2006.
254. Dulgheru R, Magne J, Capoulade R, et al. Impact of global hemodynamic load on exercise capacity in aortic stenosis. *Int J Cardiol*. 2013;168(3):2272-2277.
255. Kolwicz SC. An "Exercise" in Cardiac Metabolism. *Front Cardiovasc Med*. 2018;5:66. doi:10.3389/fcvm.2018.00066
256. Greenberg CC, Jurczak MJ, Danos AM, Brady MJ. Glycogen branches out: new perspectives on the role of glycogen metabolism in the integration of metabolic pathways. *American Journal of Physiology-Endocrinology and Metabolism*. 2006;291(1):E1-E8.
257. Stainsby WN, Barclay JK. Exercise metabolism: O 2 deficit, steady level O 2 uptake and O 2 uptake for recovery. *Med Sci Sports*. 1970;2(4):177-181.
258. Demarle AP, Slawinski JJ, Laffite LP, Bocquet VG, Koralsztein JP, Billat VL. Decrease of O2 deficit is a potential factor in increased time to exhaustion after specific endurance training. *J Appl Physiol*. 2001;90(3):947-953.
259. Nascimben L, Ingwall JS, Lorell BH, et al. Mechanisms for increased glycolysis in the hypertrophied rat heart. *Hypertension*. 2004;44(5):662-667.
260. Dalsgaard M, Kjaergaard J, Pecini R, et al. Predictors of exercise capacity and symptoms in severe aortic stenosis. *European Journal of Echocardiography*. 2010;11(6):482-487. doi:10.1093/ejechocard/jeq002
261. Francis D. Cardiopulmonary exercise testing for prognosis in chronic heart failure: continuous and independent prognostic value from VE/VCO2slope and peak VO2. *Eur Heart J*. 2000;21(2):154-161. doi:10.1053/euhj.1999.1863
262. Clyne CA, Arrighi JA, Maron BJ, Dilsizian V, Bonow RO, Cannon III RO. Systemic and left ventricular responses to exercise stress in asymptomatic patients with valvular aortic stenosis. *Am J Cardiol*. 1991;68(15):1469-1476.
263. Rajani R, Rimington H, Chambers JB. Treadmill exercise in apparently asymptomatic patients with moderate or severe aortic stenosis: relationship between cardiac index and revealed symptoms. *Heart*. 2010;96(9):689-695.
264. Moxnes JF, Sandbakk Ø. The kinetics of lactate production and removal during whole-body exercise. *Theor Biol Med Model*. 2012;9(1):7. doi:10.1186/1742-4682-9-7
265. Qiu Y, Pan X, Chen Y, Xiao J. Hallmarks of exercised heart. *J Mol Cell Cardiol*. 2022;164:126-135. doi:10.1016/j.yjmcc.2021.12.004
266. Villa E, Troise G, Cirillo M, et al. Factors affecting left ventricular remodeling after valve replacement for aortic stenosis. An overview. *Cardiovasc Ultrasound*. 2006;4(1):25. doi:10.1186/1476-7120-4-25

267. Willson TM, Brown PJ, Sternbach DD, Henke BR. The PPARs: from orphan receptors to drug discovery. *J Med Chem*. 2000;43(4):527-550.
268. Yuan J, Wu J, Han ZG. Fenofibrate improves energy metabolism and attenuates isoproterenol induced acute myocardial ischemic injury in rats via PPAR alpha activation. *Zhonghua Xin Xue Guan Bing Za Zhi*. 2008;36(9):847-850.
269. LeBrasseur NK, Duhaney TAS, De Silva DS, et al. Effects of fenofibrate on cardiac remodeling in aldosterone-induced hypertension. *Hypertension*. 2007;50(3):489-496.
270. Labinskyy V, Bellomo M, Chandler MP, et al. Chronic activation of peroxisome proliferator-activated receptor-α with fenofibrate prevents alterations in cardiac metabolic phenotype without changing the onset of decompensation in pacing-induced heart failure. *Journal of Pharmacology and Experimental Therapeutics*. 2007;321(1):165-171.
271. Ichihara S, Obata K, Yamada Y, et al. Attenuation of cardiac dysfunction by a PPAR-α agonist is associated with down-regulation of redox-regulated transcription factors. *J Mol Cell Cardiol*. 2006;41(2):318-329.
272. Keech A, Simes RJ, Barter P, et al. Effects of long-term fenofibrate therapy on cardiovascular events in 9795 people with type 2 diabetes mellitus (the FIELD study): randomised controlled trial. *Lancet*. 2005;366(9500):1849-1861. doi:10.1016/S0140-6736(05)67667-2
273. Keating GM. Fenofibrate: a review of its lipid-modifying effects in dyslipidemia and its vascular effects in type 2 diabetes mellitus. *Am J Cardiovasc Drugs*. 2011;11(4):227-247. doi:10.2165/11207690-000000000-00000
274. Irukayama-Tomobe Y, Miyauchi T, Sakai S, et al. Endothelin-1–Induced Cardiac Hypertrophy Is Inhibited by Activation of Peroxisome Proliferator–Activated Receptor-α Partly Via Blockade of c-Jun NH 2 -Terminal Kinase Pathway. *Circulation*. 2004;109(7):904-910. doi:10.1161/01.CIR.0000112596.06954.00
275. Nita C, Bala C, Porojan M, Hancu N. Fenofibrate improves endothelial function and plasma myeloperoxidase in patients with type 2 diabetes mellitus: an open-label interventional study. *Diabetol Metab Syndr*. 2014;6(1):30. doi:10.1186/1758-5996-6-30
276. Schulz-Menger J, Bluemke DA, Bremerich J, et al. Standardized image interpretation and post processing in cardiovascular magnetic resonance: Society for Cardiovascular Magnetic Resonance (SCMR) Board of Trustees Task Force on Standardized Post Processing. *Journal of Cardiovascular Magnetic Resonance*. 2013;15(1):35. doi:10.1186/1532-429X-15-35
277. van Bilsen M, van der Vusse GJ, Reneman RS. Transcriptional regulation of metabolic processes: implications for cardiac metabolism. *Pflügers Archiv*. 1998;437(1):2-14.
278. Chu Y, Zhang C, Xie M. Beta-Hydroxybutyrate, Friend or Foe for Stressed Hearts . *Frontiers in Aging* . 2021;2.
279. Shen W, Asai K, Uechi M, et al. Progressive Loss of Myocardial ATP Due to a Loss of Total Purines During the Development of Heart Failure in Dogs . *Circulation*. 1999;100(20):2113-2118. doi:10.1161/01.CIR.100.20.2113
280. Shveta M, Ladislav V, Damian T, et al. Insights Into the Metabolic Aspects of Aortic Stenosis With the Use of Magnetic Resonance Imaging. *JACC Cardiovasc Imaging*. 2022;0(0). doi:10.1016/j.jcmg.2022.04.025
281. Gjertsson P, Caidahl K, Farasati M, Odén A, Bech-Hanssen O. Preoperative moderate to severe diastolic dysfunction: A novel Doppler echocardiographic long-term prognostic factor in patients with severe aortic stenosis. *J Thorac Cardiovasc Surg*. 2005;129(4):890-896. doi:https://doi.org/10.1016/j.jtcvs.2004.09.004

282. Ng ACT, Delgado V, Bertini M, et al. Myocardial Steatosis and Biventricular Strain and Strain Rate Imaging in Patients With Type 2 Diabetes Mellitus. *Circulation*. 2010;122(24):2538-2544. doi:10.1161/CIRCULATIONAHA.110.955542
283. Hess OM, Villari B, Krayenbuehl HP. Diastolic dysfunction in aortic stenosis. *Circulation*. 1993;87(5 Suppl):IV73-6.
284. Geraldine O, Philippe P, Bjorn R, et al. Diastolic Function and Clinical Outcomes After Transcatheter Aortic Valve Replacement. *J Am Coll Cardiol*. 2020;76(25):2940-2951. doi:10.1016/j.jacc.2020.10.032
285. Park TS, Hu Y, Noh HL, et al. Ceramide is a cardiotoxin in lipotoxic cardiomyopathy*s. *J Lipid Res*. 2008;49(10):2101-2112. doi:https://doi.org/10.1194/jlr.M800147-JLR200
286. Vikramadithyan RK, Hirata K, Yagyu H, et al. Peroxisome proliferator-activated receptor agonists modulate heart function in transgenic mice with lipotoxic cardiomyopathy. *Journal of Pharmacology and Experimental Therapeutics*. 2005;313(2):586-593.
287. Sarma S, Carrick-Ranson G, Fujimoto N, et al. Effects of Age and Aerobic Fitness on Myocardial Lipid Content. *Circ Cardiovasc Imaging*. 2013;6(6):1048-1055. doi:10.1161/CIRCIMAGING.113.000565
288. Shubair MM, Kodis J, McKelvie RS, Arthur HM, Sharma AM. Metabolic profile and exercise capacity outcomes: their relationship to overweight and obesity in a Canadian cardiac rehabilitation setting. *J Cardiopulm Rehabil Prev*. 2004;24(6):405-413.
289. Grewal J, McCully RB, Kane GC, Lam C, Pellikka PA. Left Ventricular Function and Exercise Capacity. *JAMA*. 2009;301(3):286-294. doi:10.1001/jama.2008.1022
290. Vanoverschelde JJ, Essamri B, Vanbutsele R, et al. Contribution of left ventricular diastolic function to exercise capacity in normal subjects. *J Appl Physiol*. 1993;74(5):2225-2233. doi:10.1152/jappl.1993.74.5.2225
291. Cuocolo A, Sax FL, Brush JE, Maron BJ, Bacharach SL, Bonow RO. Left ventricular hypertrophy and impaired diastolic filling in essential hypertension. Diastolic mechanisms for systolic dysfunction during exercise. *Circulation*. 1990;81(3):978-986. doi:10.1161/01.CIR.81.3.978
292. Arena R, Myers J, Aslam SS, Varughese EB, Peberdy MA. Peak VO2 and VE/VCO2 slope in patients with heart failure: a prognostic comparison. *Am Heart J*. 2004;147(2):354-360. doi:10.1016/j.ahj.2003.07.014
293. Steadman CD, Jerosch-Herold M, Grundy B, et al. Determinants and Functional Significance of Myocardial Perfusion Reserve in Severe Aortic Stenosis. *JACC Cardiovasc Imaging*. 2012;5(2):182-189. doi:https://doi.org/10.1016/j.jcmg.2011.09.022
294. Domanski O, Richardson M, Coisne A, et al. Cardiopulmonary exercise testing is a better outcome predictor than exercise echocardiography in asymptomatic aortic stenosis. *Int J Cardiol*. 2017;227:908-914. doi:https://doi.org/10.1016/j.ijcard.2016.10.070
295. Dulgheru R, Magne J, Davin L, et al. Left ventricular regional function and maximal exercise capacity in aortic stenosis. *Eur Heart J Cardiovasc Imaging*. 2016;17(2):217-224. doi:10.1093/ehjci/jev147
296. Maciver DH. The relative impact of circumferential and longitudinal shortening on left ventricular ejection fraction and stroke volume. *Exp Clin Cardiol*. 2012;17(1):5-11.
297. Al Musa T, Uddin A, Swoboda PP, et al. Myocardial strain and symptom severity in severe aortic stenosis: insights from cardiovascular magnetic resonance. *Quant Imaging Med Surg*. 2017;7(1):38-47. doi:10.21037/qims.2017.02.05

298. Chamsi-Pasha MA, Zhan Y, Debs D, Shah DJ. CMR in the Evaluation of Diastolic Dysfunction and Phenotyping of HFpEF: Current Role and Future Perspectives. *JACC Cardiovasc Imaging*. 2020;13(1, Part 2):283-296. doi:https://doi.org/10.1016/j.jcmg.2019.02.031